

9-2009

Synthesis and Study of Hybrid Organic – Inorganic Polyhedral Oligomeric Silsesquioxanes (poss) Based Polymers

Gunjan A, Gadodia

University of Massachusetts Amherst, gunjangadodia@3aassociate.com

Follow this and additional works at: https://scholarworks.umass.edu/open_access_dissertations

 Part of the [Polymer Science Commons](#)

Recommended Citation

Gadodia, Gunjan A., "Synthesis and Study of Hybrid Organic – Inorganic Polyhedral Oligomeric Silsesquioxanes (poss) Based Polymers" (2009). *Open Access Dissertations*. 97.

<https://doi.org/10.7275/x6zc-t890> https://scholarworks.umass.edu/open_access_dissertations/97

This Open Access Dissertation is brought to you for free and open access by ScholarWorks@UMass Amherst. It has been accepted for inclusion in Open Access Dissertations by an authorized administrator of ScholarWorks@UMass Amherst. For more information, please contact scholarworks@library.umass.edu.

**SYNTHESIS AND STUDY OF HYBRID ORGANIC – INORGANIC
POLYHEDRAL OLIGOMERIC SILSESQUIOXANES (POSS)
BASED POLYMERS**

A Dissertation Presented

By

GUNJAN A. GADODIA

Submitted to the Graduate School of the
University of Massachusetts Amherst in partial fulfillment
of the requirements for the degree of

DOCTOR OF PHILOSOPHY

September 2009

Department of Polymer Science and Engineering

**SYNTHESIS AND STUDY OF HYBRID ORGANIC – INORGANIC
POLYHEDRAL OLIGOMERIC SILSESQUOXANES (POSS)
BASED POLYMERS**

A Dissertation Presented

By

GUNJAN A. GADODIA

Approved as to style and content by:

E. Bryan Coughlin, Chair

Alfred J. Crosby, Member

Anthony D. Dinsmore, Member

Shaw Ling Hsu, Department Head
Polymer Science and Engineering

DEDICATION

To my beloved family

ACKNOWLEDGEMENTS

I would like to express my sincerest gratitude to my advisor and mentor Prof E. Bryan Coughlin. The journey towards my PhD would not have been possible without this constant support and encouragement. I would also like to thank him for his patience and freedom he gave me to try new and different things. Working with him, I have become a more optimist person, and a better communicator. I would also like to thank Prof. Al Crosby and Prof Anthony Dinsmore for serving on my committee. I have learned a great deal through their insightful comments and constructive criticism.

I would like to acknowledge a number of collaborators with whom I have worked Prof. Sam Gido, Eric Anderson, Wim De Jeu, Ling Yang, Jiayu Wang and Prof. Tom Russell. I have learnt a lot working with them. I would especially like to thank Prof. Sam Gido, even though he was not on my committee he has always been available for discussions. Further, I would like to thank all the faculty members of Polymer Science and Engineering Department.

I would also like to thank Dr. Stephen Eyles, Dr. Greg Dabkowski, Dr. Weiguo Hu, Dr. Sekar Dhanasekaran and Jack Hirsh for keeping the facilities up and running, and helping me to run my experiments. I also need to thank the administrative staff especially Erin and Vivien for their fantastic job.

I would like to thank the sixth floor students, and the many other students with whom I have worked or interacted. It's truly a great experience working in the Polymer Science and Engineering department at University of Massachusetts Amherst.

It has been wonderful working in the Coughlin group and I would like to thank all present and past Coughlin group members. Push helped me in my first year to settle in

the group. I have learnt a lot from Nui and Brad, my fellow hybrid group members. It has been fun working around Ranga, Rich, Chris, Liz, Katie, Tsung Han, Bon-Choel, Makoto and Tarik. I have found friends for life in Ying, Shilpi, Gregoire, Yoan and Sergio. Ying has been fantastic friend for last the past 5 years, we started together and she has been very helpful to me. Hopefully in the future we will stay in touch with each other. Shilpi has also been a great friend for more than just research, we have discussed India, politics, life etc. Gregoire has been a great friend and a mentor. When I started, I had no synthetic skills and knowledge, he really helped me get started. We have been good friend since then and hopefully we will stay in touch. I think I have spent most time of my graduate life working around Yoan and Sergio. It has been a great cultural experience working with them. I am sure I will miss all of them once I go back to India.

There is a huge Indian Mafia at UMASS and they make a foreign country, 10,000 miles away from India, feel like home. My roommates and friends, present and past, Nilanjan, Gautam, Abhishek, Srikant, Neha, Swetha, Raja, Mayur, Suresh and many others have been like a family. Deepak and Ajay have been special friends and I have enjoyed conversations with them and learnt a lot from them. Keyur and Vishal my high school friends have been great support in US. My friends Shreenath, Gopal and Pushkar in India have also been very supportive.

Finally I would like to dedicate this thesis to my parents, sister Neha and girlfriend Janavi. It was only because of them that I have managed to do a Ph.D. Without their incessant love, support and patience this journey would not have been possible. It has been very difficult living away from them for 5 years and I look forward to my life with them. Thank you all!

ABSTRACT

SYNTHESIS AND STUDY OF HYBRID ORGANIC-INORGANIC
POLYHEDRAL OLIGOMERIC SILSESQUIOXANE (POSS)
BASED POLYMERS
SEPTEMBER 2009

GUNJAN A. GADODIA, B.TECH., UNIVERISTY OF MUMBAI, INDIA
M.S., UNIVERISTY OF MASSACHUSETTS, AMHERST
Ph.D., UNIVERISTY OF MASSACHUSETTS, AMHERST

Directed by: Professor E. Bryan Coughlin

Hybrid organic-inorganic materials represent a new class of materials having scientific and technological potential. In this thesis, Polyhedral Oligomeric Silsesquioxanes (POSS) are used as an inorganic building block which has been tethered to an organic polymer. POSS are silica precursors, having a well defined silsesquioxane central core surrounded by an organic periphery which makes them compatible with monomers and possibly polymers. The objectives of this study are to (1) study the basic structures of POSS homopolymers, (2) to incorporate POSS building blocks by a bottom-up approach into polymer chains and study the resulting morphologies, and (3) to study the thin film behavior of POSS block copolymers.

PMA and styryl POSS homopolymers of different peripheries were synthesized by ATRP and mass spectrometry studies were carried out by MALDI-TOF and ESI. PMA POSS chains undergo a number of fragmentations while styryl POSS chains have a

relatively robust backbone. Poly(ethylene-butylene-*b*-MAPOSS), AB type copolymers and poly(MAPOSS-*b*-styrene-*b*-MAPOSS), ABA type copolymers were synthesized by a combination of anionic and ATRP polymerization. Spheres, inverse cylinders, lamellar and crystalline lamellar morphologies were observed for the poly(ethylene-butylene-*b*-MAPOSS) copolymers. In the poly(MAPOSS-*b*-styrene-*b*-MAPOSS) copolymers, cylindrical, lamellar and perforated lamellar morphologies were obtained. Beyond the interaction parameter (χ), total degree of polymerization (N) and volume fraction (f), the conformational asymmetry (ϵ) also plays an important role in determining the morphology of these block copolymer. Crystallization of the POSS phase and better thermal properties were observed in the both block copolymers. Thin film studies of poly(MAPOSS-*b*-styrene-*b*-MAPOSS) copolymers showed that the microdomains can be oriented either parallel or perpendicular to the substrate depending upon the film thickness, morphology and relative volume fractions of the connecting blocks. By removal of the organic phase, ordered mesoporous low dielectric constant silica films were obtained. These hybrid block copolymers are a potential candidate for nanopatterning applications.

TABLE OF CONTENTS

ACKNOWLEDGEMENTS.....	v
ABSTRACT.....	vii
LIST OF TABLES.....	xii
LIST OF FIGURES.....	xiv
LIST OF SCHEMES.....	xx
LIST OF ABBREVIATIONS AND SYMBOLS.....	xxi
CHAPTER	
1. INTRODUCTION.....	1
1.1 Hybrid Organic – Inorganic Materials.....	1
1.2 Self – Assembly of Block Copolymers.....	5
1.3 Hybrid Organic - Inorganic Polymers Based on Polyhedral Oligomeric Silsesquioxanes (POSS).....	7
1.3.1 Synthesis and Properties of Polyhedral Oligomeric Silsesquioxanes (POSS).....	7
1.3.2 POSS as Fillers.....	12
1.3.3 POSS as Comonomer.....	13
1.4 Summary.....	26
1.5 References.....	28
2. SYNTHESIS, ELECTROSPRAY IONIZATION AND MALDI MASS SPECTROMETRY STUDIES OF LARGE POSS OLIGOMERS.....	33
2.1 Introduction.....	33
2.2 Experimental Section.....	36
2.2.1 Materials.....	36
2.2.2 Equipment.....	37
2.2.3 ATRP Synthesis of POSS Oligomers.....	38
2.3 Results and Discussion.....	46
2.3.1 POSS PMA Oligomers.....	46
2.3.2 POSS Styryl Oligomers.....	56
2.4 Conclusions.....	61
2.5 References.....	62
3. SYNTHESIS AND SELF-ASSEMBLY OF ORGANIC-INORGANIC POSS – POLY (ETHYLENE – BUTYLENE) BASED POLYMERS.....	67
3.1 Introduction.....	67
3.2 Experimental Section.....	69
3.2.1 Materials.....	69

3.2.2	Synthesis	70
3.2.3	Polymer Characterization.....	74
3.3	Results and Discussions.....	76
3.3.1	Synthesis and Hydrogenation of Polybutadiene	76
3.3.2	Synthesis of PEB Macroinitiator and p(EB- <i>b</i> -MA- POSS(isobutyl)) Diblock Copolymer	79
3.3.3	Polymer Characterization.....	81
3.4	Summary	95
3.5	References.....	96
4.	SYNTHESIS AND MORPHOLOGICAL STUDIES OF POSS CONTAINING ORGANIC – INORGANIC TRIBLOCK COPOLYMERS	100
4.1	Introduction.....	100
4.2	Experimental Section	103
4.2.1	Materials	103
4.2.2	Synthesis	104
4.2.3	Polymer Characterization.....	108
4.3	Results and Discussions.....	111
4.3.1	Synthesis of Hemi-telechelic & Telechelic Polystyrene.....	111
4.3.2	Synthesis of Polystyrene Macroinitiator and p(MA- POSS(isobutyl)- <i>b</i> -Styrene- <i>b</i> -MA-POSS(isobutyl)) Triblock Copolymer.....	113
4.3.3	Polymer Characterization.....	116
4.4	Conclusion	130
4.5	References.....	132
5.	Organizing Silica Nanostructures on Surfaces Using Polyhedral Oligomeric Silsesquioxane (POSS) Based Block Copolymers	136
5.1	Introduction.....	136
5.2	Experimental.....	139
5.2.1	Materials	139
5.2.2	Thin Film Preparation and Characterization.....	140
5.3	Results and Discussion	142
5.3.1	Thin Film Studies of Hybrid Organic-Inorganic Block Copolymers.....	142
5.3.2	Transformation of POSS to Silica	148
5.3.3	Dielectric Constant of Silica Thin Film.....	151
5.4	Summary	152
5.5	References.....	153
6.	SUMMARY AND FUTURE OUTLOOK	157
6.1	Summary	157
6.2	Future Outlook	160
6.3	References.....	162

APPENDIX : A MALDI AND ESI DATA of POSS OLIGOMERS.....	164
BIBLIOGRAPHY.....	190

LIST OF TABLES

Table	Page
1.1. Classification of dispersed particles based on size scale.	12
2.1. M_n and PDI values of PMA and Styryl POSS Oligomers	45
3.1. Molecular weights of poly(ethylenebutylene) and p(EB- <i>b</i> -MA-P OSS(isobutyl)) diblock copolymers.....	75
3.2. TGA and DSC data for p(EB- <i>b</i> -MA-POSS(isobutyl)) diblock copolymers.....	82
3.3. Summarized WAXS results of the homopolymers and diblock copolymers.....	86
4.1. Molecular weights of polystyrene and p(MA-POSS(isobutyl)- <i>b</i> -Styrene- <i>b</i> -MA-POSS(isobutyl)) triblock copolymers.....	113
4.2. DSC and TGA data of MA-POSS (isobutyl) homopolymer, styrene homopolymers and p(MA-POSS(isobutyl)- <i>b</i> -Styrene- <i>b</i> -MA- POSS(isobutyl)) triblock copolymers.	124
5.1. Molecular weights of polystyrene and p(MA-POSS(isobutyl)- <i>b</i> -styrene- <i>b</i> - MA-POSS(isobutyl)) triblock copolymers.	139
5.2. X-ray photoelectron spectroscopy (XPS) results of POSS ₁₀ -S ₁₃₀ -POSS ₁₀ triblock copolymer before and after thermal annealing.....	149
A. MALDI SPECTRA	164
A1. $M = CH_3CH_2COOC-C(CH_3)_2-R_7T_7propylmethacrylate]_n -Br$	164
A2. $M = CH_3CH_2COOC-C(CH_3)_2-R_7T_7propylmethacrylate]_n -Br$	168
A3. $M = C_6H_4(CO)_2NCH_2CH_2OCH_2CH_2OOC-C(CH_3)_2-$ $R_7T_7propylmethacrylate]_n-Br$	170
A4. $M = NH_2CH_2CH_2OCH_2CH_2OOC-C(CH_3)_2-[R_7T_7propylmethacrylate]_n -$ Br	173
A5. $M = [R_7T_7Propylmethacrylate]_n[(CH_3)_2CCN]_{m=1,2}$	176
A6. $M = R_7T_7Propylmethacrylate]_n[(CH_3)_2CCN]_{m=1,2}$	178

A7. $M = R_7T_7(C_6H_4CHCH_2)]_n[(CH_3)_2CCN]_{m=1,2,3}$	180
A8. $M = C_6H_4(CO)_2NCH_2CH_2OCH_2CH_2OOC-C(CH_3)_2-R_7T_7(C_6H_4CHCH_2)]_n-$ Br.....	182
A9. $M = C_6H_4(CO)_2NCH_2CH_2OCH_2CH_2OOC-C(CH_3)_2-$ $R_7T_7(C_6H_4CHCH_2)]_n-Br$	184
A10. $M = C_6H_4(CO)_2NCH_2CH_2OCH_2CH_2OOC-C(CH_3)_2-$ $R_7T_7(C_6H_4CHCH_2)]_n-Br$	186
A11. $M = NH_2CH_2CH_2OCH_2CH_2OOC-C(CH_3)_2-$ $(Cyclohexyl)_7T_7(C_6H_4CHCH_2)]_n-Br$	188

LIST OF FIGURES

Figure	Page
1.1. (a) Nacre of a shell and (b) Brick and mortar structure having alternating calcium carbonate and biopolymer layers giving hardness, strength and toughness to the shell (fig. taken from reference [1]).	1
1.2. (a) Graph comparing the properties of inorganic ceramics, organic polymers and hybrid organic-inorganic materials. Applications of inorganic materials, (b) silsesquioxane based optically clear scratch free coatings, (c) artificial bone made of hydroxyapatite-phosphazene, (d) titanium oxide based solar cells and (e) clay nanocomposites based packaging material (fig. taken from references [4,6]).	2
1.3. Different morphologies formed by self-organization of block copolymers in bulk and solution (fig. taken from reference [15]).	4
1.4. (Top) Phase diagram of linear block copolymer predicted by self-consistent mean field theory, (middle) Experimental phase diagram of linear poly(styrene-b-isoprene) diblock copolymer and (bottom) Pictorial representation of various phases of the block copolymer (fig. taken from reference [23, 27]).	6
1.5. Structures of Silsesquioxanes (fig. taken from reference [31]).	8
1.6. Basic reactions for silsesquioxane synthesis.	9
1.7. Synthesis of silsesquioxane derivatives by acid or base hydrolytic condensation.	9
1.8. Chemical structure of POSS monomer where X is the reactive group, R is the organic periphery and Y is the site of attachment.	10
1.9. Chemical structure of components of epoxy-POSS copolymers (fig. taken from reference [50]).	15
1.10. Synthesis of polyethylene-POSS copolymer by (top) metallocene and (bottom) ring-opening metathesis polymerization (ROMP) (fig. taken from reference [60]).	17
1.11. (A) TEM of PBD-POSS. The copolymer of low POSS concentration aggregate into short randomly oriented lamellae with lateral dimensions of approximately 50nm (B) Schematic drawing of PBD-POSS assembly at low POSS concentration. (C) TEM of	

<p>PBD-POSS copolymer of high POSS concentration form continuous lamellar morphology with lateral length on the order of microns (D) Schematic drawing of PBD-POSS assembly at high POSS concentration (fig. taken from reference [65]).</p>	19
<p>1.12. Transmission electron micrographs of (a) 50Cyclohexyl-POSS and (b) 50Cyclopentyl-POSS showing the different size of cylindrical structure depending upon corner groups present in POSS monomer (fig. taken from reference [68]).</p>	21
<p>1.13. Small angle X-ray scattering (SAXS) of PS-POSS copolymers, PS-POSS 2K shows mesoscopic ordering (fig. taken from reference [72]).</p>	23
<p>1.14 Synthetic methodology for the preparation of ABA triblocks containing a poly(n-butyl acrylate) middle segments and outer segments of p(MAPOSS). In the first step, difunctional pBA macroinitiator is prepared by the ATRP of BA from a dimethyl 2,6-dibromoheptanedioate initiator. Subsequent chain extension of the pBA macroinitiator with MA-POSS yielded the ABA triblock copolymer (fig. taken from reference [55]).</p>	25
<p>1.15. (Right) Chemical structure of PMMA-POSS and PS-POSS copolymer and (left) TEM image of the corresponding copolymer (fig. taken from reference [76]).</p>	26
<p>2.1. 4,4'-dihydroxyoctofluoroazobenzene matrix.</p>	35
<p>2.2. Ethyl isobutyrate POSS PMA oligomers synthesized using ATRP.</p>	47
<p>2.3. ESI mass spectrum of [(i-butyl)₇T₇propylmethacrylate]_n. Most intense peaks are assigned to sodiated and potassied parent species, the terminal Br being replaced with OH.</p>	47
<p>2.4. Ethyl isobutyrate Isobutyl POSS PMA MALDI mass spectrum using 4,4'-dihydroxyoctoflyoroazobenzene matrix. Typical series shown in expansion in region of m/z = 3900 - 4040.</p>	48
<p>2.5. Ethyl isobutyrate Phenyl POSS PMA MALDI mass spectrum using 4,4'-dihydroxyoctofluoroazobenzene matrix. Typical series shown in expansion region of m/z = 7800</p>	49
<p>2.6. ESI mass spectrum of [(phenyl)₇T₇propylmethacrylate]_n The largest peak in each series up to n = 6 corresponds to protonation of the parent.</p>	50
<p>2.7. GPC of MA-POSS(isobutyl) polymer.</p>	51

2.8. ¹ HNMR spectrum of phthalimide PMA POSS (i-butyl) (left); NH ₂ -PMA POSS (i-butyl) (right).	52
2.9. Phthalimide (i-butyl) POSS PMA oligomers, (left) GPC with UV detector at 254 nm, (right) IR spectra.	53
2.10. MSMS MALDI spectrum of phthalimido-Isobutyl POSS PMA using 4,4'-dihydroxyoctofluoroazobenzene matrix for the m/z 2397 peak.....	54
2.11. IR of phthalimide (green), primary amine (black) and benzoyl (red) Isobutyl Styryl-POSS oligomers.	57
2.12. MALDI mass spectra of (Cp) styryl POSS in dihydroxyoctofluoroazobenzene. Inset shows spectrum in HABA matrix.	58
2.13. Isobutylnitrile (i-butyl)styrylPOSS MALDI mass spectrum using 4,4'-dihydroxyoctofluoroazobenzene matrix. Labels A, B, A and C correspond to 1-3 isobutylnitrile groups	61
3.1. GPC of poly(butadiene), M _n – 5,800 g/mol and PDI 1.05 and poly(ethylenebutylene), M _n – 5,000 g/mol and PDI 1.05.	78
3.2. GPC of (a) PEB, 19,000 g/mol and (b) p(EB-b-MA-POSS (isobutyl)) diblock copolymer (E(65)B ₃₅₀ POSS ₁₇), 35,000 g/mol.	80
3.3. TGA of poly(MA-POSS (isobutyl)), a)E(44)B ₁₀₇ POSS ₉ , b) E(65)B ₃₅₀ POSS ₁₇ , c)E(63)B ₆₃₂ POSS ₂₈ , d)E(72)B ₁₀₇₂ POSS ₁₅ and poly(ethylenebutylene).	81
3.4. DSC of a)E(44)B ₁₀₇ POSS ₉ , b) E(65)B ₃₅₀ POSS ₁₇ , c)E(63)B ₆₃₂ POSS ₂₈ and d)E(72)B ₁₀₇₂ POSS ₁₅	83
3.5. (left) WAXS of (a) poly (MA-POSS (isobutyl)) homopolymer, (b) E(44)B ₁₀₇ POSS ₉ , c) E(65)B ₃₅₀ POSS ₁₇ , d) E(63)B ₆₃₂ POSS ₂₈ , e) E(72)B ₁₀₇₂ POSS ₁₅ and f) E(63)B ₆₃₂ homopolymer.....	85
3.6. SAXS of p(EB-b-MA-POSS (isobutyl)) diblock copolymers a)E(44)B ₁₀₇ POSS ₉ , b) E(65)B ₃₅₀ POSS ₁₇ , c)E(63)B ₆₃₂ POSS ₂₈ and d)E(72)B ₁₀₇₂ POSS ₁₅	87
3.7. TEM of p(EB-b-MA-POSS (isobutyl)) diblock copolymers a) E(65)B ₃₅₀ POSS ₁₇ , b) E(63)B ₆₃₂ POSS ₂₈ and c)E(72)B ₁₀₇₂ POSS ₁₅	89

3.8. Wedge of a cylinder with the chains in the core being more stretched than the chains in the periphery. The shaded plane shows the interface between the chains.	90
3.9. SAXS of E(65)B ₃₅₀ POSS ₁₇ at different temperatures.....	91
3.10. (A) SAXS of diblock copolymer (a) E(63)B ₆₃₂ POSS ₂₈ and (b) quenched- E(63)B ₆₃₂ POSS ₂₈ and (B) TEM image of quenched- E(63)B ₆₃₂ POSS ₂₈	92
3.11. DSC plots of (a) E(63)B ₆₃₂ POSS ₂₈ and (b) quenched - E(63)B ₆₃₂ POSS ₂₈ diblock copolymer.	92
3.12. Tensile test of E(72)B ₁₀₇₂ POSS ₁₅ sample.	95
4.1. IR of (top to bottom) hemi-telechelic polystyrene, telechelic polystyrene, polystyrene macroinitiator and p(MA-POSS(isobutyl)- <i>b</i> -Styrene- <i>b</i> -MA-POSS(isobutyl)) triblock copolymers.	112
4.2. ¹ H NMR of (left) hemi-telechelic (PS) and (right) telechelic PS.	112
4.3. GPC of (a) PS homopolymer (5,000 g/mol) and (b) POSS ₆ -S ₄₈ -POSS ₆ triblock copolymer (16,500 g/mol).....	115
4.4. SAXS of copolymer POSS ₁₀ -S ₁₃₀ -POSS ₁₀ at different temperatures to determine the order-disorder temperature of the triblock copolymer.	116
4.5. WAXS of (a) MA-POSS (isobutyl) monomer as received from Aldrich , (b) POSS ₆ -S ₄₈ -POSS ₆ , (c) POSS ₁₀ -S ₁₃₀ -POSS ₁₀ , (d) POSS ₈ -S ₁₃₀ -POSS ₈ , (e) POSS _{13.5} -S ₃₄₈ -POSS _{13.5} and (f) Polystyrene homopolymer.	119
4.6. Small angle X-ray Scattering (SAXS) of as cast triblock copolymer films (a) POSS ₆ -S ₄₈ -POSS ₆ , (b) POSS ₁₀ -S ₁₃₀ -POSS ₁₀ , (c) POSS ₈ -S ₁₃₀ -POSS ₈ , (d) POSS _{13.5} -S ₃₄₈ -POSS _{13.5}	120
4.7. Transmission Electron Microscopy (TEM) of p(MA-POSS(isobutyl)- <i>b</i> -Styrene- <i>b</i> -MA-POSS(isobutyl)) triblock copolymers (a) POSS ₆ -S ₄₈ -POSS ₆ , (b) POSS ₁₀ -S ₁₃₀ -POSS ₁₀ , (c) POSS ₈ -S ₁₃₀ -POSS ₈ , (d) POSS _{13.5} -S ₃₄₈ -POSS _{13.5}	122
4.8. TGA graph of p(MA-POSS)- <i>b</i> -p(PS)- <i>b</i> -p(MA-POSS), MA-POSS (char yield 45%, top), (a) POSS ₆ -S ₄₈ -POSS ₆ , (b) POSS ₁₀ -S ₁₃₀ -POSS ₁₀ , (c) POSS ₈ -S ₁₃₀ -POSS ₈ , (d) POSS _{13.5} -S ₃₄₈ -POSS _{13.5} and PS homopolymer (char yield 0%, bottom).....	126

4.9. DSC of MAPOSS isobutyl monomer.	127
4.10. DSC of p(MA-POSS(isobutyl)- <i>b</i> -Styrene- <i>b</i> -MA-POSS(isobutyl)) triblock copolymers, (a) POSS ₆ -S ₄₈ -POSS ₆ , (b) POSS ₁₀ -S ₁₃₀ - POSS ₁₀ , (c) POSS ₈ -S ₁₃₀ -POSS ₈ , (d) POSS _{13.5} -S ₃₄₈ -POSS _{13.5}	127
4.11. Static light scattering of MA-POSS (isobutyl) homopolymers at four different concentrations (2.0, 3.0, 4.0 and 5.0 g/L) and eight different angles (40°, 50°, 60°, 70°, 80°, 90°, 100° and 110°).....	130
4.12. Differential refractive index of MA-POSS (isobutyl) homopolymers at five different concentrations (1.0, 2.0, 3.0, 4.0 and 5.0 g/L) in toluene as the solvent.	131
5.1. Surface analysis of POSS ₈ -S ₁₃₀ -POSS ₈ triblock copolymer spin-coated on silicon with native silicon oxide layer. SFM (25 μm x 25 μm) height image (a) revealed interconnected-island formation. As can be seen from the phase image (c), the template was covered with one phase (one of the block copolymer domain). (b) Scanning across these islands and holes resulted in step heights of 18.6 nm which was comparable to the bulk long period of the triblock. (d) GISAXS pattern of the film shows parallel orientation of the microdomains throughout the thickness of the film.	143
5.2. Surface analysis of POSS ₁₀ -S ₁₃₀ -POSS ₁₀ triblock copolymer spin-coated on silicon with native silicon oxide layer. SFM (2 μm x 2 μm) phase image (a) revealed phase contrast with FFT (inset) of a ring that corresponds to 21.1 nm which is comparable to the bulk long period of the triblock. (b), GISAXS pattern of the thin film obtained at incident angle ($\alpha_i = 0.14^\circ$) probing only the surface of the film, scattering profile suggest that the microdomains are oriented perpendicular to the polymer/air interface. (c), GISAXS pattern of the thin film obtained at incident angle ($\alpha_i = 0.21^\circ$) probing the entire thickness of the film, scattering profile suggest that the lamellae microdomains are oriented perpendicular to the substrate and perforations layers are present parallel to the substrate. (d) 1-dimensional SAXS profile of the triblock sample obtained from the GISAXS pattern shown in 2c.	145
5.3. Surface analysis of POSS ₁₀ -S ₁₃₀ -POSS ₁₀ triblock copolymer spin-coated on gold substrate. (left), GISAXS pattern of the thin film obtained at incident angle ($\alpha_i = 0.14^\circ$) probing only the surface of the film, scattering profile suggest that the microdomains are oriented perpendicular to the polymer/air interface. (right), GISAXS pattern of the thin film obtained at incident angle ($\alpha_i = 0.20^\circ$) probing the entire thickness of the film, scattering profile suggest that the	

lamellae microdomains are oriented perpendicular to the substrate and perforations layers are present parallel to the substrate.	147
5.4. Surface analysis of POSS ₁₀ -S ₁₃₀ -POSS ₁₀ triblock copolymer after thermal annealing at 375 °C. SFM (2 μm x 2 μm) phase image (a) revealed phase contrast with FFT (inset) of a ring that corresponds to 20 nm which is comparable to the long period of the triblock before thermal annealing. (b), GISAXS pattern of the thermally annealed thin film which suggests that the silica microdomains are perpendicular to the substrate.	151
6.1 Study of conformation of molecules using MALDI-TOF and helium filled drift cell.....	161

LIST OF SCHEMES

Scheme	Page
2.1. Synthesis of Isobutyl POSS PMA polymers using phthalimide initiator by ATRP.	40
2.2. Synthesis of benzoyl isobutyl POSS PMA oligomer.....	42
2.3. Synthesis of isobutyl POSS Styryl polymers using phthalimide initiator by ATRP and conversion of phthalimide group to primary amine.....	43
2.4. Free radical termination in cyclopentyl POSS PMAoligomers. Scheme I: single i-butylnitrile; Scheme II: two i-butylnitrile groups. Cp = cyclopentyl.....	55
2.5. Free radical termination in isobutyl POSS styryl oligomers. Scheme I: single i-butylnitrile; Scheme II: two i-butylnitrile groups.	59
3.1. Synthesis of polybutadiene and poly(ethylene-butylene).....	72
3.2. Synthesis of PEB macroinitiator and p(EB- <i>b</i> -MA-POSS (isobutyl)) diblock copolymer.	74
4.1. Synthesis of hemi-telechelic and telechelic polystyrene.	105
4.2. Synthesis of polystyrene macroinitiator and p(MA-POSS(isobutyl)- <i>b</i> -Styrene- <i>b</i> -MA-POSS(isobutyl)) triblock copolymers.	107

LIST OF ABBREVIATIONS AND SYMBOLS

AFM	Atomic force microscopy
AIBN	Azobisisobutyronitrile
amu	Atomic mass unit
ATRP	Atom transfer radical polymerization
BA	<i>n</i> - butyl acrylate
BCC and <i>bcc</i>	Body-centered cubic packing
C	Spheres
<i>cLam</i>	Crystalline lamellae
Cp	Cyclopentyl
Cy	Cyclohexyl
CpPOSS-NCO	1-[isocyanotopropyldimethylsilyl]-3,5,7,9,11,13,15- ^{3,9} ^{5,15} ^{7,13} hepacyclopentylpentacyclo [9.5.1.1 .1 .1] octasiloxane
Cu(I)Cl	Copper (I) chloride
Cu(I)Br	Copper (I) bromide
<i>d</i>	Domain spacing
DGEBA	Diglycidyl ether of bisphenol A
DHB	2,5-dihydroxybenzoic acid
dn/dc	Differential refractive index
DPE	Diphenylethylene
DSC	Differential scanning calorimetry
EB	Ethylene-butylene
eV	Electron Volt
ESI	Electrospray ionization
<i>f</i>	Volume fraction
FCC and <i>fcc</i> -	Face-centered cubic packing
FFT	Fast fourier transform
FTIR	Fourier transform infrared spectroscopy
G	Bicontinuous cubic structure
GISAXS	Grazing incidence angle small angle X-ray scattering
GPC	Gel permeation chromatography
H	Hexagonally packed cylinders
HABA	2-(4-hydroxyphenylazo)benzoic acid
i-butyl	Isobutyl
IR	Infrared Spectroscopy
<i>k</i>	Dielectric constant
L	Lamellae
<i>l_o</i>	Length of repeat unit
<i>l_p</i>	Persistence length
<i>M₄</i>	4,4'-dihydroxyoctofluoroazobenzene
<i>M_n</i>	Number average molecular weight
<i>M_o</i>	monomer molecular weight
<i>M_w</i>	Weight average molecular weight

MALDI	Matrix assisted laser desorption – ionization
MA-POSS(isobutyl)	3-(3,5,7,9,11,13,15-Heptaisobutylpentacyclo[9.5.1(3,9).1(5,15).1(7,13)]octasiloxan-1-yl)propyl methacrylate [MA POSS(isobutyl)]
MS	Mass spectrometry
MS/MS	Tandem mass spectrometry
n	Index of refraction
N	Degree of polymerization
N ₂	Nitrogen
NMR	Nuclear magnetic resonance
P	Porosity
PBD	Polybutadiene
PBD-POSS	Polybutadiene- <i>co</i> -POSS
PDI	Polydispersity index
PE	Polyethylene
PE-POSS	Polyethylene- <i>co</i> -POSS
PEB	poly(ethylene-butylene)
PEO	Poly(ethylene oxide)
Ph	Phenyl
PI	Polyisoprene
PL	Perforated lamellae
PMAPOSS	poly(methacrylate-POSS (isobutyl)
PMEDTA	N,N,N',N'',N'''-pentamethyldiethylenetriamine
PMMA	Poly(methyl methacrylate)
PNB	Polynorbornene
POSS	Polyhedral oligomeric silsesquioxane
PS	Polystyrene
PS- <i>b</i> -PBD	Polystyrene- <i>block</i> -Polybutadiene
PS- <i>b</i> -PMMA	Polystyrene- <i>block</i> -Poly(methyl methacrylate)
PSOH	Hydroxy-terminated polystyrene
q	Scattering vector
q^*	Primary scattering vector
q_y	Scattering vector along y-axis
q_z	Scattering vector along z-axis
R	Organic substituents
R_{gw}	weight average radius of gyration
ROMP	Ring-opening metathesis polymerization
S	Spheres
SAXS	Small angle X-ray scattering
SALS	Static angle light scattering
SBS	Styrene-Butadiene-Styrene triblock copolymer
<i>sec</i> -BuLi	<i>sec</i> -butyl lithium
SEM	Scanning electron microscopy
SFM	Surface force microscopy
SSL	Strong segregation limit
T	Temperature

T_7	Trisilanol POSS
T_8	Fully condensed POSS
T_g	Glass transition temperature
T_{ODT}	Order-Disorder transition temperature
TBAF	Tetra <i>n</i> -butylammonium fluoride
TBDMS	Tert-butyldimethylsilyl
TEM	Transmission electron microscopy
TGA	Thermogravimetric analysis
THF	Tetrahydrofuran
TOF	Time-of-flight
UV	Ultraviolet
VASE	Variable angle spectrometric ellipsometry
WAXS	Wide-angle X-ray scattering
WSL	Weak segregation limit
wt %	Weight percent
X	Reactive group
XPS	X-ray photoelectron spectroscopy

Symbols

α_c	Critical angle
α_i	Incidence angle
β	Peak width at half maxima
χ	Flory-Huggins parameter
δ	Density
ε	Conformation asymmetry parameter
θ_A	Advancing angle
θ_R	Receding angle

CHAPTER 1

INTRODUCTION

1.1 Hybrid Organic – Inorganic Materials

Nature has combined organic and inorganic compounds to produce smart materials with synergistic properties showing extraordinary strength, toughness, hardness and functionality.¹⁻³ Nacre of shell is one of the most studied materials displaying very high strength, toughness and hardness due to the brick and mortar structural arrangement of inorganic calcium carbonate platelets and organic proteins (see Fig. 1.1).¹ Other examples include the skeletons of sponges and diatoms formed by the self-assembly of organic –inorganic components that produce superior material properties for precise functions.^{2,4}

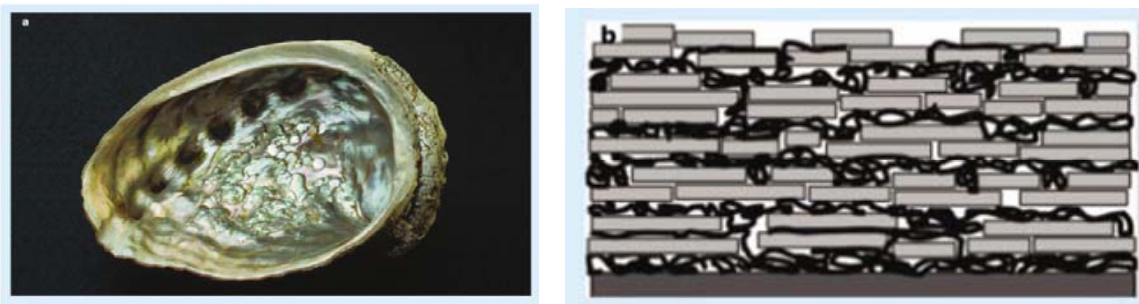


Figure 1.1. (a) Nacre of a shell and (b) Brick and mortar structure having alternating calcium carbonate and biopolymer layers giving hardness, strength and toughness to the shell (fig. taken from reference [1]).

Material scientists, inspired by nature, are trying to combine dissimilar materials which could lead to novel functions giving access to a wider spectrum of applications.^{5,6} Traditionally inorganic materials, ceramics for example, have high temperature and oxidation resistance but lack toughness and processability. On the other hand, organic materials are tough, light weight and easy to process but lack high temperature and

oxidation resistance. Synergistic combination of the properties of organic and inorganic materials could give hybrid materials with novel functionalities. These materials will open new opportunities in existing areas of science and create new opportunities in medicine, renewable energy and space technology.

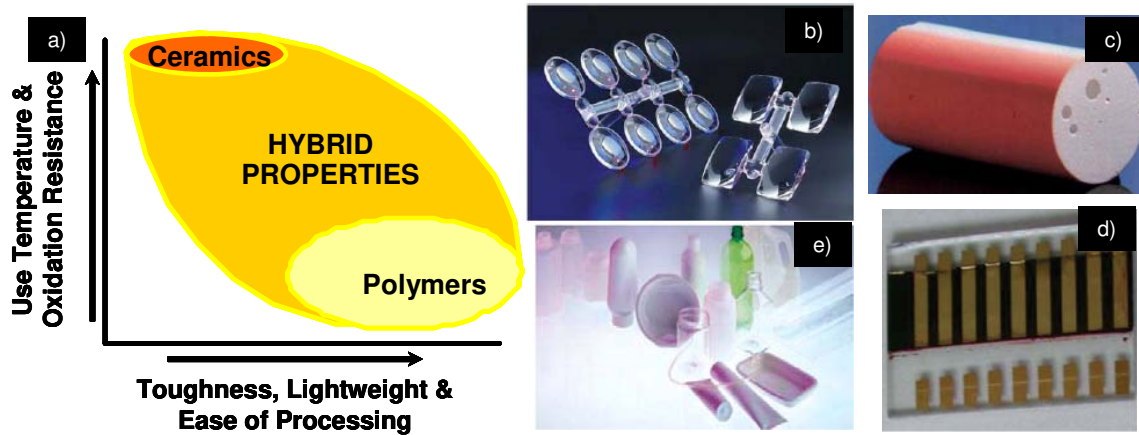


Figure 1.2. (a) Graph comparing the properties of inorganic ceramics, organic polymers and hybrid organic-inorganic materials. Applications of inorganic materials, (b) silsesquioxane based optically clear scratch free coatings, (c) artificial bone made of hydroxyapatite-phosphazene, (d) titanium oxide based solar cells and (e) clay nanocomposites based packaging material (fig. taken from references [4,6]).

Irrespective of the type of organic - inorganic material, the method of combination of the components plays a very important role in the final structure, property and application of the hybrid material. Various top-down and bottom-up approaches have been developed to combine organic and inorganic materials.^{4,7,8} Sanchez *et al.* have reviewed different approaches to combine organic and inorganic components.⁴ Top-down approaches involve mixing mesoscopic organic and inorganic components with the assistance of an external source of energy such as heat or mechanical work. Clay composites produced by top-down approaches are one of the most widely studied hybrid materials.⁹ Exfoliated structures of the composites lead to superior thermal and mechanical properties.¹⁰ However, the top-down approach is an energy intensive

approach and does not offer control over the molecular and supramolecular architectures which control the macroscopic properties of the polymer composites. It also suffers from serious limitations of non-uniform dispersion of the clay in the organic matrix leading to non-uniform properties. On the other hand, the bottom-up approach covalently combines organic - inorganic materials to form truly molecular dispersed nanocomposites with complete control over the molecular architecture. Organizing inorganic matter with organic molecules at a mesoscale was first discovered by scientists at the Mobil Corporation.¹¹ Sol-gel the most widely used bottom-up approach is an extremely cost effective technique leading to molecular dispersed nanocomposites.¹² A variety of metal alkoxides (Si, Ti, Al, Zr) have been used to generate inorganic networks. However sol-gel does not offer complete control over the mesoscopic scale, length scales of tens to hundreds of nanometers. Thus bottom-up approaches like self-assembly and templated-assembly have gained importance as they offer control over mesoscopic length scales.⁴ Self-assembly of block copolymers offers control over nanometer length scales and provides a mean to make hierarchical structures for various applications.^{13,14} Self-assembly of block copolymers is driven by the weak non-covalent interactions between the polymer segments of the block copolymer leading to phase segregation and thus forming a range of morphologies in both bulk and solution (see Fig. 1.3).^{14,15}

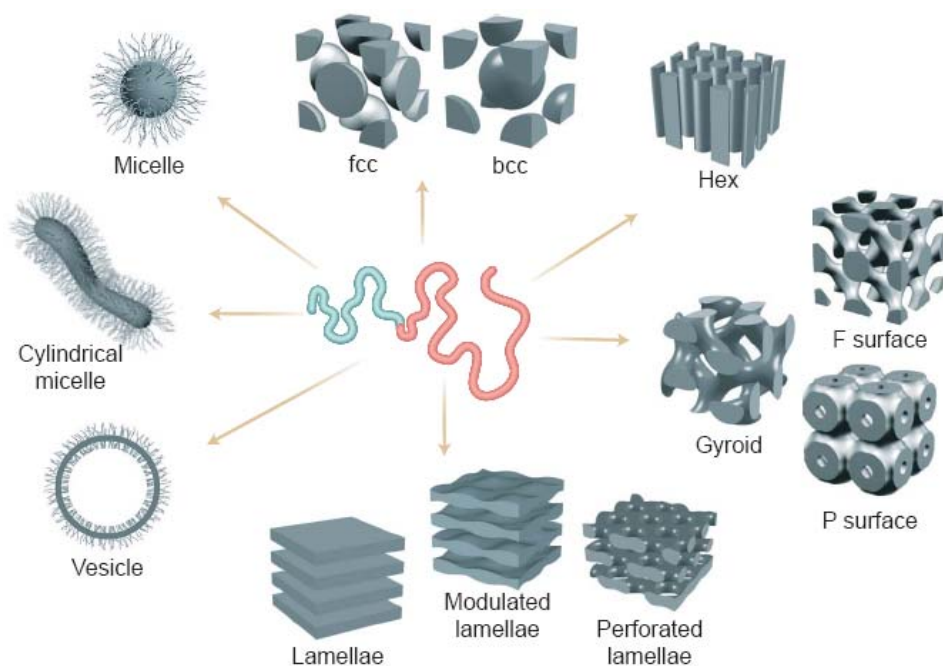


Figure 1.3. Different morphologies formed by self-organization of block copolymers in bulk and solution (fig. taken from reference [15]).

Inorganic building blocks (containing Si, P, Fe and other elements) have been used as comonomers to synthesize block copolymers.^{16,17} Different morphologies with ordering from nano to mesoscale were obtained in these block copolymers. Templated self-assembly approaches have also received considerable attention. Russell used a combination of top-down and bottom up approaches by blending nanoparticles with block copolymers to obtain ordered morphologies of the inorganic matter.¹⁸ Stucky, Weisner, and others have combined sol-gel and self-assembly of block copolymers to generate various nano-structures which were converted by calcination to inorganic nanoobjects.¹⁹⁻²² Thus self-assembly of block copolymers has become an important tool to obtain hybrid materials with desired supramolecular structures. However, in order to obtain the desired structure of the block copolymer, we need to understand the factors

governing the phase behavior of block copolymers. This topic is discussed in the next section.

1.2 Self – Assembly of Block Copolymers

“Block copolymers are macromolecules composed of sequences, or blocks, of chemically distinct repeat units.”¹⁴ The weak non-covalent interactions between the chemically distinct repeat units lead to phase separation in block copolymers. The phase behavior of the copolymer is determined by the overall degree of polymerization N , the composition f (volume fraction of one of the connecting blocks) and the segment-segment interaction parameter χ . A number of theoretical approaches have been used by Leibler and others to describe the phase behavior of block copolymers.²³⁻²⁶ The weak Segregation Limit (WSL) where composition fluctuations are represented by a single wave function, and the strong segregation limit (SSL) where composition fluctuations are represented by step wave functions are two of the most common approaches to describe the phase behavior of block copolymers.^{25,26} Spheres (S or C), hexagonally packed cylinders (H), gyroid (G) and lamellae (L) are various morphologies predicted by theory. The phase diagram for a linear block copolymer as predicted by theory is shown at the top of Fig 1.4, this theoretical phase diagram is very similar to the experimentally determined phase diagram of linear poly(styrene-*b*-isoprene) (middle of fig. 1.4).^{23,27} The experimentally observed perforated lamellae (PL) phase in poly(styrene-*b*-isoprene) diblock copolymer was not predicted by theory and is a metastable state of the more stable bicontinuous phase.

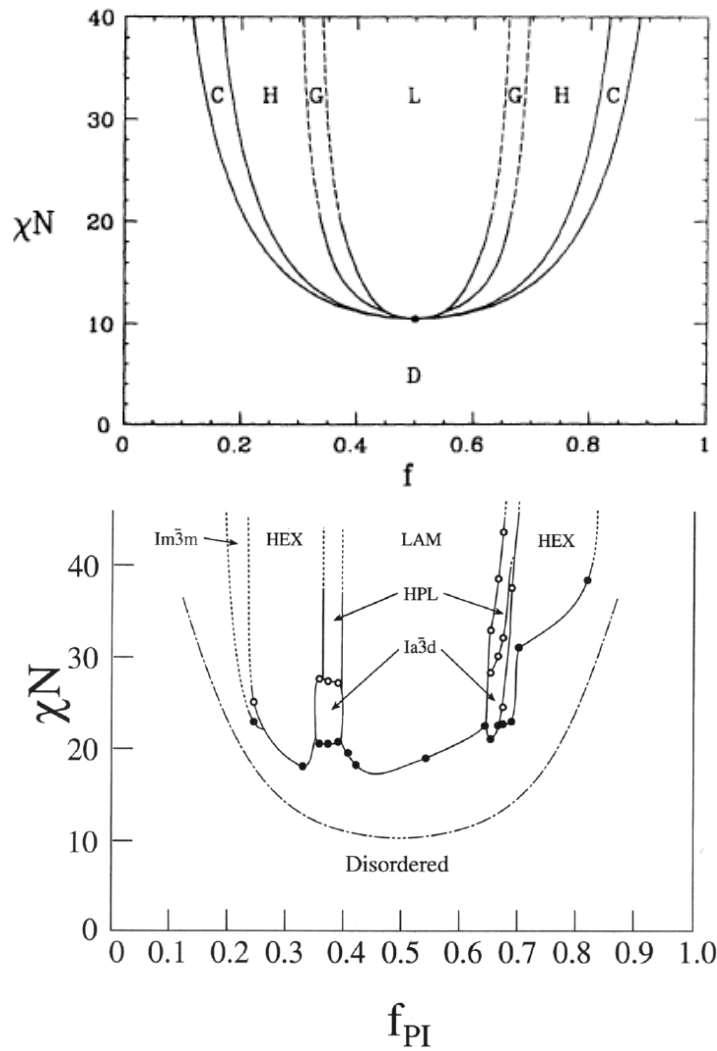


Figure 1.4. (Top) Phase diagram of linear block copolymer predicted by self-consistent mean field theory, (middle) Experimental phase diagram of linear poly(styrene-*b*-isoprene) diblock copolymer and (bottom) Pictorial representation of various phases of the block copolymer (fig. taken from reference [23, 27]).

When $\chi N < 10$ entropic terms dominate and the chains are in a phase mixed state, as χN increases, enthalpic terms began to dominate and chains begin to phase separate. χ is inversely proportional to temperature (T), by cooling a block copolymer from the melt state the chains begin to phase separate and there is a loss of entropy as the chains begin to order. The temperature at which phase separation occurs is called the order-disorder temperature (T_{ODT}). The morphology obtained in block copolymers depends upon the relative volume fractions of the phases. There are other factors like architecture, conformational asymmetric, fluctuations and crystallization that also affect the phase behavior of block copolymers.²⁸⁻³⁰

1.3 Hybrid Organic - Inorganic Polymers Based on Polyhedral Oligomeric Silsesquioxanes (POSS)

1.3.1 Synthesis and Properties of Polyhedral Oligomeric Silsesquioxanes (POSS)

Depending upon the degree of oxygen functionality around a silicon atom they are M, D, T and Q resins where M, D, T and Q stand for mono, di, tri and quaternary oxygen substitution around silicon. Silsesquioxanes are a class of organosilicon materials having empirical formula $R\text{SiO}_{3/2}$ where R is a hydrogen, alky or aryl substituent.

Silsesquioxanes have trifunctionality (T-type) and form cages, ladders or three dimensional network structures (Figure 1.5).³¹

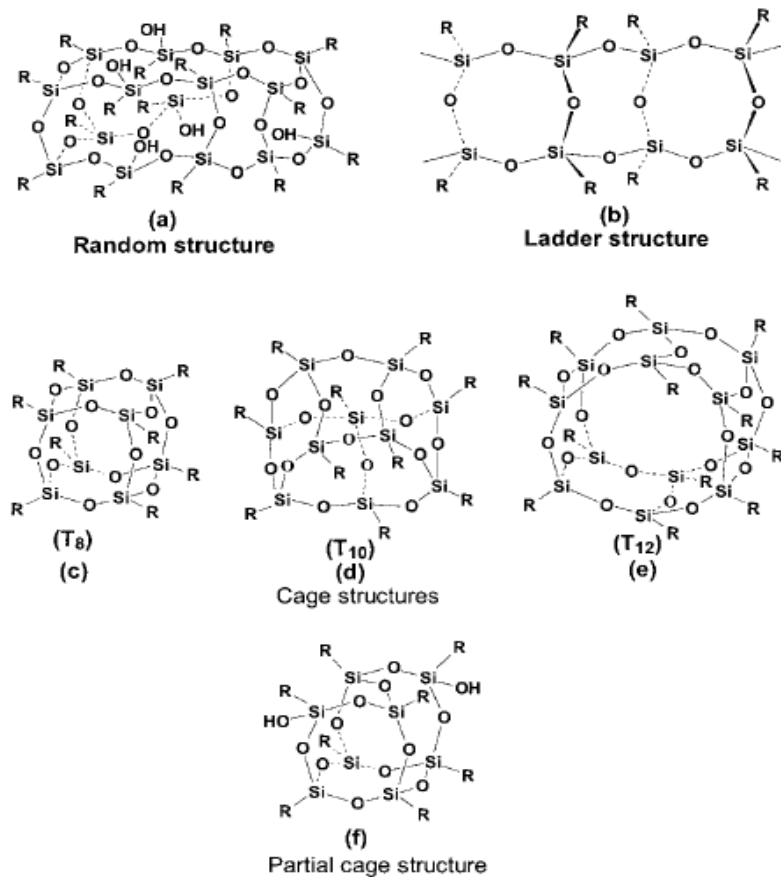


Figure 1.5. Structures of Silsesquioxanes (fig. taken from reference [31]).

The structure of a silsesquioxane is dependent upon the process by which it is prepared. The first oligomeric organosilsesquioxane was isolated by Scott in 1946 along with other volatile compounds through thermolysis of the polymeric products obtained from cohydrolysis of methyltrichlorosilane and dimethylchlorosilane.³² Silsesquioxanes are synthesized by acid or base catalyzed condensation of alkyl trichlorosilanes. Chlorosilanes are hydrolysed to silanols which then undergo condensation to form siloxane bonds represented by the general equations shown below.³³

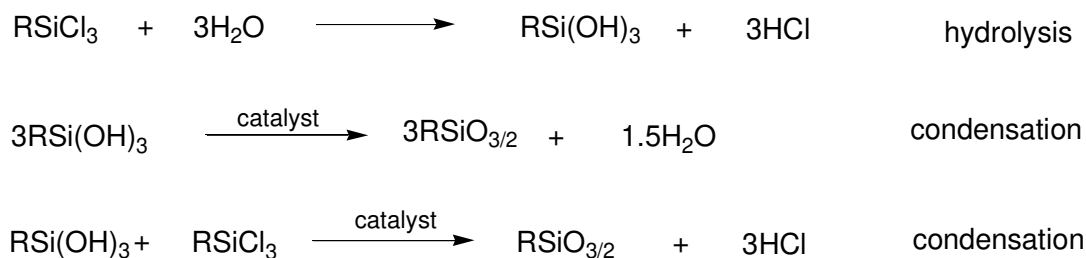


Figure 1.6 Basic reactions for silsesquioxane synthesis.

The ladder polysilsesquioxanes have outstanding thermal stability and exhibit high temperature oxidation resistance.³¹ They also have good insulating properties and high gas permeability. However in recent years greater attention has been paid to specific cage structures, the so called polyhedral oligomeric silsesquioxane (POSS). POSS cubes (T₈) can be obtained directly by hydrolysis and condensation of alkyl trichlorosilanes or by corner capping reactions of non-fully condensed POSS cubes (T₇) with alkyl trichlorosilanes bearing a reactive/polymerization group (see Fig. 1.7).³⁴

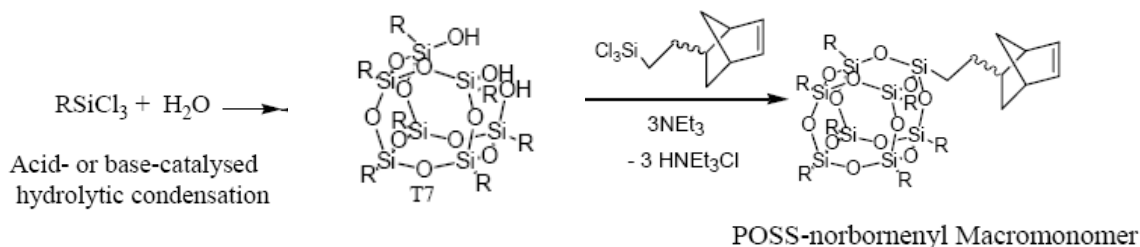


Figure 1.7 Synthesis of silsesquioxane derivatives by acid or base hydrolytic condensation.

The most common molecular formula of POSS is (R)₇(SiO_{1.5})₈X₁ where R is an organic substituent which renders the cube soluble in common solvents and possibly miscible with certain polymers. The lone reactive group (X) can be used for homo or copolymerization or grafting reactions. Depending upon the functionality of POSS, it can be used either as a filler, comonomer or cross-linking agent. The choice of organic periphery (R) and reactive group (X) depends upon the desired structure, property and application

of the material. Some of the commercially available peripheries and reactive groups are shown in Fig. 1.8. Depending upon the organic periphery (R_1) POSS is available either as a solid or a viscous liquid. A number of reviews have been written on POSS based materials.^{33,35-39}

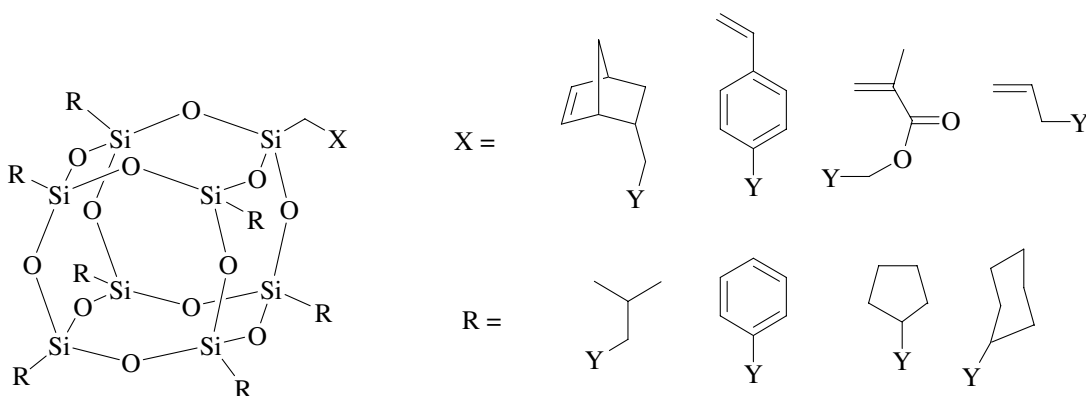


Figure 1.8. Chemical structure of POSS monomer where X is the reactive group, R is the organic periphery and Y is the site of attachment.

A POSS molecule with an isobutyl periphery and an isocyanate functional group has a diameter of approximately 1.5 nm. POSS has an inorganic core with eight silicon atoms bridged by twelve oxygen atoms and has dimensions comparable to polymer segments and coils (~ 0.5 nm). POSS monomers arrange in planar hexagonal arrays and these planes form a three dimensional structure by stacking in an ABCA sequence.⁴⁰ Depending upon the type of POSS used, amount of POSS and the polymer system, POSS can enhance various properties of the host polymer viz. mechanical, thermal, optical and other properties.⁴¹

A synopsis of POSS effect on material properties is given below;

- Mechanical Properties
 - It can improve modulus of the material by several orders of magnitude especially the high temperature modulus of the material
 - It can improve the elongation at break
 - It improves the flow properties of the material leading to easier processing of high T_g polymers
 - It lowers the friction of the material
- Optical Properties
 - Due to its small size it maintains optical transparency
 - It can reduce or totally remove the color from the polymer
- Thermal Properties
 - It can increase the thermal decomposition temperature of the material
 - It can increase the glass transition temperature of the polymer
 - It can lower the thermal conductivity of the material
- Other properties
 - It can improve the oxidation resistance and reduce the flammability of the material
 - It can improve the corrosion resistance of the material
 - It can lower the dielectric constant of the material and improve the quantum efficiency.
 - It can selectively change the permeability of gases through the material
 - It can increase hydrophobicity and oleophobicity of the material

1.3.2 POSS as Fillers

Fillers are mixed in a number of polymeric systems to improve the mechanical, physical, thermal and other properties of the polymeric matrix and to lower the cost of the manufacture. Dispersed particles of fillers can be classified into three types depending upon the number of dimensions (1, 2 or 3) in the nanometer scale.⁴²

Table 1.1. Classification of dispersed particles based on size scale.

Number of dimensions of dispersed particle in the nanometer scale i.e. < 100 nm	Dispersed particle structure	Examples
1	Laminates, Sheets	Clay sheets
2	Nanotubes, Whiskers	Carbon nanotubes, cellulose whiskers
3	Isodimensional particles	Silica particles, POSS

When only one dimension of the dispersed particle is on the nanometer scale (i.e. < 100 nm) and other dimensions are hundred to thousands of nanometers in size scales, the dispersed particles form layers or sheets in the polymer matrix. When two dimensions of the dispersed particles are on the nanometer scale and the third dimension is larger, dispersed particles form elongated structures like nanotubes and whiskers. When all the three dimensions of the dispersion are on the nanometer scale the dispersion particles are considered to be “isodimensional” nanoparticles.⁴² POSS are isodimensional spherical particles which can form truly dispersed nanocomposites and thus have been used as fillers in a number of polymeric matrices. POSS have been added to epoxies and polycarbonates to improve thermal and mechanical properties.^{43,44} When used as filler in polypropylene,

depending upon the amount of loading POSS influences the crystallization of the polymer matrix thereby affecting the final microstructure and properties of the material.⁴⁵ In recent years, an important class of POSS nanoparticles i.e. fluoroPOSS nanoparticles have gained a lot of attention.⁴⁶ By mixing different amount of fluoroPOSS nanoparticles in PMMA, the surface energy of the polymer composite film can be controlled. Different processing conditions (e.g. spin coating and electrospaying) can change the roughness and the curvature of the surface of the polymer composite. By electrospaying, the first example of truly superoleophobic surface with low energy POSS particles at the PMMA-air interface obtained.⁴⁶ POSS nanoparticle reinforced polymers have also been used as dental composites and high performance fibers.^{47,48}

Although POSS improves physical, mechanical, thermal and other properties, formation of composites by melt blending or other means is an energy intensive process. Also when used as filler POSS does not offer complete control over the mesoscopic structure of the material. Therefore, it is better to use POSS as a comonomer in thermoplastic and thermoset materials to obtain copolymer with superior properties, and to have a degree of control on the mesoscopic structure of the material.

1.3.3 POSS as Comonomer

POSS is used as comonomer in a number of thermoset and thermoplastic polymers leading to dramatic changes in the structure-property relationship of the final copolymer.

1.3.3.1 Thermosets Based on POSS

A number of studies have been performed on POSS incorporation into epoxies,^{36,46,49,50} imides,^{51,52} urethanes and other thermoset resins.^{36,53} Epoxy resins are among the most commercially successful materials known, either as composite matrices, adhesives, or coating materials. A number of publications dealing with incorporation of POSS particles into epoxy resins have been published in the past few years. Abad *et al.* synthesized an epoxy-POSS network and studied the thermal and mechanical properties of the copolymer (see Fig. 1.9).⁵⁰ Hindered motion of polymer chains led to an increase in T_g which was due to the pendant POSS groups acting as anchors. A macrophase separation between POSS-rich regions and epoxy-rich regions was observed by scanning electron microscopy (SEM) and differential scanning calorimetry (DSC). Mechanical properties (rubbery modulus, fracture toughness, tensile modulus) of POSS-modified epoxy resins were found to be equivalent, or better than, non-modified epoxy resins. A few general concepts can be taken from this above work. Incorporation of a POSS particle into an organic polymeric system tends to increase the T_g of the polymer due the size of a POSS particle and/or its crystallization behavior. The incompatibility between organic segments and POSS particles tend to result in macrophase (or microphase) separation.

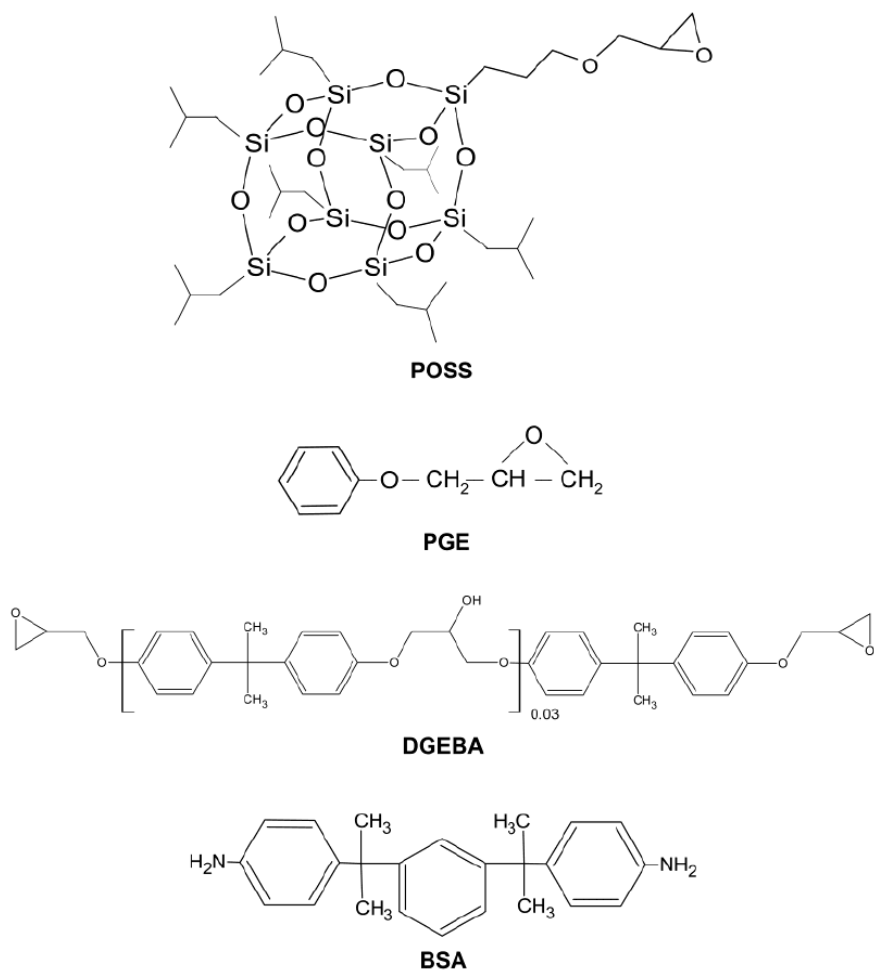


Figure 1.9. Chemical structure of components of epoxy-POSS copolymers (fig. taken from reference [50]).

Another polymer-POSS composite which have attracted considerable interest in recent years are polyimide-POSS composite. Polyimides are well-known for their high temperature stability and are used as interlayer dielectrics in microelectronic applications. POSS macromolecules due to their nano-porosity have low dielectric constants in the range of 2.1 – 2.7 and thus have been used as comonomer in polyimides. Leu *et al.* synthesized the polyimide-POSS copolymers and studied the morphology of these materials.^{51,52} POSS was incorporated in polyimides by two different methods, it was added to the polyimide backbone as an end-capping unit with each polyimide chain

having a one POSS unit, or as pendant units from the copolymer backbone. Transmission electron microscopy (TEM) of POSS end-capped polyimide showed cylinders having a persistence length of 60 nm. Pendant POSS did not aggregate as well as the POSS end-capped polyimides due to the reduced mobility because of multiple bulky POSS units. POSS lowered the dielectric constant of the copolymer by 28% compared to the dielectric constant of a polyimide film. POSS also lowered the mechanical properties of the polyimide i.e. Young's modulus and maximum stress reduced in polyimide-POSS copolymers as POSS screened the interactions between the polyimide chains.

Conclusions to be drawn from epoxy-POSS and polyimide-POSS studies would be that final properties of the copolymers depend strongly on polymer-POSS interactions. POSS incorporation in epoxy polymers improved the mechanical property of the composite whereas in polyimides incorporation of POSS lowered the mechanical property by screening the interaction between polyimide chains. The microstructure of the copolymers depends on the amount of POSS units incorporated and how the POSS units are attached to the polymer backbone.

1.3.3.2 Thermoplastics Based on POSS

POSS has also been incorporated into a number of thermoplastic polymers for examples polyacrylates,^{12,54-56} polystyrenics,^{38,57} polyethylene,⁵⁸⁻⁶¹ polypropylene,⁶² and polyoxazolines.^{63,64} It has been mainly incorporated in thermoplastics to improve their mechanical, thermal and physical properties.

1.3.3.2.1 Polyolefin Based Materials.

Extensive work has been carried out to incorporate POSS in polyethylene (PE).⁵⁸⁻

⁶¹ Due to a number of different reactive groups available on POSS, different chemistries can be used to incorporate POSS. Random copolymers of POSS and PE have been synthesized by metallocene catalyst and ring - opening metathesis polymerization (ROMP) (see Fig. 1.10)

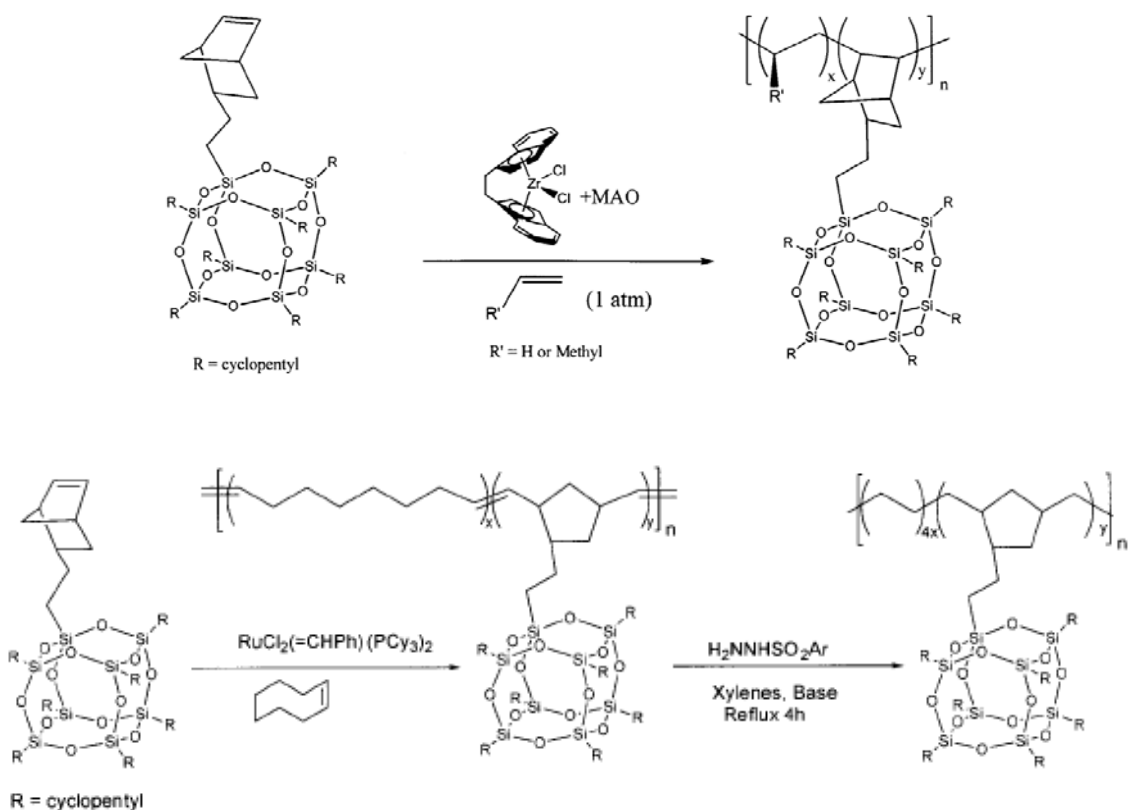


Figure 1.10. Synthesis of polyethylene-POSS copolymer by (top) metallocene and (bottom) ring-opening metathesis polymerization (ROMP) (fig. taken from reference [60]).

The POSS loadings in the sample were varied from 0 to 56 wt%. Optically clear films were obtained by melt pressing PE-POSS copolymers. POSS disrupted the crystallization of PE leading to small PE crystals thereby giving transparent films.

Processing conditions were seen to have profound effect on the microstructure, thermal and optical properties of the copolymer films. Crystallization of PE-POSS copolymer films were studied by casting films from xylene solution (solution crystallization) and by cooling from the melt (melt crystallization). From solution PE – POSS copolymers precipitated first laying a scaffold of PE crystallites, the POSS components were then confined in the spatial environment between preexisting PE crystals. The opposite of this situation was observed when the samples were melt crystallized. POSS crystallized first and then crystallization of PE was subject to geometric and topological constraint. Both cases lead to self-assembly of two distinct but molecularly connected crystalline phases. The dramatic difference in structures in PE-POSS copolymers gave rise to significantly different thermal properties. In melt crystallized sample, significant weight loss (10%) was observed above ~ 400 °C, while in xylene crystallized samples, the same weight loss occurred in the range of ~ 230-330 °C.

1.3.3.2.2 Raft Forming Polybutadiene-POSS Copolymers

Zheng *et al.* synthesized random copolymers of POSS and butadiene.⁶⁵ In PE-POSS composites, PE competes with POSS for crystallization, thus polybutadiene – POSS composites were synthesized to study the POSS crystallization/aggregation without the polymer host competing for crystallization. Also it was anticipated that POSS hard blocks would reinforce the soft polybutadiene materials to give elastomeric properties for PBD-POSS composites. Copolymerization of 1,5- cyclooctadiene and norbornene-POSS (cyclopentyl) macromonomer was carried out using Grubbs First Generation Catalyst. The POSS content was varied from 0 wt % to a maximum of 50 wt

% and the PDI's were obtained in the range of 1.7 to 2.0. The wide angle X-ray scattering (WAXS) of PBD-POSS samples showed an amorphous halo of PBD and crystalline peaks of POSS. As the content of POSS in the copolymer increases crystalline peaks become more intense and sharp. Fig. 1.11 shows the TEM image of PBD-POSS with 12 wt % (a) and 43 wt % POSS (c). In 1.11a POSS aggregates were directly observed as short randomly oriented lamellae with the lateral dimensions of approximately 50 nm. The thickness of the lamellae was found to be approximately 3-5 nm and corresponded to roughly twice the diameter of POSS nanoparticle. Increasing the POSS ratio to 43 wt % resulted in continuous lamellae with lateral lengths on the order of microns (Fig 1.11c). The morphology bears similarity to the lamellar morphology formed by precise diblock copolymers.

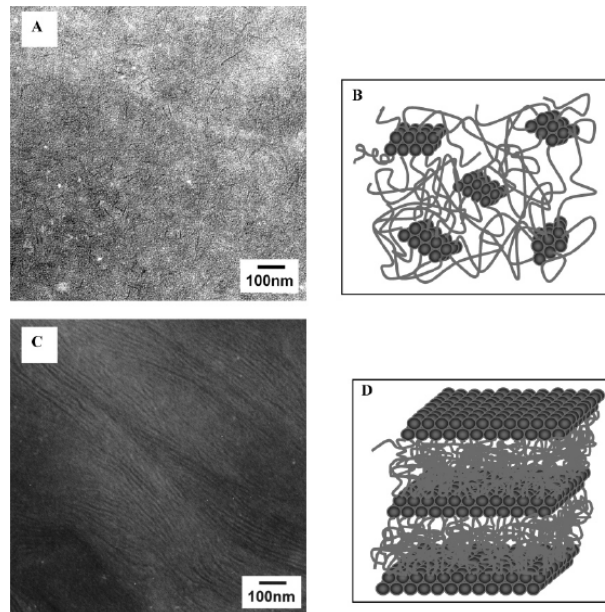


Figure 1.11. (A) TEM of PBD-POSS. The copolymer of low POSS concentration aggregate into short randomly oriented lamellae with lateral dimensions of approximately 50nm (B) Schematic drawing of PBD-POSS assembly at low POSS concentration. (C) TEM of PBD-POSS copolymer of high POSS concentration form continuous lamellar morphology with lateral length on the order of microns (D) Schematic drawing of PBD-POSS assembly at high POSS concentration (fig. taken from reference [65]).

The lamellar morphology was confirmed by SAXS where a broad maxima was observed. The average distance between the POSS layers (d-spacing) is ~ 12 nm. The spacing between the lamellar could be altered by changing the relative ratio between POSS and PBD. Thus by incorporating POSS onto an amorphous polymer backbone exfoliated structures similar to clay/nanocomposites could be obtained. The exfoliated structures have shown substantial improvements in mechanical and thermal properties of the composite materials and thus similar effect would be seen for POSS incorporation into amorphous thermoplastic composites.

Computer simulation work has been done to study interaction of POSS with polymer matrices and to understand, and perhaps predict, the experimental behavior of polymer-POSS composites. Experimental work on random copolymers of PE-POSS and PBD-POSS showed that POSS cubes tend to separate from the PE and PBD phases and aggregate together. Atomistic simulation by Rutledge on blends of PE and POSS showed attraction between the POSS cages leading to aggregation and possible phase separation.⁶⁶ Glotzer did Monte Carlo simulations of polymer-POSS systems and showed strong face-face packing induced by bulkiness, cubic geometry and attraction of the POSS cages.⁶⁷ These simulation results explain the lamellar and the raft structures seen in PE-POSS and PBD-POSS copolymers.^{60,61,65}

In general we can conclude that irrespective of the nature of the copolymer, POSS cubes tend to phase separate and aggregate. Mesoscopic ordering can be obtained at sufficiently high POSS loadings. However long-range order was not observed in random PE-POSS and PBD-POSS copolymers.

1.3.3.2.3 Effect of Periphery on POSS Properties

POSS is a general class of material whose properties and interactions with the polymer matrix depends upon on the functionality and periphery attached to the silicon cage. The periphery of POSS occupies approximately 70% of the POSS molecule volume and plays a very important role in determining the properties of the polymer-POSS composites. Mather studied the effect of different peripheries (cyclopentyl and cyclohexyl) of POSS by synthesizing random copolymers of norbornene and norbornyl-POSS.^{34,68} Grey domains in 50 wt% POSS (cyclopentyl and cyclohexyl) correspond to cylinders of POSS in a norbornene matrix (see Fig. 1.12). POSS (cyclopentyl) cylinders were found to have a diameter of 6 nm and length 36 nm whereas POSS (cyclohexyl) cylinders had a diameter of 12 nm and length 62 nm. Cyclopentyl-POSS packs better than cyclohexyl-POSS, thus cyclopentyl-POSS show stronger crystallization peaks in Wide Angle X-ray Scattering (WAXS) and better cylindrical order.

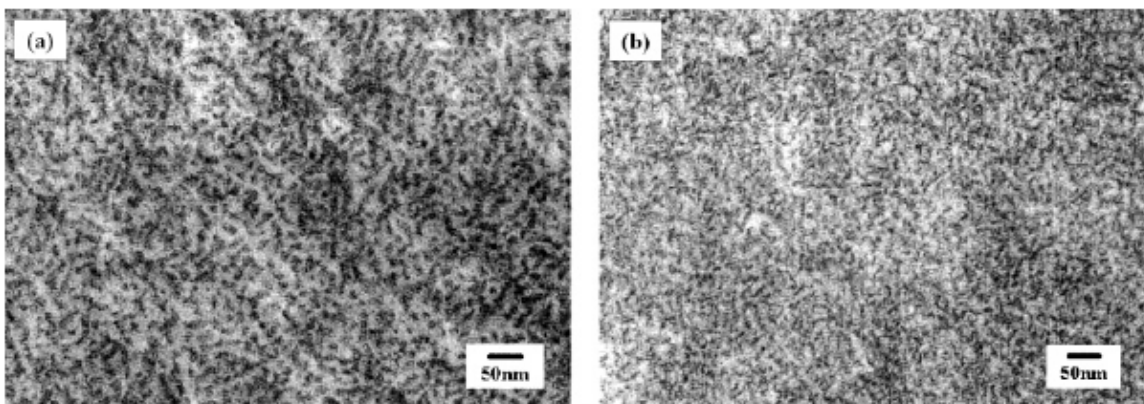


Figure 1.12. Transmission electron micrographs of (a) 50Cyclohexyl-POSS and (b) 50Cyclopentyl-POSS showing the different size of cylindrical structure depending upon corner groups present in POSS monomer (fig. taken from reference [68]).

Slight changes in the domain size due to different periphery lead to dramatic changes in the glass transition temperature (T_g) of the composite. There was also

enhancement in the tensile modulus at the room temperature and significant enhancement in storage modulus at low temperatures.

Berry *et al.* carried out simulation studies on norbornene-POSS copolymers and showed an increase in T_g based on the volume-temperature curve obtained for these polymer-POSS composites.⁶⁹ Bizet *et al.* compared the effect of periphery on the packing of POSS cages.⁷⁰ They compared the packing of POSS with cyclohexyl and isobutyl peripheries and observed that the smaller periphery group make it easier for the chains to pack. Both results explain the increase in T_g observed by Mather *et al.* for the norbornyl-POSS copolymers described in the previous section.^{34,68} Bizet and Berry claimed that the improvements in the properties of the copolymer were entirely due to the presence of POSS and not due to aggregation. They showed that the pendant POSS acts as anchor and reduces the overall mobility of the copolymer which causes improvement in mechanical and thermal properties of the copolymer.

1.3.3.2.4 POSS Based Block Copolymers

All the systems described above are polymer-POSS random copolymers. POSS tends to phase separate and form ordered structures. However to obtain complete control over the mesoscopic structure of the material, well-defined POSS block copolymers need to be synthesized and fully characterized.

Cardoen *et al.* synthesized POSS chain-end polystyrene by anionic polymerization.^{71,72} Hydroxyl end-capped polystyrene chains were obtained by end-capping living polystyryl anion with ethylene oxide. Equimolar quantity of isocyanate-POSS was reacted with hydroxyl-polystyrene to attach POSS to polystyrene chains with a connecting urethane linkage. Small aggregates of POSS were seen in WAXS. For high

molecular weight PS-POSS copolymer, (i.e. above 4,000 g/mol) diffraction peaks were not observed by small angle X-ray scattering (SAXS). On the other hand, SAXS of a PS-POSS sample with PS molecular weight 873 g/mol shows a diffraction pattern with a first and a second order peak (see fig. 1.13). The first order peak was found at $q = 0.0769 \text{ \AA}^{-1}$ which correspond to a long period L spacing of 8.17 nm. The long period found here is equal to approximately two times the radius of gyration of a polystyrene polymer with $M_n = 900 \text{ g/mol}$. From these dimensional considerations, a plausible model for the organization of the hemi-telechelic PS-POSS polymer would be a head-to-head and tail-to-tail aggregation. The second order peak offers some proof of the mesoscopic organization of the system.

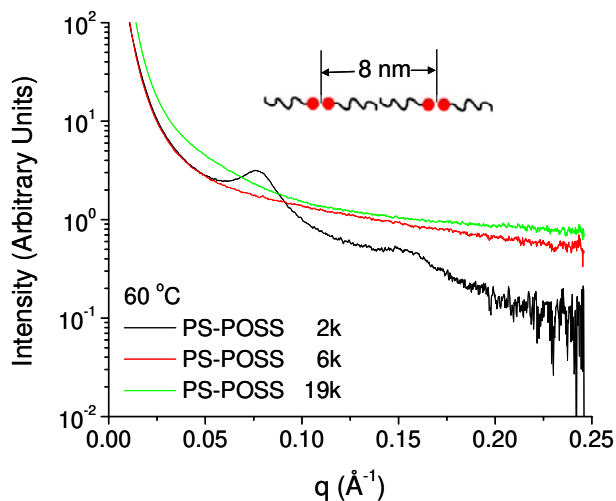


Figure 1.13. Small angle X-ray scattering (SAXS) of PS-POSS copolymers, PS-POSS 2K shows mesoscopic ordering (fig. taken from reference [72]).

Glotzer has performed simulations to understand the self-assembly of mono-tethered,⁷³ tetra-tethered and cyclic-tethered POSS nanocubes.^{74,75} Studies on mono-tethered POSS molecules show they can behave like surfactants or block copolymers forming stable lamellae or cylindrical structures.⁷³ Formation of lamellae in POSS end-

capped PS copolymers can be explained by both surfactant or block copolymer behavior of PS-POSS chains. When the tether lengths are long, tethered-POSS molecules can be considered as block copolymers. They demonstrated that thermodynamically driven immiscibility of tethers and nanocubes can be used to self-assemble POSS cubes into structures analogous to those observed in block copolymers.

In rest of this section we will discuss the behavior of POSS block copolymers having multiple POSS units pendant from the chain. Matyjaszewski and Mather group were the first to synthesize and study block copolymer of POSS.^{7,55} They were also the first to report living polymerization of POSS particles by Atom Transfer Radical Polymerization (ATRP). Dimethyl 2,6-dibromoheptanedioate was used as a difunctional initiator to polymerize *n*-butylacrylate (see fig. 1.14). The catalyst/ligand system has Copper (I) Bromide (Cu(I)Br) and N,N,N',N'',N'''-pentamethyldiethylenetriamine (PMEDTA). The *n*-butylacrylate difunctional macroinitiator was then chain extended with CpPOSS-MA (POSS bearing one methyl methacrylate unit and having a cyclopentyl periphery). The resulting ABA triblock copolymer exhibited narrow molecular weight distribution (PDI=1.2). Surprisingly enough, the degree of polymerization of the POSS block did not exceed 10, presumably because of the bulkiness of the POSS monomer. Cylinders of poly(*n*-butyl acrylate) in a POSS matrix were observed by TEM for the p(MA-POSS)₁₀-*b*-p(BA)₂₀₁-*b*-p(MA-POSS)₁₀ polymer, where the subscripts indicate the degree of polymerization of each block. The cylinders were locally well ordered but macroscopically disordered. Matyjaszewski reviewed different architectures that can be obtained using a similar strategy using a multifunctional initiator.⁷

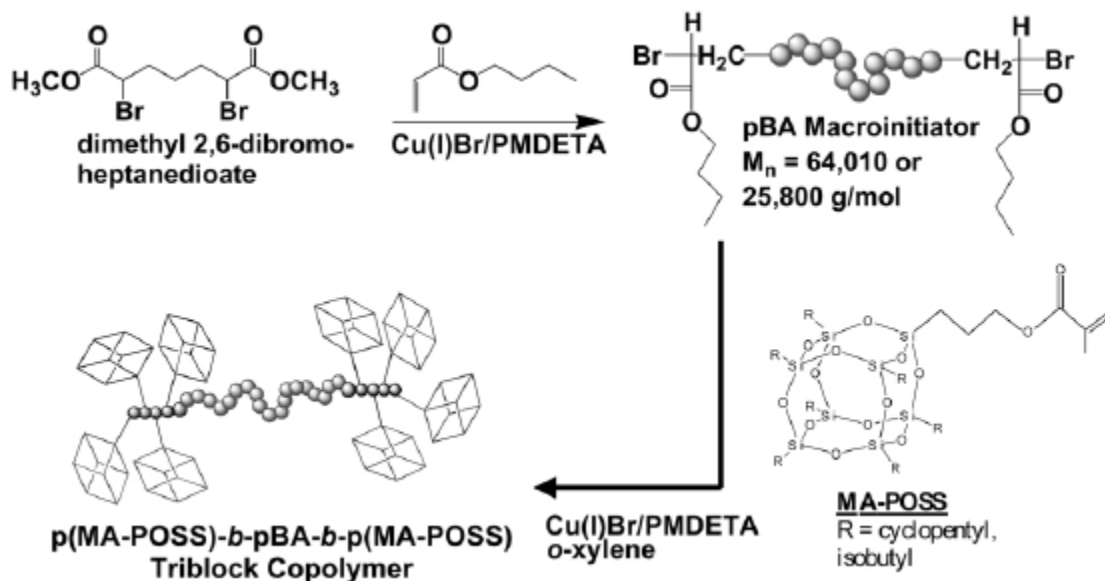


Figure 1.14 Synthetic methodology for the preparation of ABA triblocks containing a poly(n-butyl acrylate) middle segments and outer segments of p(MAPOSS). In the first step, difunctional pBA macroinitiator is prepared by the ATRP of BA from a dimethyl 2,6-dibromoheptanedioate initiator. Subsequent chain extension of the pBA macroinitiator with MA-POSS yielded the ABA triblock copolymer (fig. taken from reference [55]).

Recently Hirai *et al.* synthesized PS-POSS and PMMA-POSS diblock copolymers by anionic polymerization.⁷⁶ *Sec*-butyl lithium was used as the initiator, PMMA or PS block were first synthesized and POSS was added as the second block. The volume fraction of PS:POSS and PMMA:POSS were maintained close to 0.5. The morphology of the diblock copolymer was studied by SAXS, TEM and WAXS. Lamellae of POSS and PS were obtained and the TEM images are shown in fig. 1.15

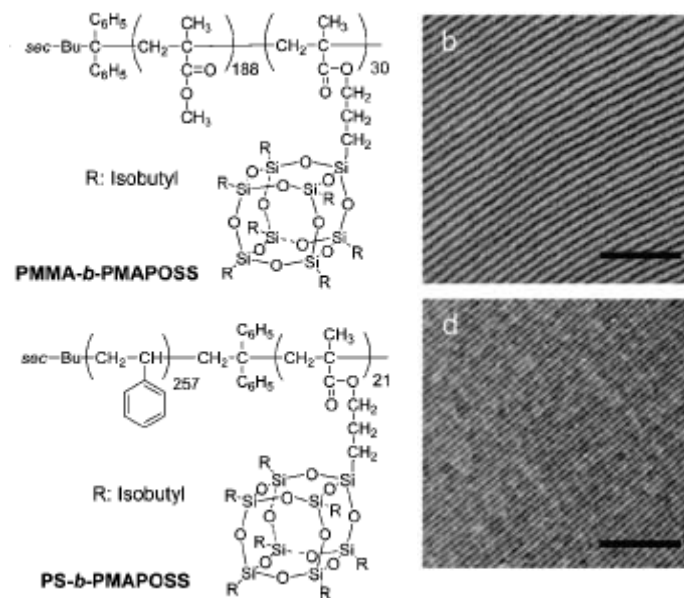


Figure 1.15. (Right) Chemical structure of PMMA-POSS and PS-POSS copolymer and (left) TEM image of the corresponding copolymer (fig. taken from reference [76]).

1.4 Summary

POSS are unique hybrid organic – inorganic materials with excellent material properties which can enhance mechanical, thermal, physical and other properties when physically or chemically incorporated into a range of polymers. It is a general class of materials having a number of different functionalities and different peripheries. Due to various functionalities available on POSS, it can be chemically incorporated into polymers by different reaction chemistries. The periphery occupies 70% volume of the POSS molecule and plays an important role in determining the interactions of POSS with the host polymer. Random copolymers of POSS with PE and PBD have better thermal and mechanical properties compared to the host polymer and also exhibit mesoscopic ordering. Cylinders and lamellae of POSS were observed when POSS was incorporated in block copolymers either *n*-butyl acrylate or polystyrene as the other block.

Although a great deal of work has been done, and is ongoing, on POSS based materials there are a number of scientific questions that need to be answered. An empirical approach has been used to improve the properties of polymers by incorporating POSS as fillers and comonomers. Structure – property studies of POSS homopolymers have been restricted to dimers and trimers of POSS. In chapter 2, we investigate the structure – property relationship of higher molecular weight POSS homopolymers of different peripheries and backbones by matrix assisted laser desorption – ionization (MALDI) and ion mobility experiments. MA-POSS-*b*-(*n*-butylacrylate)-*b*-MA-POSS triblock copolymers and MA-POSS-*b*-styrene diblock copolymers are the only block copolymers of POSS which have been synthesized and studied. A systematic study by varying the volume fractions of the blocks has not been performed. Factors such as the asymmetry of the blocks, crystallization and architecture have also not been investigated. In chapter 3 we synthesize and study poly(ethylenebutylene-*b*-MA-POSS) diblock copolymers. The poly(ethylenebutylene) block is a saturated hydrocarbon and chemically distinct than previously studied POSS block copolymers. It has a low T_g and potential to crystallize depending upon the ethylene content. Ethylene-butylene and MA-POSS repeat units of different sizes and thus conformational asymmetry was also considered as a factor affecting the observed morphologies of these block copolymers. In chapter 4 we synthesize and study poly(MA-POSS(isobutyl)-*b*-styrene-*b*-MA-POSS(isobutyl)) triblock copolymers. The polystyrene block is an amorphous, high T_g block and the ABA architecture does have an affect on the morphology of the copolymer. In chapter 5 we study the application of poly(MA-POSS(isobutyl)-*b*-styrene-*b*-MA-POSS(isobutyl)) triblock copolymers by spin coating the copolymers on different

surfaces and patterning inorganic structures on the surface. Finally we summarize the conclusions of our work and propose future studies in chapter 6.

1.5 References

- (1) Rubner, M. *Nature* **2003**, *423*, 925-926.
- (2) Aizenberg, J.; Weaver, J. C.; Thanawala, M. S.; Sundar, V. C.; Morse, D. E.; Fratzl, P. *Science* **2005**, *309*, 275-278.
- (3) Sanchez, C.; Arribart, H.; Guille, M. M. G. *Nature Materials* **2005**, *4*, 277-288.
- (4) Sanchez, C.; Julian, B.; Belleville, P.; Popall, M. *Journal of Materials Chemistry* **2005**, *15*, 3559-3592.
- (5) Gomez-Romero, P. *Advanced Materials* **2001**, *13*, 163-174.
- (6) <http://research.chem.psu.edu/hragroup/biomaterials.htm>.
- (7) Pyun, J.; Matyjaszewski, K. *Chemistry of Materials* **2001**, *13*, 3436-3448.
- (8) Kickelbick, G. *Progress in Polymer Science* **2003**, *28*, 83-114.
- (9) Karak, N. *Journal of Polymer Materials* **2006**, *23*, 1-20.
- (10) Sur, G. S.; Sun, H. L.; Lyu, S. G.; Mark, J. E. *Polymer* **2001**, *42*, 9783-9789.
- (11) Kresge, C. T.; Leonowicz, M. E.; Roth, W. J.; Vartuli, J. C.; Beck, J. S. *Nature* **1992**, *359*, 710-712.
- (12) Zou, H.; Wu, S. S.; Shen, J. *Chemical Reviews* **2008**, *108*, 3893-3957.
- (13) Mackay, M. E.; Tuteja, A.; Duxbury, P. M.; Hawker, C. J.; Van Horn, B.; Guan, Z. B.; Chen, G. H.; Krishnan, R. S. *Science* **2006**, *311*, 1740-1743.
- (14) Bates, F. S.; Fredrickson, G. H. *Annual Review of Physical Chemistry* **1990**, *41*, 525-557.
- (15) Bucknall, D. G.; Anderson, H. L. *Science* **2003**, *302*, 1904-1905.
- (16) Uddin, M. H.; Rodriguez, C.; Lopez-Quintela, A.; Leisner, D.; Solans, C.; Esquena, J.; Kunieda, H. *Macromolecules* **2003**, *36*, 1261-1271.

- (17) Cheng, J. Y.; Ross, C. A.; Thomas, E. L.; Smith, H. I.; Vancso, G. J. *Advanced Materials* **2003**, *15*, 1599-+.
- (18) Lin, Y.; Boker, A.; He, J. B.; Sill, K.; Xiang, H. Q.; Abetz, C.; Li, X. F.; Wang, J.; Emrick, T.; Long, S.; Wang, Q.; Balazs, A.; Russell, T. P. *Nature* **2005**, *434*, 55-59.
- (19) Yang, P. D.; Deng, T.; Zhao, D. Y.; Feng, P. Y.; Pine, D.; Chmelka, B. F.; Whitesides, G. M.; Stucky, G. D. *Science* **1998**, *282*, 2244-2246.
- (20) Yang, P. D.; Zhao, D. Y.; Margolese, D. I.; Chmelka, B. F.; Stucky, G. D. *Nature* **1998**, *396*, 152-155.
- (21) Zhao, D. Y.; Feng, J. L.; Huo, Q. S.; Melosh, N.; Fredrickson, G. H.; Chmelka, B. F.; Stucky, G. D. *Science* **1998**, *279*, 548-552.
- (22) Templin, M.; Franck, A.; DuChesne, A.; Leist, H.; Zhang, Y. M.; Ulrich, R.; Schadler, V.; Wiesner, U. *Science* **1997**, *278*, 1795-1798.
- (23) Matsen, M. W.; Schick, M. *Physical Review Letters* **1994**, *72*, 2660-2663.
- (24) Matsen, M. W.; Schick, M. *Macromolecules* **1994**, *27*, 7157-7163.
- (25) Leibler, L. *Macromolecules* **1980**, *13*, 1602-1617.
- (26) Semenov, A. N. *Macromolecules* **1993**, *26*, 6617-6621.
- (27) Khandpur, A. K.; Forster, S.; Bates, F. S.; Hamley, I. W.; Ryan, A. J.; Bras, W.; Almdal, K.; Mortensen, K. *Macromolecules* **1995**, *28*, 8796-8806.
- (28) Matsen, M. W.; Schick, M. *Macromolecules* **1994**, *27*, 6761-6767.
- (29) Matsen, M. W.; Schick, M. *Macromolecules* **1994**, *27*, 4014-4015.
- (30) Floudas, G.; Vazaiou, B.; Schipper, F.; Ulrich, R.; Wiesner, U.; Iatrou, H.; Hadjichristidis, N. *Macromolecules* **2001**, *34*, 2947-2957.
- (31) Baney, R. H.; Itoh, M.; Sakakibara, A.; Suzuki, T. *Chemical Reviews* **1995**, *95*, 1409-1430.
- (32) Scott, D. W. *Journal of the American Chemical Society* **1946**, *68*, 356-358.

- (33) Baney, R. H.; Cao, X. In *Silicon Containing Polymers*; Jones, R. G., Ando, W., Chojnowski, J., Eds.; Klumer Academic Publishers: Netherlands, 2000, p 157-184.
- (34) Mather, P. T.; Jeon, H. G.; Romo-Uribe, A.; Haddad, T. S.; Lichtenhan, J. D. *Macromolecules* **1999**, *32*, 1194-1203.
- (35) Joshi, M.; Butola, B. S. *Journal of Macromolecular Science-Polymer Reviews* **2004**, *C44*, 389-410.
- (36) Li, G. Z.; Wang, L. C.; Ni, H. L.; Pittman, C. U. *Journal of Inorganic and Organometallic Polymers* **2001**, *11*, 123-154.
- (37) Mark, J. E. *Accounts of Chemical Research* **2004**, *37*, 946-953.
- (38) Phillips, S. H.; Haddad, T. S.; Tomczak, S. J. *Current Opinion in Solid State & Materials Science* **2004**, *8*, 21-29.
- (39) Pielichowski, K.; Njuguna, J.; Janowski, B.; Pielichowski, J. In *Supramolecular Polymers Polymeric Betains Oligomers* 2006; Vol. 201, p 225-296.
- (40) Waddon, A. J.; Coughlin, E. B. *Chemistry of Materials* **2003**, *15*, 4555-4561.
- (41) <http://www.hybridplastics.com>.
- (42) Alexandre, M.; Dubois, P. *Materials Science & Engineering R-Reports* **2000**, *28*, 1-63.
- (43) Rashid, E. S. A.; Ariffin, K.; Kooi, C. C.; Akil, H. M. *Materials & Design* **2009**, *30*, 1-8.
- (44) Zhao, Y. Q.; Schiraldi, D. A. *Polymer* **2005**, *46*, 11640-11647.
- (45) Pracella, M.; Chionna, D.; Fina, A.; Tabuani, D.; Frache, A.; Camino, G. *Macromolecular Symposia* **2006**, *234*, 59-67.
- (46) Tuteja, A.; Choi, W.; Ma, M. L.; Mabry, J. M.; Mazzella, S. A.; Rutledge, G. C.; McKinley, G. H.; Cohen, R. E. *Science* **2007**, *318*, 1618-1622.
- (47) Soh, M. S.; Sellinger, A.; Yap, A. U. J. *Current Nanoscience* **2006**, *2*, 373-381.
- (48) Zeng, J.; Kumar, S.; Iyer, S.; Schiraldi, D. A.; Gonzalez, R. I. *High Performance Polymers* **2005**, *17*, 403-424.

- (49) Matejka, L.; Strachota, A.; Plestil, J.; Whelan, P.; Steinhart, M.; Slouf, M. *Macromolecules* **2004**, *37*, 9449-9456.
- (50) Abad, M. J.; Barral, L.; Fasce, D. P.; Williams, R. J. J. *Macromolecules* **2003**, *36*, 3128-3135.
- (51) Leu, C. M.; Reddy, G. M.; Wei, K. H.; Shu, C. F. *Chemistry of Materials* **2003**, *15*, 2261-2265.
- (52) Leu, C. M.; Chang, Y. T.; Wei, K. H. *Macromolecules* **2003**, *36*, 9122-9127.
- (53) Constable, G. S.; Lesser, A. J.; Coughlin, E. B. *Macromolecules* **2004**, *37*, 1276-1282.
- (54) Nair, M. B.; Blum, F. D. *Abstracts of Papers of the American Chemical Society* **2005**, 229, U961-U961.
- (55) Pyun, J.; Matyjaszewski, K.; Wu, J.; Kim, G. M.; Chun, S. B.; Mather, P. T. *Polymer* **2003**, *44*, 2739-2750.
- (56) Kopesky, E. T.; Haddad, T. S.; Cohen, R. E.; McKinley, G. H. *Macromolecules* **2004**, *37*, 8992-9004.
- (57) Zheng, L.; Kasi, R. M.; Farris, R. J.; Coughlin, E. B. *Journal of Polymer Science Part a-Polymer Chemistry* **2002**, *40*, 885-891.
- (58) Zheng, L.; Waddon, A. J.; Farris, R. J.; Coughlin, E. B. *Macromolecules* **2002**, *35*, 2375-2379.
- (59) Waddon, A. J.; Zheng, L.; Farris, R. J.; Coughlin, E. B. *Nano Letters* **2002**, *2*, 1149-1155.
- (60) Zheng, L.; Farris, R. J.; Coughlin, E. B. *Macromolecules* **2001**, *34*, 8034-8039.
- (61) Zheng, L.; Farris, R. J.; Coughlin, E. B. *Journal of Polymer Science Part a-Polymer Chemistry* **2001**, *39*, 2920-2928.
- (62) Zhao, J. Q.; Fu, Y.; Liu, S. M. *Polymers & Polymer Composites* **2008**, *16*, 483-500.
- (63) Kim, K. M.; Keum, D. K.; Chujo, Y. *Macromolecules* **2003**, *36*, 867-875.
- (64) Kim, K. M.; Ouchi, Y.; Chujo, Y. *Polymer Bulletin* **2003**, *49*, 341-348.

- (65) Zheng, L.; Hong, S.; Cardoen, G.; Burgaz, E.; Gido, S. P.; Coughlin, E. B. *Macromolecules* **2004**, *37*, 8606-8611.
- (66) Capaldi, F. M.; Rutledge, G. C.; Boyce, M. C. *Macromolecules* **2005**, *38*, 6700-6709.
- (67) Zhang, Z. L.; Horsch, M. A.; Lamm, M. H.; Glotzer, S. C. *Nano Letters* **2003**, *3*, 1341-1346.
- (68) Jeon, H. G.; Mather, P. T.; Haddad, T. S. *Polymer International* **2000**, *49*, 453-457.
- (69) Bharadwaj, R. K.; Berry, R. J.; Farmer, B. L. *Polymer* **2000**, *41*, 7209-7221.
- (70) Bizet, S.; Galy, J.; Gerard, J. F. *Polymer* **2006**, *47*, 8219-8227.
- (71) Cardoen, G.; Coughlin, E. B. *Macromolecules* **2004**, *37*, 5123-5126.
- (72) Cardoen, G., University of Massachusetts AMherst, 2006.
- (73) Zhang, X.; Chan, E. R.; Glotzer, S. C. *Journal of Chemical Physics* **2005**, *123*.
- (74) Zhang, X.; Zhang, Z. L.; Glotzer, S. C. *Nanotechnology* **2007**, *18*.
- (75) Chan, E. R.; Zhang, X.; Lee, C. Y.; Neurock, M.; Glotzer, S. C. *Macromolecules* **2005**, *38*, 6168-6180.
- (76) Hirai, T.; Leolukman, M.; Hayakawa, T.; Kakimoto, M.; Gopalan, P. *Macromolecules* **2008**, *41*, 4558-4560.

CHAPTER 2

SYNTHESIS, ELECTROSPRAY IONIZATION AND MALDI MASS SPECTROMETRY STUDIES OF LARGE POSS OLIGOMERS

2.1 Introduction

Polyhedral Oligomeric Silsesquioxanes (POSS) are a class of important hybrid organic - inorganic materials of the form $(\text{RSiO}_{3/2})_n$, or R_nT_n , where organic substituents are attached to a silicon-oxygen cage.¹ The most common and stable POSS cage is the T_8 (a molecule with a cubic array of silicon atoms bridged by oxygen atoms with an R group at each of the silicon vertices of the cube); other cages with well-defined geometries include $n = 6, 10, 12, 14, 16$ and 18 .^{2,3} When these silsesquioxane cages are introduced into organic polymers, new and useful materials are often realized,⁴⁻⁹ with enhanced properties superior to the original organic polymer. Current research on POSS materials has focused on developing new synthetic routes and creating POSS compounds with different cage sizes and organic substituents to obtain tailor-designed physical properties and to allow for the incorporation of POSS into a wide variety of polymer systems. Therefore, the goal of specifying structure-property relationships for these materials has important ramifications and significant applications.

The goal of this research has been to characterize the conformational preferences of various R_7T_8 -POSS cages when coupled to oligomers in the $N = 2$ to 20 range ($N =$ degree of polymerization) and to determine conformer structures and isomer distributions of new materials using ion mobility mass spectrometry. Our collaborators, the Bowers group at UCSB has been successful in characterizing two oligomer systems, POSS propylmethacrylates and siloxanes, but only up to species with three POSS cages,^{10,11}

due to limitations in mass signal intensity. The ion mobility methodology is predicated on obtaining strong signals in the mass spectrum.

There are to date only a few papers reporting mass spectra of POSS polymers and oligomers.¹²⁻²⁰ These studies all investigate systems, and especially synthetic intermediates, in which there are a large number of -OH groups. In our experience, the presence of such electronegative groups aids mass spectrometry by both MALDI and ESI because they facilitate cationization. This condition is seldom met for most POSS polymers and oligomers that do not have many electronegative groups. Another crucial condition for studying large POSS ions in the gas phase is the absence of substantial fragmentation. While ion formation mechanisms in MALDI have been extensively reviewed, in general they are complicated and poorly understood.^{21,22} The choice of an appropriate matrix is critical to obtaining mass spectra, POSS materials have been understudied because often there are not suitable matrices.

Ion mobility mass spectrometry has been quite successful in studying large conventional polymers or biopolymers including DNA and peptides.²³⁻²⁹ Initial work with POSS materials using MALDI techniques,^{30,31} employed 2,5-dihydroxybenzoic acid (DHB) as a matrix. The parent compounds are efficiently ionized due to electronegative atoms or localized π -electron density in the R-groups and readily bind protons or alkali metal cations to give abundant positive ions. Cage fragmentation does occur to some extent in all of these systems, especially at high laser power, but that did not prevent observation of a strong molecular ion peaks for monomers and dimers. Trimers of mass ~ 3000 g/mol were more of a challenge, particularly to obtain enough intensity for ion mobility measurements. The nature of the cage R-group was found to be important.

Bulky alkyl R-groups seem to inhibit the formation of positive ions and mass spectra for such POSS species are difficult to obtain. We hypothesize that larger POSS oligomers have lower ionization efficiencies than the monomers, most likely due to decreased charge density, since the POSS cages seem to be efficient in delocalizing electron density. Large systems also have an increased probability of fragmentation, e.g. loss of POSS side-chains

For these reasons, the intensity of the “molecular ion” (generally, sodiated or potassiated oligomer molecules) generally decreases with increasing oligomer size to the point that it becomes impossible to obtain ion mobility data. To facilitate the observation of higher POSS oligomers it has been necessary to develop new strategies to enhance cationization (or anionization) efficiency. The discovery by Bassingdale,^{32,33} that certain POSS monomers efficiently incorporate fluoride ion into the cage center suggested using fluoride as a structural probe. This proved successful for POSS monomers containing R-groups which are electron-withdrawing or have delocalized π electron density. Unfortunately, this approach was complicated by the fact that non-aqueous F^- is a good nucleophile and degrades and/or isomerizes POSS cages. The presence of even trace water enhances these processes. Fluoride incorporation therefore was not as successful a probe for oligomers as we had hoped.³⁴

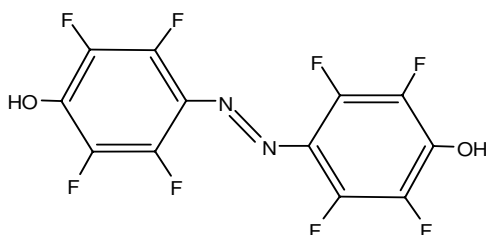


Figure 2.1. 4,4'-dihydroxyoctafluoroazobenzene matrix.

A remaining strategy is to find a better matrix for MALDI. Somogyi, *et al.* have recently described a number of new matrices and especially the newly synthesized matrix 4,4'-dihydroxyoctafluoroazobenzene (see Figure 2.1).³⁵ It has prove successful for intractable polyester polymers such as Vectra ® and this suggests it might be suitable for large POSS oligomers. This matrix ostensibly works so well because the powerfully solvating tetrafluorophenolic group is incorporated directly into the matrix structure as well as the azobenzene functionality to impart appropriate UV-absorbing characteristics. We wish to report MALDI studies using this matrix on a number of representative POSS PMA and styryl systems that were difficult, or even impossible, to investigate using standard matrices.

2.2 Experimental Section

2.2.1 Materials

Phthalic anhydride (99%+) , 2-(2-aminoethoxy) ethanol (98%) , N,N,N',N',N''-pentamethyldiethyltriamine (PMDETA) (99%+), Cu(I)Cl (99.99%+), hydrazine hydrate, 3-(3,5,7,9,11,13,15-Heptaioisbutylpentacyclo[9.5.1(3,9).1(5,15).1(7,13)]octasiloxan-1-yl)propyl methacrylate [MA POSS(isobutyl)], azoisobutylnitrile (AIBN) and ethyl 2-bromoisobutyrate (all from Aldrich) were used as received. Benzoyl chloride (from Fluka) was used as received. Methylene chloride (from VWR) was used as received. 2-bromoisobutyrylbromide, triethylamine both were dried over CaH₂ before distillation and were stored and used under N₂ atmosphere after purification. THF and Toluene were distilled over sodium/benzophenone mixture.

2.2.2 Equipment

All NMR spectra were collected on a Bruker 300 MHz instrument and obtained in either CDCl₃ or CD₂Cl₂ solutions. ¹H NMR spectra (reported in ppm using the δ scale) were referenced to either residual CHCl₃ at 7.26 ppm or residual CH₂Cl₂ at 5.3 ppm. Gel Permeation Chromatography was performed with THF as mobile phase with a flow rate of 1ml/min using Polymer Laboratories PL Gel 5μm Mixed-D columns, Knauer K-501 HPLC Pump equipped with Knauer K-2301 differential refractometer detector and Knauer K-2600 dual wavelength UV Detector. Molecular weights were calibrated versus PMMA or PS standards. All FTIR spectra were obtained on a Perkin Elmer Spectrum One.

Matrix assisted laser desorption/ionization (MALDI) spectra were recorded on either a Bruker Reflex-III MALDI time-of-flight (TOF) instrument or on a Bruker Ultraflex III MALDI-TOF-TOF tandem mass spectrometer (Bruker Daltonics, Billerica, MA). These instruments are equipped with a N₂ and Nd:YAG laser, respectively. The synthesis and other applications of the 4,4'-dihydroxyoctafluoroazobenzene (traditionally denoted as **M4**) are discussed in detail in reference 35. The matrix was dissolved in THF (ca. 10 mg/ml) and this matrix solution was mixed with THF solutions (ca. 1 mg/ml) of the POSS polymer analytes in a 10:1 ratio. Both the linear (lower resolution but larger mass range) and the reflectron (higher resolution but smaller mass range) ion detection modes were applied. The laser power was varied to obtain the best quality spectra but avoid significant fragmentation in the MS studies. The MS/MS tandem experiments were performed on an Ultraflex III MALDI TOF-TOF instrument by using the LIFT technique and applying higher laser powers than for the MS studies.

An extended m/z range Waters QToF was used to perform the ESI experiments described. The instrument makes use of nanoelectrospray ionization. The extended m/z range of the quad allows selection of very large oligomers which have m/z in excess of 20,000 g/mol.

2.2.3 ATRP Synthesis of POSS Oligomers

2.2.3.1 PMA-POSS Oligomers

To a heat-dried 10 mL Schlenk flask with a magnetic stir bar were added Cu(I)Cl (10.5 mg, 0.106 mmol), THF (0.5 mL), and PMDETA (22.2 μ L, 0.106 mmol). After the mixture was stirred for 10 minutes, MAPOSS (isobutyl) (1.00 g, 1.06 mmol), ethyl 2-bromoisobutyrate (15.55 μ L, 0.106 mmol) and THF (1.0 mL) were added to the dark green solution of the catalyst and stabilizing agent. Three freeze-pump-thaw cycles were then performed to remove oxygen. After polymerization at 50 °C for 16 h, the reaction was cooled to room temperature and diluted with THF and passed through a wet activated neutral alumina column to remove the catalyst and stabilizing agent. The colorless and transparent dilute solution was concentrated by evaporation and precipitated in methanol and dried under vacuum overnight. Monomer residues were removed by Soxhlet extraction in methanol or acetonitrile for 5 days. The white polymer powder was vacuum dried.

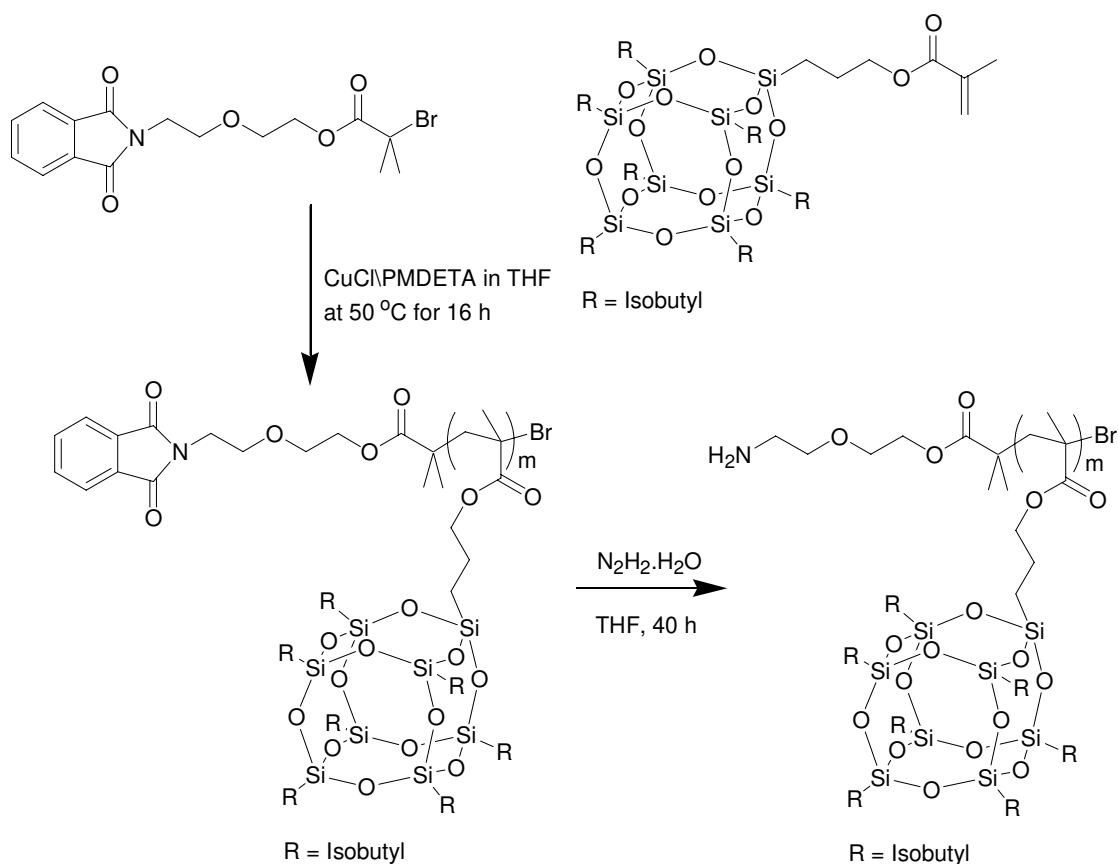
^1H NMR (CDCl_3 , 300 MHz): δ 0.54 (d, 14H, $\text{SiCH}_2\text{CH}(\text{CH}_3)_2$), 0.58 (t, 2H $\text{SiCH}_2\text{CH}_2\text{CH}_2\text{OC}(\text{O})-$), 1.01 (d, 42H, $\text{SiCH}_2\text{CH}(\text{CH}_3)_2$), 1.29 (s, 6H, $-(\text{CH}_3)_2\text{C}$), 1.34 (s, 3H, $-\text{CH}_2\text{C}(\text{CH}_3)$), 1.6 (m, 2H $\text{SiCH}_2\text{CH}_2\text{CH}_2\text{OC}(\text{O})-$), 1.8 (m 7H, $\text{SiCH}_2\text{CH}(\text{CH}_3)_2$), 1.81 (t, 3H $\text{CH}_3\text{CH}_2\text{OC}(\text{O})-$), 1.91 (s, 2H, $-\text{CH}_2\text{C}(\text{CH}_3)$), 3.9 (t, 2H

SiCH₂CH₂CH₂OC(O)-), 4.27 (q, 2H, -CH₂OC(O)-) ppm. Gel permeation chromatography using THF as mobile phase gave M_n of 8,480 g/mol (degree of polymerization (X) = 9) and PDI of 1.05.

Ethyl isobutyrate (phenyl) POSS PMA oligomers was synthesized under identical reaction conditions and fully characterized. Ethyl isobutyrate (Ph) POSS PMA oligomers, ¹H NMR of PMA-POSS (phenyl) oligomer (CDCl₃, 300 MHz): δ 0.58 (t, 18H SiCH₂CH₂CH₂OC(O)-), 1.29 (s, 6H, -(CH₃)₂C), 1.34 (s, 27H, -CH₂C(CH₃)), 1.6 (m, 18H SiCH₂CH₂CH₂OC(O)-), 1.81 (t, 3H CH₃CH₂OC(O)-), 1.91 (s, 18H, -CH₂C(CH₃)), 3.9 (t, 18H SiCH₂CH₂CH₂OC(O)-), 4.27 (q, 2H, -CH₂OC(O)-), 7.0 – 7.8 (m, 378H aromatic protons) ppm. Gel permeation chromatography using THF as mobile phase gave M_n of 8,250 g/mol (X= 9) and PDI of 1.05.

2.2.3.2 Synthesis of Phthalimide POSS PMA Samples and Derivatives

ATRP was carried out using N-2-(2-(2-bromoisobutyryloxy)ethoxy)ethyl phthalimide (81.2 mg, 0.211 mmol) (synthesized as described by Lecolley *et al.*)³⁷ as initiator under similar conditions as described above. Yield: 1.65 g of a white powder (85%, 0.12 mmol). ¹H NMR (CDCl₃, 300 MHz): δ 0.54 (d, 8H, SiCH₂CH(CH₃)₂), 0.58 (t, 2H SiCH₂CH₂CH₂OC(O)-), 1.01 (d, 42H, SiCH₂CH(CH₃)₂), 1.29 (s, 6H, -(CH₃)₂C), 1.34 (s, 3H, -CH₂C(CH₃)), 1.6 (m, 2H SiCH₂CH₂CH₂OC(O)-), 1.8 (m 7H, SiCH₂CH(CH₃)₂), 1.91 (s, 2H, -CH₂C(CH₃)), 3.72 (t, 2H CH₂CH₂OC(O)-), 3.76 (t, 2H, -OCH₂CH₂N-), 3.90 (t, 2H, -NCH₂-), 3.9 (t, 2H SiCH₂CH₂CH₂OC(O)-), 4.27 (t, 2H, -CH₂OC(O)-), 7.70 – 7.86 (m, 4H aromatic protons) ppm. Gel permeation chromatography using THF as mobile phase gave M_n of 6500 g/mol (X= 7) and PDI of 1.05. IR 2953, 1729 (ester C=O stretch), 1464, 1383, 1366, 1332, 1228, 1087 (Si-O stretch), 836, 739 cm⁻¹.



Scheme 2.1. Synthesis of isobutyl POSS PMA polymers using phthalimide initiator by ATRP.

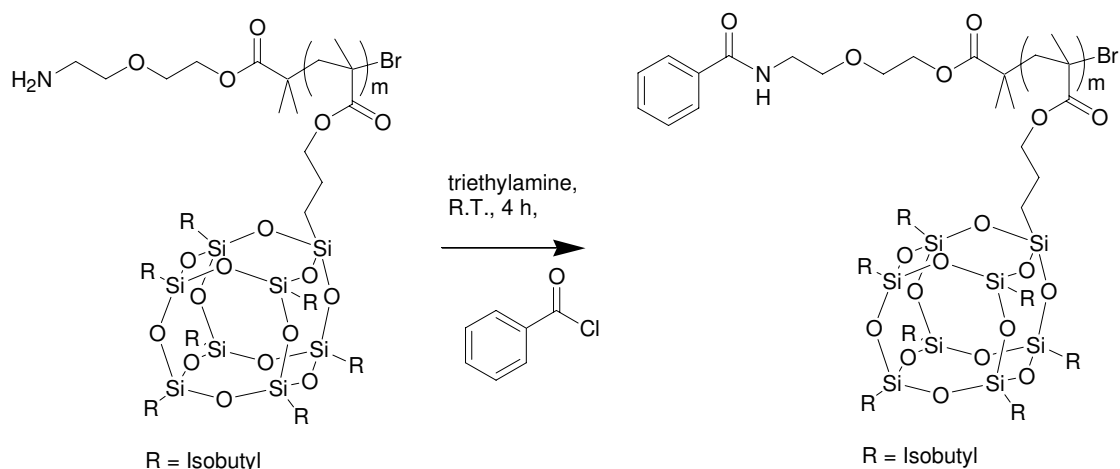
2.2.3.3 Conversion of Phthalimide (i-butyl) POSS PMA to Primary Amine

Phthalimide (i-butyl) POSS PMA oligomer (0.5 g, 76.9 μmol) was dissolved in THF (10 mL) to which was added hydrazine hydrate (5 mL, 100 mmol). The solution was refluxed for 40 h. Deprotection was accompanied by the formation of a white precipitate of phthalhydrazide. The salt was separated by filtration and the polymer was then precipitated in methanol. The removal of solvent in vacuo gave the desired product, which was further dried under high vacuum. Yield: 0.281 g (57 %, 44.1 μmol) white powder. $^1\text{H NMR}$ (CDCl_3 , 300 MHz): δ 0.54 (d, 14H, $\text{SiCH}_2\text{CH}(\text{CH}_3)_2$), 0.58 (t, 2H $\text{SiCH}_2\text{CH}_2\text{CH}_2\text{OC}(\text{O})-$), 1.01 (d, 42H, $\text{SiCH}_2\text{CH}(\text{CH}_3)_2$), 1.29 (s, 6H, $-(\text{CH}_3)_2\text{C}$), 1.34 (s, 3H, $-\text{CH}_2\text{C}(\text{CH}_3)$), 1.6 (m, 2H $\text{SiCH}_2\text{CH}_2\text{CH}_2\text{OC}(\text{O})-$), 1.8 (m 7H, $\text{SiCH}_2\text{CH}(\text{CH}_3)_2$),

1.91 (s, 2H, -CH₂C(CH₃)), 2.8 (t, 2H, NH₂), 3.72 (t, 2H CH₂CH₂OC(O)-), 3.76 (t, 2H, -OCH₂CH₂N-), 3.90 (t, 2H, -NCH₂-), 3.9 (t, 2H SiCH₂CH₂CH₂OC(O)-), 4.27 (t, 2H, -CH₂OC(O)-) ppm. Gel permeation chromatography using THF as mobile phase gave a M_n of 6200 g/mol (X=7) and PDI of 1.1, IR 2953 (N-H stretch), 1729 (ester C=O stretch), 1459,1366,1266,1087 (Si -O stretch), 834, 735 cm⁻¹.

2.2.3.4 Reaction of Primary Amine with Benzoyl Chloride

H₂N (i-butyl) POSS PMA oligomer (50 mg, 7.6 μmol) was dissolved in methylene chloride and triethylamine was used as base. Benzoyl chloride (18μL, 153 μmol) (Ratio polymer: benzoyl chloride 1:20) was added and reaction was continued for 6 h (see Scheme 2.2). The solution was washed with water (3 x 10 mL) and the solvent was removed in vacuo. The white powder was washed with methanol to remove the benzoic acid formed and then vacuum dried. Yield = 38 mg (76%, 5.7μmol). ¹H NMR (CD₂Cl₂, 300 MHz): δ 0.54 (d, 14H, SiCH₂CH(CH₃)₂), 0.58 (t, 2H SiCH₂CH₂CH₂OC(O)-), 1.01 (d, 42H, SiCH₂CH(CH₃)₂), 1.29 (s, 6H, -(CH₃)₂C), 1.34 (s, 3H, -CH₂C(CH₃)), 1.6 (m, 2H SiCH₂CH₂CH₂OC(O)-), 1.8 (m 7H, SiCH₂CH(CH₃)₂), 1.91 (s, 2H, -CH₂C(CH₃)), 3.72 (t, 2H CH₂CH₂OC(O)-), 3.76 (t, 2H, -OCH₂CH₂N-), 3.90 (t, 2H, -NCH₂-), 3.9 (t, 2H SiCH₂CH₂CH₂OC(O)-), 4.27 (t, 2H, -CH₂OC(O)-), 7.4 (t, 1H, NHCO), 7.70 – 7.8 (m, 4H aromatic protons) ppm. Gel permeation chromatography using THF as mobile phase gave a M_n of 7000 g/mol (X=7) and PDI of 1.1. IR 2953, 2870, 1785 (amide C=O stretch), 1726 (ester C=O stretch), 1599 (amide -NHCO stretch) 1464, 1451, 1401, 1383, 1366, 1322, 1228, 1211, 1170, 1087 (Si-O stretch), 996, 836, 739, 702 cm⁻¹.



Scheme 2.2. Synthesis of Benzoyl isobutyl POSS PMA oligomer.

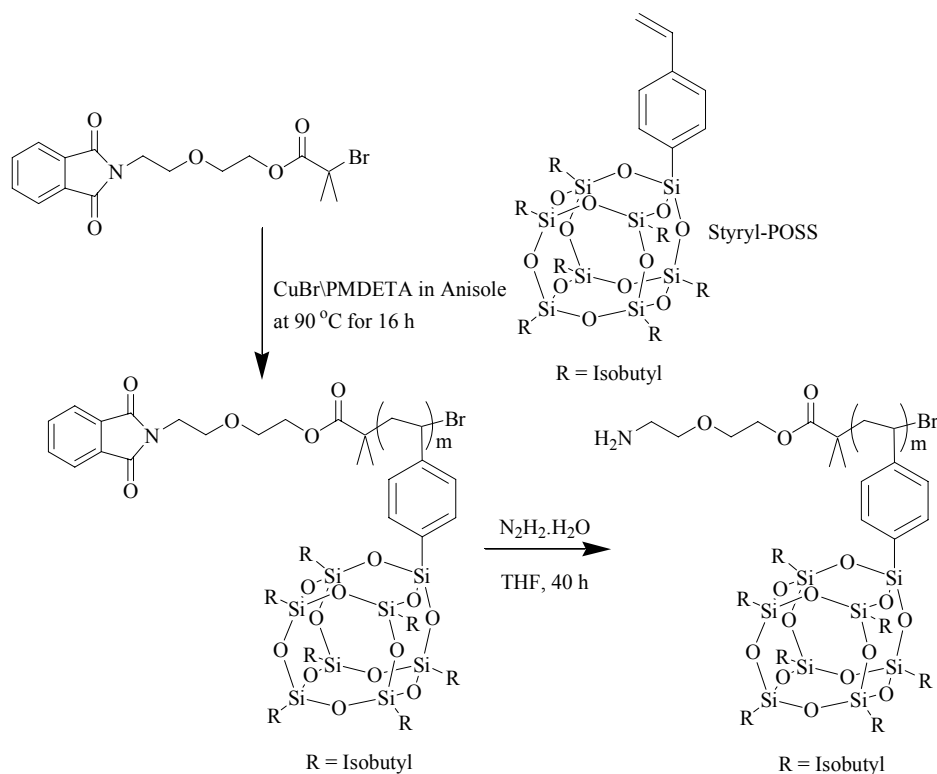
To compare with ATRP synthesized oligomers, POSS oligomers were also synthesized by conventional free radical polymerization using AIBN. To an oven dried round bottom flask was added (i-butyl) MA POSS (0.210 g, 0.22 mmol), AIBN (3.1 mg, 0.018 mmol) and degassed toluene (1.7 mL). The reaction was carried out for 2 days at 60 °C. The polymer was then precipitated as a white powder in methanol and dried under vacuum overnight.

Isobutylnitrile (Cp) POSS PMA oligomers were synthesized by identical reaction and fully characterized.

2.2.3.5 ATRP synthesis of phthalimide Styryl-POSS oligomers

To an oven dried 10 mL Schlenk flask was added Cu(I)Br (7.79 mg, 54.3 μmol), Anisole (3 mL) and PMDETA (11.39 μL , 54.3 μmol). The mixture was stirred for 10 min. Styryl-Poss (isobutyl) (0.5 g, 0.54 mmol), initiator N-2-(2-(2-bromoisobutyryloxy)ethoxy)ethyl phthalimide (20.8 mg, 54.3 μmol) were added to the flask and three freeze-pump-thaw cycles were performed (see Scheme 2.3).

Polymerization was carried out for 16 h at 90 °C. The reaction solution was then diluted with 10 mL THF and passed through a column of neutral alumina to remove excess catalyst. The colorless and transparent solution was concentrated by evaporation. The polymer was then precipitated in methanol. The polymer was vacuum dried. Yield: 0.290 g White powder (58%). ¹H NMR (CDCl₃, 300 MHz): δ 0.54 (d, 14H, SiCH₂CH(CH₃)₂), 1.01 (d, 42H, SiCH₂CH(CH₃)₂), 1.29 (s, 6H, -(CH₃)₂C), 1.8 (m 7H, SiCH₂CH(CH₃)₂), 1.91 (s, 2H, -CH₂C), 2.9 (t, 2H, -NCH₂-), 3.4 (t, 2H, -OCH₂CH₂N-), 3.6 (t, 2H CH₂CH₂OC(O)-), 3.8 (t, 2H, -CH₂OC(O)-), 7.70 – 7.86 (m, 36H aromatic protons) ppm. Gel permeation chromatography using THF as mobile phase gave a M_n of 7,200 g/mol (X= 8) and PDI of 1.07. IR 2953, 1729 (ester C=O stretch), 1464,1383,1366,1332, 1228,1087 (Si-O stretch), 836, 739 cm⁻¹.



Scheme 2.3. Synthesis of isobutyl POSS Styryl polymers using phthalimide initiator by ATRP and conversion of phthalimide group to primary amine.

Conversion of phthalimide (i-butyl) Styryl-POSS to primary amine and reaction of primary amine with benzoyl chloride was carried out in a procedure similar to the one described for phthalimide POSS PMA oligomers.

Primary-amine (i-butyl) Styryl-POSS oligomer, Yield: 0.290g white powder (58%). ^1H NMR (CDCl_3 , 300 MHz): δ 0.54 (d, 112H, $\text{SiCH}_2\text{CH}(\text{CH}_3)_2$), 1.01 (d, 336H, $\text{SiCH}_2\text{CH}(\text{CH}_3)_2$), 1.29 (s, 6H, $-(\text{CH}_3)_2\text{C}$), 1.8 (m 42H, $\text{SiCH}_2\text{CH}(\text{CH}_3)_2$), 1.91 (s, 16H, $-\text{CH}_2\text{C}$), 2.8 (t, 2H, $-\text{NCH}_2-$), 3.4 (t, 2H $\text{CH}_2\text{CH}_2\text{OC}(\text{O})-$), 3.6 (t, 2H, $-\text{OCH}_2\text{CH}_2\text{N}-$), 3.8 (t, 2H, $-\text{CH}_2\text{OC}(\text{O})-$), 6.4 (t, 2H, NH_2), 7.70 – 7.86 (m, 32H aromatic protons) ppm. Gel permeation chromatography using THF as mobile phase gave a M_n of 5,800 g/mol ($X=5$) and PDI of 1.05. IR 3200-3000 (N-H stretch), 1650-1580 (N-H bending), 1459, 1366, 1266, 1087 (Si –O stretch), 834, 735 cm^{-1} .

Benzoyl (i-butyl) Styryl-POSS oligomer, Yield = 38 mg (76%, 5.7 μmole) white powder. IR 2953, 2870, 1730 (ester C = O stretch), 1670 (amide C=O stretch), 1464, 1451, 1401, 1383, 1366, 1322, 1228, 1211, 1170, 1087 (Si-O stretch), 996, 836, 739, 702 cm^{-1} .

The cyclopentyl and cyclohexyl species were prepared by identical reaction conditions and fully characterized. Phthalimide (Cy) Styryl-POSS oligomer, ^1H NMR (CDCl_3 , 300 MHz): δ 0.60 (t, 42H, $\text{SiCHCH}_2\text{CH}_2\text{CH}_2$), 1.24 (m, 168H, $\text{SiCHCH}_2\text{CH}_2\text{CH}_2$), 1.29 (s, 6H, $-(\text{CH}_3)_2\text{C}$), 1.75 (m, 252H, $\text{SiCHCH}_2\text{CH}_2\text{CH}_2$), 1.91 (s, 16H, $-\text{CH}_2\text{C}$), 2.9 (t, 2H, $-\text{NCH}_2-$), 3.4 (t, 2H, $-\text{OCH}_2\text{CH}_2\text{N}-$), 3.6 (t, 2H $\text{CH}_2\text{CH}_2\text{OC}(\text{O})-$), 3.8 (t, 2H, $-\text{CH}_2\text{OC}(\text{O})-$), 7.70 – 7.86 (m, 28H aromatic protons) ppm. Gel permeation chromatography using THF as mobile phase gave a M_n of 5,800 g/mol ($X= 6$) and PDI

of 1.07. IR 2953, 1729 (ester C=O stretch), 1464,1383,1366,1332, 1228,1087 (Si-O stretch), 836, 739 cm^{-1} .

Phthalimide Styryl-POSS (cyclohexyl) oligomer, ^1H NMR (CDCl_3 , 300 MHz): δ 0.60 (t, 42H, $\text{SiCHCH}_2\text{CH}_2\text{CH}_2$), 1.24 (m, 168H, $\text{SiCHCH}_2\text{CH}_2\text{CH}_2$), 1.29 (s, 6H, $-(\text{CH}_3)_2\text{C}$), 1.75 (m, 252H, $\text{SiCHCH}_2\text{CH}_2\text{CH}_2$), 1.91 (s, 16H, $-\text{CH}_2\text{C}$), 2.9 (t, 2H, $-\text{NCH}_2-$), 3.4 (t, 2H, $-\text{OCH}_2\text{CH}_2\text{N}-$), 3.6 (t, 2H $\text{CH}_2\text{CH}_2\text{OC}(\text{O})-$), 3.8 (t, 2H, $-\text{CH}_2\text{OC}(\text{O})-$), 7.70 – 7.86 (m, 28H aromatic protons) ppm. Gel permeation chromatography using THF as mobile phase gave an M_n of 5,800 g/mol ($X=6$) and PDI of 1.07. IR 2953, 1729 (ester C=O stretch), 1464,1383,1366,1332, 1228,1087 (Si-O stretch), 836, 739 cm^{-1} .

The GPC data is summarized in Table 2.1.

Table 2.1. M_n and PDI values of PMA and Styryl POSS Oligomers

R group (Periphery)	Ethyl isobutyrate-POSS g/mol (PDI)	Phthalimide-POSS g/mol (PDI)	Primary Amine – POSS g/mol (PDI)
Isobutyl PMA	8,480 (1.05)	-	-
Phenyl PMA	8,250 (1.05)	-	-
Isobutyl PMA	-	6,500 (1.05)	6,200 (1.10)
Isobutyl Styryl	-	7,300 (1.07)	5,800 (1.05)
Cyclohexyl Styryl	-	5,800 (1.08)	5,700 (1.08)
Cyclopentyl Styryl	-	4,500 (1.08)	3,500 (1.07)

2.3 Results and Discussion

2.3.1 POSS PMA Oligomers



The generalized structure of the ethyl isobutyrate POSS PMA oligomer is given in Figure 2.2. It is the product of an ATRP synthesis and is terminated with a bromine atom. Analysis by ^1H and ^{13}C NMR and GPC, coupled with mass spectrometry are consistent with this structure. Focusing on the MALDI and ESI results, (see ESI spectrum in Figure 2.3) different series in the mass spectra are clearly evident and give evidence for the range of oligomers synthesized by the ATRP. In fact, this series represents the molecular mass limit under the ATRP conditions employed. The repeat unit mass of 944 g/mol is common to both and corresponds to the structure shown in the fig. 2.2. In the ESI spectrum the two closely spaced most intense peaks can be assigned to sodiated and potassiated parent species, formed by the presence of adventitious ions. The terminal Br has been replaced by an –OH group. The third most intense peak to the right of these in each series is simply the protonated parent ion. The MSMS of the 2042 g/mol peak shows fragmentation corresponding to two paths. The first path involves loss of $(i\text{-butyl})_7\text{T}_8(\text{CH}_2)_3\text{OCO}$ and the second to loss of $(i\text{-butyl})_7\text{T}_8(\text{CH}_2)_3\text{O}$ fragments. This provided guidance in the interpretation of the MALDI spectra.

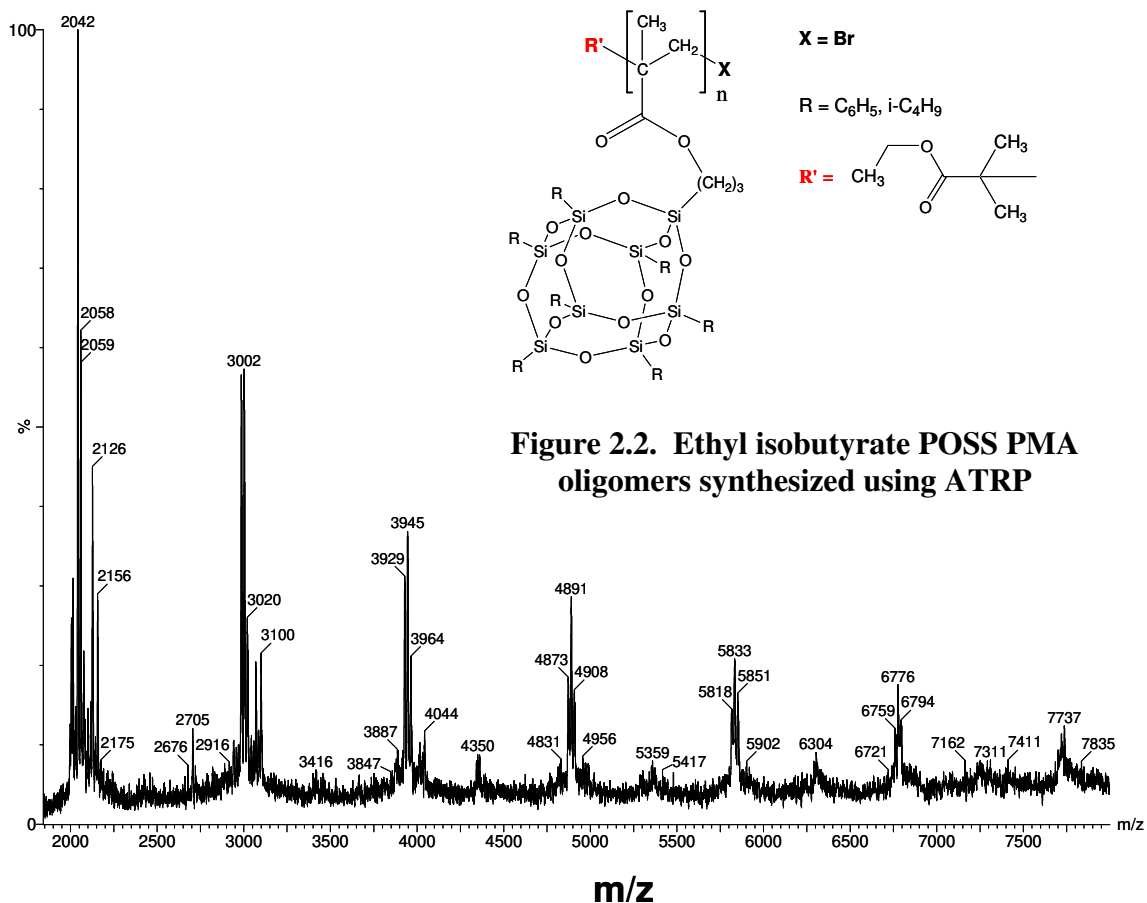


Figure 2.3. ESI mass spectrum of $[(i\text{-butyl})_7\text{T}_7\text{propylmethacrylate}]_n$. Most intense peaks are assigned to sodiated and potassiated parent species, the terminal Br being replaced with OH.

Figure 2.4 gives the MALDI spectrum obtained in the linear mode and shows a progression of peaks out to $n = 12$ with the terminal Br replaced by an H atom. The inset is an expansion of the typical set of three peaks centered on $m/z \sim 3,929$ with clearly defined isotope splitting. The peak at $m/z = 3,913$ is the sodiated species while the peak at $3,929$ is the potassiated species. The less intense third peak (e.g. $m/z 3,997$) of the repeating series can be assigned to the sodiated $n+1$ oligomer minus a $(i\text{-bu})_7\text{T}_8(\text{CH}_2)_3$ -fragment which is replaced by a hydrogen. The fragmentation occurs due to the thermal elimination reaction in esters at high temperature in the gaseous state. This assignment has been confirmed by MSMS spectra of the $m/z 3,929$ and the analogous $2,982$ peaks

which show fragmentations corresponding to the loss of one or more (i-bu)₇T₈(CH₂)₃-units from the PMA backbone. The theoretical isotope distribution pattern for these two peaks fits the experimental exactly, further supporting our assignment.

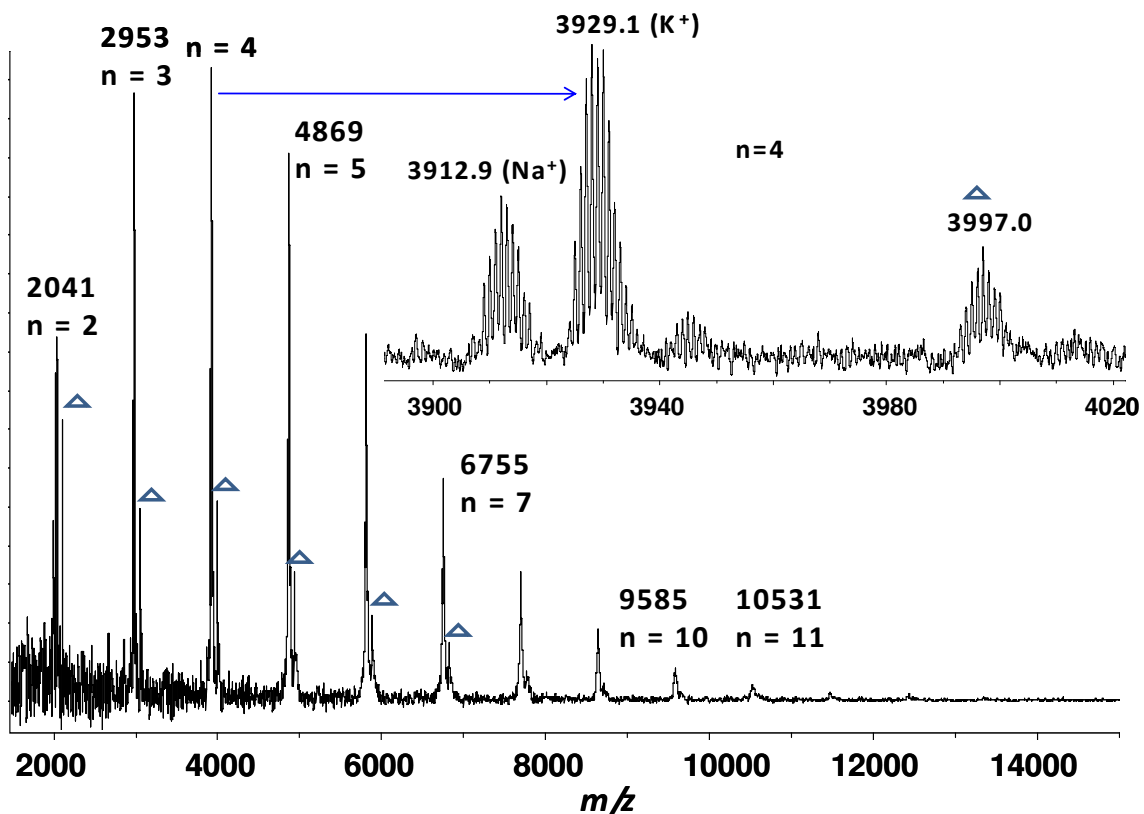


Figure 2.4. Ethyl isobutyrate Isobutyl POSS PMA MALDI mass spectrum using 4,4'-dihydroxyoctofluoroazobenzene matrix. Typical series shown in expansion in region of $m/z = 3900 - 4040$.

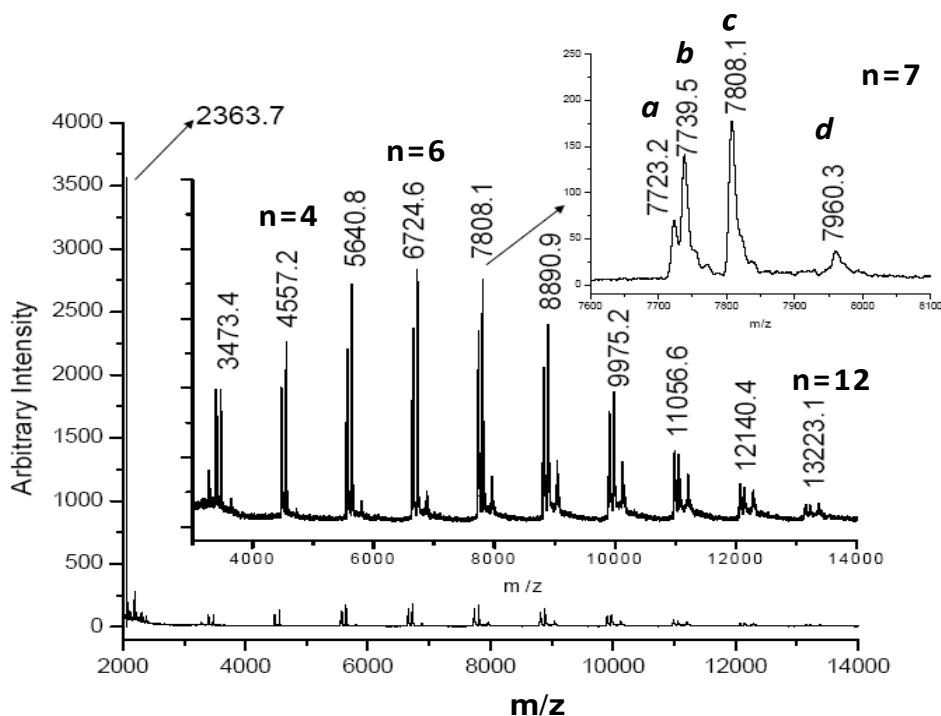
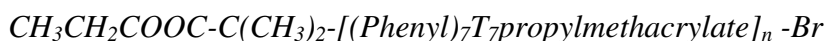


Figure 2.5. Ethyl isobutyrate Phenyl POSS PMA mass spectrum using 4,4'-dihydroxyoctafluoroazobenzene matrix. Typical series shown in expansion region of $m/z = 7800$.

This closely related material again was well characterized by NMR, GPC and mass spectrometry. The MALDI mass spectrum when R = phenyl is shown in Figure 2.5.⁴⁰ The repeat unit mass is 1,083 amu. Clearly resolved series are again observed out to $n = 12$, even though the synthesis stoichiometry was targeted for an octamer. GPC data (see Table 2.1) shows that the average molecular weight of $\sim 8,250$ does correspond to this stoichiometry and this is roughly reflected in the MALDI mass distribution which has maximum in the octamer region. Similar to the isobutyl POSS PMA species above, the two most intense peaks in an n -mer set, such as depicted in the inset, can be assigned to adventitious sodiated and potassiated parent species that have Br replaced by an H-atom. The intense third peak of the repeating series (e.g. $m/z \sim 7808$) can be assigned to the

sodiated (n+1) oligomer minus a (phenyl)₇T₈(CH₂)₃- fragment with the terminal Br replaced by an H-atom. Relative intensity of this peak compared with the parent ion increases with chain length since the increasing number of POSS side chains increases the probability of their loss by fragmentation. The fourth peak of each sub-series (e.g. m/z ~7960) grows in relative intensity and is best interpreted as the loss of a second (phenyl)₇T₈(CH₂)₃- fragment from the (n + 2) oligomer.

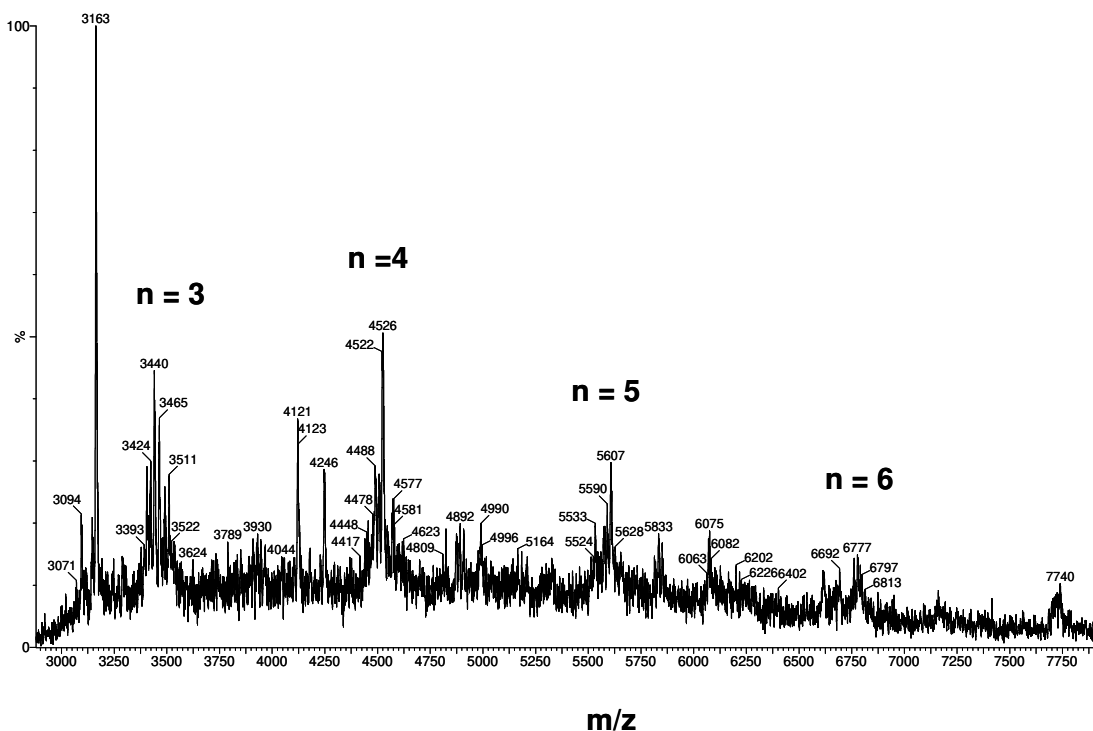


Figure 2.6. ESI mass spectrum of [(phenyl)₇T₇propylmethacrylate]_n. The largest peak in each series up to n = 6 corresponds to protonation of the parent.

The ESI mass spectrum is shown in Figure 2.6. A somewhat different series of mass peaks arises under electrospray conditions in contrast to the isobutyl case. The major mass peaks at m/z 3,440, 4,524 and 5,607 can be accounted for by protonation of the parent bromo species rather than replacement of the terminal Br by -OH. The best explanation of the peaks at m/z 3,163 and 4,246 is the potassiumated species accompanied

by fragmentation involving loss of a PhSiO-OSiPh edge from *one* of the trimer or tetramer T₈ cages.



In an attempt to obtain NH₂- substituted series of oligomers, intermediate phthalimido-POSS PMA materials were synthesized which showed interesting studies in themselves because they gave

quite good MALDI mass spectra.

The phthalimido-POSS PMA (isobutyl) oligomer series were successfully synthesized using the initiator N-2-(2-(2-bromoisobutyryloxy)ethoxy)ethyl phthalimide. Gel permeation chromatography (GPC) gave number average

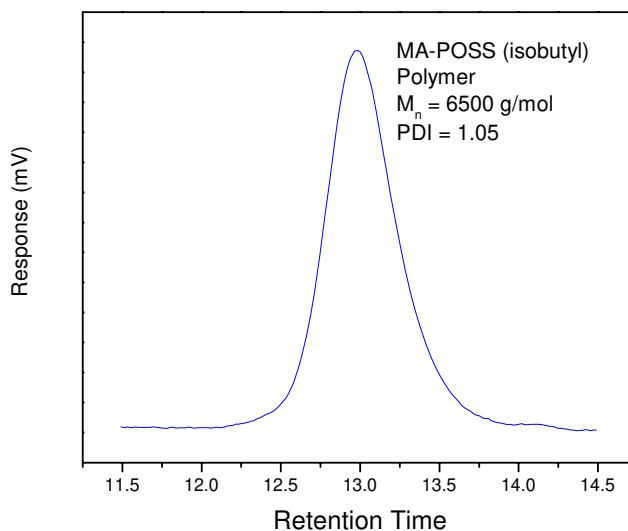


Figure 2.7. GPC of MA-POSS(isobutyl) polymer.

molecular weight of 6,500 g/mol (degree of polymerization X=7) and PDI 1.05 (see Figure 2.7). Reaction of the phthalimide-POSS PMA (isobutyl) polymer with hydrazine hydrate in THF reduced the phthalimide group to the primary amine giving H₂N-POSS PMA (isobutyl). Conversion from phthalimide to primary amine was studied by GPC with UV detector, ¹H NMR and IR spectroscopy (see Figure 2.8 & Figure 2.9). UV-active phthalimide compounds were observed in GPC trace using the UV detector at 254 nm. After the deprotection, the disappearance of absorbance in the GPC trace at 254 nm confirmed the removal of the protecting group. In ¹H NMR there was no resonance

detected between δ 7.00 to 8.00 ppm further confirming the removal of the protecting phthalimide group. In ^1H NMR and the IR spectrum the primary amine signals were observed at δ 2.8 ppm and $3000 - 3300\text{ cm}^{-1}$ respectively.

To further confirm the presence of the primary amine, primary amine PMA POSS oligomer was reacted with benzoyl chloride in methylene chloride employing triethylamine as a base (see Scheme 2.2). The benzoyl derivative of PMA POSS (isobutyl) oligomer was observed in GPC at 254 nm having a M_n of 6,800 g/mol ($X=7$) and PDI of 1.06. In ^1H NMR, resonances at δ 7.7 to 7.8 ppm showed the presence of the benzoyl group. The newly formed amide linkage was observed both in the ^1H NMR and IR spectrums at δ 7.4 ppm and 1599 cm^{-1} respectively. The detection of the amide bond formed by the reaction of benzoyl chloride with primary amine confirmed the presence of amine group in PMA POSS oligomers.

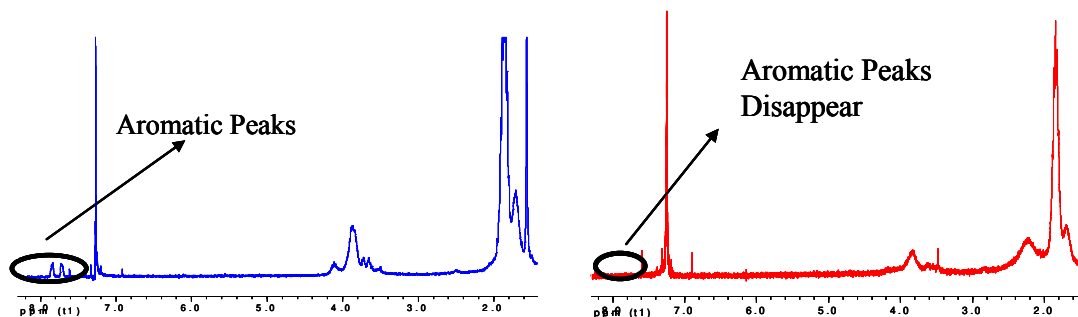


Figure 2.8. ^1H NMR spectrum of phthalimide PMA POSS (i-butyl) (left); NH_2 -PMA POSS (i-butyl) (right).

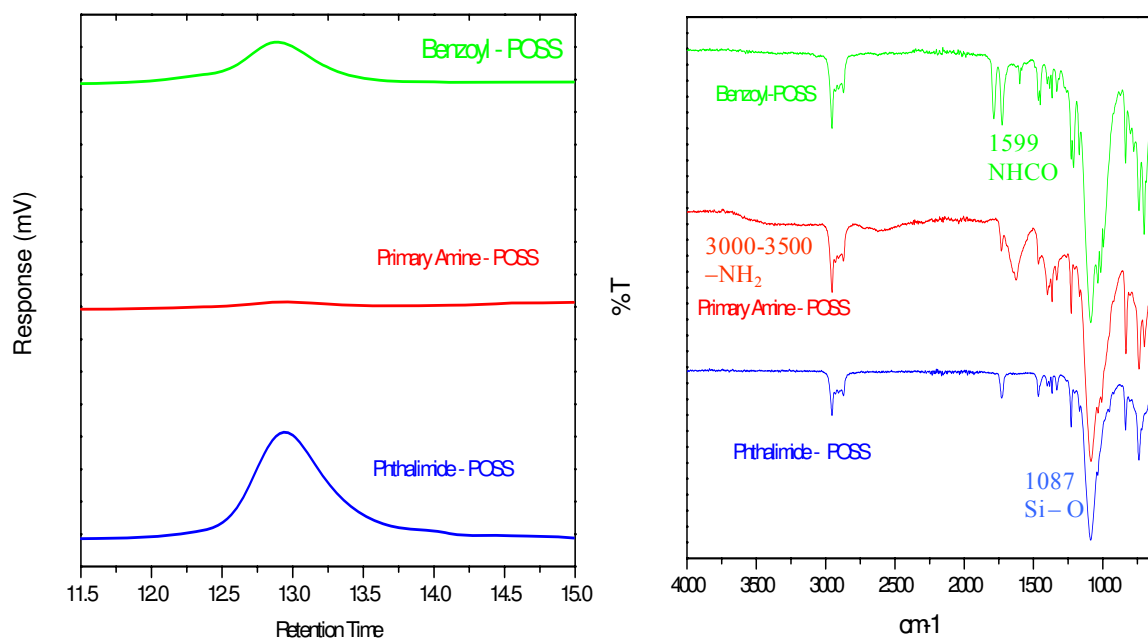


Figure 2.9. Phthalimide (i-butyl) POSS PMA oligomers, (left) GPC with UV detector at 254 nm, (right) IR spectra.

The MALDI mass spectrum of this phthalimidoester oligomer is quite similar to the ethyl isobutyrate (i-butyl)POSS and phenyl POSS PMA species already discussed. The total spectrum is characterized by the isobutyl POSS repeat unit of 944 amu and clearly resolved series of three peaks observed up to $n = 10$, for the nominal octamer. The mass spectra of the phthalimidoesters do show some unique features due to fragmentation of the parent ion.

Assignment of fragment peaks is illustrated in Figure 2.10 which displays the MALDI MSMS spectrum of one the highest mass trimer fragments at m/z 2,397. The m/z 1,541 peak corresponds to the loss of a $(ibu)_7T_8(CH_2)_3$ - fragment from one of the side chains. The broad hump at $\sim 2,020$ corresponds to the loss of the phthalimide ester end-group from the parent 2,397 peak. This 2,397 peak itself by similar analysis is the disodiated parent ion minus a $(ibu)_7T_8(CH_2)_3$ - cage fragment, the terminal Br being replaced by a hydrogen.

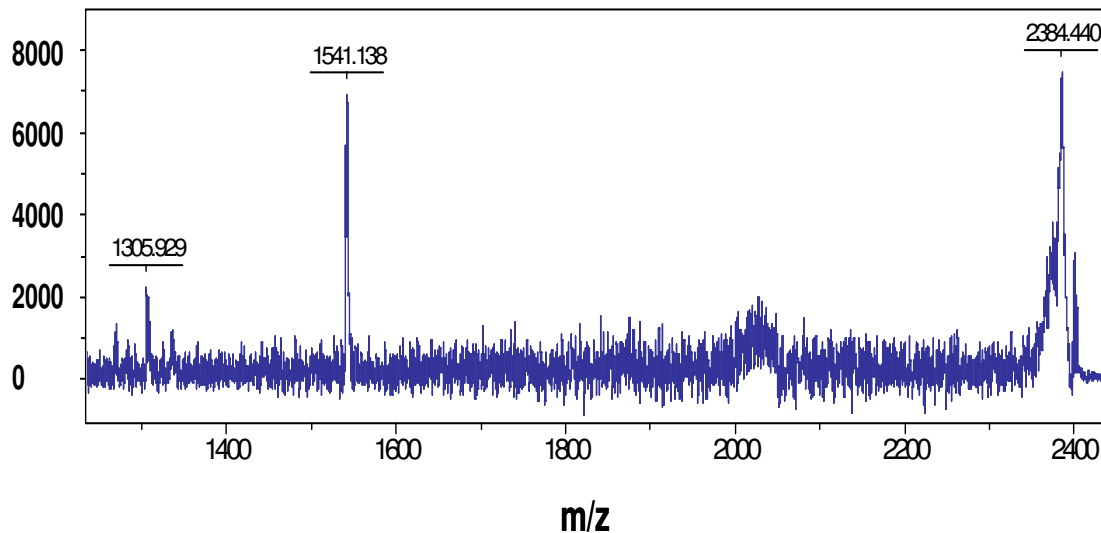
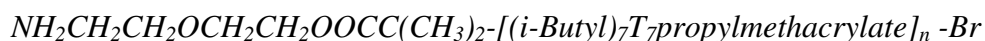
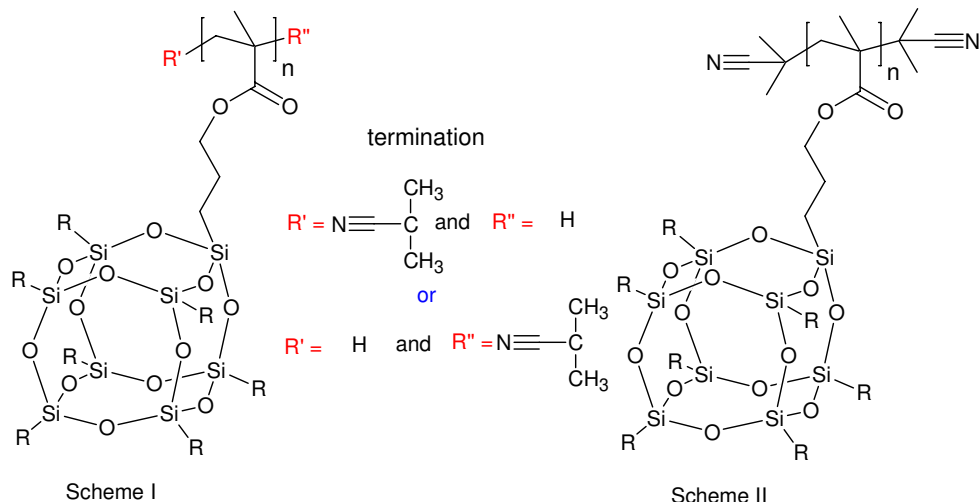


Figure 2.10. MSMS MALDI spectrum of phthalimido-Isobutyl POSS PMA using 4,4'-dihydroxyoctofluoroazobenzene matrix for the m/z 2397 peak.



This series of oligomers is prepared by converting this phthalimide material to the amine as described in the experimental section. The interpretation of the MALDI spectrum is complicated due to ion chemistry, in which the terminal amine reacts with the ester linkages of the oligomer backbone, perhaps producing a series of cyclic amides in the process. Complex spectra result in which the dominant peaks seem to arise by loss of cage fragments such as C_4H_9Si , C_4H_9SiO , and $C_4H_9SiO_2$.

A weak series of high m/z peaks can be observed, however, which represent the oligomer series. A potassium parent ion can be confidently assigned with the terminal bromine replaced with a hydrogen. Sodiated peaks are occasionally observed. The spectra and assignments are tabulated in the Appendix A.



Scheme 2.4. Free radical termination in cyclopentyl POSS PMA oligomers. Scheme I: single *i*-butylnitrile; Scheme II: two *i*-butylnitrile groups. Cp = cyclopentyl.

$[(R)_7T_7\text{Propylmethacrylate}]_n[(\text{CH}_3)_2\text{CCN}]_{m=1,2}$; $R = i\text{-butyl and cyclopentyl(Cp)}$

Isobutylnitrile isobutyl and cyclopentyl (Cp) POSS PMA materials were synthesized using a conventional free radical procedure employing various mole ratios of azoisobutyronitrile (AIBN). Scheme 2.4 shows the variety of ways in which these oligomers (Cp in this example) can be terminated, either by an H atom or the isobutyronitrile radical. The mass spectra obtained for the range of syntheses were of very good quality and give evidence for oligomers out to the pentamer with peaks clearly assigned to one or two isobutylnitrile terminal groups. Both sodiated and potassiated species are observed with no di-H termination evident except for the dimer. This is expected for relatively large amounts of AIBN used in the synthesis. The mass spectrum repeat unit is 1028 amu for the cyclopentyl materials and 944 amu for the isobutyl species, based on the monomer stoichiometry.

The isobutyl oligomer also shows a series of very low intensity peaks evident for masses corresponding to the presence of *three* isobutyl nitrile groups. This occurs when higher concentration of the initiator is present and is due to abstraction of a hydrogen

radical from the backbone or periphery (R) group and subsequent reaction with a third AIBN radical. Spectra and assignments are tabulated in Appendix A.

2.3.2 POSS Styryl Oligomers

Synthesis of styryl oligomers by ATRP provided an important contrast to the PMA POSS oligomers already described. The phthalimido-StyrylPOSS oligomers were successfully synthesized using N-2-(2-(2-bromoisobutyryloxy)ethoxy)ethyl phthalimide as the initiator. Gel permeation chromatography gave a number average molecular weight of 7,200 g/mol for R = isobutyl (degree of polymerization $X=8$. PDI = 1.07). Traces of unreacted monomer were seen in gel permeation chromatography.

The reaction of phthalimido-StyrylPOSS(R) oligomers, where R = isobutyl, cyclopentyl and cyclohexyl with hydrazine hydrate in THF reduced phthalimide to the primary amine giving H₂N-StyrylPOSS (isobutyl).^{38,39} The reactions were characterized using IR spectroscopy (see Figure 2.11). In IR spectra, the intensity of the carbonyl peak of the phthalimido-StyrylPOSS (R) polymer at 1720 ppm decreased by 90-95% (relative to bands at 1080 cm⁻¹ and 2000-2250 cm⁻¹) after reaction with hydrazine hydrate confirming the deprotection of the protecting phthalimide group. The newly formed primary amine peaks were observed in the IR spectrum at 3200–3000 cm⁻¹ (stretching) and 1650-1580 cm⁻¹ (bending).

Similar to the PMA POSS oligomer series the presence of the primary amine group was verified by the reaction of H₂N-StyrylPOSS(R) oligomers with benzoyl chloride. The success of the reaction was confirmed by the formation of an amide peak at

1690 cm^{-1} in the IR spectrum, see Fig. 2.11.

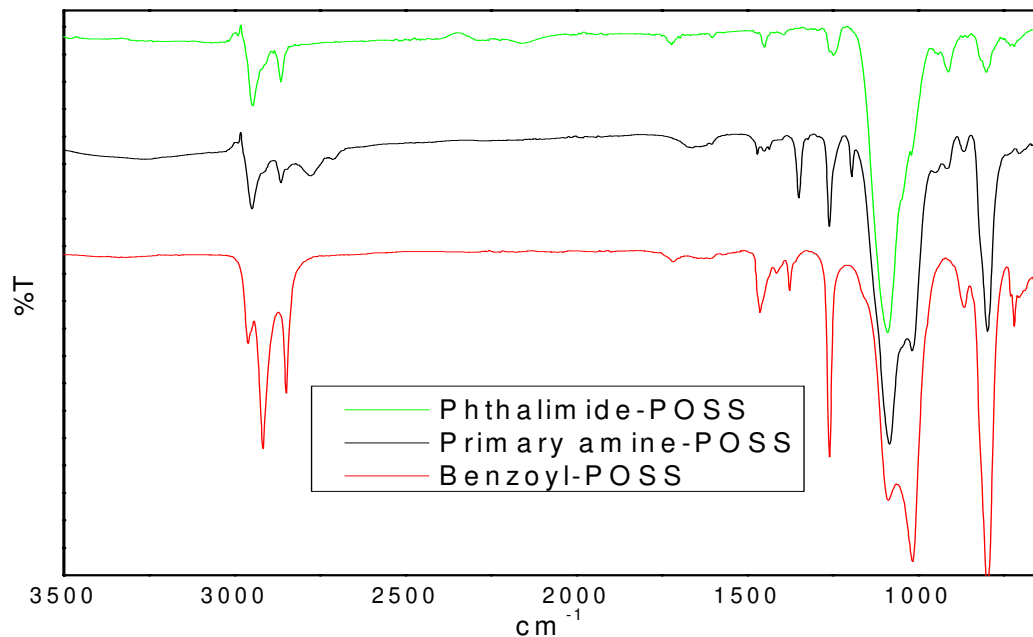


Figure 2.11. IR of phthalimide (green), primary amine (black) and benzoyl (red) Isobutyl Styryl-POSS oligomers.

$C_6H_4(CO)_2NCH_2CH_2OCH_2CH_2OOC-C(CH_3)_2-R)_7T_7(C_6H_4CHCH_2)]_n-Br$; R = i-Butyl, Cp, and Cy

The phthalimidoester styrylPOSS intermediates gave very good to excellent mass spectra, once again giving evidence for ion chemistry products rather than simple parent ions. These species are characterized by oligomer repeat units of 919, 1003 and 1001 mass units for the i-butyl, cyclopentyl and cyclohexyl R-groups, respectively. Figure 2.12 shows a comparison between spectra obtained in the new matrix and the standard 2-(4hydroxyphenylazo)benzoic acid (HABA). The signal-to-noise ratio and resolution show a significant improvement compared to the standard matrix. In fact, this is one of the few examples of POSS oligomers for which any MALDI spectrum could be obtained with a standard matrix.

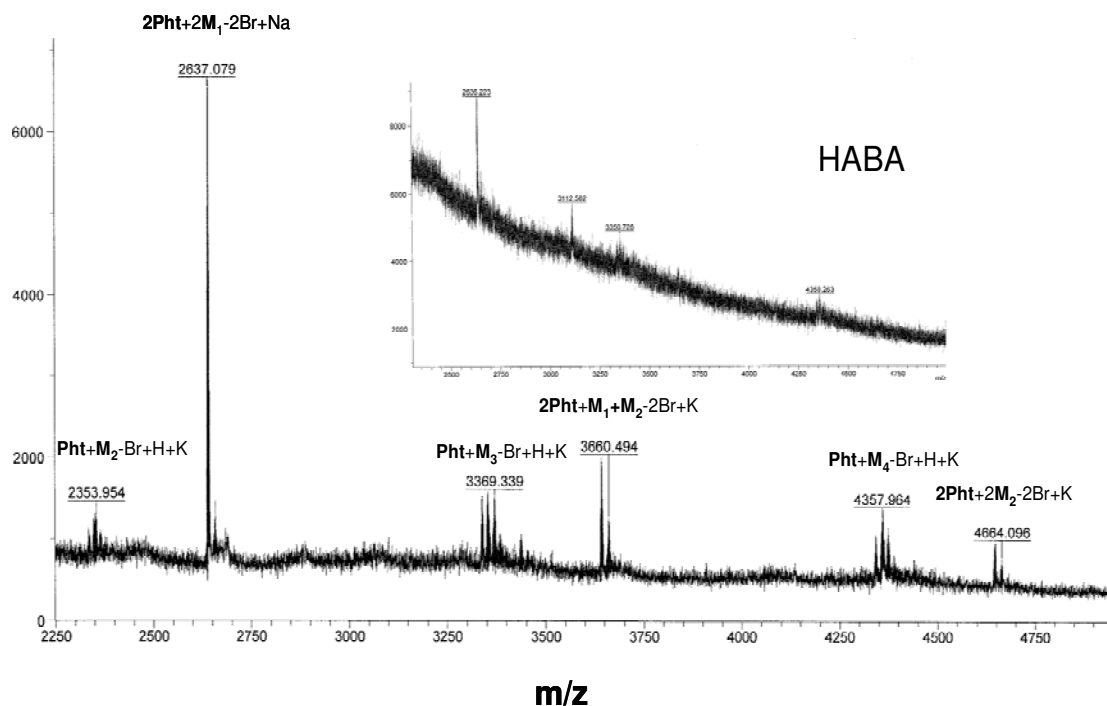
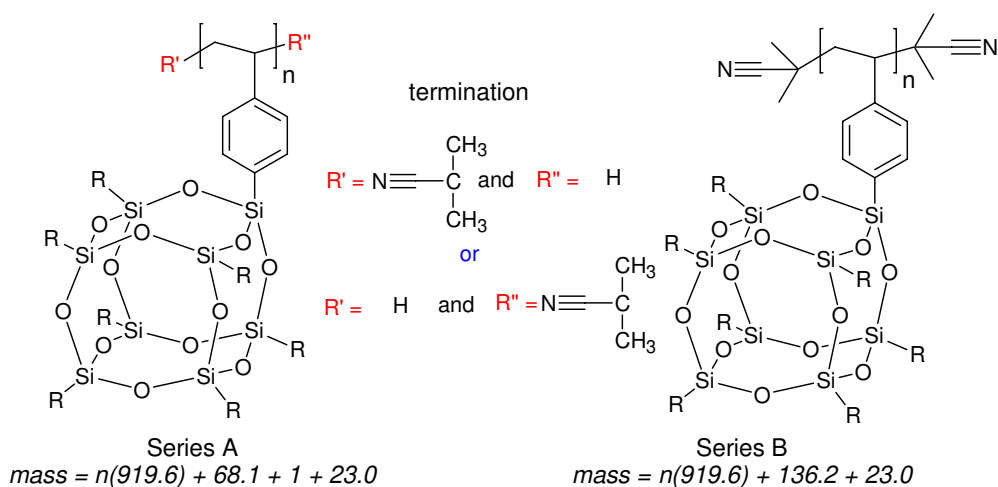


Figure 2.12. MALDI mass spectra of (Cp) styryl POSS in dihydroxy-octafluoroazobenzene. Inset shows spectrum in HABA matrix.

The spectra of the styryl species are similar to the PMA materials, but are more complex and show some very interesting differences. These differences are primarily due to two steric factors, namely the nature of the all carbon backbone of the styryl POSS series versus the ester backbone of the POSS PMAs, and the effect of the R-group size on the conformation of the backbone and ability to protect the terminus.

The styryl POSS oligomer spectrum (Figure 2.12) is typified by the cyclopentyl phthalimidoester (see Appendix A). Potassiated parent ions ($\text{M} + \text{K}^+$) are observed, but are of low intensity. Assigned peaks show multiplets corresponding to sodiated and potassiated species (e.g. 2354, 3369 and 4357) which have lost the terminal Br atom and added a H atom as in the PMA series. The most intense peaks cannot be assigned to simple molecular ion derived species, but correspond to the products of ion chemistry in

the source. For example, when a terminal Br atom is lost, it is possible for the radicals produced to couple and we observe mass peaks consistent with head-to-head coupling of these fragments to generate protonated, sodiated and potassiated dimers (peaks at 2637, 3660, 4646, 4660, 5642 and 6647) up to 6-mers. The cyclopentyl group seems to be of optimum size to “straighten” out the backbone so that the terminus of separate fragments are exposed and can bond. Since the presence of a cation will not influence the conformation of the styryl backbone as happens in the case of the PMAs via coordination to carbonyl groups, backbone extension would be facilitated. For the larger R = cyclohexyl only dimer and trimer coupling products are observed and none of the higher oligomers present in the Cp mass spectrum were observed. This is presumably due to steric reasons. When R = Cy and $n > 3$, more crowded species result which “protect” the terminus so that it cannot couple. Instead, it adds a small H atom. Assignments involving analyte/matrix complexes can be ruled out for all R-groups since all mass peaks are common to spectra obtained in both 4,4'-dihydroxyoctafluoroazobenzene and HABA matrices.



Scheme 2.5. Free radical termination in i-butyl POSS styryl oligomers. Scheme I: single i-butyl nitrile; Scheme II: two i-butyl nitrile groups.

In the case of R = i-butyl, only dimer and trimer coupling reaction products are evident, similar to the R- cyclohexyl oligomers, but for different reasons. The i-butyl group is much smaller than the cyclopentyl or cyclohexyl groups. We have previously observed that cages have a tendency to cluster due to van der Waals interactions which become more important as the oligomer gets larger.¹¹ A small R-group enables closer association of the cages as shown by modeling, the effect of which is to cause the backbone to wrap around rather than to “straighten” and the species to become very compact. The overall effect is the same as a large R = cyclohexyl group blocking the terminus; if the terminus is buried in the center of compacted oligomer it cannot couple with another radical. It will be less accessible, especially for longer chains. High resolution ion mobility studies will allow us to further characterize such structures.



Isobutylnitrile styryl-POSS oligomers were synthesized in the same way as the POSS-propylmethacrylates under free radical conditions with the initiator concentration ranging from 2 – 30 mol %. Scheme 2.5 depicts the synthetic routes which give rise to two isobutylnitrile terminated species corresponding to the most intense observed peak (B) in the mass spectrum (see Figure 2.13). The same series of very low intensity peaks corresponding to the presence of *three* isobutylnitrile groups similar to that seen previously in the isobutylPOSS PMA spectra is evident.

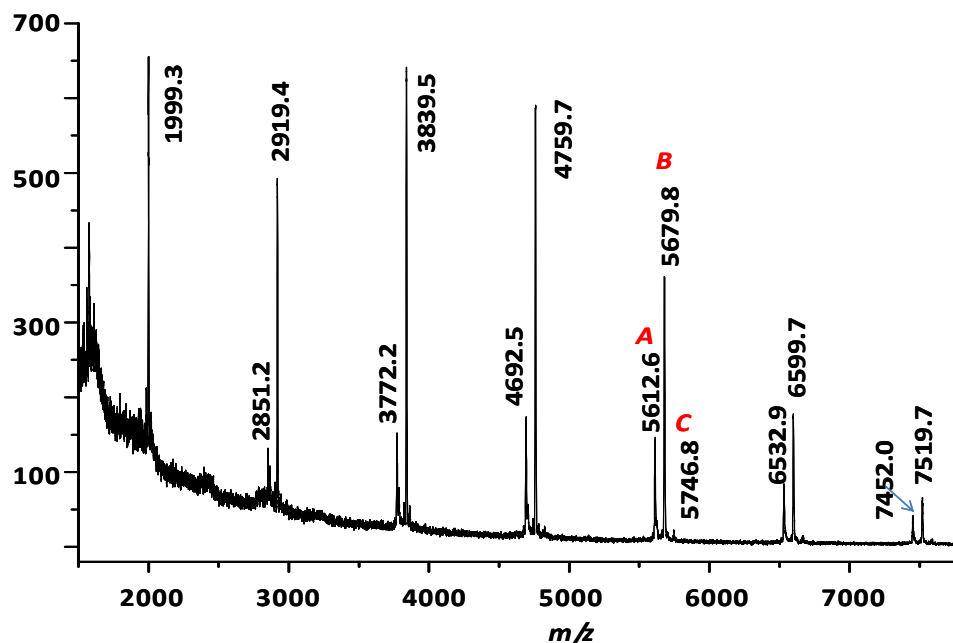


Figure 2.13. Isobutylnitrile (i-butyl)styrylPOSS MALDI mass spectrum using 4,4'-dihydroxyoctafluoroazobenzene matrix. Labels A, B, And C correspond to 1-3 isobutylnitrile groups.

2.4 Conclusions

We have succeeded in obtaining ESI and MALDI mass spectra on a variety of PMA and styryl POSS oligomers, in some cases out to mass ~16,000 g/mol. MALDI spectra were greatly enhanced with the use of a new matrix, 4,4'-dihydroxyoctafluoroazobenzene. ATRP syntheses were much more effective than free radical procedures in creating oligomers with many repeat units. ESI and MALDI mass spectra of the ATRP products rarely gave true molecular ion peaks for any oligomer; rather the terminal halogen was invariably replaced with a hydroxyl or hydrogen atom, respectively. Single atom substitutions are not expected to change the conformation relative to the parent species.

For the PMA series, the most intense peaks observed in the mass spectra correspond to simple sodiated or potassiated species related to the substituted parent ion. Less

intense peaks arise from fragmentations (generally loss of one or more of the POSS side chains) and recombinations, since these processes have relatively low probabilities. These are not of primary structural interest since they represent degraded parent oligomers, but may give insight into how side chains affect backbone conformation. MSMS was used to assign the major peaks for several sets of oligomers, and by analogy, to develop a consistent explanation of the observed spectra for the PMA oligomers studied.

The all-carbon backbone of the styryl materials was resistant to fragmentation but the mass spectra obtained did show recombinations arising from the loss of the terminal Br atom not observed with the POSS PMAs. Coupling of radicals produced by Br atom loss gave rise to multimers. Differences in these ion chemistry products allowed us to draw conclusions about the structures of the styryl species.

Free radical methods did not give materials with more than seven repeat units in any case studied. Termination occurs via a H atom and/or one or two isobutylnitrile moieties from the initiator depending on the amount present in the synthesis. The intensity of peaks in the MALDI spectra in most cases is sufficient to obtain ion mobility data.

2.5 References

1. Voronkov, M. G.; Lavrentyev, V. I. *Top. Curr. Chem.* **1982**, *102*, 199-236.
2. Agaskar, P. A. *Inorg. Chem.* **1991**, *30*, 2707-2708.
3. Agaskar, P. A.; Klemperer, W. G. *Inorg. Chim. Acta* **1995**, *229*, 355-364.
4. Baney, R. H.; Itoh, M.; Sakakibara, A.; Suzuki, T. *Chem. Rev.*, **1995**, *92*, 1409-1430.
5. Lichtenhan, J. D. *Comments Inorg. Chem.*, **1995**, *17*, 115-130.

6. Lichtenhan, J. D. in *Polymeric Materials Encyclopedia*, J. C. Salamore (ed.) CRC Press, NY, **1996** 7769-7778.
7. Li, G. Z.; Wang, L. C.; Ni, H. L.; Pittman, C. U. *J. Inorg. Organomet. Polym.*, **2001**, *11* 123-154.
8. Phillips, S. H.; Haddad, T. S.; Tomczak, S. J. *Curr. Opin. Sol. State Mat. Sci.*, **2004**, *8*, 21-29.
9. Li, G. Z.; Pittman, C. U., Chapter 5 in *Macromolecules Containing Metals and Metal-like Elements. Vol. 5 Group IVA Polymers*, Abd El Aziz, A.S.; Carraher, C.E.; Pittman, C.U.; Zeldin, M., Editors, John Wiley & Sons, Hoboken, NJ, 2005, pp 79-131.
10. Anderson, S. E.; Mitchell, C.; Haddad, T. S.; Vij, A.; Schwab, J. J.; Bowers, M. T., *Chemistry of Materials* **2006**, *18*, 1490-1497.
11. Anderson, S. E.; Mitchell, C.; Bowers, M. T.; and T. S. Haddad, *Chem. Mater.*, **2005**, *17*, 2537-2545.
12. Wallace, W.E.; Guttman, C. M.; and Antonucci, J.M., *J. Am. Soc. Mass Spectrom.*, **1999**, *10*, 224-230.
13. Farahani, M.; Antonucci, J. M.; Guttman, C. M., *Polymer Preprints (American Chemical Society, Division of Polymer Chemistry)*, **2004**, *45*, 350-351.
14. Farahani, M.; Wallace, W. E.; Antonucci, J. M.; Guttman, C. M., *Journal of Applied Polymer Science*, **2006**, *99*, 1842-1847.
15. Wallace, W. E.; Guttman, C. M.; Antonucci, J. M., *Polymer*, **1999**, *41*, 2219-2226.
16. Williams, R. J. J.; Erra-Balsells, R.; Ishikawa, Y.; Nonami, H.; Mauri, A. N.; Riccardi, C. C., *Macromolecular Chemistry and Physics*, **2001**, *202*, 2425-2433.

17. Fasce, D. P.; Williams, R. J. J.; Erra-Balsells, R.; Ishikawa, Y.; Nonami, H.,
Macromolecules, **2001**, *34*, 3534-3539.
18. Valencia, M.; Dempwolf, W.; Guenzler, F.; Knoepfelmacher, O.; Schmidt-Naake, G.,
Macromolecules, **2007**, *40*, 40-46.
19. Auner, N.; Ziemer, B.; Herrschaft, B.; Ziche, W.; John, P.; Weis, J., *European
Journal of Inorganic Chemistry*, **1999**, 1087-1094.
- Eisenberg, P.; Erra-Balsells, R.; Ishikawa, Y.; Lucas, J.C.; Mauri, A. N.; Nonami, H.;
Riccardi, C. C., Williams, R. J. J.; *Macromolecules*, **2000**, *33*, 1940-1947.
21. Karas, M.; Krueger, R., Ion formation in MALDI: *Chemical Reviews*, **2003**, *103*,
427-439.
22. Knochenmuss, R., *The Analyst*, **2006**, *131*, 966-86.
23. Baker, E.S.; Gidden, J.; Fee, D.P.; Kemper, P.R.; Anderson, S.E.; Bowers, M.T., *Int.
J. Mass Spectrom.*, **2003**, *227*, 205-216.
24. Gidden, J. ; Kemper, P.R.; Shammel, E. ; Fee, D.P.; Anderson, S.E.; and Bowers,
M.T., *Int. J. Mass Spectrom.*, **2003** *222*, 63-73.
25. Baker, E. S.; Gidden, J.; Anderson, S. E.; Haddad, T. S.; and Bowers, M.T., *Nano
Lett.*, **2004**, *4*, 779-785.
26. Erin Shammel Baker, Summer L. Bernstein, and Michael T. Bowers, *J. Am. Soc.
Mass Spectrom.* **2005**, *16*, 989-997.
27. Erin Shammel Baker, John E. Bushnell, Stephen R. Wecksler, Mark D. Lim, Manuel
J. Manard, Nicholas F. Dupuis, Peter C. Ford, and Michael T. Bowers, *J. Am. Chem.
Soc.* **2005**, *127*, 18222-18228.

28. Andrij Baumketner, Summer L. Bernstein, Thomas Wyttenbach, Gal Bitan, David B. Teplow, Michael T. Bowers, and Joan-Emma Shea, *Protein Sci.* **2006**, *15*, 420-428
29. Valerie Gabelica, Erin Shammel Baker, Marie-Paule Teulade-Fichou, Edwin De Pauw, and Michael T. Bowers, *J. Am. Chem. Soc.* **2007**, *129*, 895-904.
30. Bakhtiar, R., *Rapid Communications in Mass Spectrometry*, **1999**, *13*, 87-89.
31. Bakhtiar, R.; Feher, F. J., *Rapid Communications in Mass Spectrometry*, **1999**, *13*, 687-694.
32. Bassindale, A.R.; Pourny, M.; Taylor, P.G.; Hursthouse, M.B.; Light, M.E. *Angew. Chem., Int. Ed.*, **2003**, *42*, 3488-3490.
33. Bassindale, A.R.; Parker, D.J.; Pourny, M.; Taylor, P. G.; Horton, P. N.; and Hursthouse, M.B., *J. Organomet. Chem.*, **2004**, *23*, 4400-4405.
34. Anderson, S. E.; Bodzin, D.; Haddad, T. S.; Boatz, J. A.; Dupuis, N. F.; Mitchell, C.; and Bowers, M. T.: *Chem Mater.* **2008**, *20*, 4299-4309.
35. Somogyi, A.; Elandaloussi, E. H.; Hall, D. E.; Buyle Padias, A.; Bates, R. B.; Hall, H. K., Jr., *Macromolecules*, **2007**, *40*, 5311-5321.
36. Pyun, J.; Matyjaszewski, K. *Macromolecules* **2000**, *33*, 217-220.
37. Lecolley, F.; Waterson, C.; Carmichael, A. J.; Mantovani, G.; Harrisson, S.; Chappell, H.; Limer, A.; Williams, P.; Ohno, K.; Haddleton, D. M. *Journal of Materials Chemistry* **2003**, *13*, 2689-2695.
38. Harrison S., W. K., *Polymer Preprints (American Chemical Society, Division of Polymer Chemistry)* **2004**, *45*, (2), 545-546.
39. Almar Posta, T. D., Richard Evans, Guoxin Li, Graeme Mod, Micheal O`Shea, *Macromolecules* **2006**, *39*, (16), 5293-5306.

40. Somogyi, A.; Shu, P.; Padias, A. B. ; Hall, D. E.; Hall, H. K., Jr. “MALDI-TOF Analysis of Polymers by Using Tailor-Made Fluorinated Azobenzene and Stilbene Matrices”, presented at 55th ASMS Conference on Mass Spectrometry and Allied Topics, **2007**, Indianapolis, IN

CHAPTER 3

SYNTHESIS AND SELF-ASSEMBLY OF ORGANIC-INORGANIC POSS – POLY (ETHYLENE – BUTYLENE) BASED POLYMERS.

3.1 Introduction

Self-assembly in nature produces hierarchical structured materials with order on length scales of a few nanometers to micrometers that are capable of performing extremely complex functions. Extraordinary toughness in shells, functionality in echinoderms (sea cucumbers) and cell mitosis are some of the features made possible by the self-assembly of biological components.¹⁻³ Self-assembly is defined as “creation of material from its constituent components in a spontaneous `natural` manner, i.e. by an interaction between the components or by specific rearrangement of them, that proceeds naturally without any external impetus”.⁴ Inspired by nature’s ability to combine dissimilar materials in an ordered manner, similar process have been replicated to produce materials for novel applications.⁵ Composite materials are a form of materials that combine two or more separate components into a form suitable for the required application.⁶ The components of the composite retain their individual identity but exhibit superior properties as compared to either of the individual components. Different top-down and bottom-up approaches can be used to combine materials. Because of the cost advantage the top-down approaches are the most widely used approach, however this approach does not always provide complete control over the microscopic structure of the material.⁷ The bottom-up approach using block copolymers has shown immense promise as it provides control over the microscopic structure, and thus also offers control over the macroscopic properties of the hybrid materials.^{7,8}

In this thesis, a bottom-up approach was used to combine the newly emerging class of Polyhedral Oligomeric Silsesquioxanes (POSS) with conventional polymers to produce hybrid materials which can be used for novel applications. A POSS has a generic formula of $R_n(\text{SiO}_{1.5})_n$ where R are alkyl groups used for polymerization, grafting or solubility and n is an even integer with $n \geq 4$.⁹ The POSS molecule has an inorganic silicon-oxygen core which is surrounded by organic alkyl periphery. The periphery of the POSS occupies 70% volume of the molecule and plays a very important role in determining the physical properties of the molecule. A cubic POSS molecule with seven non-reactive groups and one reactive group has been the most commonly used POSS molecule. It has been incorporated into a number of polymers such as epoxy resins,^{10,11} polyimides,^{12,13} polyacrylates,^{14,15} polyethylene oxide,^{15,16} polyethylene and polystyrene.^{17,18} However, as of today, only a few reports are concerned with utilizing POSS as a building block to generate mesoscopically - ordered structures. POSS lamellae were observed in random copolymers of POSS with epoxy resins and polyimides.^{12,19} In both studies, POSS was attached as pendant group from the backbone, the formation of lamellae was due to entropic and intermolecular interactions of the POSS groups. POSS molecules with short peripheral groups act as spheres and pack in a hexagonal arrangement.²⁰ However, when POSS is attached to the backbone, the connecting linkage restricts the mobility of the cage and imposes considerable spatial constraints on the crystal shape.²⁰ Zheng *et al.* synthesized and studied butadiene – POSS random copolymers and experimentally observed raft structures due to face to face packing of POSS spheres.¹⁷ In the above study, though the phase separation was observed in random copolymers, no long range order was observed. There are very few examples of

incorporating POSS molecules in block copolymers. Pyun *et al.* synthesized poly(methylacrylate-POSS(isobutyl)-*b-n*-butylacrylate-*b*-methacrylate-POSS(isobutyl)) triblock copolymers with varying block lengths, and at higher POSS content observed cylinders of POSS with fairly good order.¹⁵ Recently, Hirai *et al.* synthesized POSS diblocks with either poly(methyl methacrylate) or polystyrene and observed POSS lamellae with very good long range order.²¹

In the present work, the synthesis of poly(ethylene-butylene-*b*-MA-POSS(isobutyl)) diblock copolymers has been achieved, and the study of the block copolymer morphologies by varying the volume fractions of MA-POSS and poly(ethylene-butylene) (PEB). Hemi-telechelic hydroxyl-terminated polybutadiene homopolymers were synthesized by anionic polymerization and hydrogenated to poly(ethylene-butylene) (PEB) homopolymers. These were subsequently allowed to react with EB – bromoisobutyryl bromide to obtain PEB macroinitiators for ATRP. A methacrylate functionalized POSS was then polymerized by ATRP. The resulting diblock copolymers have been fully characterized and the resulting morphologies investigated.

3.2 Experimental Section

3.2.1 Materials

The purification of hexane (99.9%+) (from Aldrich) to the standards required for anionic polymerization has been described elsewhere.²² *n*-butyl lithium (1.6 M) in hexanes, N,N,N',N',N''-pentamethyldiethyltri-amine (PMDETA) (99%+), Cu(I)Cl (99.99%+), Cu(II)Br (99.99%), 3-(3,5,7,9,11,13,15-hepta-*n*-butylpentacyclo[9.5.1(3,9).1(5,15).1(7,13)] octasiloxan-1-yl)propyl methacrylate [MaPOSS(isobutyl)] (all from

Aldrich) were used as received. EB-bromoisobutyrylbromide, triethylamine were dried over CaH_2 , distilled and stored under N_2 atmosphere, THF was distilled over sodium/benzophenone mixture (all from Aldrich). Ethylene oxide and butadiene (both from Aldrich) were purified over *n*-butyl lithium using a manifold as described earlier.²³

3.2.2 Synthesis

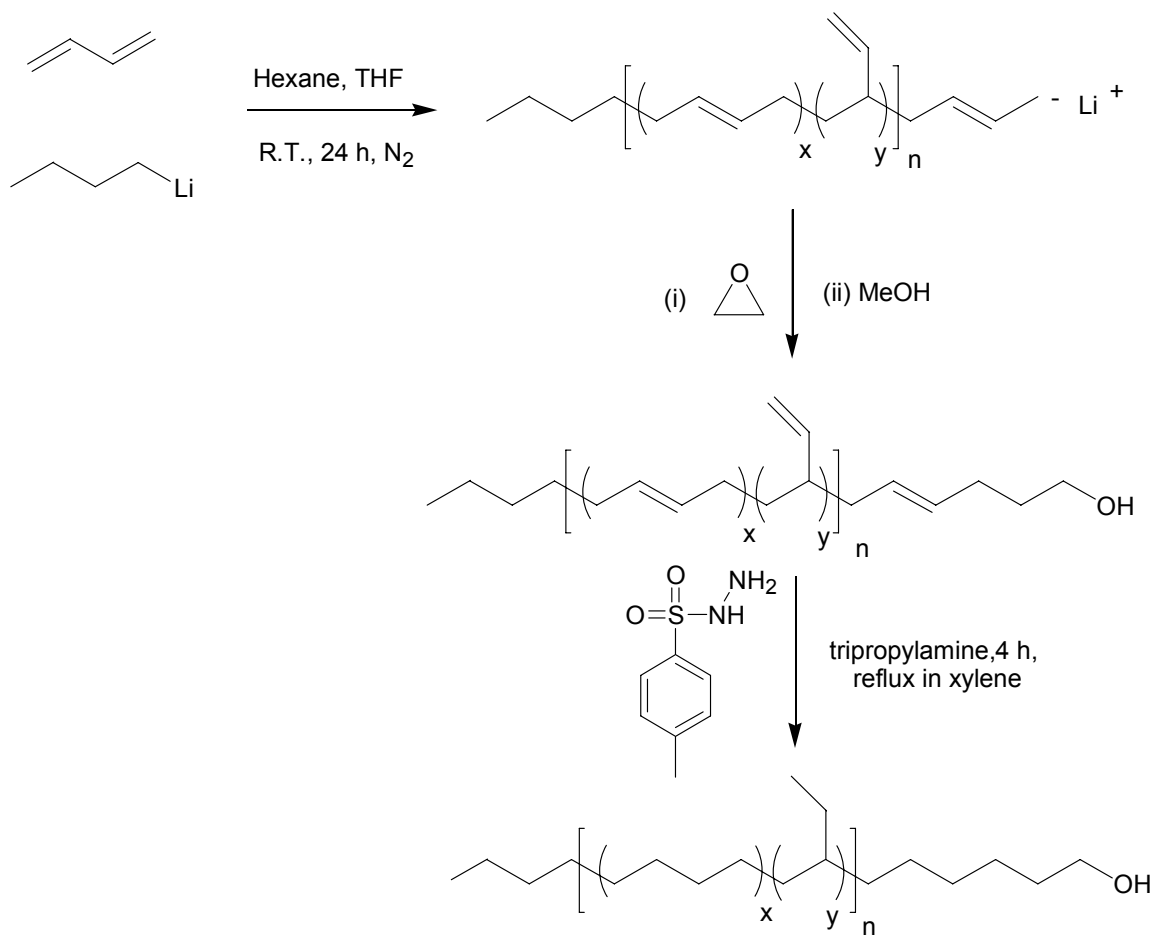
3.2.2.1 Hydroxyl terminated polybutadiene

Dry hexane (300 mL) was distilled into a round bottom flask. THF (0.72 mL, 10.2 mmol) and *n*-butyl lithium (1.2 mL, 2.0 mmol) were cannulae transferred into the flask. Butadiene (11.1 g, 0.20 mol), purified over *n*-butyl lithium at $-10\text{ }^\circ\text{C}$ for 1 hour was transferred into the reaction flask using a manifold as described earlier.²³ The ratio of THF : *n*-butyl lithium was 5 : 1. The reaction was performed at room temperature for 24 h. Ethylene oxide (0.44 g, 10.2 mmol), purified over *n*-butyl lithium was transferred into the reaction flask using the same manifold. The reaction was continued for 30 min and terminated by the addition of methanol. The polymer was precipitated in cold methanol, filtered and vacuum dried. Yield 10 g of viscous clear liquid (90%). M_n 5,800 g/mol against PS standards with THF as the mobile phase. ^1H NMR (CDCl_3 , 400 MHz): δ 0.8 – 2.2 (aliphatic protons of all trans, cis and vinyl), 3.5 ($\text{CH}_2\text{--OH}$), 4.9 (CH_2 vinylic), 5.4 (CH trans and cis), 5.5 – 5.6 (CH vinylic) ppm. ^{13}C NMR (CDCl_3 , 400 MHz): 24 – 45 (aliphatic protons of all trans, cis and vinyl), 50.85 ($\text{CH}_2\text{--OH}$), 114 (CH_2 vinylic), 127–133 (CH trans and cis), 143 (CH vinylic) ppm.

Caution: Extreme care has to be taken during the purification of butadiene to maintain the temperature at -10 °C, b.p. of butadiene is -4 °C. Polymerization of butadiene is an extremely dangerous reaction.

3.2.2.2 Hydrogenation of polybutadiene to poly(ethylene-butylene)

Polybutadiene (3 g, 0.055 mol of butadiene), *p*-toluene sulfonyl hydrazide (11.3 g, 0.061 mol) and tripropyl amine (13.9 mL, 0.073 mol) were dissolved in *o*-xylene (75 mL) and refluxed for 4 h. The color of the reaction solution changes from colorless to orange. The reaction solution was then washed with deionized water (4 X 30 mL) and the organic layer was passed through basic alumina layer till colorless solution was obtained. The polymer was precipitated in cold methanol, filtered and vacuum dried. Yield 2.8 g of a viscous clear liquid (93%). ¹H NMR (CDCl₃, 400 MHz): δ 0.8 (CH₂CHCH₂CH₃) 1.1 – 2.0 (all methylene protons), 1.64 (CH₂CHCH₂CH₃), 3.5 (CH₂–OH). ¹³C NMR (CDCl₃, 400 MHz): 10-11 (CH₂CHCH₂CH₃), 24 – 38 (all methylene protons), 35 - 39 (CH₂CHCH₂CH₃) ppm.



Scheme 3.1. Synthesis of polybutadiene and poly(ethylene-butylene).

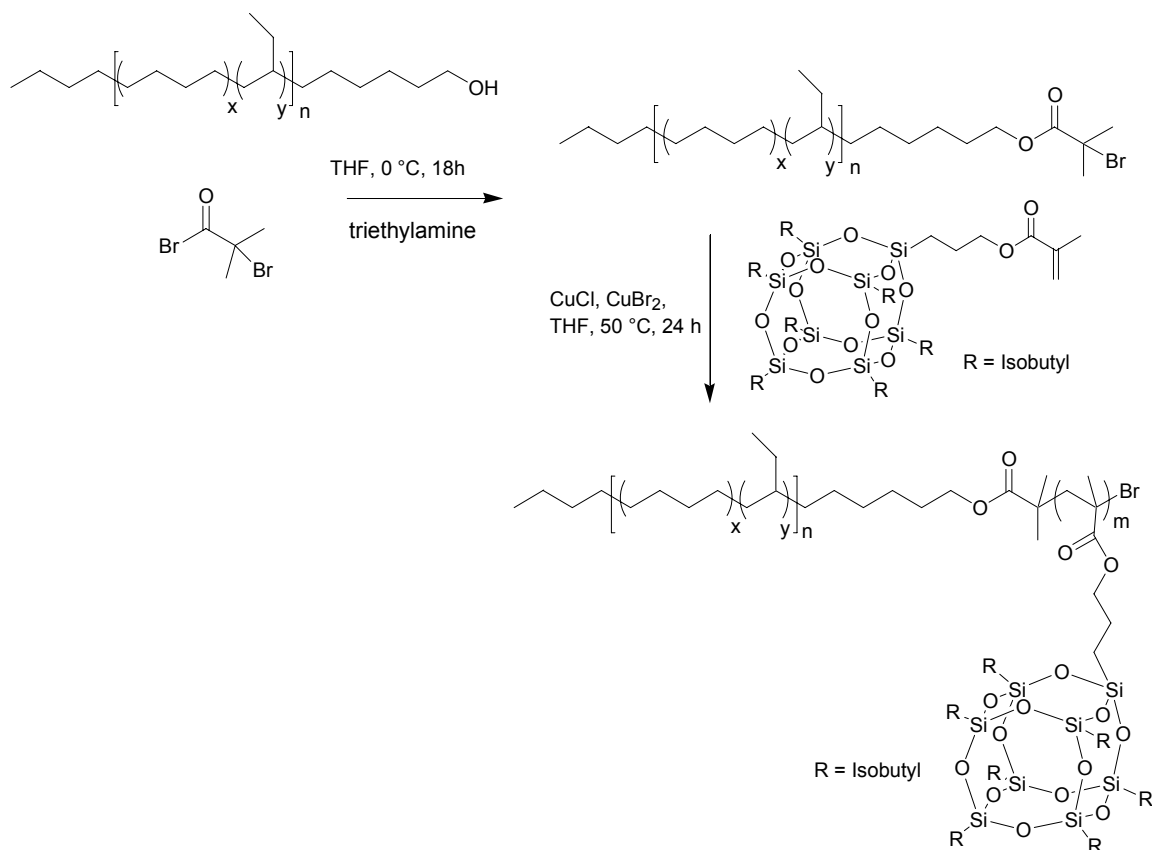
3.2.2.3 Synthesis of poly(ethylene-butylene) macroinitiator

Poly(ethylene-butylene) homopolymer (3 g, 0.51 mmol) was dissolved in THF (10 mL) containing triethylamine (2.22 mL, 1.61 g, 16 mmol), the temperature was reduced to 0 °C and EB-bromoisobutyryl bromide (0.61 mL, 1.14 g, 5.0 mmol) was added to the flask dropwise over 15 min. After stirring for 24 h, the reaction solution was dissolved in 20 mL methylene chloride. The solution was washed with water (2 x 20 mL), 2% HCl solution (1 x 20 mL) and water (1 x 20 mL) and then filtered over a plug of silica with dichloromethane as eluent. Column chromatography was carried out with hexane : ethyl acetate (20 : 1) as eluent. The solution was precipitated in cold methanol,

filtered and vacuum dried. Yield 1.00 g of a viscous clear liquid (33%). ^1H NMR (CDCl_3 , 400 MHz): δ 0.8 ($\text{CH}_2\text{CHCH}_2\text{CH}_3$) 1.1 – 2.0 (all methylene protons), 1.29 ($(\text{CH}_3)_2\text{C}$), 1.64 ($\text{CH}_2\text{CHCH}_2\text{CH}_3$), 4.2 ($\text{CH}_2\text{CH}_2\text{OCO}$).

3.2.2.4 Synthesis of poly(EB-*b*-MA-POSS (isobutyl)) diblock copolymers

To an oven dried 10 mL round bottom flask was added poly(ethylene-butylene) macroinitiator (0.14 g, 0.0241 mmol), MA-POSS(isobutyl) (0.91 g, 0.96 mmol) (Ratio of PEB macroinitiator : MA-POSS(isobutyl) 1 : 40), PMDETA (5.55 μL , 0.0265 mmol), THF (1.0 mL). Three freeze-pump-thaw cycles were performed. CuCl (2.38 mg, 0.024 mmol), CuBr₂ (0.539 mg, 0.00241 mmol, 10 mol% relative to CuCl) were added to the mixture and again three freeze-pump thaw cycles were performed. Polymerization was carried out for 24 h at 50 °C. The reaction solution was then diluted with 10 mL THF and passed through a column of neutral alumina to remove catalyst. The colorless transparent solution was concentrated by evaporation. The polymer was then precipitated in methanol. The polymer was vacuum dried. Yield 0.21 g of a white powder (19.0%). ^1H NMR (CDCl_3 , 400 MHz): δ 0.54 ($\text{SiCH}_2\text{CH}(\text{CH}_3)_2$), 0.58 ($\text{SiCH}_2\text{CH}_2\text{CH}_2\text{OC}(\text{O})-$), δ 0.8 ($\text{CH}_2\text{CHCH}_2\text{CH}_3$), 1.01 ($\text{SiCH}_2\text{CH}(\text{CH}_3)_2$), 1.1 – 2.0 (all PEB methylene protons), 1.29 ($(\text{CH}_3)_2\text{C}$), 1.34 ($\text{CH}_2\text{C}(\text{CH}_3)$), 1.6 ($\text{SiCH}_2\text{CH}_2\text{CH}_2\text{OC}(\text{O})-$), 1.64 ($\text{CH}_2\text{CHCH}_2\text{CH}_3$), 1.8 ($\text{SiCH}_2\text{CH}(\text{CH}_3)_2$), 1.91 ($\text{CH}_2\text{C}(\text{CH}_3)$), 3.9 ($\text{SiCH}_2\text{CH}_2\text{CH}_2\text{OC}(\text{O})$), 4.2 ($\text{CH}_2\text{CH}_2\text{OC}(\text{O})$) ppm.



Scheme 3.2. Synthesis of PEB macroinitiator and p(EB-b-MA-POSS (isobutyl)) diblock copolymers.

3.2.3 Polymer Characterization

Gel permeation chromatography (GPC) measurements were performed in tetrahydrofuran (THF) at 1.0 mL/min using a Knauer K-501 pump with a K-2301 refractive index detector and K-2600 UV detector, and a column bank consisting of two Polymer Labs PLGel Mixed D columns at 40 °C. Molecular weights are reported relative to polystyrene standards (Polymer Labs, Inc.). Nuclear magnetic resonance (NMR) spectra were collected on Bruker 400 MHz instrument and obtained from CDCl₃ solution. ¹H NMR spectra were referenced to residual CHCl₃ at 7.26 ppm and ¹³C NMR spectra were referenced to residual CHCl₃ at 77.16 ppm. Infrared (IR) spectra were obtained on a

Perkin-Elmer Spectrum One FTIR spectrometer equipped with an ATR accessory. The spectra were obtained on vacuum dried bulk samples.

Thermogravimetric analysis (TGA) was carried out using a TA Instruments TGA 2950 thermogravimetric analyzer with a heating rate of 10° C/min from room temperature to 700° C under air. (40 mL/min). Samples for Differential Scanning Calorimetry (DSC) were thermally annealed at 150 °C and allowed to cool to room temperature over a period of 3 h. DSC was performed on TA Instruments DSC Q1000 and the heating and cooling rates of the sample were 10 °C / min.

Samples for Small angle X-ray scattering (SAXS), Wide angle X-ray scattering (WAXS) and Transmissions electron microscopy (TEM) were cast from concentrated solutions of polymer in toluene and then thermally annealed at 150 °C under vacuum for 48 h. SAXS was performed using Ni-filtered Cu K α radiation ($\lambda=1.54 \text{ \AA}$) from a Rigaku rotating anode (operated at 60 kV, 45 mA). The X-ray was collimated by a set of three pinholes. A CCD detector (Siemens Hi-Star), located at a camera length of 1192.5 mm, was used to record scattering patterns. WAXS was carried out on the thermally annealed materials with a Siemens D500 diffractometer in transmission mode and Cu K α radiation. MA POSS (isobutyl) monomer was studied as received. The scan range of 2θ was 5°- 30° with a step interval of 0.1°. A photographic plate was used as detector kept at a distance of 119 mm from the sample. Samples for electron microscopy were prepared by microtoming the annealed samples at different temperature (-60° to -30°) using a diamond knife. Approximately 50-100 nm thick sections were collected. TEM studies were performed using a JEOL 1000CX transmission electron microscope operated at 100 kV. No staining of the samples was performed.

Diblock samples for tensile testing were prepared by compression molding at 130 °C under a pressure of 5 metric ton for 20 mins. The temperature was allowed to gradually cool down to room temperature. Mechanical properties were measured using an Instron 4411 series tensile tester equipped with a 100 N load cell and data was collected with LabView software. Tests were conducted on specimens of width and thickness equal to approximately 0.4 – 0.8 mm and 0.17 mm respectively, using a crosshead velocity of 10 mm/minute and a gauge length of the samples were 4mm and 8mm. The tensile specimens were prepared according the methods suggested in ASTM standards C 1557-03 and D 3379-75. Though these standards have been developed for single filament materials, we have applied the same technique to test a small quantity of synthesized polymer. The method involved gluing the specimens at each end to a cardboard backing using Devcon five-minute epoxy. Two holes in the cardboard backing were used to ensure a consistent gauge length. The center section of the backing was removed after the sample was fixed in the Instron grips. The grips were arranged with pin ends between the Instron foundation and the gripping surface so the direction of applied force and vertical axis of the specimen were coincident.

3.3 Results and Discussions

3.3.1 Synthesis and Hydrogenation of Polybutadiene

Anionic polymerization is the preferred technique for synthesis of polybutadiene of desired molecular weights with low polydispersity indexes.²⁴ The reactions were carried out in hexane and *n*-butyl lithium was used as the initiator. A stoichiometric amount of THF relative to *n*-butyl lithium was used to control the 1,4 and 1,2 content in

the polymer.^{25,26} The 1,2 content in the polybutadiene backbone can be increased, by increasing the amount of THF added to the reaction solution. ¹H NMR and quantitative ¹³C NMR were used to quantitatively determine the amount of 1,2 content in the polybutadiene homopolymer.²⁷ The use of THF also helps in lowering the reaction time of the polymerization by breaking the hexameric aggregates of *n* – butyl lithium in hexane to dimeric aggregates. Smaller aggregates lead to faster initiation and also help in lowering the PDI of the polymer.²⁸ The reaction was end capped with ethylene oxide and then terminated with methanol. During the ethylene oxide transfer a small oxygen leak leads to radical-radical coupling which can be seen by the presence of a high molecular weight shoulder in the GPC. Four different molecular weights of polybutadiene were synthesized with varying 1,2 content from 56% to 28% as shown in table 3.1.

Table 3.1. Molecular weights of poly(ethylenebutylene) and p(EB-*b*-MA-POSS(isobutyl)) diblock copolymers.

No.	Copolymer	M _n PEB g/mol (PDI) ^a	% 1,4 content	M _n p(EB- <i>b</i> - MA-POSS (isobutyl)) g/mol (PDI) ^a	N _(ethylene- butylene)	N _(POSS)	<i>f</i> _(EB)
1	E(44)B ₁₀₇ POSS ₉	5,800 (1.04)	44	14,200 (1.05)	107	9	0.46
2	E(65)B ₃₅₀ POSS ₁₇	19,000 (1.14)	65	35,000 (1.1)	350	17	0.60
3	E(63)B ₆₃₂ POSS ₂₈	34,200 (1.09)	63	60,600 (1.08)	632	28	0.62
4	E(72)B ₁₀₇₂ POSS ₁₅	56,000 (1.05)	72	70,100 (1.06)	1072	15	0.84

a - Molecular weight determined by GPC against PS standard, b - Molecular weight determined by ¹H NMR, N - number of repeat units, *f* - volume fraction, assuming density of poly(ethylene-butylene) 0.91 g/cm³ and density of poly(MA-POSS (isobutyl)) 1.15 g/cm³ (by ASTM D792-00).

Hydrogenation of the butadiene samples was carried out using the procedure developed by Hahn.²⁹ Poly(ethylene-butylene) formed by hydrogenation of polybutadiene has an apparently slightly lower molecular weight than the corresponding polybutadiene as determined by GPC (Fig. 3.1).

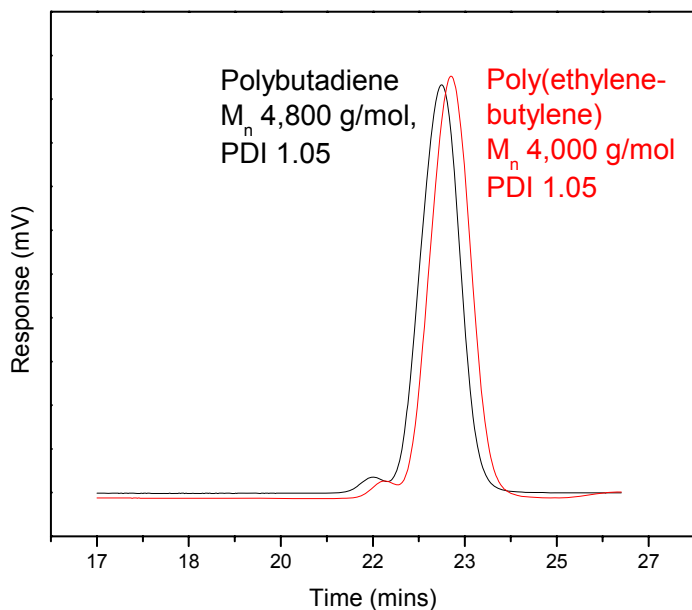


Figure 3.1 GPC of poly(butadiene), M_n – 5,800 g/mol and PDI 1.05 and poly(ethylenebutylene), M_n – 5,000 g/mol and PDI 1.05.

The saturated hydrocarbon backbone formed after hydrogenation increases the flexibility of the backbone, thereby reducing the radius of gyration (R_g) of the polymer thus apparently lowering the molecular weight of the polymer. No significant change is observed in the PDI of the polymer after hydrogenation. In ^1H and ^{13}C NMR spectra, the resonances corresponding to the unsaturated protons in the region δ 4.9-6.0 and the unsaturated carbon peaks at δ 114-143 either completely disappear or are reduced by over 99% confirming nearly quantitative hydrogenation.³⁰ The hydrogenation reaction was also characterized by IR spectroscopy, absorbance of alkene stretching at 1630 cm^{-1}

disappears after hydrogenation and new peak at 720 cm^{-1} appears due to CH_2 rocking vibration in PEB.

3.3.2 Synthesis of PEB Macroinitiator and p(EB-*b*-MA-POSS(isobutyl)) Diblock Copolymer

The hydroxyl terminated PEB was reacted with α -bromoisobutyryl bromide in the presence of triethylamine to obtain PEB macroinitiators for atom transfer radical polymerization (ATRP) (Scheme 3.2). The macroinitiator synthesis was monitored by ^1H NMR, the resonances corresponding to methylene protons α to the hydroxyl group in PEB shift downfield from $\delta = 3.4\text{ ppm}$ to $\delta = 4.2\text{ ppm}$ indicating the formation of an ester bond and no residual resonance is observed at $\delta 3.4\text{ ppm}$ after the reaction indicating complete consumption of the starting material. Methacrylate functionalized POSS monomer was polymerized by ATRP using standard conditions and the PEB macroinitiator (Scheme 3.2). Unreacted monomer was removed either by precipitation or by Soxhlet extraction in methanol for 2 – 7 days. The GPC traces of PEB of molecular weight M_n 19,000 g/mol and p(EB-*b*-MAPOSS (isobutyl)) of molecular weight M_n 35,000 g/mol are shown in Fig. 3.2.

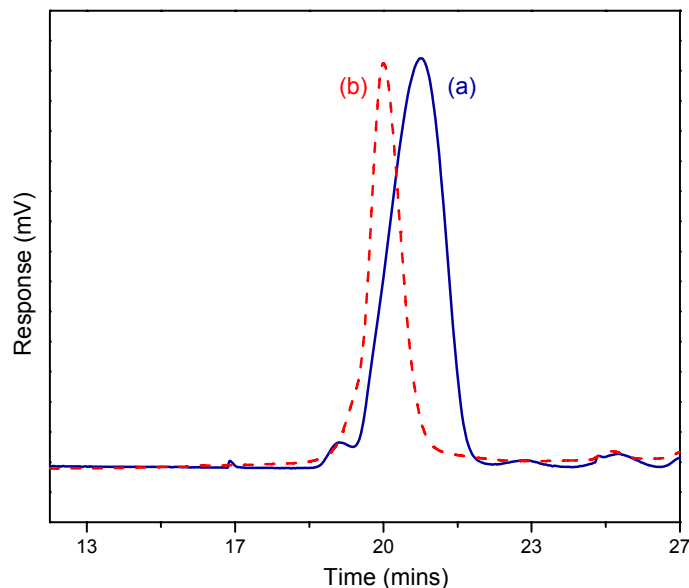


Figure 3.2. GPC of (a) PEB, 19,000 g/mol and (b) p(EB-*b*-MA-POSS (isobutyl)) diblock copolymer (E(65)B₃₅₀POSS₁₇), 35,000 g/mol.

A clear shift in the peak to higher molecular weight and very little overlap with the peak corresponding to the macroinitiator clearly shows the incorporation of the POSS block. The PDI of the p(EB-*b*-MA-POSS (isobutyl)) diblock copolymers was fairly narrow (PDI < 1.14). The number of units of POSS attached to PEB backbone were calculated by comparing the methyl peak integrations of the butylene units at $\delta = 0.8$ to the integration of methyl peaks of the isobutyl periphery of POSS at $\delta = 1.01$. The maximum number of units of POSS attached to PEB backbone was 28. Various compositions of the diblocks synthesized are listed in Table 1. The nomenclature of the diblock copolymers is on the basis of number of repeat units of EB and POSS and % ethylene content in PEB block, copolymer **1** with 107 units of EB, 9 units of POSS and a ethylene content of 44% is thus named E(44)B₁₀₇POSS₉.

3.3.3 Polymer Characterization

3.3.3.1 Thermal Stability

The thermal stability of the polymers under atmospheric conditions was studied using TGA. MA-POSS (isobutyl) homopolymer (PMAPOSS) having 10 repeat units were synthesized by ATRP as a control sample. Decomposition temperatures (5 wt % loss temperature) of PMAPOSS and PEB under air are 324 °C and 311 °C respectively (Fig. 3.3).

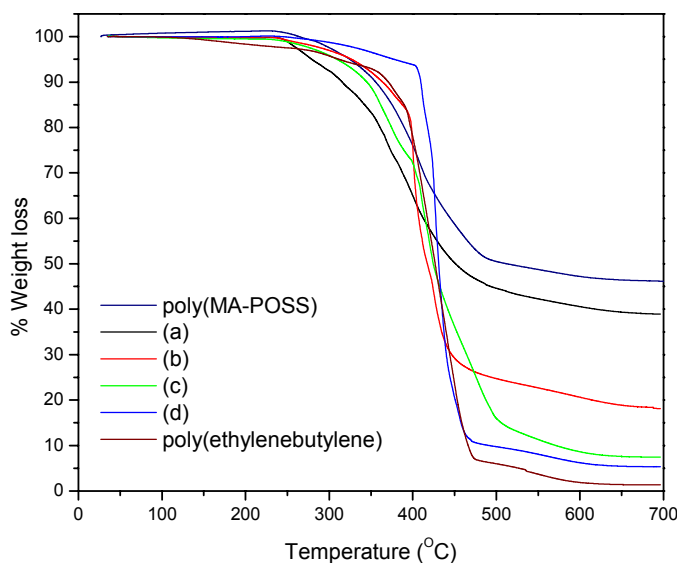


Figure 3.3. TGA of poly(MA-POSS (isobutyl)), a)E(44)B₁₀₇POSS₉, b) E(65)B₃₅₀POSS₁₇, c)E(63)B₆₃₂POSS₂₈, d)E(72)B₁₀₇₂POSS₁₅ and poly(ethylenebutylene).

The decomposition temperatures of the copolymers vary from 279 °C to 377 °C and are reported in table 3.2. The char yield percentages of the homopolymers and the diblock copolymers are also reported in table 3.2. As anticipated, as the amount of POSS is reduced, the char yield of the copolymer also reduces.

Table 3.2. TGA and DSC data for p(EB-*b*-MA-POSS(isobutyl)) diblock copolymers.

No	Copolymer	Decomp. Temp. (° C)	% Char yield	T _g (EB) (° C)	T _m (EB) (° C)	T _g (POSS) (° C)	T _m (POSS) (° C)	ΔH(POSS) J/g
1	E(44)B ₁₀₇ POSS ₉	279	38.9	-58	-	80	118	0.18
2	E(65)B ₃₅₀ POSS ₁₇	326	18.1	-44	15	69	113	0.03
3	E(63)B ₆₃₂ POSS ₂₈	309	7.4	-44	16	85	105	2.77
4	E(72)B ₁₀₇₂ POSS ₁₅	377	5.3	-32	43	-	-	-

T_g – glass temperature transition, T_m – Melting point, ΔH – endothermic heat of melting, Decomp. Temp. – Decomposition Temperature

3.3.3.2 DSC Studies

The thermal behavior, phase separation and crystallization in p(EB-*b*-MA POSS (isobutyl)) block copolymers was studied by DSC. The DSC results for the diblock copolymers are shown in Table 3.2 and Fig. 3.4. Diblock copolymer E(44)B₁₀₇POSS₉ has two different glass transition temperatures. The first T_g(EB) at -58 °C corresponds to the glass transition temperature of the EB phase and the second T_g(MAPOSS) at 80 °C corresponds to the glass transition temperature of the MAPOSS phase. This sample has a melting point T_m(MAPOSS) at 118 °C which corresponds to the melting of POSS crystals. The presence of two glass transitions in the copolymer indicates that the chains of the POSS and EB phase are immiscible and are phase separated. The weak melting peak at 118 °C with a heat of melting (ΔH) of 0.18 J/g shows that the POSS crystals are very small and ill-defined. Copolymer E(44)B₁₀₇POSS₉ has more butylene segments than

ethylene segments which prevents the crystallization of ethylene chains and thus we do not observe a melting point corresponding to the EB phase.

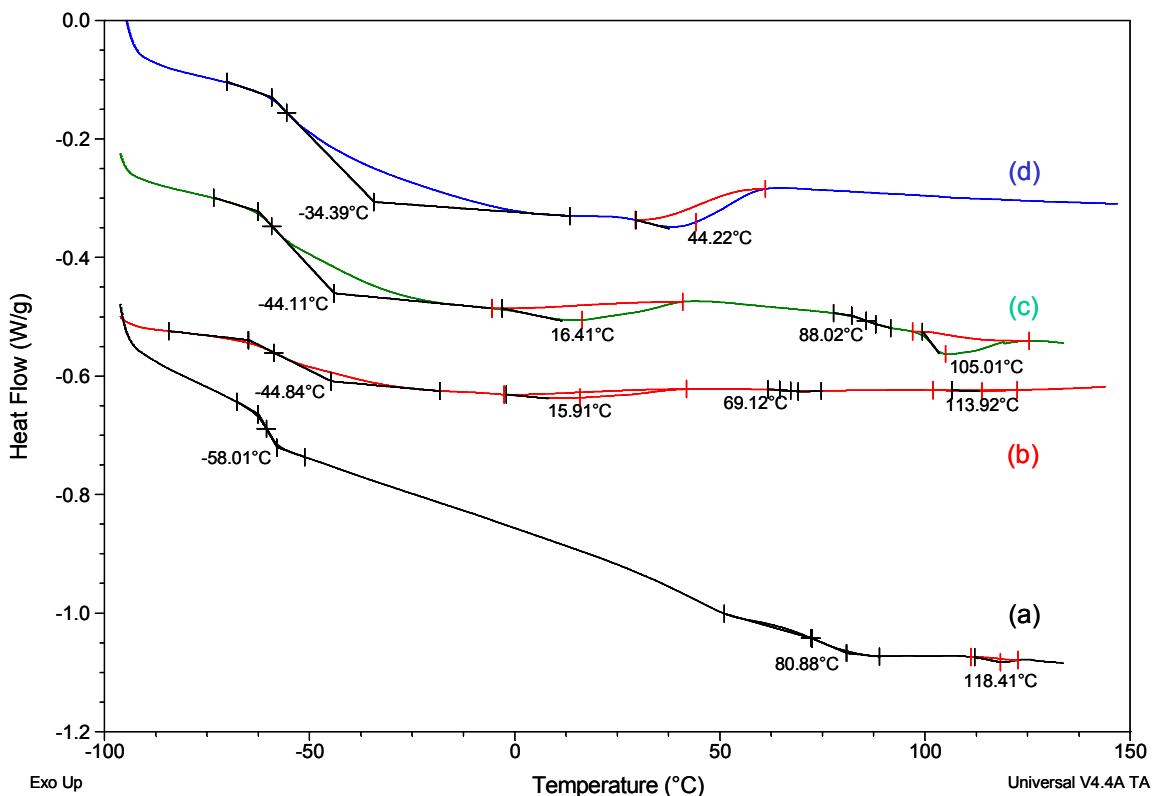


Figure 3.4. DSC of a)E(44)B₁₀₇POSS₉, b) E(65)B₃₅₀POSS₁₇, c)E(63)B₆₃₂POSS₂₈ and d)E(72)B₁₀₇₂POSS₁₅.

Two glass transition temperatures and two melting points were observed for E(65)B₃₅₀POSS₁₇ diblock copolymer. As the EB phase in these diblock copolymers has higher ethylene content, the $T_{g(EB)}$ increases to $-44\text{ }^{\circ}\text{C}$. The $T_{g(MAPOSS)}$ is at $69\text{ }^{\circ}\text{C}$. The melting point $T_{m(EB)}$ of the ethylene crystals in the EB phase is observed around $15\text{ }^{\circ}\text{C}$ and the $T_{m(MAPOSS)}$ is at $113\text{ }^{\circ}\text{C}$. Both EB and MAPOSS phases crystallize and are phase separated.

Two glass transition temperatures and two melting points were also observed for diblock copolymer E(63)B₆₃₂POSS₂₈. The thermal transitions corresponding to the EB

phase are similar to the thermal transitions observed in diblock copolymer E(65)B₃₅₀POSS₁₇. The $T_{g(\text{MAPOSS})}$ is at 89 °C. The difference in T_g of the MAPOSS phase in all three diblock copolymers is due to the different morphologies of the diblock copolymers (as discussed below) and due to the different crystalline content of POSS in the MAPOSS phase. Copolymer E(63)B₆₃₂POSS₂₈ with maximum 28 units of POSS shows the highest ΔH of 2.7 J/g.

Copolymer E(72)B₁₀₇₂POSS₁₅ with the highest ethylene content has the highest $T_{g(\text{EB})}$ at -32 °C and highest $T_{m(\text{EB})}$ at 43 °C. Due to the low weight percent of POSS (20 wt %) in the copolymer, the thermal transitions corresponding to the POSS phase could not be detected by DSC.

Based on the thermal data from the DSC, both phases of the p(EB-*b*-MAPOSS (isobutyl)) copolymers are semi-crystalline. There are only a few studies on the morphological behavior of diblock copolymers with two semi-crystalline phases.^{31,32} The crystallization of the phases can significantly affect the phase separation of the block copolymer and can lead to unexpected non-equilibrium structures.

3.3.3.3 WAXS Studies

The crystallization behavior of the diblock copolymer was studied using Wide angle X-ray scattering (Fig. 3.5). The MAPOSS monomer is a highly crystalline material, where POSS packs as spheres or cubes in an hexagonal arrangement.²⁰ However, when POSS is covalently attached to a polymer backbone their crystallization is restricted to 2D sheets due to the geometric constraints of attaching POSS to the polymer chain.¹⁷ The WAXS profile of PMAPOSS and PEB are shown in Fig. 3.5. The WAXS of the PMAPOSS (Fig. 3.5a) has two broad peaks centered at $2\theta = 8.61^\circ$ and 18.36° . There was

no crystallization observed in the homopolymer, the attachment of POSS spheres to the backbone and the short propyl acrylate chain joining the POSS cubes to the backbone restricts the mobility of the cubes and presumably prevents crystallization. In figure 3.5f, the top trace of PEB homopolymer of molecular weight 34,200 g/mol shows two broad peaks centered at two theta values of 11.0° and 19.0°. The broad peaks observed in WAXS profile of PEB indicate that the 37% butylene content in PEB homopolymer prevents crystallization of the ethylene segments in the EB phase.

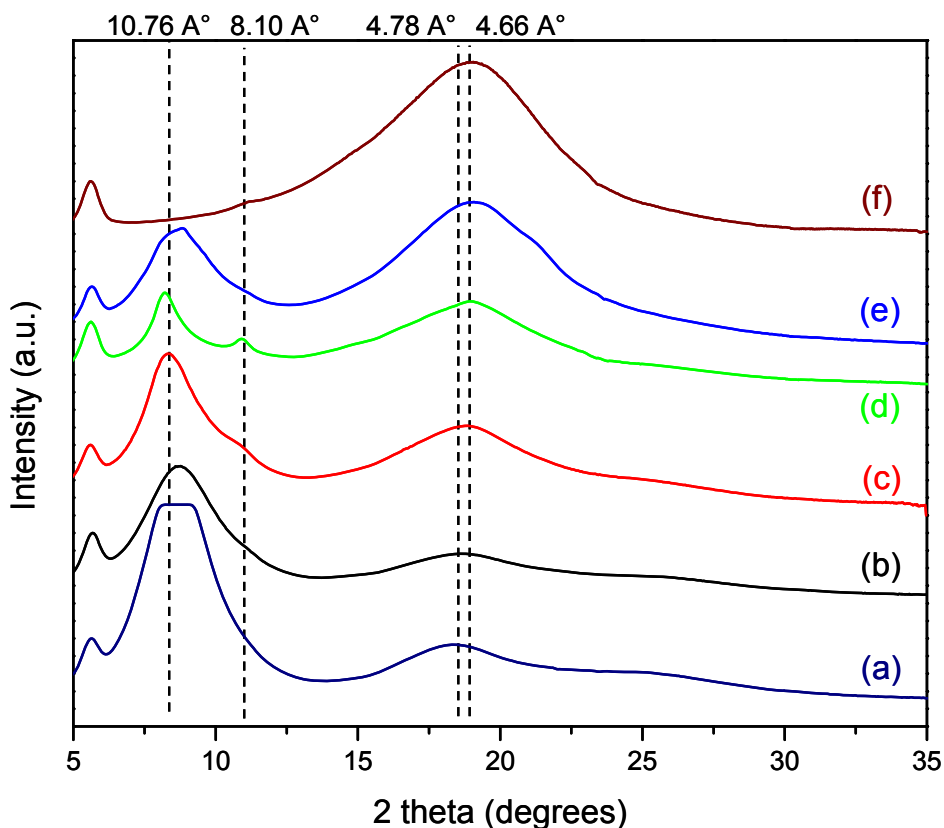


Figure 3.5. (left) WAXS of (a) poly (MA-POSS (isobutyl)) homopolymer, (b) E(44)B₁₀₇POSS₉, c) E(65)B₃₅₀POSS₁₇, d) E(63)B₆₃₂POSS₂₈, e) E(72)B₁₀₇₂POSS₁₅ and f) E(63)B₆₃₂ homopolymer.

The WAXS profile of the p(EB-*b*-MA-POSS (isobutyl)) copolymers also do not show sharp crystalline peaks. The positions of the peaks in the diblocks are summarized

in Table 3.3. All of the diblock copolymer samples have peaks centered at 2θ around 8.4° and 18.8° . As the number of POSS units are increased, an additional peak centered at $2\theta = 11.01^\circ$ is observed. With increasing POSS content, the position of the peak shift to lower 2θ values indicating an increase in d-spacing of the crystal. The absence of the sharp peaks in the WAXS profile of the diblock copolymers along with the presence of melting transitions in the DSC suggests that both the ethylene and POSS crystals formed in the diblock copolymer are very small and ill-defined.

Table 3.3. Summarized WAXS results of the homopolymers and diblock copolymers.

No.	Copolymer	2θ values (degrees)
(a)	Poly (MA-POSS (isobutyl))	8.61, 18.36
(b)	E(44)B ₁₀₇ POSS ₉	8.67, 18.52
(c)	E(65)B ₃₅₀ POSS ₁₇	8.34, 11.01, 18.79
(d)	E(63)B ₆₃₂ POSS ₂₈	8.23, 10.90, 18.98
(e)	E(72)B ₁₀₇₂ POSS ₁₅	8.83, 19.01
(f)	E(63)B ₆₃₂	11.17, 19.06

3.3.3.4 Morphology Studies

Small angle X-ray scattering (SAXS) was used to study the phase separation of the diblock copolymers. Intensity (I) versus scattering vector (q) plots are shown in Fig. 3.6, where q^* is defined as the scattering vector of the Bragg peak with the lowest scattering angle. The TEM images of p(EB-*b*-MAPOSS (isobutyl)) diblock copolymers are shown in fig. 3.7. Diblock copolymers were not stained since the silicon in the POSS

phase provides sufficient mass contrast. The black domains in the TEM images correspond to the POSS phase while the white phase corresponds to the PEB phase. Diblock copolymer E(44)B₁₀₇POSS₉ has a number average molecular weight of 14,200 g/mol with relative volume fraction of EB:POSS of 0.44:0.56. The SAXS profile of E(44)B₁₀₇POSS₉ shows only one broad peak with a maximum at $q^* = 0.43 \text{ nm}^{-1}$ and a corresponding d-spacing of 14.6 nm. The broad shape of the peak indicates that the copolymer is in a phase-mixed state. The corresponding TEM image (not shown here) also does not show a phase separated block copolymer morphology. Copolymer E(44)B₁₀₇POSS₉ has low total degree of polymerization (N) and thus it does not phase separate. By increasing the total number of repeat units in the copolymer, phase separation would be expected.

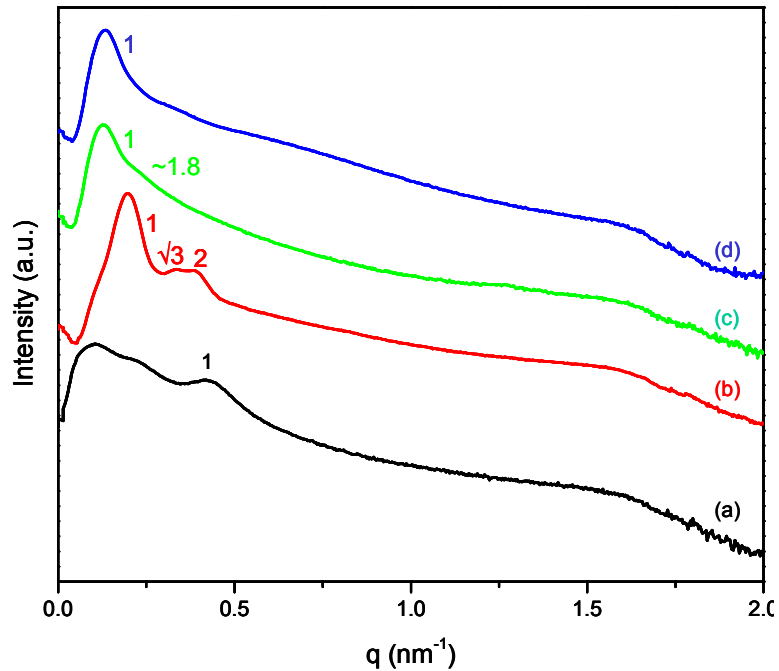


Figure 3.6. SAXS of p(EB-b-MA-POSS (isobutyl)) diblock copolymers
a)E(44)B₁₀₇POSS₉, b) E(65)B₃₅₀POSS₁₇, c)E(63)B₆₃₂POSS₂₈ and d)E(72)B₁₀₇₂POSS₁₅.

Diblock copolymer E(65)B₃₅₀POSS₁₇ has a total molecular weight of 35,000 g/mol with relative volume fraction of EB:POSS of 0.60:0.40. The SAXS profile of E(65)B₃₅₀POSS₁₇ has three peaks in scattering ratio of $q^* : \sqrt{3}q^* : 2q^*$ with a d-spacing of 31.7 nm. The scattering profile of the sample indicates a cylindrical morphology. The TEM image of the corresponding sample shows white cylinders of EB phase hexagonally packed in black POSS phase. The average of 10 images of the hexagonally packed cylinders shows that the volume occupied by the EB cylinders is 60 % of the total volume of the hexagons. The SAXS profile and the TEM image suggests an inverse cylindrical morphology where the majority volume EB phase packs as cylindrical structures and the minority MAPOSS phases occupies the matrix around the cylinders.

The formation of inverse cylindrical morphology can be explained based on two factors; conformational asymmetry (ϵ) and/or the flexibility of the connecting blocks. Milner, Matsen and others have independently predicated that there is a shift of order – order transition towards the compositions richer in the segments possessing longer statistical segment length and away from the segment possessing higher segmental volume.³³⁻³⁷ The backbone of PMAPOSS copolymer would have comparable statistical segment length to the PMMA homopolymer but due to the size of the POSS cage attached to the back bone the segmental volume of the PMAPOSS copolymer would be very large. The diameter of a single POSS molecule with an isobutyl periphery is around 1.5 nm, the difference in segmental length and segmental volume can lead to an asymmetry in the block copolymers. This would shift the phase diagram away from the MAPOSS segments and towards the EB segments. Even at higher POSS fractions, the morphologies rich in EB segments would be obtained and would explain the formation of

EB cylinders in the POSS matrix at the relative volume fractions of EB:POSS at 0.60:0.40.

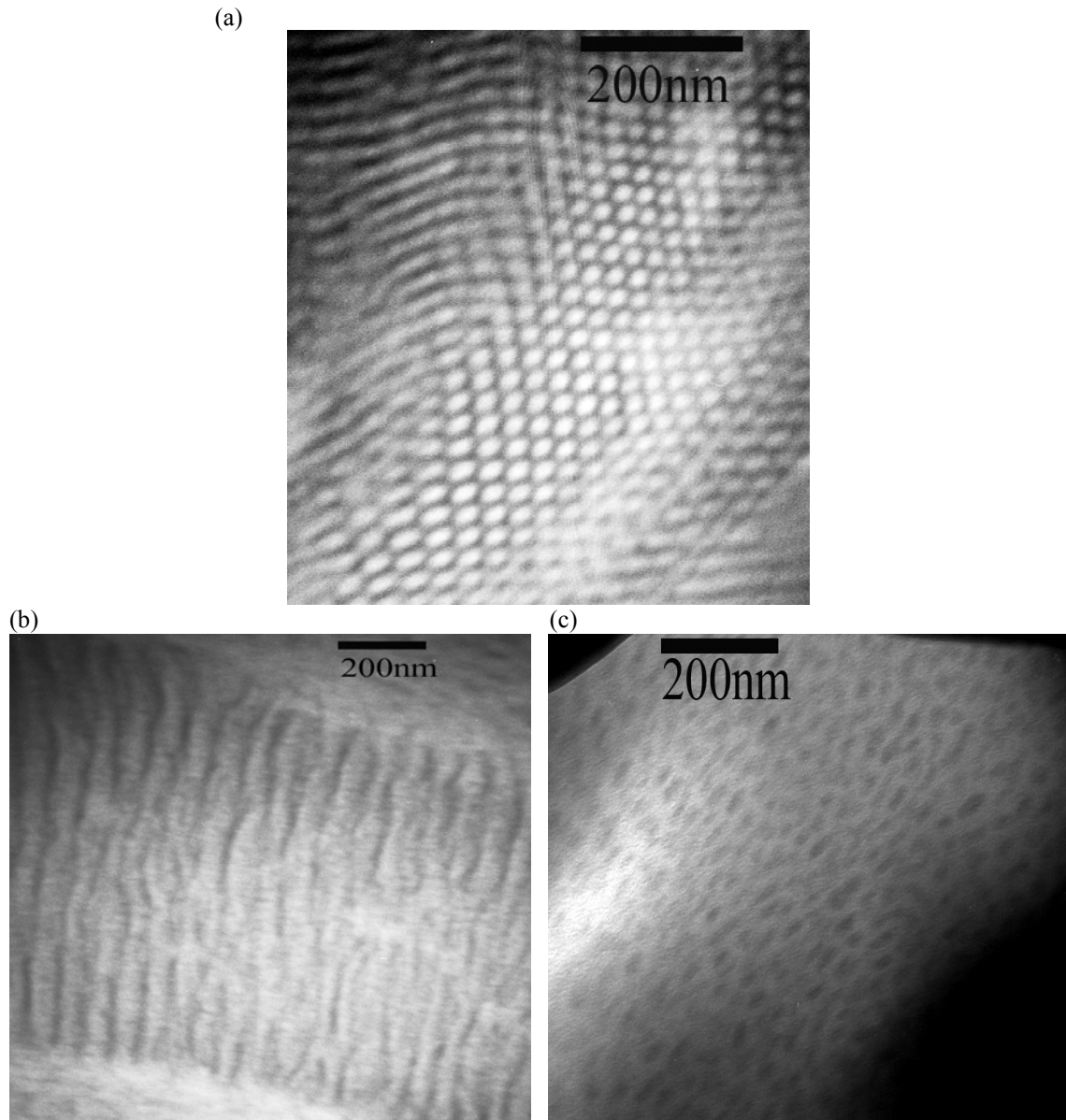


Figure 3.7. TEM of p(EB-b-MA-POSS (isobutyl)) diblock copolymers a) E(65)B₃₅₀POSS₁₇, b) E(63)B₆₃₂POSS₂₈ and c)E(72)B₁₀₇₂POSS₁₅.

Another factor which can lead to inverse cylindrical morphology is the relative flexibility of the EB and MAPOSS chains. In the cylindrical morphology, the chains in the core of the cylinder are more stretched than the chains which occupy the matrix

around the cylindrical domains.³⁸ Thus, the flexible chains tend to occupy the center of the cylinders while the stiffer chains occupy the matrix surrounding the cylinder.³⁹ It is observed in coil-comb copolymers, where flexible coils occupy the center of the cylindrical morphology and the comb phase occupies the matrix around the cylinders.⁴⁰ The bulky POSS groups attached to methacrylate backbone can act as anchors and prevent the stretching of the MAPOSS chains. Thus the MAPOSS segments could occupy the periphery of the cylinder and the flexible EB segments would occupy the core of the cylinder. In figure 3.8, a wedge of the cylinder shows that the chains in the core are more stretched than the chains in the periphery of the cylinder.

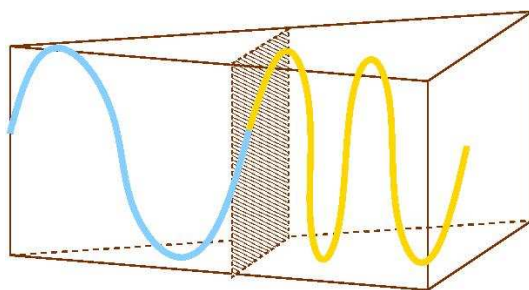


Figure 3.8. Wedge of a cylinder with the chains in the core being more stretched than the chains in the periphery. The shaded plane shows the interface between the chains.

To determine the order-disorder transition temperature (T_{ODT}) of the diblock copolymer, the SAXS profiles of the diblock copolymer were obtained at temperature intervals of 10 °C from 150 °C to 270 °C. Above 200 °C, the $\sqrt{3}q^*$ peak in SAXS begins to diminish and a new peak appears at the scattering ratio of $3q^*$. The cylindrical morphology of the diblock copolymer transforms to lamellar morphology with three Bragg peaks in the scattering ratio $q^*: 2q^*: 3q^*$ (Fig 3.9). The d-spacing of the lamellae is 26.9 nm which is lower than the d-spacing of the corresponding cylinders (31.7 nm). Transformation of the cylindrical to lamellae morphology by annealing at higher temperature and reduction in d-spacing indicates that the cylindrical morphology is an

intermediate morphology and lamellae is the equilibrium morphology for the E(65)B₃₅₀POSS₁₇ block copolymer. The T_{ODT} of the diblock copolymer is greater than 270 °C, which is the upper temperature limit of our SAXS instrument.

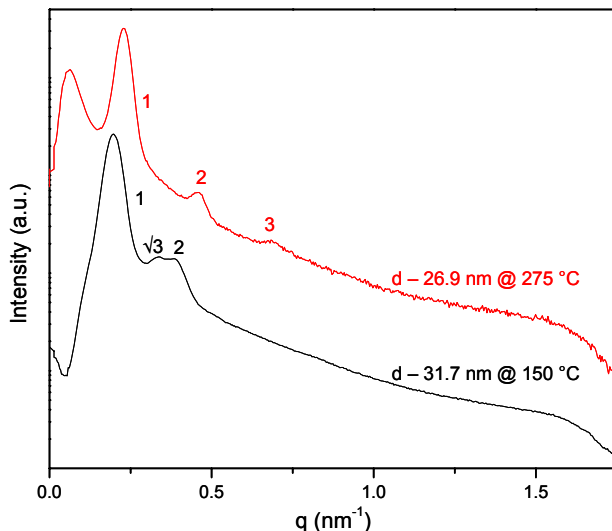


Figure 3.9. SAXS of E(65)B₃₅₀POSS₁₇ at different temperatures

Diblock copolymer E(63)B₆₃₂POSS₂₈ has a total molecular weight of 60,600 g/mol with relative volume fraction of EB:POSS of 0.62:0.38. The SAXS profile of E(63)B₆₃₂POSS₂₈ has two peaks, the first peak at $q^* = 0.128 \text{ nm}^{-1}$ with a d-spacing of 49.6 nm and second broad peak around $1.8q^*$ (Fig. 3.6c). The scattering profile of the sample does not clearly indicate the morphology of the block copolymer. The TEM image of the corresponding sample shows random lamellae of POSS in the PEB matrix (Fig. 3.7b).

The sample was again annealed at 150 °C for 48 h and quenched to room temperature. The quenched sample E(63)B₆₃₂POSS₂₈ is called q-E(63)B₆₃₂POSS₂₈. The SAXS profile of copolymer q-E(63)B₆₃₂POSS₂₈ has scattering ratio $q^* : 2q^*$ and a d-spacing of 46.8 nm (Fig. 3.10A). The TEM image of the sample shows lamellae morphology with good long range order (Fig. 3.10B).

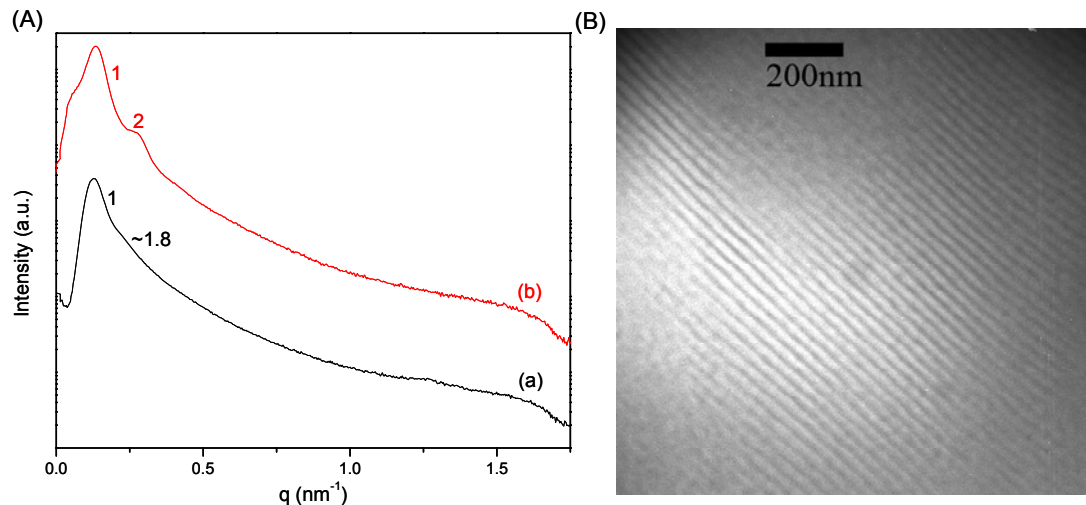


Figure 3.10. (A) SAXS of diblock copolymer (a) E(63)B₆₃₂POSS₂₈ and (b) quenched-E(63)B₆₃₂POSS₂₈ and (B) TEM image of quenched-E(63)B₆₃₂POSS₂₈.

The quenched sample has better order than the sample which was allowed to slowly cool to room temperature. The DSC result of slowly cooled diblock copolymer E(63)B₆₃₂POSS₂₈ (Fig. 3.11a) showed a melting peak of POSS at 105 °C and heat of melting ΔH 2.76 J/g whereas no melting point was observed for quenched copolymer q-E(63)B₆₃₂POSS₂₈ (Fig. 3.11b).

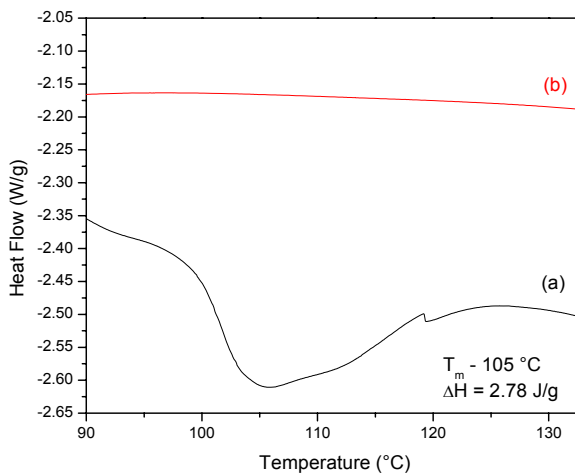


Figure 3.11. DSC plots of (a) E(63)B₆₃₂POSS₂₈ and (b) quenched - E(63)B₆₃₂POSS₂₈ diblock copolymer.

Formation of highly ordered lamellar structure at high temperature and random lamellar structure at room temperature can be explained by the crystallization in the POSS phase and dependence of morphology on χ of the polymer. During the slow cooling of the block copolymer, crystallization occurs in the phase separated melt domains of MAPOSS and EB phases. Due to the lower Gibbs free energy associated with crystallization, the crystallization is favored over the block copolymer morphologies. The block copolymer lamellar domains are disrupted by the crystallization, leading to formation of random lamellar structures in the slowly cooled samples.

Diblock copolymer E(72)B₁₀₇₂POSS₁₅ has a molecular weight of 70,100 g/mol with relative volume fraction of EB:POSS of 0.84:0.16. The SAXS profile of E(72)B₁₀₇₂POSS₁₅ has only one peak with the maximum at $q^* = 0.129 \text{ nm}^{-1}$ and the corresponding d-spacing is 48.6 nm (Fig. 3.6d). The TEM image of the corresponding sample shows the block copolymer has POSS spheres confined in a EB matrix (Fig. 3.7c). Due to the spherical shape of the POSS cage, it is difficult for POSS cubes to pack into spherical geometry. The absence of higher order peaks in the SAXS profile and the TEM image shows that the spheres do not pack in body centered cubic or face centered cubic arrangements.

Confirmation asymmetry (ε) can be estimated using the formula $\varepsilon = \beta_A/\beta_B$ where $\beta = v_o/b^2$ (v_o = statistical segmental volume and b = statistical segmental length).³³ In EB chain, the ethylene segment has 4 carbon units in the backbone and thus the segmental length (b_{ethylene}) would be approximately 0.5 nm whereas in the butylene segments there are 2 carbon units in the backbone and the segmental length (b_{butylene}) would be approximately 0.25 nm. The average segmental length of EB unit (b_{EB}) would be 0.375

nm. The POSS repeat unit with 2 carbon atoms would have b_{MAPOSS} of approximately 0.25 nm. Assuming that the statistical segmental volume is proportional to the length of the pendant unit, the length of EB unit with pendant butylene units would be approximately 0.25 nm and the length of MAPOSS unit would be 1.5 nm. Thus the ϵ for the diblock copolymer would be $\epsilon = (v_{\text{o(POSS)}}/v_{\text{o(EB)}})(b_{\text{EB}}^2/b_{\text{POSS}}^2)$, $\epsilon = (1.5/0.25)(0.375^2/0.25^2)$ i.e. $\epsilon = 13.5$.

3.3.3.5 Tensile testing

Mechanical studies were performed on copolymer E(72)B₁₀₇₂POSS₁₅ using a Instron 4411. Copolymer E(72)B₁₀₇₂POSS₁₅ contains flexible PEB block and hard MAPOSS (isobutyl) (block) and thus can be expected to show elastomeric character. Figure 3.12 shows the tensile test of three different samples of copolymer E(72)B₁₀₇₂POSS₁₅ having slightly different thickness and width and two different gauge lengths (4 mm and 8 mm).

The tensile testing result of copolymer E(72)B₁₀₇₂POSS₁₅ shows that the copolymer has ultimate tensile strength on the order of ~ 1 MPa and elongation at break in the range 40 - 52% (see Fig. 3.12). The modulus of the material is in the range 3.6 – 5.2 MPa. Modulus and tensile strength are both comparable to conventional SEBS polymers. The elongation of the copolymer E(72)B₁₀₇₂POSS₅ is lower at 50% which could be due to high ethylene content and crystallinity in PEB block. Preliminary mechanical results for copolymer E(72)B₁₀₇₂POSS₁₅ look promising even though the samples were not annealed nor were the processing conditions optimized. Systematic mechanical studies will be carried to study the mechanical response of these materials comparing them with conventional thermoplastic elastomers.

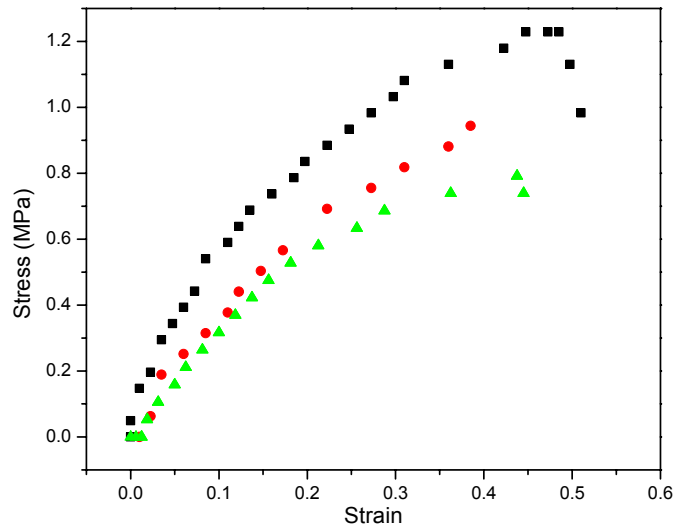


Figure 3.12. Tensile test of E(72)B₁₀₇₂POSS₁₅ sample.

3.4 Summary

Low PDI poly(ethylene-butylene) homopolymers and p(EB-*b*-MA-POSS(isobutyl)) diblock copolymers were synthesized by a combination of anionic polymerization and ATRP. Both phases of MA-POSS and EB crystallize depending upon the number of repeat units of MAPOSS and 1,4-content in the EB chains. Three different morphologies i.e. cylinders, lamellae and spheres of the semicrystalline diblock copolymer were obtained by changing the relative volume fractions of EB and POSS phases. Inverse cylindrical morphology was observed, with majority 60 volume % EB block forming the cylindrical phase while the minor MAPOSS phase occupies the periphery around the cylinder. This is presumably was due to conformational asymmetry or relative flexibility of the phases. Crystalline lamellar morphology was obtained due to the crystallization of the POSS cubes or due to high χ values. Further investigations are ongoing to study the morphology of the block copolymers under different annealing conditions, different crystalline content and lowering EB volume fractions.

3.5 References

- (1) Rubner, M. *Nature* **2003**, *423*, 925-926.
- (2) Capadona, J. R.; Shanmuganathan, K.; Tyler, D. J.; Rowan, S. J.; Weder, C. *Science* **2008**, *319*, 1370-1374.
- (3) Whitesides, G. M.; Grzybowski, B. *Science* **2002**, *295*, 2418-2421.
- (4) Donald, A. M. *Materials Today* **2005**, *8*, 56.
- (5) Sanchez, C.; Arribart, H.; Guille, M. M. G. *Nature Materials* **2005**, *4*, 277-288.
- (6) <http://www.egr.msu.edu/cmsc/>.
- (7) Sanchez, C.; Julian, B.; Belleville, P.; Popall, M. *Journal of Materials Chemistry* **2005**, *15*, 3559-3592.
- (8) Hawker, C. J.; Russell, T. P. *Mrs Bulletin* **2005**, *30*, 952-966.
- (9) Li, G. Z.; Wang, L. C.; Ni, H. L.; Pittman, C. U. *Journal of Inorganic and Organometallic Polymers* **2001**, *11*, 123-154.
- (10) Lee, A.; Lichtenhan, J. D. *Journal of Applied Polymer Science* **1999**, *73*, 1993-2001.
- (11) Lee, A.; Lichtenhan, J. D. *Macromolecules* **1998**, *31*, 4970-4974.
- (12) Leu, C. M.; Chang, Y. T.; Wei, K. H. *Macromolecules* **2003**, *36*, 9122-9127.
- (13) Gilman, J. W.; Schlitzer, D. S.; Lichtenhan, J. D. *Journal of Applied Polymer Science* **1996**, *60*, 591-596.
- (14) Kopesky, E. T.; Haddad, T. S.; Cohen, R. E.; McKinley, G. H. *Macromolecules* **2004**, *37*, 8992-9004.
- (15) Pyun, J.; Matyjaszewski, K.; Wu, J.; Kim, G. M.; Chun, S. B.; Mather, P. T. *Polymer* **2003**, *44*, 2739-2750.

- (16) Miao, J. J.; Cui, L.; Lau, H. P.; Mather, P. T.; Zhu, L. *Macromolecules* **2007**, *40*, 5460-5470.
- (17) Zheng, L.; Hong, S.; Cardoen, G.; Burgaz, E.; Gido, S. P.; Coughlin, E. B. *Macromolecules* **2004**, *37*, 8606-8611.
- (18) Drazkowski, D. B.; Lee, A.; Haddad, T. S.; Cookson, D. J. *Macromolecules* **2006**, *39*, 1854-1863.
- (19) Matejka, L.; Strachota, A.; Plestil, J.; Whelan, P.; Steinhart, M.; Slouf, M. *Macromolecules* **2004**, *37*, 9449-9456.
- (20) Waddon, A. J.; Coughlin, E. B. *Chemistry of Materials* **2003**, *15*, 4555-4561.
- (21) Hirai, T.; Leolukman, M.; Hayakawa, T.; Kakimoto, M.; Gopalan, P. *Macromolecules* **2008**, *41*, 4558-4560.
- (22) Hadjichristidis, N.; Iatrou, H.; Pispas, S.; Pitsikalis, M. *Journal of Polymer Science Part a-Polymer Chemistry* **2000**, *38*, 3211-3234.
- (23) Cardoen, G. B., K.; Emrick T.; Coughlin E.B. *Macromolecules* **2006**, *39*, 7170-7173.
- (24) Hsieh, H. L.; Quirk, R. P.; Editors *Anionic Polymerization : Principles And Practical Applications 1st Edition*, 1996.
- (25) Halasa, A. F.; Lohr, D. F.; Hall, J. E. *Journal of Polymer Science Part a-Polymer Chemistry* **1981**, *19*, 1357-1360.
- (26) Antkowiak, T.; Tate, D. P.; Oberster, A. E.; Halasa, A. F. *Journal of Polymer Science Part a-1-Polymer Chemistry* **1972**, *10*, 1319-&.

- (27) Frankland, J. A.; Edwards, H. G. M.; Johnson, A. F.; Lewis, I. R.; Poshyachinda, S. *Spectrochimica Acta Part a-Molecular and Biomolecular Spectroscopy* **1991**, *47*, 1511-1524.
- (28) Uraneck, C. A. *Journal of Polymer Science Part a-1-Polymer Chemistry* **1971**, *9*, 2273-&.
- (29) Hahn, S. F. *Journal of Polymer Science Part a-Polymer Chemistry* **1992**, *30*, 397-408.
- (30) Singha, N. K.; Mohandas, T. P. *Journal of Macromolecular Science-Pure and Applied Chemistry* **1997**, *A34*, 2269-2278.
- (31) Castillo, R. V.; Muller, A. J.; Lin, M. C.; Chen, H. L.; Jeng, U. S.; Hillmyer, M. A. *Macromolecules* **2008**, *41*, 6154-6164.
- (32) Hamley, I. W. In *Interfaces Crystallization Viscoelasticity* 1999; Vol. 148, p 113-137.
- (33) Matsen, M. W.; Bates, F. S. *Journal of Polymer Science Part B-Polymer Physics* **1997**, *35*, 945-952.
- (34) Milner, S. T. *Macromolecules* **1994**, *27*, 2333-2335.
- (35) Vavasour, J. D.; Whitmore, M. D. *Macromolecules* **1993**, *26*, 7070-7075.
- (36) Gehlsen, M. D.; Bates, F. S. *Macromolecules* **1994**, *27*, 3611-3618.
- (37) Bates, F. S.; Fredrickson, G. H. *Macromolecules* **1994**, *27*, 1065-1067.
- (38) Gido, S. P.; Schwark, D. W.; Thomas, E. L.; Goncalves, M. D. *Macromolecules* **1993**, *26*, 2636-2640.
- (39) Grason, G. M.; Kamien, R. D. *Macromolecules* **2004**, *37*, 7371-7380.

- (40) Chiang, W. S.; Lin, C. H.; Yeh, C. L.; Nandan, B.; Hsu, P. N.; Lin, C. W.; Chen, H. L.; Chen, W. C. *Macromolecules* **2009**, *42*, 2304-2308.

CHAPTER 4

SYNTHESIS AND MORPHOLOGICAL STUDIES OF POSS CONTAINING ORGANIC – INORGANIC TRIBLOCK COPOLYMERS

4.1 Introduction

Nature has combined organic and inorganic compounds to produce materials with synergistic properties showing extraordinary strength, toughness, hardness and functionality.¹⁻³ Nacre of shell is one of the most studied material displaying very high strength, toughness and hardness due to the brick and mortar structural arrangement of inorganic calcium carbonate platelets and organic proteins.¹ Other examples include the skeleton of sponge and diatoms formed by the self-assembly of organic–inorganic components and produce superior material properties for precise functions.^{2,4}

Material scientist, inspired by nature, are trying to combine dissimilar materials which could lead to novel functions giving access to a wider spectrum of applications.⁵ A number of approaches (bottom-up and top-down) have been developed to combine organic and inorganic materials.^{6,7} Clay composites produced by top-down approaches are one of the most widely studied hybrid materials.⁸ Exfoliated structures of the composites lead to superior thermal and mechanical properties.⁹ However, the top-down approach is an energy intensive approach and does not offer control over the molecular and supramolecular architectures which control the macroscopic properties of the nanocomposites. It also suffers from serious limitations of non-uniform dispersion of the clay in the organic matrix leading to non-uniform properties. On the other hand, the bottom-up approach covalently combines organic-inorganic materials to form truly molecular dispersed nanocomposites with complete control over the molecular

architecture. Sol-gel the most widely used bottom-up approach is an extremely cost effective technique leading to molecular dispersed nanocomposites.¹⁰ However it does not offer complete control over the mesoscopic scale that is at length scale of tens to hundreds of nanometers. Other bottom-up approaches like self-assembly and templated-assembly have gained importance as they offer control over mesoscopic length scales.⁴ Self-assembly of block copolymers offer control over the nanometer length scales and provides a mean to make hierarchical structures for various applications.^{11,12} Self-assembly of block copolymers is formed by weak non-covalent interactions between the polymer segments of the block copolymer leading to phase segregation and thus forming different morphologies in both bulk and solution.^{12,13}

In this thesis, we describe the use of Polyhedral Oligomeric Silsesquioxanes (POSS) as nanoscopic inorganic building blocks in triblock copolymers to generate hybrid organic-inorganic materials. Silsesquioxanes are regarded as one of the most promising and rapidly emerging nanobuilding blocks in the field of organic-inorganic nanocomposites.¹⁴ A common molecular formula of POSS is $R_7(SiO_{1.5})_8X$. It has an inorganic core that resembles silica with eight silicon atoms bridged by twelve oxygen atoms; core has dimensions comparable to polymer segments and coils. It has seven organic substituents which make it compatible with monomers/polymers and one reactive group (X) which can be used for polymerization or grafting. POSS monomers act as spheres or cubes and arrange in one plane on hexagonal arrays.^{15,16} POSS has been successfully incorporated as filler for material reinforcement in several different polymeric systems to improve the mechanical, thermal and other properties.^{17,18} However it is difficult to obtain uniform dispersion of POSS in the matrix and this leads to non-

uniform macroscopic properties. POSS has also been covalently bonded to polymers such as epoxy resins,¹⁹ polyimides,²⁰ polyethylenes,²¹ polystyrenes²¹ and polynorbornenes.⁶ However, as of today, only a few reports are concerned with utilizing POSS as a building block to generate mesoscopically-ordered structures.^{6,22} POSS lamellae were observed in random copolymers of POSS with epoxy resins and polyimides.^{19,20} However, the lamellae were not continuous and their length was less than 100 nm. Formation of lamellae as explained by simulations was due to strong face-to-face packing of bulky POSS groups.²³ Zheng et al. have synthesized random copolymers of POSS and butadiene by ring-opening metathesis polymerization (ROMP) and experimentally observed raft structures due to the tendency of POSS particles to pack face-to-face.²¹ Pyun et al. have used atom transfer radical polymerization (ATRP) to synthesize p[(MA-POSS)-*b*-(n-butylacrylate)-*b*-(MA-POSS)] (ABA) triblock copolymers.⁶ Microphase separation and cylindrical structures could be observed for samples with a higher POSS content. A similar synthetic strategy was adopted by Intasanta et al. to synthesize diblock copolymers of POSS and poly(methyl methacrylate).²⁴ It was hypothesized that because of the steric hindrance of bulky POSS group, maximum number of repeat units of POSS that can be polymerized by ATRP is 10. Recently, Hirai *et al.* synthesized POSS diblocks with either poly(methyl methacrylate) or polystyrene and observed POSS lamellae with very good long range order.²²

In the present work, we report the synthesis of a series of p(MA-POSS(isobutyl)-*b*-Styrene-*b*-MA-POSS(isobutyl)) triblock copolymers and study the block copolymer morphologies by varying the volume fractions of MA-POSS and polystyrene (PS). Telechelic hydroxyl-terminated polystyrene homopolymers for the central block were

synthesized by anionic polymerization. These were subsequently allowed to react with α -bromoisobutyryl bromide to form α - ω difunctional macroinitiators for ATRP. A methacrylate functionalized POSS was then polymerized by ATRP. The resulting triblock copolymers have been fully characterized and the resulting morphologies investigated.

4.2 Experimental Section

4.2.1 Materials

The purification of styrene (99%), benzene (99.9%+) (both from Aldrich) to the standards required for anionic polymerization has been described elsewhere.²⁵ *t*-Butyldimethylsiloxypropyl lithium (0.5 M) in hexane (from FMC Lithium) was used as received. Tetrabutyl ammonium fluoride (1.0 M) (TBAF) in THF, pyridine, N,N,N',N',N''-pentamethyldiethyltriamine (PMDETA) (99%+), Cu(I)Cl (99.99%+), Cu(II)Br (99.99%), 3-(3,5,7,9,11,13,15-heptaioisbutylpentacyclo[9.5.1(3,9).1(5,15).1(7,13)] octasiloxan-1-yl)propyl methacrylate [Ma-POSS (isobutyl)] (all from Aldrich) were used as received. α -Bromoisobutyrylbromide, triethylamine were dried over CaH₂, distilled and stored under N₂ atmosphere, THF was distilled over sodium/benzophenone mixture (all from Aldrich). Ethylene oxide (from Fluka) was purified over *n*-butyl lithium using a manifold as described earlier.²⁶

4.2.2 Synthesis

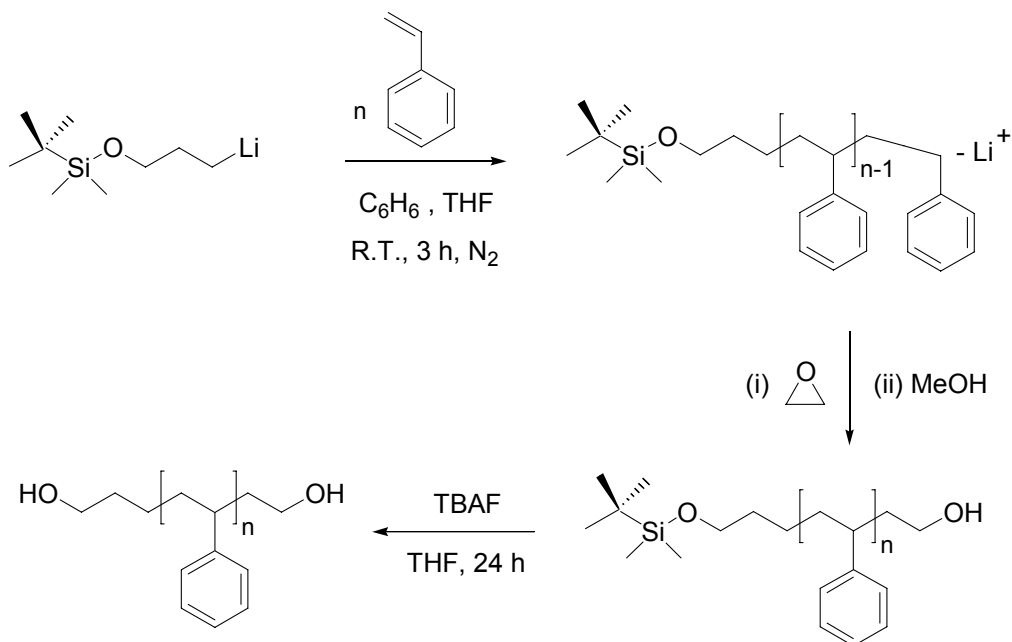
4.2.2.1 Synthesis of Hemi-telechelic Polystyrene

Dry benzene (300 mL) was cannulae transferred into a 500 mL round bottom flask under dry nitrogen. Dry THF (2.2 mL, 0.027 mol) and styrene (30 mL, 0.260 mol) were then cannulae transferred into the flask. The reaction solution was titrated with *t*-butyldimethylsiloxypropyl lithium initiator until a light yellow color appeared followed by immediate addition of the desired quantity of *t*-butyldimethylsiloxypropyl lithium (5.32 mL, 2.71 mmol) to achieve the target molecular weight. The molar ratio of THF:initiator was 10:1. The reaction was performed at room temperature for 4 hours. Ethylene oxide (0.59 g, 13.58 mmol), purified over *n*-butyl lithium, was transferred into the reaction flask using a manifold as described earlier.²⁶ The reaction was continued for 30 min and terminated by addition of methanol. The polymer was precipitated in cold methanol, filtered and vacuum dried. Yield 26 g of a white powder (96%). ¹H NMR (CDCl₃, 400 MHz): δ 0.2 (s, 6H, Si(CH₃)₂C(CH₃)₃), 0.9 (s, 9H, Si(CH₃)₂C(CH₃)₃), 1.1 (m, 2H, SiOCH₂CH₂CH₂), 1.2 – 2.2 (m, 3H, -CH₂CH(C₆H₅)), 1.48 (m, 2H, SiOCH₂CH₂CH₂), 1.77 (m, 2H, CH₂CH₂OH), 3.4 (t, 1H, CH₂CH₂OH), 3.5 (m, 2H, CH₂CH₂OH), 3.5 (m, 2H, SiOCH₂CH₂CH₂), 6.3 – 7.4 (m, 5H, aromatic protons).

4.2.2.2 Deprotection of Siloxyl group

Hemi-telechelic polystyrene (M_n 5,000 g/mol, 10 g, 2.0 mmol) was dissolved in THF (50 mL). TBAF (2 mL, 2.0 mmol) was added and the cleavage reaction was conducted at room temperature for 24 hours. The reaction product was then passed through the column of silica with THF as solvent and then precipitated in cold methanol.

Yield 9.3 g of a white powder (93%). $^1\text{H NMR}$ (CDCl_3 , 400 MHz): δ 1.1 (m, 2H, $\text{HOCH}_2\text{CH}_2\text{CH}_2$), 1.2 – 2.2 (m, 3H, $-\text{CH}_2\text{CH}(\text{C}_6\text{H}_5)$), 1.48 (m, 2H, $\text{HOCH}_2\text{CH}_2\text{CH}_2$), 1.77 (m, 2H, $\text{CH}_2\text{CH}_2\text{OH}$), 3.5 (m, 2H, $\text{CH}_2\text{CH}_2\text{OH}$), 3.5 (m, 2H, $\text{HOCH}_2\text{CH}_2\text{CH}_2$), 3.7 (t, 2H, $\text{HOCH}_2\text{CH}_2\text{CH}_2$), 3.7 (t, 1H, $\text{CH}_2\text{CH}_2\text{OH}$), 6.3 – 7.4 (m, 5H aromatic protons) ppm.



Scheme 4.1. Synthesis of hemi-telechelic and telechelic polystyrene.

4.2.2.3 Synthesis of Polystyrene Macroinitiator

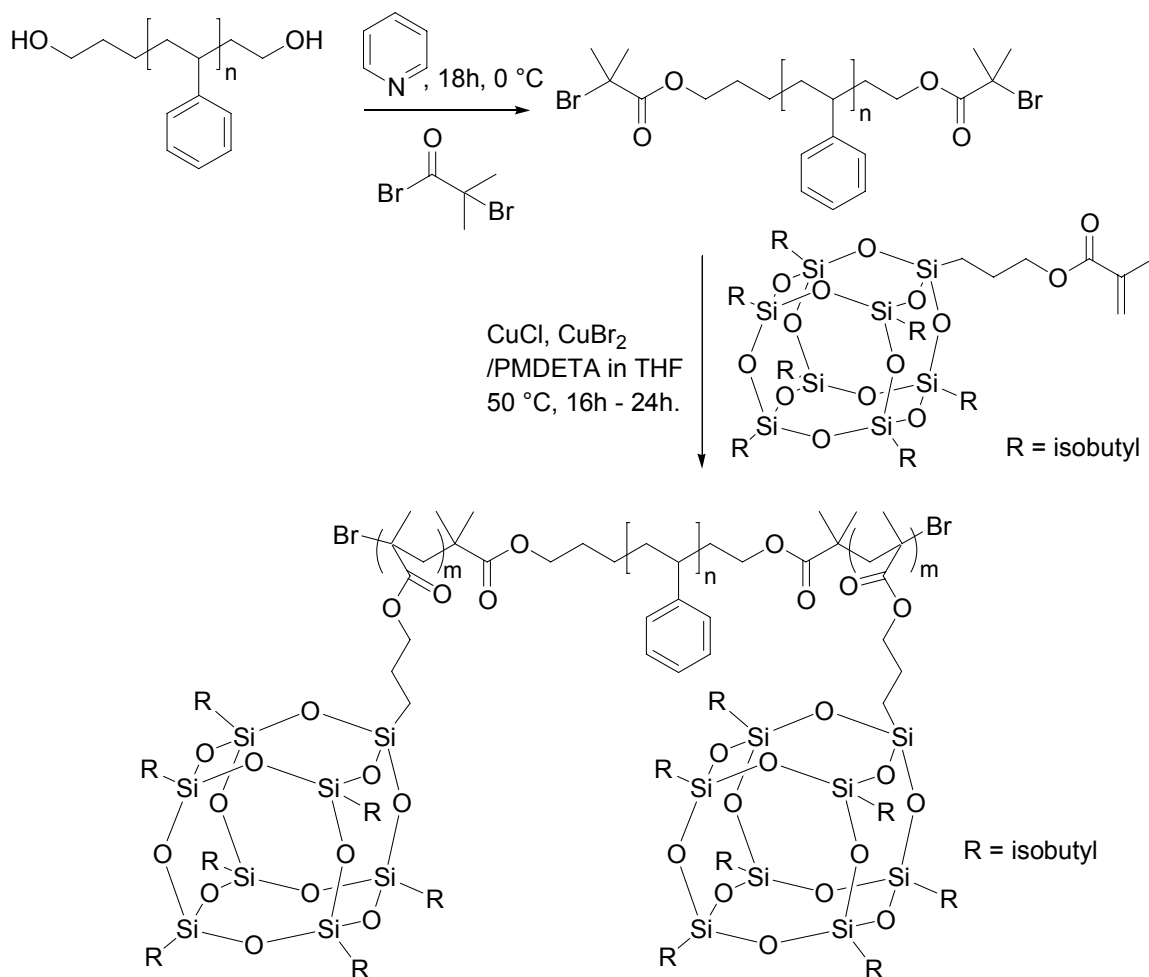
Telechelic polystyrene (M_n 5000 g/mol, 1 g, 0.2 mmol) was dissolved in pyridine (50 mL), the temperature was reduced to 0 °C and α -bromoisobutyryl bromide (4.6 mL, 0.2 mol) was added dropwise to the flask over 15 min. The contents of the flask immediately turned milky yellow. After stirring for 24 hours, the reaction solution was dissolved in 100 mL methylene chloride. The solution was washed with water (2 x 25 mL), 1% HCl solution (2 x 25 mL) and water (1 x 20 mL) and then filtered over a plug of silica with THF as eluent. The product was precipitated in cold methanol and vacuum

dried. Yield 0.71 g of a white powder (71%). $^1\text{H NMR}$ (CDCl_3 , 400 MHz): δ 1.1 (m, 2H, $\text{OCOCH}_2\text{CH}_2\text{CH}_2$), 1.2 – 2.2 (m, 3H, $-\text{CH}_2\text{CH}(\text{C}_6\text{H}_5)$), 1.29 (s, 6H, $-(\text{CH}_3)_2\text{CBr}$), 1.48 (m, 2H, $\text{OCOCH}_2\text{CH}_2\text{CH}_2$), 1.77 (m, 2H, $\text{CH}_2\text{CH}_2\text{OCO}$), 3.5 (m, 2H, $\text{CH}_2\text{CH}_2\text{OCO}$), 3.5 (m, 2H, $\text{OCOCH}_2\text{CH}_2\text{CH}_2$), 6.3 – 7.4 (m, 5H aromatic protons) ppm.

4.2.2.4 Synthesis of p(MA-POSS(isobutyl)-*b*-Styrene-*b*-MA-POSS(isobutyl)) triblock copolymers

To an oven dried 10 mL round bottom flask was added polystyrene macroinitiator (M_n 5,000 g/mol, 0.2 g, 0.04 mmol), MA-POSS(isobutyl) (1.509 g, 1.6 mmol), PMDETA (16.72 μL , 0.08 mmol) and THF (1.5 ml). Three freeze-pump-thaw cycles were performed. CuCl (7.9 mg, 0.08 mmol), CuBr₂ (1.7 mg, 10 mol% relative to CuCl) were added to the mixture and again three freeze-pump thaw cycles were performed.

Polymerization was carried out for 24 hours at 50 °C. The reaction solution was then diluted with 10 ml THF and passed through a column of neutral alumina to remove excess catalyst. The colorless transparent solution was concentrated by evaporation. The polymer was then precipitated in methanol. The polymer was vacuum dried. Yield 0.95 g of a white powder (52.7%). $^1\text{H NMR}$ (CD_2Cl_2 , 400 MHz): δ 0.54 (d, 112H, $\text{SiCH}_2\text{CH}(\text{CH}_3)_2$), 0.58 (t, 16H $\text{SiCH}_2\text{CH}_2\text{CH}_2\text{OC}(\text{O})-$), 1.01 (d, 336H, $\text{SiCH}_2\text{CH}(\text{CH}_3)_2$), 1.29 (s, 6H, $-(\text{CH}_3)_2\text{C}$), 1.34 (s, 24H, $-\text{CH}_2\text{C}(\text{CH}_3)_2$), 1.6 (m, 16H $\text{SiCH}_2\text{CH}_2\text{CH}_2\text{OC}(\text{O})-$), 1.8 (m 42H, $\text{SiCH}_2\text{CH}(\text{CH}_3)_2$), 1.91 (s, 16H, $-\text{CH}_2\text{C}(\text{CH}_3)_2$), 3.72 (t, 2H $\text{CH}_2\text{CH}_2\text{OC}(\text{O})-$), 3.76 (t, 2H, $-\text{OCH}_2\text{CH}_2\text{N}-$), 3.90 (t, 2H, $-\text{NCH}_2-$), 3.9 (t, 16H $\text{SiCH}_2\text{CH}_2\text{CH}_2\text{OC}(\text{O})-$), 4.27 (t, 2H, $-\text{CH}_2\text{OC}(\text{O})-$), 7.70 – 7.86 (m, 4H, aromatic protons) ppm.



Scheme 4.2. Synthesis of polystyrene macroinitiator and p(MA-POSS(isobutyl))-*b*-Styrene-*b*-MA-POSS(isobutyl)) triblock copolymers.

4.2.2.5 Synthesis of PMMA-POSS samples

To an oven dried 10 ml Schlenk flask was added Cu(I)Cl (20.4 mg, 0.211 mmol), THF (0.5ml) and PMDETA (44 μ l, 0.211 mmol). The mixture was stirred for 10 min. MAPoss(isobutyl) (2.00 g, 2.12 mmol), initiator N-2-(2-(2-bromoisobutyryloxy)ethoxy)ethyl phthalimide (81.2mg, 0.211 mmol) (synthesized as described by Lecolley et al.) and THF (1mL) were added to the flask and three freeze-pump thaw cycles were performed.²⁷ Polymerization was carried out for 16 hours at 50 $^\circ$ C. The reaction solution was then diluted with 10 mL THF and passed through a column

of neutral alumina to remove catalyst. The colorless and transparent solution was concentrated by evaporation. The polymer was then precipitated in methanol. Unreacted monomer was then removed by Soxhlet extraction in methanol for 3 days. The polymer was vacuum dried. Yield: 1.65g of a white powder (85%, 0.12 mmol).

^1H NMR (CDCl_3 , 300 MHz): δ 0.54 (d, 112H, $\text{SiCH}_2\text{CH}(\text{CH}_3)_2$), 0.58 (t, 16H $\text{SiCH}_2\text{CH}_2\text{CH}_2\text{OC}(\text{O})-$), 1.01 (d, 336H, $\text{SiCH}_2\text{CH}(\text{CH}_3)_2$), 1.29 (s, 6H, $-(\text{CH}_3)_2\text{C}$), 1.34 (s, 24H, $-\text{CH}_2\text{C}(\text{CH}_3)$), 1.6 (m, 16H $\text{SiCH}_2\text{CH}_2\text{CH}_2\text{OC}(\text{O})-$), 1.8 (m 42H, $\text{SiCH}_2\text{CH}(\text{CH}_3)_2$), 1.91 (s, 16H, $-\text{CH}_2\text{C}(\text{CH}_3)$), 3.72 (t, 2H $\text{CH}_2\text{CH}_2\text{OC}(\text{O})-$), 3.76 (t, 2H, $-\text{OCH}_2\text{CH}_2\text{N}-$), 3.90 (t, 2H, $-\text{NCH}_2-$), 3.9 (t, 16H $\text{SiCH}_2\text{CH}_2\text{CH}_2\text{OC}(\text{O})-$), 4.27 (t, 2H, $-\text{CH}_2\text{OC}(\text{O})-$), 7.70 – 7.86 (m, 4H aromatic protons) ppm. Gel permeation chromatography using THF as mobile phase gave M_n of 6500 g/mol ($X=7$) and PDI of 1.05. IR 2953, 1729 (ester C=O stretch), 1464, 1383, 1366, 1332, 1228, 1087 (Si-O stretch), 836, 739 cm^{-1} .

4.2.3 Polymer Characterization

Gel permeation chromatography (GPC): GPC measurements were performed in tetrahydrofuran (THF) at 1.0 mL/min using a Knauer K-501 pump with a K-2301 refractive index detector and K-2600 UV detector, and a column bank consisting of two Polymer Labs PLGel Mixed D columns at 40°C. Molecular weights are reported relative to polystyrene standards (Polymer Labs, Inc.). Preparative GPC was carried out in THF at 5 mL/min using a pump (HP Series 1050) with a refractive index detector (HP 1047A) and one Polymer Labs ResiPore 3 μm (300 x 7.5 mm) columns. THF solutions containing 25 mg/mL of polymers were used.

Nuclear magnetic resonance (NMR): All NMR spectra were collected on Bruker 400 MHz instrument and obtained from either CDCl_3 solutions or CD_2Cl_2 solutions. ^1H NMR spectra were referenced to either residual CHCl_3 at 7.26 ppm or residual CH_2Cl_2 at 5.30 ppm. ^{13}C NMR spectra were recorded on 400 MHz and were referenced to residual CHCl_3 at 77.16 ppm

Infrared (IR) spectroscopy: Infrared spectra were obtained on a Perkin-Elmer Spectrum One FTIR spectrometer equipped with an ATR accessory. The spectra were obtained on vacuum dried bulk samples.

Thermogravimetric analysis (TGA): TGA was carried out using a TA Instruments TGA 2950 thermogravimetric analyzer with a heating rate of $10^\circ\text{C}/\text{min}$ from room temperature to 800°C or 750°C under air at a flow rate of $40\text{ mL}/\text{min}$.

Differential Scanning Calorimetry (DSC): Samples for DSC were thermally annealed at 150°C and allowed to cool to room temperature over a period of 3h. DSC was performed on TA Instruments DSC Q1000 and the heating and cooling rates of the sample were $10^\circ\text{C}/\text{min}$.

Small angle X-ray scattering (SAXS), wide angle X-ray scattering (WAXS) and Transmission Electron Microscopy (TEM): Samples for SAXS, WAXS and TEM were cast from concentrated solutions of polymer in toluene and then thermally annealed at 150°C under vacuum for two days. SAXS and WAXS were performed using Ni-filtered $\text{Cu K}\alpha$ radiation ($\lambda=1.54\text{ \AA}$) from a Rigaku rotating anode (operated at 60 kV, 45 mA). The X-ray was collimated by a set of three pinholes. A CCD detector (Siemens Hi-Star), located at a camera length of 1192.5 mm was used to record SAXS patterns. A photographic plate kept at a distance of 139 mm was used to collect WAXS patterns.

Samples for electron microscopy were prepared by microtoming the annealed samples at room temperature using a diamond knife. Approximately 50-100 nm thick sections were collected. TEM studies were performed using a JEOL 2000CX transmission electron microscope operated at 200 kV. No staining of the samples was performed.

Static Light Scattering (SLS): SLS experiments were performed at room temperature using an ALV unit equipped with an ALV/SP-125 precision goniometer (ALV-Laser Vertiebsgesellschaft m.b.h., Langen, Germany), an Innova 70 argon laser ($\lambda = 514.5$ nm, maximum power 3 W, Coherent Inc.) operated at 300 mW, and a photomultiplier detector (Thorn EMI Electron Tubes). Signal from the detector was processed by an ALV5000 Multiple Tau Digital Correlator board and associated software. The sample was vacuum dried prior to use. Four different samples having different concentrations (2.0, 3.0, 4.0 and 5.0 mg/mL) were prepared by using HPLC grade toluene as solvent. Each sample was analyzed at eight different angles (40° , 50° , 60° , 70° , 80° , 90° , 100° and 110°).

Determination of Specific Refractive Index Increments (dn/dc): The specific refractive index measurement of MA-POSS (isobutyl) homopolymer was determined on a Wyatt Optilab rEX refractive index detector, operating at laser wavelength of 685.0 nm and 25°C . The sample was vacuum dried prior to use. Five different concentrations (1.0, 2.0, 3.0, 4.0, and 5.0 mg/mL) were prepared using toluene as solvent. Sample preparation was done according to the same procedure used for the SLS experiment. Samples were introduced at 1.0 ml/min rate to the RI detector at ambient conditions using a syringe pump. The dn/dc values were determined by using Wyatt Astra V software.

4.3 Results and Discussions

4.3.1 Synthesis of Hemi-telechelic & Telechelic Polystyrene

Anionic polymerization was chosen to synthesize hemi-telechelic polystyrene because of the ability to precisely control the molecular weight and obtain narrow polydispersities. A common method to synthesize difunctional monomodal polymers by anionic polymer require difunctional initiators and high vacuum polymerization techniques.^{6,28} An alternative approach was used, in which monofunctional *t*-butyldimethylsiloxy propyl lithium was used as the initiator and the polymerization of styrene was performed under an inert atmosphere. The polystyryl anion was end-capped with ethylene oxide and then terminated with methanol. This procedure provides a hemi-telechelic polystyrene block with the *t*-butyldimethylsiloxy (TBDMS) protecting group on one end and a hydroxyl group on the other end (Scheme 1).

To accelerate the initiation step, THF was added to the reaction, the hexameric aggregates of *n*-butyllithium in benzene are broken into dimeric aggregates in the presence of THF thereby lowering both reaction times and polydispersity.²⁹ Three different samples of hemi-telechelic-polystyrene i.e. M_n 5,000, 15,000 and 40,000 g/mol with low polydispersities (PDI<1.1) were obtained (Table 4.1). The hemi-telechelic polystyrenes were reacted with tetrabutyl ammonium fluoride (TBAF) to cleave the TBDMS protecting group (Scheme 4.1). The deprotection of hemi-telechelic PS to telechelic PS was confirmed by IR and ¹H NMR spectroscopy. In IR spectroscopy (Fig. 4.1) the Si-CH₃ stretching band at 840 cm⁻¹ and in ¹H NMR (Fig. 4.2) the *t*-butyl peaks at $\delta = 0.9$ ppm and dimethyl peaks at $\delta = 0.3$ ppm of hemi-telechelic polystyrene disappear

after the deprotection with TBAF indicating complete deprotection of the protecting group.

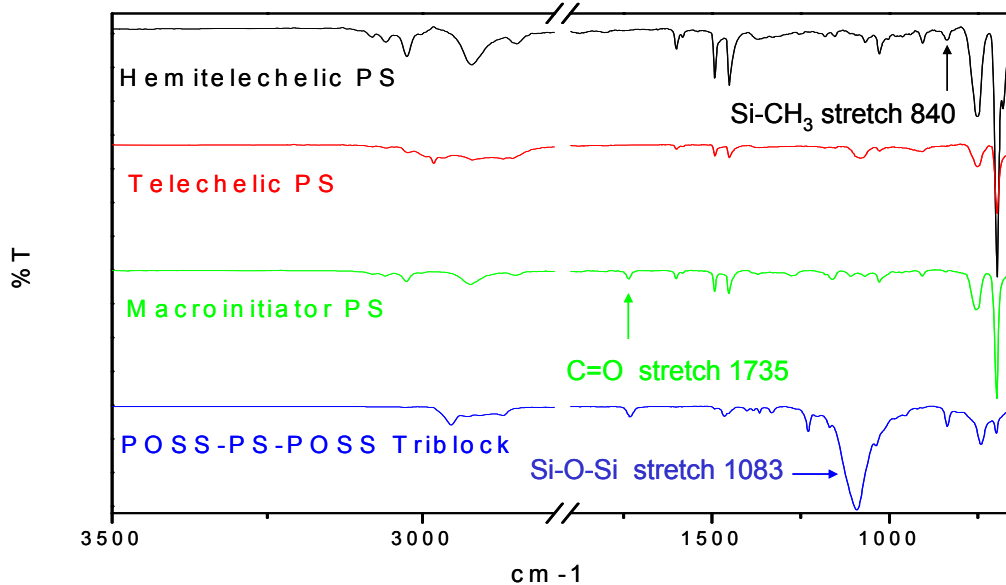


Figure 4.1. IR of (top to bottom) hemi-telechelic polystyrene, telechelic polystyrene, polystyrene macroinitiator and p(MA-POSS(isobutyl)-*b*-Styrene-*b*-MA-POSS(isobutyl)) triblock copolymers.

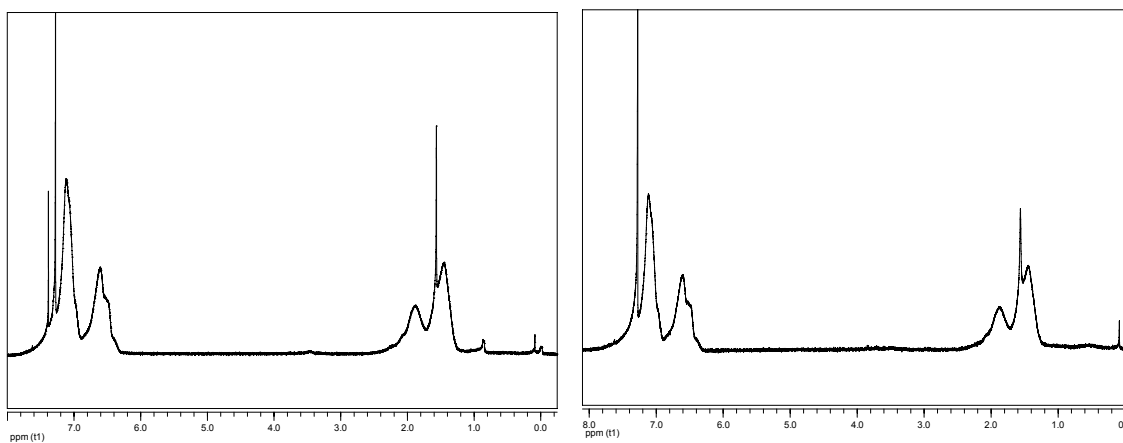


Figure 4.2. ¹H NMR of (left) hemi-telechelic (PS) and (right) telechelic PS.

Table 4.1. Molecular weights of polystyrene and p(MA-POSS(isobutyl)-*b*-Styrene-*b*-MA-POSS(isobutyl)) triblock copolymers.

No.	Sample	M_n Polystyrene g/mol (PDI) ^a	M_n p(MA- POSS(isobutyl) - <i>b</i> -Styrene- <i>b</i> - MA- POSS(isobutyl)) (PDI) ^b	$N_{(\text{Styrene})}$	$N_{(\text{POSS})}$	$f_{(\text{polystyrene})}$
1	POSS ₆ -S ₄₈ - POSS ₆	5,000 (1.1)	16,320 (1.2)	48	12	0.32
2	POSS ₁₀ -S ₁₃₀ - POSS ₁₀	13,500 (1.06)	32,370 (1.1)	130	20	0.43
3	POSS ₈ -S ₁₃₀ - POSS ₈	13,500 (1.06)	28,600 (1.1)	130	16	0.49
4	POSS _{13.5} - S ₃₈₄ - POSS _{13.5}	40,000 (1.03)	65,480 (1.04)	384	27	0.63

a: Molecular weight determined by GPC, b: Molecular weight determined by ¹H NMR, N is number of repeat units, *f* is the volume fraction, assuming a density of polystyrene – 1.05 g/cc and density of MA-POSS (isobutyl) – 1.15 g/cc (by ASTM D792-00).

4.3.2 Synthesis of Polystyrene Macroinitiator and p(MA-POSS(isobutyl)-*b*-Styrene-*b*-MA-POSS(isobutyl)) Triblock Copolymer

The hydroxyl terminated telechelic polystyrene was allowed to react with α -bromoisobutyryl bromide in pyridine to obtain a α - ω difunctional polystyrene ATRP macroinitiators (Scheme 4.2).

The formation of macroinitiators were monitored by ¹H NMR, the resonances for the methylene protons α to the hydroxyl group in telechelic PS shift from δ 3.4 to δ 4.0 ppm indicating the formation of an ester bond and no peak is observed at δ 3.4 ppm after

the reaction indicating consumption of the starting material. The formation of the difunctional macroinitiators was further confirmed by IR spectroscopy, the band at 1735 cm^{-1} confirmed the presence of the newly formed carbonyl (C=O) groups (Fig. 4.1). Methacrylate functionalized POSS monomer was polymerized by ATRP using standard conditions and the α - ω difunctional macroinitiator. Previous work in our group,²⁴ and by others have shown that due to the steric hindrance, the number of repeat units of MA-POSS that can be attached by ATRP is limited to approximately 10.⁶ However, we have now found that the use of copper(II) bromide as a co-catalyst in ATRP allows for an increase of the number of repeat units of POSS above 10 and also results in a lowering of the PDI. Triblock copolymers of p(MA-POSS(isobutyl)-*b*-Styrene-*b*-MA-POSS(isobutyl)) were obtained that have PDI values lower than 1.3. The ATRP reactions were monitored by ^1H NMR, as the reaction progressed, the intensity of the vinyl protons of the MA-POSS monomer at δ 5.6 ppm and δ 6.1 ppm decreased, thus by comparing the vinyl resonances of the monomer with the aromatic resonances of PS macro-double initiator the percentage of monomer consumption was calculated. The GPC traces of polystyrene of molecular weight M_n 5,000 g/mol and p(MA-POSS(isobutyl)-*b*-Styrene-*b*-MA-POSS(isobutyl)) of molecular weight M_n 16,500 g/mol are shown in Fig. 4.3.

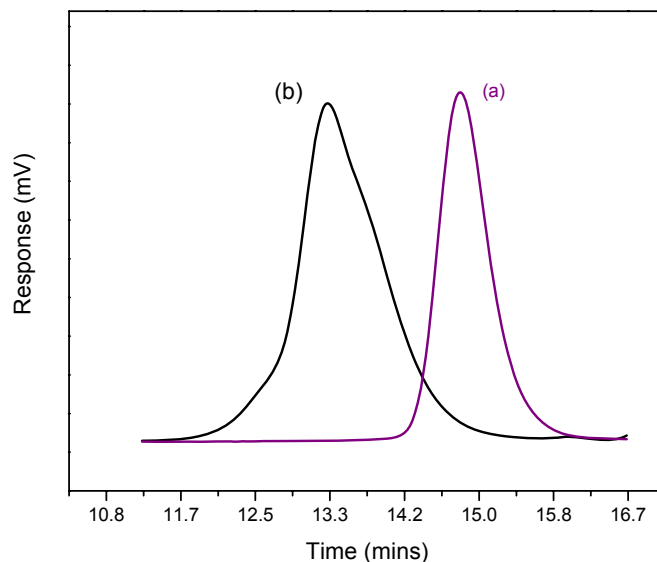


Figure 4.3. GPC of (a) PS homopolymer (5,000 g/mol) and (b) POSS₆-S₄₈-POSS₆ triblock copolymer (16,500 g/mol).

A clear shift in the peak to higher molecular weight and very little overlap with the peak corresponding to the macroinitiator clearly shows the incorporation of the POSS block. Unreacted monomer was removed either by precipitation, Soxhlet extraction or preparative GPC. The number of POSS units attached to the polystyrene backbone were calculated by comparing the integrations of the methylene resonances α to the acrylate bond in MA-POSS (isobutyl) to the aromatic polystyrene resonances in ¹H NMR spectra. Various compositions of the triblock copolymers synthesized are listed in Table 4.1. The nomenclature of the triblock copolymers is on the basis of number of repeat units of styrene and POSS, copolymer **1** with 48 units of styrene and 12 units of POSS is named POSS₆-S₄₈-POSS₆. We have assumed equal distribution of POSS units on both sides of the central PS block.

4.3.3 Polymer Characterization

4.3.3.1 Morphology

The morphology and aggregation of POSS triblock copolymers were studied by WAXS, SAXS and TEM. The samples were thermally annealed at 150 °C for 2 days which is well above the glass transition temperature (T_g) of either blocks (PS \sim 100 °C and MA-POSS (isobutyl) homopolymer \sim 30 °C). The annealing temperature was selected to be below the order-to-disorder transition (ODT) temperature (185 °C as determined by SAXS shown in Fig 4.4) as well as the decomposition temperature of the triblocks (230 °C under N₂ atmosphere). It is expected that after thermal annealing, the copolymers would reach their thermal equilibrium states. Fig. 4.5 shows WAXS profile of the triblock copolymers and MA-POSS (isobutyl) monomer and PS homopolymers.

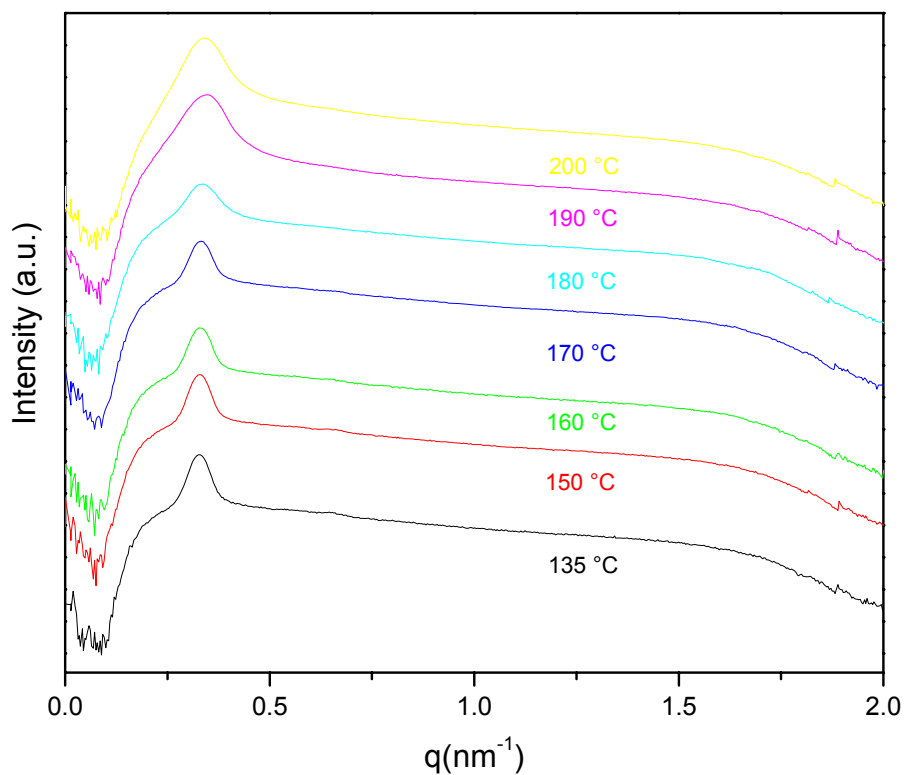


Figure 4.4. SAXS of copolymer POSS₁₀-S₁₃₀-POSS₁₀ at different temperatures to determine the order-disorder temperature of the triblock copolymer.

Going from bottom to top POSS content reduces, with bottom trace of MA-POSS isobutyl monomer and top trace of PS homopolymer. WAXS of MA-POSS monomer shows that it is a highly crystalline material with scattering peaks at two theta values of 7.3, 8.0, 8.6, 9.1, 11.6, 18.5, 19.6, 19.8 and 24.2 degrees. POSS monomers are known to pack as spheres or cubes in a hexagonal arrangement.¹⁶ However when POSS is covalently attached to the polymer backbone their crystallization is restricted to 2D sheets due to the geometric constraints of attaching POSS to the polymer chain.²¹ MA-POSS (isobutyl) homopolymer having 10 repeat units was synthesized by ATRP. There was no crystallization observed in the homopolymer, the attachment of POSS spheres to the backbone and the short propyl acrylate chain joining the POSS cubes to the backbone restricts the mobility of the cubes and presumably prevents crystallization. Similarly it would be expected that in triblock copolymers POSS would not be able to act as independent sphere and attachment to the polymeric backbone will restrict crystallization. The top trace of Figure 4.5 is PS has two scattering peaks centered at 2θ values of 10.28° and 19.53° corresponding to lattice spacing of 8.5 \AA and 4.51 \AA . The scattering peaks are not sharp which indicates amorphous character. Triblock copolymer POSS₆-S₄₈-POSS₆ has two scattering peaks centered at 2θ values of 8.0° and 18.0° . These scattering peaks are fairly broad and indicate that either POSS does not crystallize, or forms very small crystallites. Triblocks POSS₈-S₁₃₀-POSS₈, POSS₁₀-S₁₃₀-POSS₁₀ and POSS_{13.5}-S₃₄₈-POSS_{13.5} have three scattering peaks centered at 2θ value of 8.0° , 11.0° and 18.0° . The scattering peaks correspond to lattice spacings of 10.83 , 8.06 and 4.67 \AA which are signature spacing of POSS crystallization corresponding to lattice planes $(101)/(\bar{1} 11)$, $(110)/(2 \bar{1} 0)/(2 \bar{1} 0)$ and $(113)/(\bar{2} 13)/(\bar{1} 23)$ or $(300)/(330)$ respectively.¹⁶ Intensity of

the scatterings peaks in three triblock copolymers differ depending upon the number of repeat units of POSS. As the number of units of POSS increases the intensity of scattering peaks becomes stronger which indicate stronger crystallization. Copolymer POSS_{13.5}-S₃₄₈-POSS_{13.5} with a total of 27 units of POSS shows the strongest evidence of crystallization.

Crystallization in block copolymers depends upon the nature of the other connecting block and the annealing temperature.³⁰ In p(MA-POSS(isobutyl)-*b*-Styrene-*b*-MA-POSS(isobutyl)) triblock copolymer, the polystyrene phase is the amorphous block and POSS is the crystalline block. During the annealing at 150 °C, polystyrene and POSS are in a phase-separated amorphous melt state. As the samples are cooled POSS cubes start to crystallize and pack in hexagonal arrays. However below T_g of PS, the rigid PS domains restrict the crystallization of POSS cubes resulting in small crystallites. The size of the POSS crystals was calculated using Scherrer equation $L = 0.9\lambda/\beta\cos\theta$ where L is the domain length, λ is the wavelength of the X-ray, β is the peak width at half maximum, and θ is the angle. For POSS_{13.5}-S₃₄₈-POSS_{13.5}, β is selected at half-width of the crystalline peak at lattice spacing 10.8 Å and 8.06 Å and the calculated L are 7.8 nm and 3.5 nm respectively. Assuming the size of each POSS molecule is ~ 1.5 nm, an average of 5-6 units of POSS molecules aggregate in each crystal of POSS. The value of L is not calculated for copolymers POSS₆-S₄₈-POSS₆, POSS₁₀-S₁₃₀-POSS₁₀ and POSS₈-S₁₃₀-POSS₈ as the scattering peaks are very broad or the intensity of the peaks is very weak.

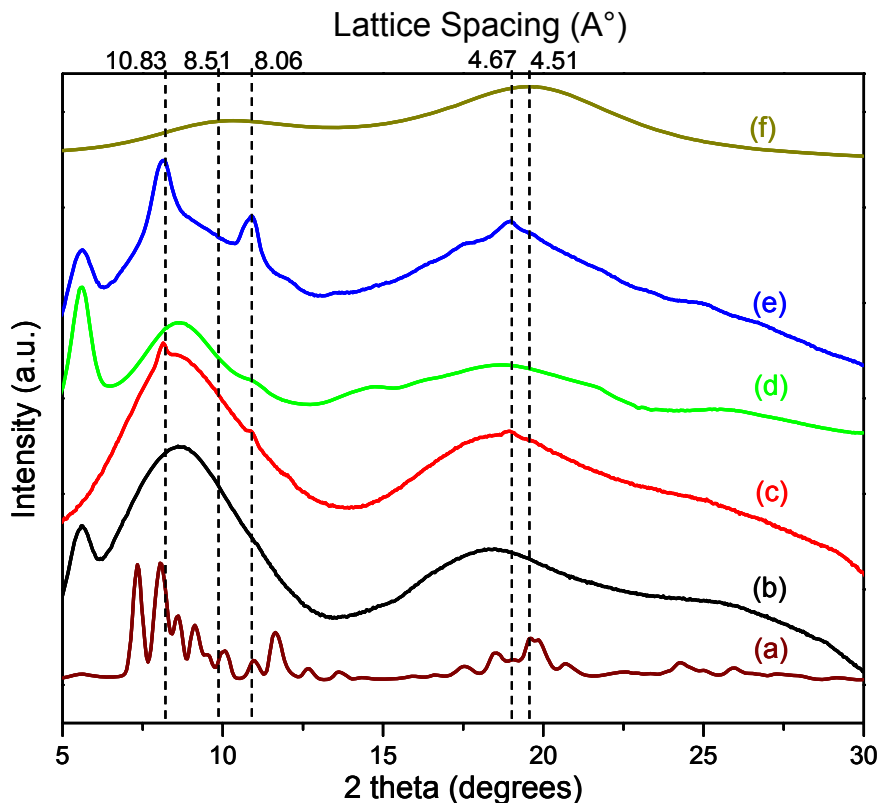


Figure 4.5. WAXS of (a) MA-POSS (isobutyl) monomer as received from Aldrich , (b) POSS₆-S₄₈-POSS₆, (c) POSS₁₀-S₁₃₀-POSS₁₀, (d) POSS₈-S₁₃₀-POSS₈, (e) POSS_{13.5}-S₃₄₈-POSS_{13.5} and (f) Polystyrene homopolymer.

The SAXS profiles of different compositions of the block copolymers are shown in Fig 4.6. For POSS₆-S₄₈-POSS₆, the SAXS profile shows a single, broad peak with a maximum at $q^* = 0.532 \text{ nm}^{-1}$ (q^* = primary scattering wave vector), which is attributed to the correlation hole effect, indicating the copolymer is in a phase-mixed state. For TEM measurements, no staining was required since the silicon in POSS provides sufficient mass contrast. The black domains in the TEM images correspond to the POSS phase while the white domains correspond to the polystyrene. The corresponding TEM image (Fig. 4.7a) shows a typical morphology of a phase-mixed block copolymer, in agreement with the SAXS result. Copolymer POSS₆-S₄₈-POSS₆ having a low total degree of

polymerization (N) and especially very few repeat units of POSS i.e. 12 and thus it does not phase separate. Pyun et al. had reported that $p[(MA-POSS)_6-b-(n\text{-butylacrylate})_{481}-b-(MA-POSS)_6]$ copolymers containing only a few units of POSS do not phase separate while copolymers with a greater number of POSS units, i.e. $p[(MA-POSS)_{10}-b-(n\text{-butylacrylate})_{201}-b-(MA-POSS)_{10}]$ phase separated into a cylindrical microstructure.⁶ Thus by increasing the number of repeat units of POSS in the copolymer, phase separation would be expected.

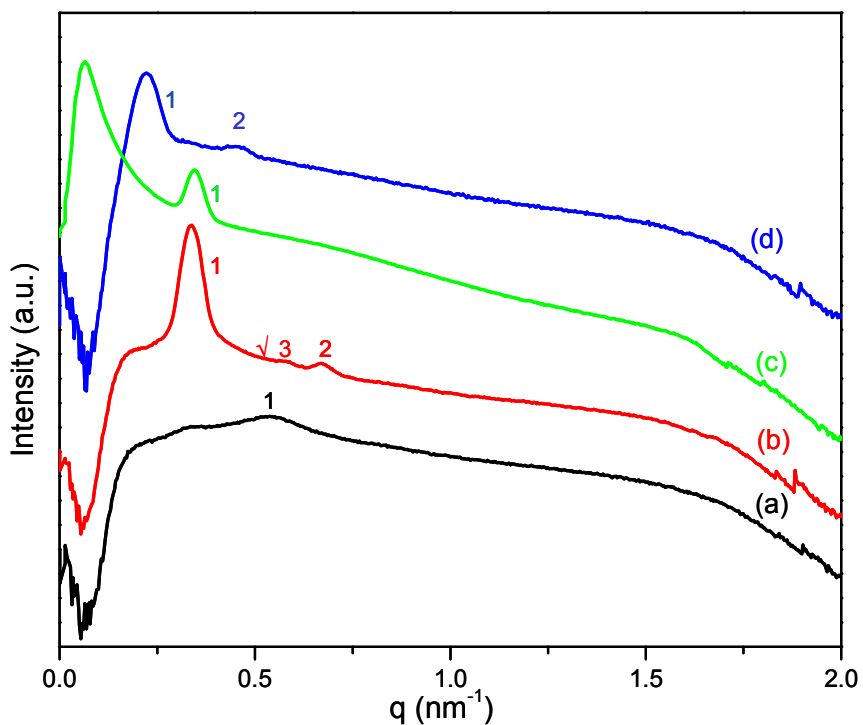


Figure 4.6. Small angle X-ray Scattering (SAXS) of as cast triblock copolymer films (a) $POSS_6-S_{48}-POSS_6$, (b) $POSS_{10}-S_{130}-POSS_{10}$, (c) $POSS_8-S_{130}-POSS_8$, (d) $POSS_{13.5}-S_{348}-POSS_{13.5}$.

Triblock $POSS_{10}-S_{130}-POSS_{10}$ has a higher molecular weight of 32,370 g/mol with total number of 20 repeat units of POSS and relatively volume fraction of POSS:PS at 57:43. The TEM image shows the formation of hexagonally perforated lamellae (PL)

morphology (Fig. 4.7b). It has alternate POSS-PS lamellae with perforations of the majority phase POSS in the lamellae of the minority PS layer. The perforations provide the three dimensional continuity of the majority phase POSS and hence is considered as the monocontinuous morphology.³¹ Perforate lamellae is a metastable state of the more stable bicontinuous gyroid state.³² Stable perforated lamellae phases are formed when the connecting blocks are in the intermediate or weak segregation limit or have a higher packing frustration due to asymmetric connecting blocks.³¹

It can be expected that the two blocks of PS and POSS are asymmetric and given the low values of N , they reside in the weak ($\chi N \sim 10$) or intermediate ($\chi N \sim 15 - 30$) segregation regime.³³ Previous reports of SAXS of perforated lamellae have observed Bragg peaks at ratio $q^* : 1.8q^*$,³⁴ however the SAXS profile of POSS₁₀-S₁₃₀-POSS₁₀ has three Bragg peaks in ratio of $q^* : \sqrt{3}q^* : 2q^*$ and a d-spacing of 18.7 nm. The ratio of the peaks in SAXS indicates that the peaks are deconvoluted and the presence of higher order peaks indicates that there is have a fairly good long-range order in the sample.

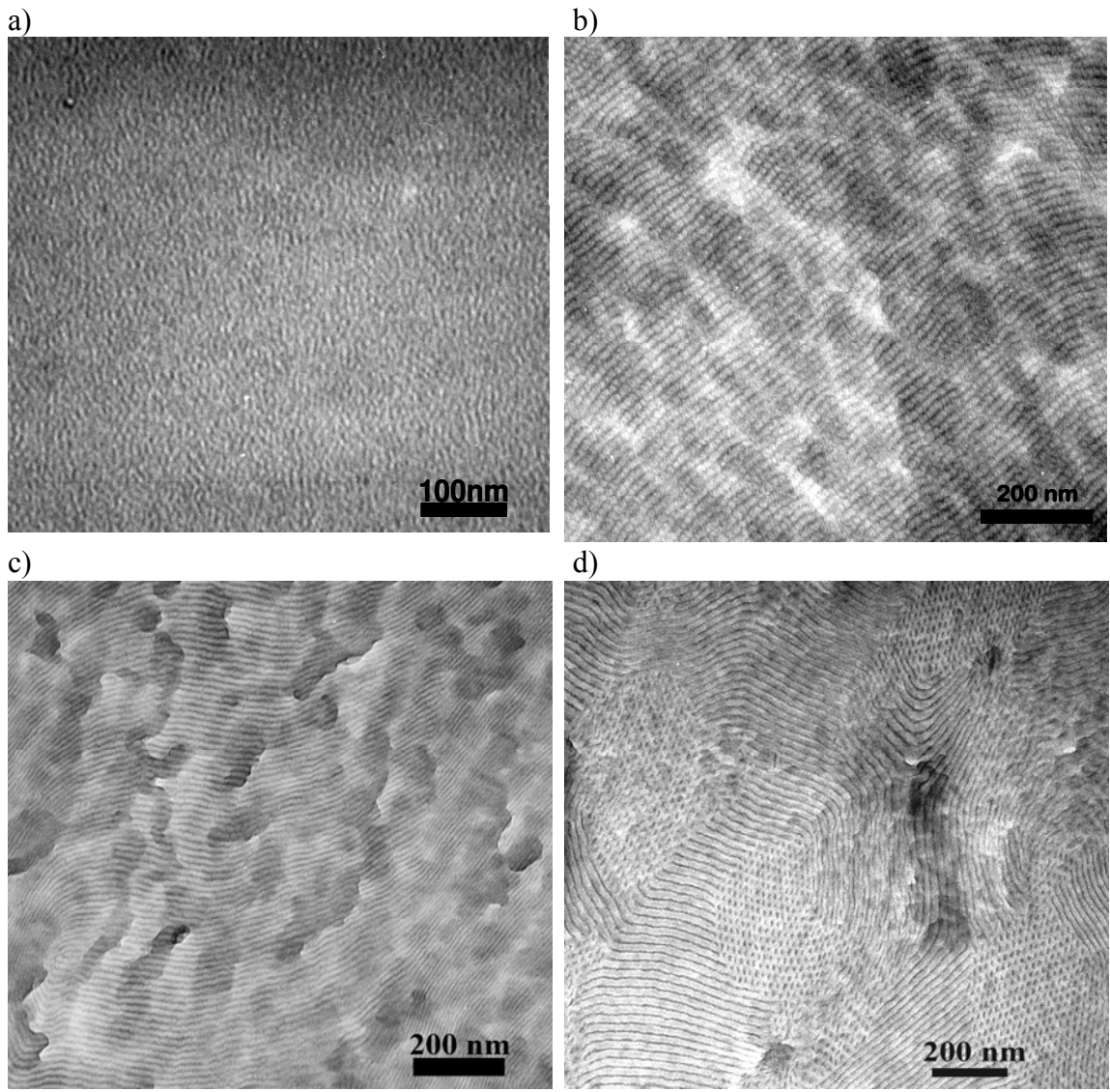


Figure 4.7. Transmission Electron Microscopy (TEM) of p(MA-POSS(isobutyl))-*b*-Styrene-*b*-MA-POSS(isobutyl) triblock copolymers (a) POSS₆-S₄₈-POSS₆, (b) POSS₁₀-S₁₃₀-POSS₁₀, (c) POSS₈-S₁₃₀-POSS₈, (d) POSS_{13.5}-S₃₄₈-POSS_{13.5}.

In order to obtain the lamellae morphology, the molecular weight of PS was kept constant as in POSS₁₀-S₁₃₀-POSS₁₀ and the amount of POSS was reduced. POSS₈-S₁₃₀-POSS₈ has a total molecular weight of 28,600 g/mol and a POSS:PS volume fraction of 0.51:0.49. TEM shows a lamellar morphology with alternating layers of PS and POSS (Fig. 4.7c). Only one Bragg peak is observed in SAXS profile (d-spacing of 18.2 nm). As

the relative volume fraction of the connecting blocks is almost 0.50, the Flory interaction – parameter (χ) for the block copolymer can be estimated using equation $\chi_{ODT}N = 10.5$. The estimated χ of the triblock copolymer at ODT (190 °C) is 0.0719. The estimated value of χ at 190 °C is approximately 18 times the value of χ for poly(styrene-*b*-butadiene). Previous studies on silicon containing polydimethylsiloxane (PDMS) – polystyrene block copolymers show that the calculated and estimated values of χ are very large.^{35,36} The solubility parameter of Si containing polymers like PDMS ($7.3 \text{ cal}^{1/2}\text{cm}^{-3/2}$) and POSS could be very different than the solubility parameter of polystyrene ($9.1 \text{ cal}^{1/2}\text{cm}^{-3/2}$),³⁷ this difference in solubility parameter leads to high χ values. High χ values also explain the phase separation observed in POSS₁₀-S₁₃₀-POSS₁₀ triblock copolymers with only 20 repeat units.

The fourth copolymer POSS_{13.5}-S₃₄₈-POSS_{13.5} was synthesized using PS of molecular weight M_n 40,000 g/mol and has total molecular weight of 65,480 g/mol with PS:POSS volume fraction of 63:37 and displays cylinders of POSS confined in a PS matrix as observed by TEM. As shown in Fig. 4.7d, clear grain boundaries are observed with POSS cylinders parallel to the z-axis and cylinders aligned horizontally. The corresponding SAXS profile showed a d-spacing of 28.2 nm with two scattering peaks at ratio $q^* : 2q^*$. The absence of the scattering peak at $\sqrt{3}q^*$ might be due to the cylindrical form factor of the sample. Thus by varying the volume fractions of both PS and POSS blocks, three different morphologies have been observed and the d-spacing of the polymers can be controlled by changing the molecular weight.

4.3.3.2 Thermal stability

The thermal stability of the polymers under atmospheric conditions was studied using TGA. Decomposition temperatures (5 wt% loss temperature) of the MA-POSS (isobutyl) homopolymer, styrene homopolymer and p(MA-POSS(isobutyl)-*b*-Styrene-*b*-MA-POSS(isobutyl)) triblock copolymers are reported in Table 4.2 and the plots are shown in Fig 4.8.

Table 4.2. DSC and TGA data of MA-POSS (isobutyl) homopolymer, styrene homopolymers and p(MA-POSS(isobutyl)-*b*-Styrene-*b*-MA-POSS(isobutyl)) triblock copolymers.

Sample	T _g (POSS) (°C)	T _g (PS) (°C)	T _m (°C)	Decomposition Temperature (°C)	% Theoretical char yield	% Experimental char yield
MA –POSS (isobutyl) homopolymer	30	-	-	324	50	45
POSS ₆ -S ₄₈ - POSS ₆	49	94	-	336	34	44
POSS ₁₀ -S ₁₃₀ - POSS ₁₀	67	75	-	331	29	25
POSS ₈ -S ₁₃₀ - POSS ₈	50	88	-	304	26	22
POSS _{13.5} -S ₃₄₈ - POSS _{13.5}	77	99	126	330	19	18
Polystyrene homopolymer	-	91 100 105	-	280	0	0

T_g – glass transition temperature, T_m – melting point

The decomposition temperature of the homopolymer of styrene is lowest at 280 °C and that of homopolymer of MA-POSS (isobutyl) is 320 °C. The decomposition

temperature of the triblock copolymers are in the range of 303 °C and 336 °C with copolymers POSS₆-S₄₈-POSS₆, POSS₁₀-S₁₃₀-POSS₁₀ and POSS_{13.5}-S₃₄₈-POSS_{13.5} having decomposition temperatures higher than the decomposition temperatures of either PS and MA-POSS (isobutyl) homopolymer. High decomposition temperatures in block copolymers compared to both the blocks may be due to crystallization of the POSS and confinement effects of different morphologies.³⁸ Phase-mixed POSS₆-S₄₈-POSS₆ with maximum 69 wt% POSS shows the highest decomposition temperature at 336 °C. In general with the decreasing weight percentage of POSS the decomposition temperature of the copolymer reduces with the exception of copolymer POSS_{13.5}-S₃₄₈-POSS_{13.5}. Copolymers POSS₁₀-S₁₃₀-POSS₁₀ and POSS_{13.5}-S₃₄₈-POSS_{13.5} having cylindrical morphology and 59 wt% and 39 wt% of POSS have comparable decomposition temperature at 331 °C and 330 °C whereas copolymer POSS₈-S₁₃₀-POSS₈ having lamellae morphology and 52 wt% of POSS shows the lowest thermal decomposition temperature at 303 °C. POSS crystallization in POSS_{13.5}-S₃₄₈-POSS_{13.5} and confinement effects of cylindrical POSS domains lead to a higher decomposition temperature than POSS₈-S₁₃₀-POSS₈ which does not show crystallization and has lamellar morphology. The percent char yields of the homopolymers and triblocks is also reported in Table 4.2. As the amount of POSS decreases the percent char yield also decreases. There is a slight increase in the mass of sample during the burning process due to the oxidation of the POSS cage to silica.

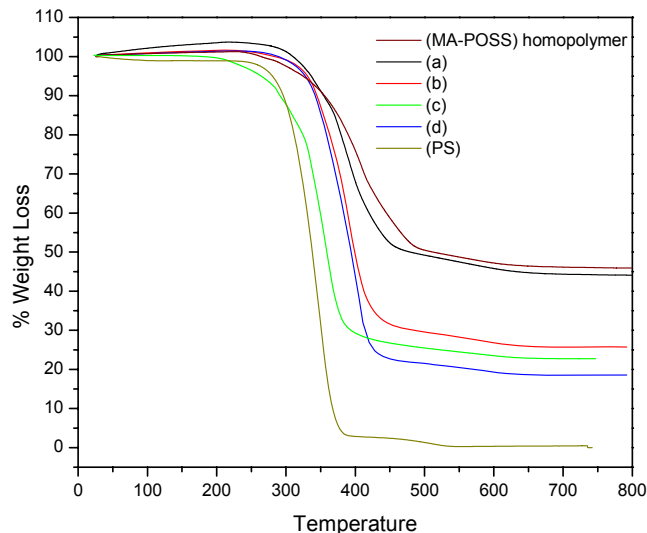


Figure 4.8. TGA graph of p(MA-POSS)-*b*-p(PS)-*b*-p(MA-POSS), MA-POSS (char yield 45%, top), (a) POSS₆-S₄₈-POSS₆, (b) POSS₁₀-S₁₃₀-POSS₁₀, (c) POSS₈-S₁₃₀-POSS₈, (d) POSS_{13.5}-S₃₄₈-POSS_{13.5} and PS homopolymer (char yield 0%, bottom).

The DSC results of the first heating cycle for the triblock copolymers are shown in Table 4.2. The DSC plots are shown in Fig. 4.9 and 4.10. The glass transition temperature of MA-POSS (isobutyl) homopolymer is 30 °C whereas the T_g of polystyrene of M_n 5,000, 15,000 and 40,000 g/mol are 91 °C, 100 °C and 105 °C respectively. The phase-mix POSS₆-S₄₈-POSS₆ sample, shows two thermal transitions, first a strong endothermic thermal transition at 50 °C and second a step glass transition at 94 °C. Even though we do not obtain a phase-separated block copolymer morphology the chains are not completely miscible and thus two T_g are observed.

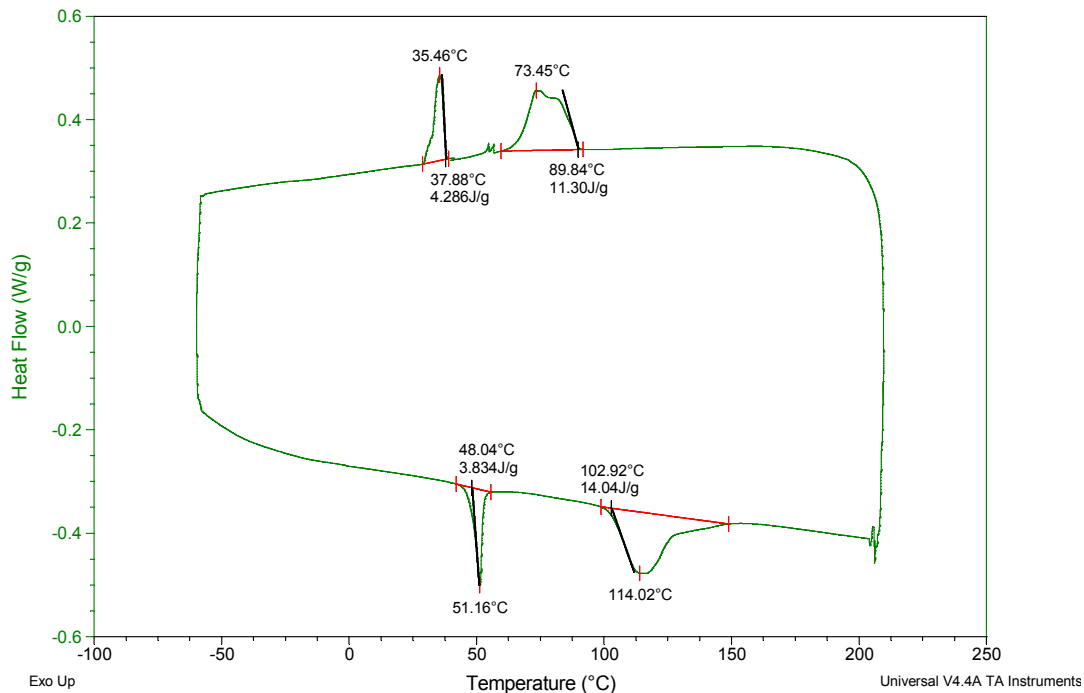


Figure 4.9. DSC of MAPOSS isobutyl monomer.

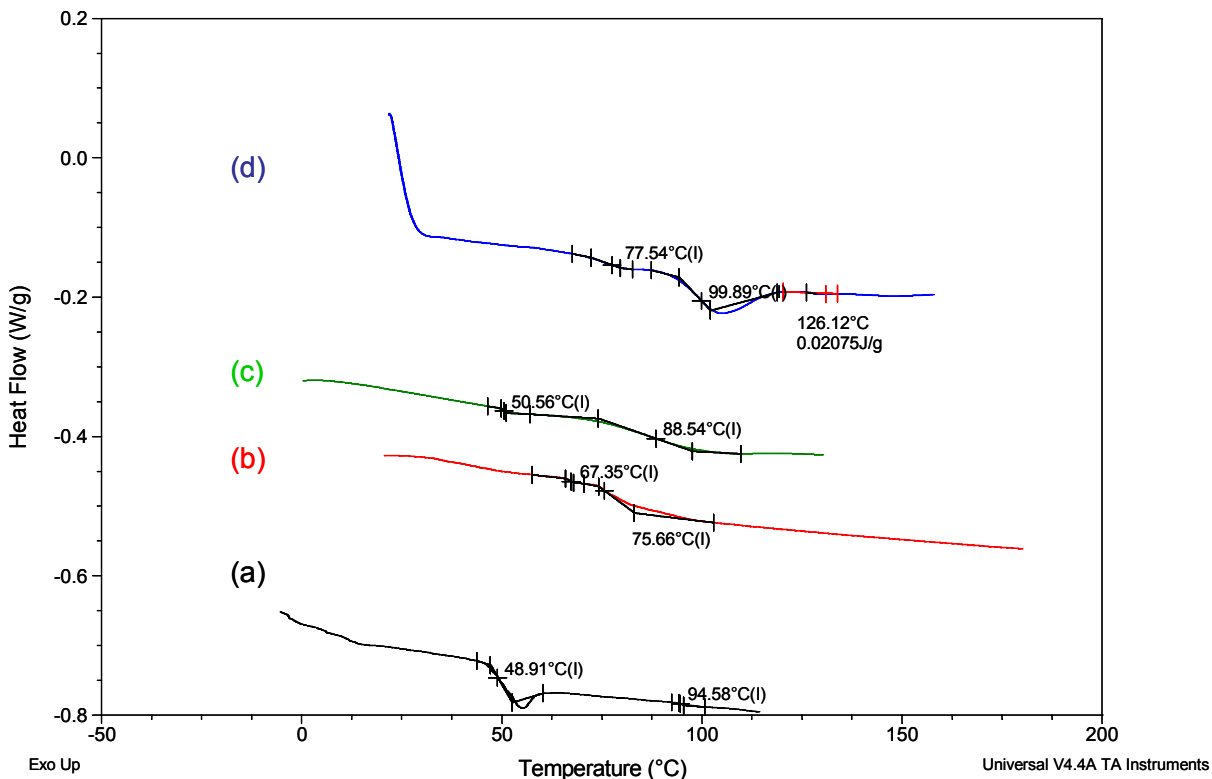


Figure 4.10. DSC of p(MA-POSS(isobutyl)-*b*-Styrene-*b*-MA-POSS(isobutyl)) triblock copolymers, (a) POSS₆-S₄₈-POSS₆, (b) POSS₁₀-S₁₃₀-POSS₁₀, (c) POSS₈-S₁₃₀-POSS₈, (d) POSS_{13.5}-S₃₄₈-POSS_{13.5}.

The endothermic thermal transition observed at 50 °C is due to overlap of the enthalpy relaxation endotherm and the glass transition of the POSS phase. During the second heating relaxation endotherm is not observed and only the step glass transition is observed. Enthalpy relaxation endotherm is a non-reversible transition which depends upon the thermal history of the sample and is caused due to slower cooling rate compared to the faster heating rate during DSC.^{39,40} There is a 20 °C increase in the T_g of the MA-POSS phase in the block copolymer compared to the homopolymer of MA-POSS and is discussed further in the next section.

Copolymers POSS₁₀-S₁₃₀-POSS₁₀, POSS₈-S₁₃₀-POSS₈ and POSS_{13.5}-S₃₄₈-POSS_{13.5} each have two glass transition temperatures at 67 °C and 80 °C, 50 °C and 88 °C and 77 °C and 94 °C respectively. Copolymer POSS_{13.5}-S₃₄₈-POSS_{13.5} also has a melting point at 126 °C. There is increase in the T_g of the lower glass transition temperature MA-POSS block and decrease in the the T_g of the higher glass transition temperature polystyrene block. When flexible and hard blocks are connected to each other the hard block restricts the mobility of the flexible block thereby increasing the T_g of the flexible block and the flexible block lowers the T_g of the hard block. The increase and the decrease in the T_g of the two blocks is also due to crystallization. Crystalline domains restrict the mobility of the chains increasing the T_g of the material.

The degree of increase and decrease of the T_g depends upon the relative fractions of the connecting blocks, morphology and the degree of crystallization of the polymer. In cylindrical morphology there is a huge change in the T_g of the confined block due to large area of contact with the surrounding matrix. This is observed by the huge decrease in the

T_g of PS phase in POSS₁₀-S₁₃₀-POSS₁₀ copolymers and a huge increase in the T_g of MA-POSS block in POSS_{13.5}-S₃₄₈-POSS_{13.5} copolymer. Likewise crystallization of POSS in POSS₁₀-S₁₃₀-POSS₁₀ and POSS_{13.5}-S₃₄₈-POSS_{13.5} also leads to an increase in T_g of MA-POSS. In triblock copolymers asymmetric broadening is observed in T_g 's of PS phase. At the interface of the POSS and PS, PS chains are stretched forming an interlayer of PS which has a different density of styrene chains compared to the density of chains in the PS domain. Due to the PS density gradient and stretching, this interlayer has T_g different than the T_g of the PS domain which leads to asymmetric broadening. Thus DSC data provides important information about the thermal behavior, crystallization and the phase separated structure of the block copolymer.

4.3.3.3 Conformational Asymmetry

Conformational asymmetry (ϵ) was calculated using the density and the persistence length (l_p) of polystyrene and MA-POSS (isobutyl) homopolymers.⁴¹ The density of MA-POSS (isobutyl) homopolymer was calculated using the ATSM D749-00 standard and the persistence length was calculated by the random-walk like model and static light scattering.⁴² For SLS, high molecular weight MA-POSS homopolymer were synthesized by free radical polymerization with AIBN as the initiator.

$$l_p = 3R_{gw}^2 M_o / M_w l_o$$

where R_{gw} is the weight average radius of gyration, M_o is the monomer molecular weight, M_w is the weight average molecular weight and l_o is the length of the repeat unit. The differential index of refraction (dn/dc) for the MA-POSS (isobutyl) homopolymer was calculated as -0.028 g/mL with toluene as the reference solvent (Fig. 4.12). The z -average radius of gyration and M_w were obtained by Zimm plots and l_o for the C-C-C

bond was estimated at 0.253 nm (Fig. 4.11). The weight average molecular weight (R_{gw}) was estimated using the Schulz-Zimm distribution. The calculated l_p of the MA-POSS (isobutyl) homopolymer is 4.4 nm which is 3 - 4 times the persistence length of PS (1.2 nm). Thus the conformational asymmetry of the PS-POSS block copolymer is 13.8. Though the random-walk model is a simplified approach to calculate the persistence length of a polymer, it does show that the PS-POSS polymers are very asymmetric which could lead to a shift in the phase diagram.

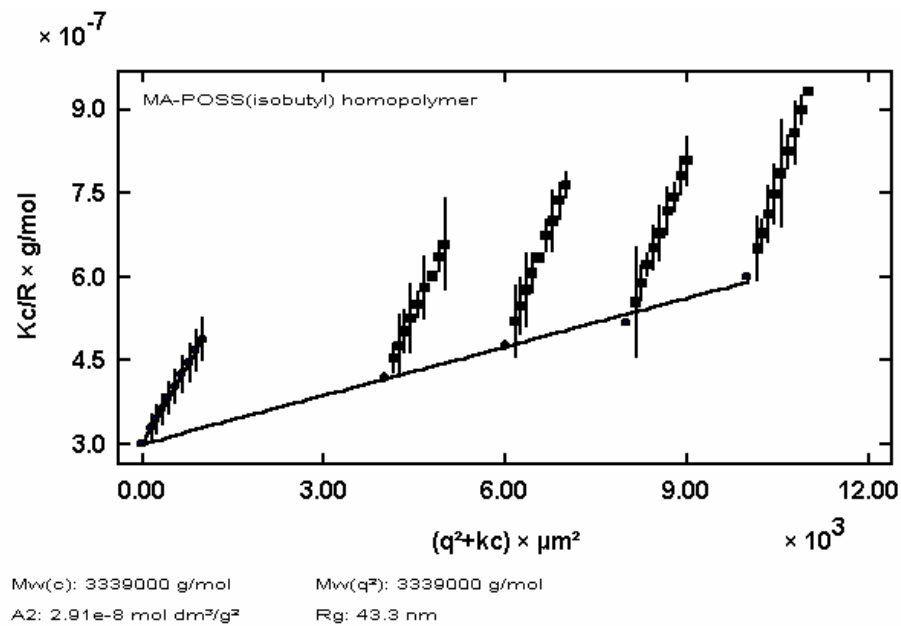


Figure 4.11. Static light scattering of MA-POSS (isobutyl) homopolymers at four different concentrations (2.0, 3.0, 4.0 and 5.0 g/L) and eight different angles (40°, 50°, 60°, 70°, 80°, 90°, 100° and 110°).

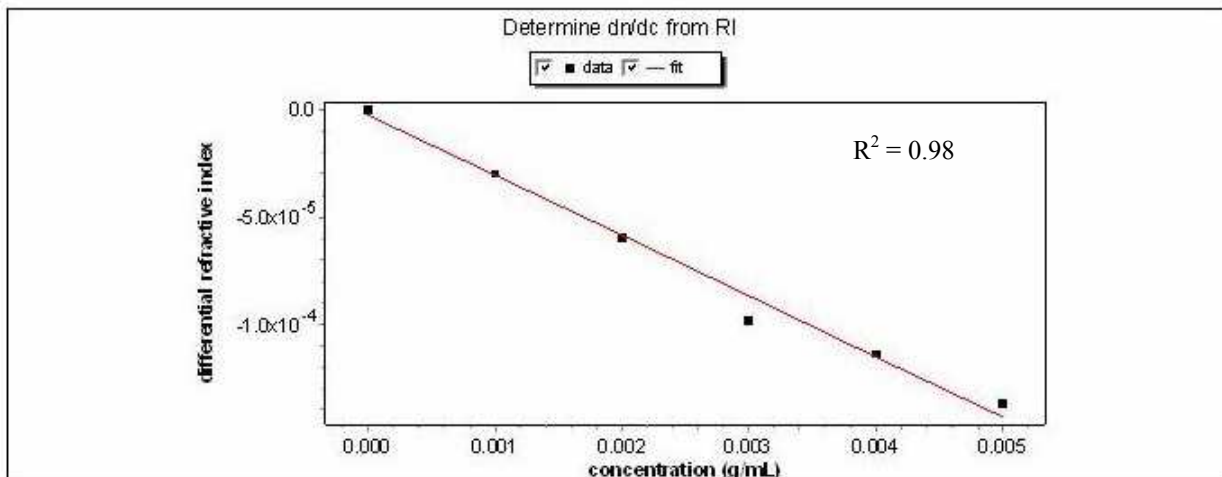


Figure 4.12. Differential refractive index of MA-POSS (isobutyl) homopolymers at five different concentrations (1.0, 2.0, 3.0, 4.0 and 5.0 g/L) in toluene as the solvent.

Confirmation asymmetry (ε) can also be estimated using the formula $\varepsilon = \beta_A/\beta_B$ where $\beta = v_o/b^2$ (v_o = statistical segmental volume and b = statistical segmental length).³¹ In both PS and POSS, the number of carbon atoms in the repeat units is the same i.e. 2, thus we assume that the statistical segmental length (b) for both PS and POSS is same i.e. $b_{POSS} = b_{PS}$. Assuming that the statistical segmental volume is proportional to the length of the pendant unit, the length of styrene unit with phenyl ring (0.5 nm) would be approximately 0.6 nm and the length of MAPOSS unit would be 1.5 nm. Thus the ε for the triblock copolymer would be $\varepsilon = v_o(POSS)/v_o(PS)$ i.e. $\varepsilon = 2.5$.

4.4 Conclusion

Precise molecular weight and low PDI polystyrene homopolymers and p(MA-POSS(isobutyl)-*b*-Styrene-*b*-MA-POSS(isobutyl)) triblock copolymers were synthesized by a combination of anionic polymerization and ATRP. The use of CuBr₂ as co-catalyst increased the number of POSS units that can be attached by ATRP. Hierarchical

nanostructures of the inorganic POSS block were observed in the block copolymers with POSS crystals of the size 7 – 8 nm inside the phase separated block copolymer POSS domains. The triblock copolymer was in a phase mixed state at lower molecular weights, and by increasing the molecular weight, phase separated morphologies were obtained. Three different morphologies, i.e. lamellae, cylinders and perforated lamellae have been observed by changing the relative volume fractions of POSS and PS. The phase diagram was slightly shifted due to the conformational asymmetry of the PS and POSS blocks. The length of the crystal and the d-spacing of the block copolymer could be controlled by varying the molecular weight of the copolymers. Further studies are ongoing to study the thin film morphologies of the copolymers and to fabricate mesoporous silica using the triblock copolymers.

4.5 References

- (1) Rubner, M. *Nature* **2003**, *423*, 925-926.
- (2) Aizenberg, J.; Weaver, J. C.; Thanawala, M. S.; Sundar, V. C.; Morse, D. E.; Fratzl, P. *Science* **2005**, *309*, 275-278.
- (3) Sanchez, C.; Arribart, H.; Guille, M. M. G. *Nature Materials* **2005**, *4*, 277-288.
- (4) Sanchez, C.; Julian, B.; Belleville, P.; Popall, M. *Journal of Materials Chemistry* **2005**, *15*, 3559-3592.
- (5) Gomez-Romero, P. *Advanced Materials* **2001**, *13*, 163-174.
- (6) Pyun, J.; Matyjaszewski, K.; Wu, J.; Kim, G. M.; Chun, S. B.; Mather, P. T. *Polymer* **2003**, *44*, 2739-2750.
- (7) KICKELBICK, G. *Progress in Polymer Science* **2003**, *28*, 83-114.

- (8) Karak, N. *Journal of Polymer Materials* **2006**, *23*, 1-20.
- (9) Sur, G. S.; Sun, H. L.; Lyu, S. G.; Mark, J. E. *Polymer* **2001**, *42*, 9783-9789.
- (10) Zou, H.; Wu, S. S.; Shen, J. *Chemical Reviews* **2008**, *108*, 3893-3957.
- (11) Hawker, C. J.; Russell, T. P. *Mrs Bulletin* **2005**, *30*, 952-966.
- (12) Bates, F. S.; Fredrickson, G. H. *Physics Today* **1999**, *52*, 32-38.
- (13) Bucknall, D. G.; Anderson, H. L. *Science* **2003**, *302*, 1904-1905.
- (14) Pielichowski, K.; Njuguna, J.; Janowski, B.; Pielichowski, J. In *Supramolecular Polymers Polymeric Betains Oligomers* 2006; Vol. 201, p 225-296.
- (15) Larsson, K. *Arkiv for Kemi* **1961**, *16*, 209-214.
- (16) Waddon, A. J.; Coughlin, E. B. *Chemistry of Materials* **2003**, *15*, 4555-4561.
- (17) Kopesky, E. T.; McKinley, G. H.; Cohen, R. E. *Polymer* **2006**, *47*, 299-309.
- (18) Kopesky, E. T.; Haddad, T. S.; Cohen, R. E.; McKinley, G. H. *Macromolecules* **2004**, *37*, 8992-9004.
- (19) Matejka, L.; Strachota, A.; Plestil, J.; Whelan, P.; Steinhart, M.; Slouf, M. *Macromolecules* **2004**, *37*, 9449-9456.
- (20) Leu, C. M.; Chang, Y. T.; Wei, K. H. *Macromolecules* **2003**, *36*, 9122-9127.
- (21) Zheng, L.; Hong, S.; Cardoen, G.; Burgaz, E.; Gido, S. P.; Coughlin, E. B. *Macromolecules* **2004**, *37*, 8606-8611.
- (22) Hirai, T.; Leolukman, M.; Hayakawa, T.; Kakimoto, M.; Gopalan, P. *Macromolecules* **2008**, *41*, 4558-4560.
- (23) Zhang, X.; Chan, E. R.; Glotzer, S. C. *Journal of Chemical Physics* **2005**, *123*.
- (24) Intasanta, N.; Russell, T. P.; Coughlin, E. B. *Abstracts of Papers of the American Chemical Society* **2004**, *227*, U513-U513.

- (25) Hadjichristidis, N.; Iatrou, H.; Pispas, S.; Pitsikalis, M. *Journal of Polymer Science Part a-Polymer Chemistry* **2000**, *38*, 3211-3234.
- (26) Cardoen, G. B., K.; Emrick T.; Coughlin E.B. *Macromolecules* **2006**, *39*, 7170-7173.
- (27) Lecolley, F.; Waterson, C.; Carmichael, A. J.; Mantovani, G.; Harrison, S.; Chappell, H.; Limer, A.; Williams, P.; Ohno, K.; Haddleton, D. M. *Journal of Materials Chemistry* **2003**, *13*, 2689-2695.
- (28) Quirk, R. P.; Yoo, T.; Lee, B. J. *Journal of Macromolecular Science-Pure and Applied Chemistry* **1994**, *A31*, 911-926.
- (29) Bywater, S.; Worsfold, D. J. *Canadian Journal of Chemistry-Revue Canadienne De Chimie* **1962**, *40*, 1564-&.
- (30) Hamley, I. W. In *Interfaces Crystallization Viscoelasticity* 1999; Vol. 148, p 113-137.
- (31) Matsen, M. W.; Bates, F. S. *Journal of Polymer Science Part B-Polymer Physics* **1997**, *35*, 945-952.
- (32) Hajduk, D. A.; Takenouchi, H.; Hillmyer, M. A.; Bates, F. S.; Vigild, M. E.; Almdal, K. *Macromolecules* **1997**, *30*, 3788-3795.
- (33) Papadakis, C. M.; Almdal, K.; Mortensen, K.; Posselt, D. *Europhysics Letters* **1996**, *36*, 289-294.
- (34) Khandpur, A. K.; Forster, S.; Bates, F. S.; Hamley, I. W.; Ryan, A. J.; Bras, W.; Almdal, K.; Mortensen, K. *Macromolecules* **1995**, *28*, 8796-8806.
- (35) Nose, T. *Polymer* **1995**, *36*, 2243-2248.

- (36) Chu, J. H.; Rangarajan, P.; Adams, J. L.; Register, R. A. *Polymer* **1995**, *36*, 1569-1575.
- (37) Dong, J.; Zhang, N. Q.; Liu, Z. L. *Journal of Applied Polymer Science* **2009**, *112*, 985-990.
- (38) Osuji, C. O.; Chen, J. T.; Mao, G.; Ober, C. K.; Thomas, E. L. *Polymer* **2000**, *41*, 8897-8907.
- (39) Floudas, G.; Vazaiou, B.; Schipper, F.; Ulrich, R.; Wiesner, U.; Iatrou, H.; Hadjichristidis, N. *Macromolecules* **2001**, *34*, 2947-2957.
- (40) Moreseseguela, B.; Stjacques, M.; Renaud, J. M.; Prudhomme, J. *Macromolecules* **1980**, *13*, 100-106.
- (41) Vavasour, J. D.; Whitmore, M. D. *Macromolecules* **1993**, *26*, 7070-7075.
- (42) Gettinger, C. L.; Heeger, A. J.; Drake, J. M.; Pine, D. J. *Journal of Chemical Physics* **1994**, *101*, 1673-1678.

CHAPTER 5

ORGANIZING SILICA NANOSTRUCTURES ON SURFACES USING POLYHEDRAL OLIGOMERIC SILSESQUOXANE (POSS) BASED BLOCK COPOLYMERS

5.1 Introduction

Fabricating small feature sizes with conventional photolithography is increasingly becoming more difficult and expensive. Different novel lithography techniques have been proposed to obtain feature sizes below 30 nm.^{1,2} Self-assembly in synthetic materials is emerging as a procedure to fabricate sub-30 nm size features. These nanopatterned surfaces can also be used for fabrication of semiconductors,^{3,4} quantum dots or antidots,⁵ the synthesis of DNA electrophoresis media,^{6,7} fabrication of magnetic recording devices, data storage devices and as filters with nanometer pore sizes.⁸⁻¹⁰ Block copolymers have been successfully used as templates to pattern nano-scale features on surfaces.^{11,12} By controlling the molecular weight, chemical composition and the molecular architecture a number of different morphologies of block copolymer can be obtained in both bulk and solution.^{13,14} Commonly observed microdomain morphologies in the bulk are periodic arrangements of lamellae, cylinders and spheres. By selective plasma or chemical treatment, one of the two domains can be etched to obtain features of sub-30 nm size scale. Park *et al.* coated polystyrene-*b*-polybutadiene copolymers on silicon nitride surface and then selectively etched one of the two blocks to generate holes and islands in the silicon nitride surface.¹⁵ In another report, Kim *et al.* deposited silica on polystyrene-*b*-poly(methyl methacrylate) copolymer and used them as templates to obtain vertically standing silica cylinders.¹⁶ Due to the organic nature of the polymers, most block

copolymers that have been studied give poor plasma etch contrast. A robust, self-assembled inorganic nanostructure will be ideal to simplify the patterning process as it can be used as hard mask to generate sub-30 nm size features.

There are only few reports of organizing inorganic nanostructures with organic self-assembled structures to produce functional hybrid materials.^{17,18} Lin *et al.* oriented cadmium selenide particles by blending them with polystyrene-*b*-poly(2-vinylpyridine) copolymers, the inorganic particles arranged on the interface of the connecting blocks and lead to oriented inorganic structures on the surface. In another example, Templin *et al.* performed sol-gel chemistries in polyisoprene-*b*-poly(ethylene oxide) copolymers and using them as templates to generate inorganic silica rich lamellar domains.¹⁸ Other than being used as hard mask, inorganic silica is also an optimal material in silicon microelectronic applications.¹⁹ Silica is used as an insulator in microelectronics, and as the size scales of device features are reduced there is a need to lower the dielectric constant (k) of silica.²⁰ By generating pores in silica structures, the dielectric constant can be lowered for insulating applications.²¹ Thus the combination of inorganic silica with block copolymers represents an opportunity to generate an inorganic mask for patterning applications, and mesoporous silica for ultra-low k applications. Other potential applications of mesoporous silica include nanoreactors, sensors, storage devices and filters.

Polyhedral Oligomeric Silsesquioxane (POSS) is a silica precursor, which can be incorporated in block copolymers to generate mesoscopically-ordered structures. A common molecular formula of POSS is $R_7(\text{SiO}_{1.5})_8X$. It has a silsesquioxane core which is a sub-oxide of silica, with a base stoichiometry of $\text{SiO}_{1.5}$. The central core has eight

silicon atoms bridged by twelve oxygen atoms and organic substituents (R) which make it compatible with monomers and possibly polymers. It has a reactive group (X) which can be used for polymerization or grafting. POSS has been covalently bonded to polymers such as epoxy resins,²² polyimides,²³ polyethylenes,²⁴ polystyrenes and polynorbornenes.^{25,26} Due to the strong face-to-face packing of POSS cubes, lamellae of POSS were observed in random copolymers of POSS with epoxy resins and polyimides and raft structures of POSS were formed in random copolymers of POSS with butadiene.^{22,23,27} The first synthesized block copolymer of POSS was poly[(methacrylate-POSS)-*b*-(*n*-butylacrylate)-*b*-(methacrylate-POSS)] (ABA) triblock copolymers where cylinders of POSS were confined in a poly(*n*-butylacrylate) matrix.²⁸ Recently diblock copolymers of POSS were synthesized with PS or PMMA and lamellae structures with good long range order were obtained.²⁹

In chapter 4 we synthesized a series of poly(methacrylate-POSS(isobutyl)-*b*-styrene-*b*-methacrylate-POSS(isobutyl)) triblock copolymers by a combination of anionic polymerization and atom transfer radical polymerization (ATRP). We observed three different morphologies i.e. cylindrical, perforated lamellae and lamellae by varying the volume fractions of the connecting blocks. The objective of this study is to examine the thin film behavior of p(MA-POSS(isobutyl)-*b*-Styrene-*b*-MA-POSS(isobutyl)) triblock copolymers. Triblock copolymers of different bulk morphologies were spin coated on silicon oxide and gold substrates to investigate the orientation and the order of the resulting morphologies. The triblock copolymers were subsequently thermally annealed to remove the organic phase and to oxidize POSS to obtain ordered mesoporous silica.

5.2 Experimental

5.2.1 Materials

Two different poly(methacrylate-POSS(isobutyl)-*b*-styrene-*b*-methacrylate-POSS(isobutyl)) triblock copolymer having lamellae and hexagonal perforated lamellae morphologies were used for thin film studies. The bulk morphologies of the triblock were characterized by transmission electron microscopy (TEM) and small angle X-ray scattering (SAXS). The molecular weights of the individual blocks and volume fractions are shown in Table 5.1.

Table 5.1. Molecular weights of polystyrene and p(MA-POSS(isobutyl)-*b*-styrene-*b*-MA-POSS(isobutyl)) triblock copolymers.

No	Sample	M _n Polystyrene g/mol (PDI) ^a	M _n p(MA- POSS(isobu tyl)- <i>b</i> - styrene- <i>b</i> - MA- POSS(isobu tyl)) (PDI) ^b	<i>f</i> _(polystyrene)	Bulk Morphology	Surface Morphology
1	POSS ₈ - S ₁₃₀ - POSS ₈	13,500 (1.06)	28,600 (1.1)	0.49	Lamellae	Lamellae
2	POSS ₁₀ - S ₁₃₀ - POSS ₁₀	13,500 (1.06)	32,370 (1.1)	0.43	Hexagonal Perforated Lamellae	Perforated Lamellae

a: Molecular weight determined by GPC, b: Molecular weight determined by ¹H NMR, N is number of repeat units, *f* is the volume fraction, assuming density of polystyrene – 1.05 g/cc and density of MA-POSS (isobutyl) – 1.15 g/cc (by ASTM D792-00)

The nomenclature of the triblock copolymers is on the basis of number of repeat units of styrene and POSS, triblock copolymer with 130 repeat units of styrene and 16 units of POSS is thus POSS₈-S₁₃₀-POSS₈. We have assumed equal distribution of POSS units on both sides of the central PS block. Triblock copolymer POSS₈-S₁₃₀-POSS₈ has a total molecular weight of 28,600 g/mol with POSS:PS volume fraction of 51:49. The SAXS of the bulk sample has one peak with a *d*-spacing of 18.2 nm and the TEM image shows a lamellar morphology. Triblock copolymer POSS₁₀-S₁₃₀-POSS₁₀ has a total molecular weight of 32,370 g/mol with POSS:PS volume fraction of 57:43. The SAXS of the bulk sample has three peaks with the scattering ratio of the peaks q^* : $\sqrt{3}q^*$: $2q^*$ and has a *d*-spacing of 18.7 nm. The TEM image of the bulk sample shows mono-continuous hexagonal perforated lamellae morphology with alternating lamellae of PS and POSS and hexagonally arranged perforations of the POSS phase through the PS domains.

5.2.2 Thin Film Preparation and Characterization

Silicon wafers were cleaned by dipping in H₂O₂/H₂SO₄ solution and were then washed under R.O. water. Gold surfaces were prepared by vapor depositing gold on silicon wafers. Solutions of triblock copolymers (2-5 wt %) were prepared in toluene and were spin coated at 2000 - 4000 rpm using a Headway Research Inc. spin coater. Film thickness was controlled by adjusting the solution concentration and the spinning speed. The spin coated samples were thermally annealed in a vacuum oven at 150 °C for 48 h. The thickness of the film was calculated by Filmetrics (F20 thin film analyzer) and Ellipsometry. The film thickness was confirmed by Grazing incident angle small angle X-ray scattering (GISAXS). GISAXS measurements were performed at the 8-ID-E

beamline at the Advanced Photon Source (Argonne National Laboratory) with X-ray wavelength of 1.68 Å. The sample to detector distance was 2056 mm.

Ultraviolet (UV) crosslinking of the polymer thin films were carried out under vacuum at 254 nm for 1 h using two 15 W UV lamps. Thermal treatment was performed in a high temperature furnace (1500 Thermolyne) in air at 375 °C. The temperature was raised from room temperature at rate of 25 °C/min.

Scanning force microscopy (SFM) was done on Digital Instrument, Dimension TM 3100) using Nanoscope ® IIIa version 5.12r3 software. In the tapping mode, height and phase images were collected. X-ray Photoelectron Spectroscopy (XPS) was performed on Physical Electronics, Quantum 2000, Scanning ESCA Microscope at two different angles 15° and 75°. The data was analyzed using Multipak software. The analysis at 15° has a penetration depth of ~10 Å and that at 75° corresponds to a penetration depth of ~40 Å.

Dynamic Contact Angle measurements were made with a Ramè-Hart telescopic goniometer and a Gilmont syringe with a 24-gauge flat-tipped needle. Milli-Q water was used as a probe liquid. Advancing and receding contact angles were recorded while the water was added and withdrawn from the drop, respectively. The values are averages of 4–5 measurements made on different areas of samples.

Variable Angle Spectrometric Ellipsometry (VASE) were carried out on Sopra Inc., GES5 Ellipsometer.

5.3 Results and Discussion

5.3.1 Thin Film Studies of Hybrid Organic-Inorganic Block Copolymers

For simplicity, first the triblock copolymer POSS₈-S₁₃₀-POSS₈ with a lamellar morphology was used to investigate surface-induced orientation. Thick films of 185 nm thickness were spin coated from 5 wt% toluene solutions at 25000 rpm. After spin coating, the block copolymer was thermally annealed at 150 °C; above T_g of both the blocks, for 48 h. It is expected that after annealing the thin film will reach its thermal equilibrium structure. Scanning Force Microscopy (SFM) studies showed that the surface of the film has isolated islands and holes (Fig. 5.1a and 5.1b) with a step-height of 18.6 nm (Fig. 5.1c), comparable to the bulk long period, across the film surface. This indicates that the microdomains of the block copolymer are oriented parallel to the surface. From the SFM result (Fig. 5.1a and 5.1b), it can be seen that the topographic features are of micrometer length scales. However, SFM provides information only about the surface of the thin film. Grazing incident small angle X-ray scattering (GISAXS) was used to investigate the entire thickness of the thin film, and was performed on films with similar thickness where the incident X-ray beam was delivered onto the film surface at shallow incidence angles and the scattering profiles were collected. In the scattering profiles (Fig. 5.1d), the streaks along the q_y axis can be observed. These long streaks are Bragg rods and the relative scattering wave vector profile is q*: 2q*, where q* is the primary scattering vector. The position and the scattering ratio of the peaks indicate that POSS₈-S₁₃₀-POSS₈ triblock copolymer has lamellae morphology and the lamellae microdomains are oriented parallel to the substrate throughout the thickness of the film.

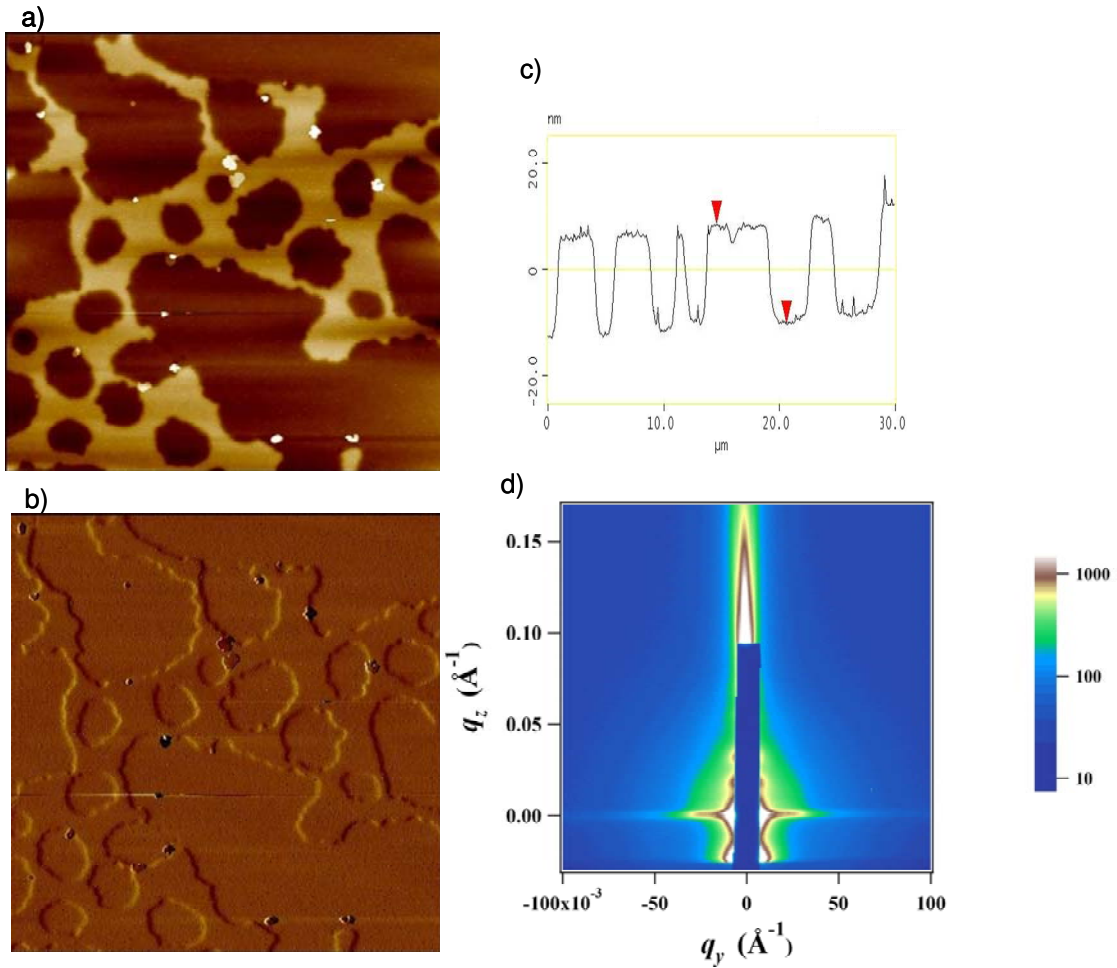


Figure 5.1. Surface analysis of POSS₈-S₁₃₀-POSS₈ triblock copolymer spin-coated on silicon with native silicon oxide layer. SFM (25 μm x 25 μm) height image (a) revealed interconnected-island formation. As can be seen from the phase image (c), the template was covered with one phase (one of the block copolymer domain). (b) Scanning across these islands and holes resulted in step heights of 18.6 nm which was comparable to the bulk long period of the triblock. (d) GISAXS pattern of the film shows parallel orientation of the microdomains throughout the thickness of the film.

Dynamic contact angle measurements on the film's surface with water yielded advancing and receding angles (θ_A/θ_R) of 110°/94°, close to the contact angle of poly(methacrylate-POSS isobutyl) (PMAPOSS) homopolymer ($\theta_A \sim 109^\circ$ for PMAPOSS (isobutyl) and $\theta_A \sim 99^\circ$ for PS film's surface). Therefore, it is likely that PMAPOSS is at

the polymer/air interface. X-ray photoelectron spectroscopy (XPS) was performed on the thin film samples to obtain the composition of the film at the surface. At 15°, the elemental composition of the surface is carbon (53%), oxygen (31%) and silicon (16%) which corresponds to the composition of the elements in the PMAPOSS calculated (percentage of C, O and Si are 55, 28 and 16 respectively). From the surface analysis we can conclude that PMAPOSS phase forms an interface with air at the top of the film. The triblock copolymer POSS₈-S₁₃₀-POSS₈ has a lamellar morphology on the silicon oxide surface with lamellae orientated parallel to the substrate and POSS phase occupying the polymer/air interface.

Thick films of triblock copolymer POSS₁₀-S₁₃₀-POSS₁₀ of 100 nm thickness were spin coated from a 5 wt % toluene solutions at 4000 rpm. The films were thermally annealed as previously described. The SFM phase image (Fig. 5.2a) showed a phase contrast between the microdomains of the block copolymer indicating a difference in moduli of the two blocks. For the phase contrast to be detected by SFM analysis, both the PMAPOSS and PS microdomains must be located at, or near, the surface. The phase contrast suggests that there was an alignment of the block copolymer microdomains normal to the surface near the polymer/air interface. Fast Fourier Transform of the SFM phase image (Figure 5.2a Inset) yielded a ring corresponding to 21.1 nm, which is greater than bulk long period as measured by SAXS (18.7 nm). Perpendicular alignment of the microdomains was confirmed by GISAXS, Fig. 5.2c shows a typical 2D GISAXS pattern obtained at the incident angle (α_i) of 0.14° which is lower than the critical angle ($\alpha_c = 0.17^\circ$) of the film and investigates only the top surface of the film. In the scattering profile, Bragg rods were observed along the q_z axis at $2\theta_f$ value of 0.48° which

corresponds to a d - spacing of 20.1 nm. The vertical Bragg rods indicate that the microdomains on the surface are normal to the polymer/air interface.

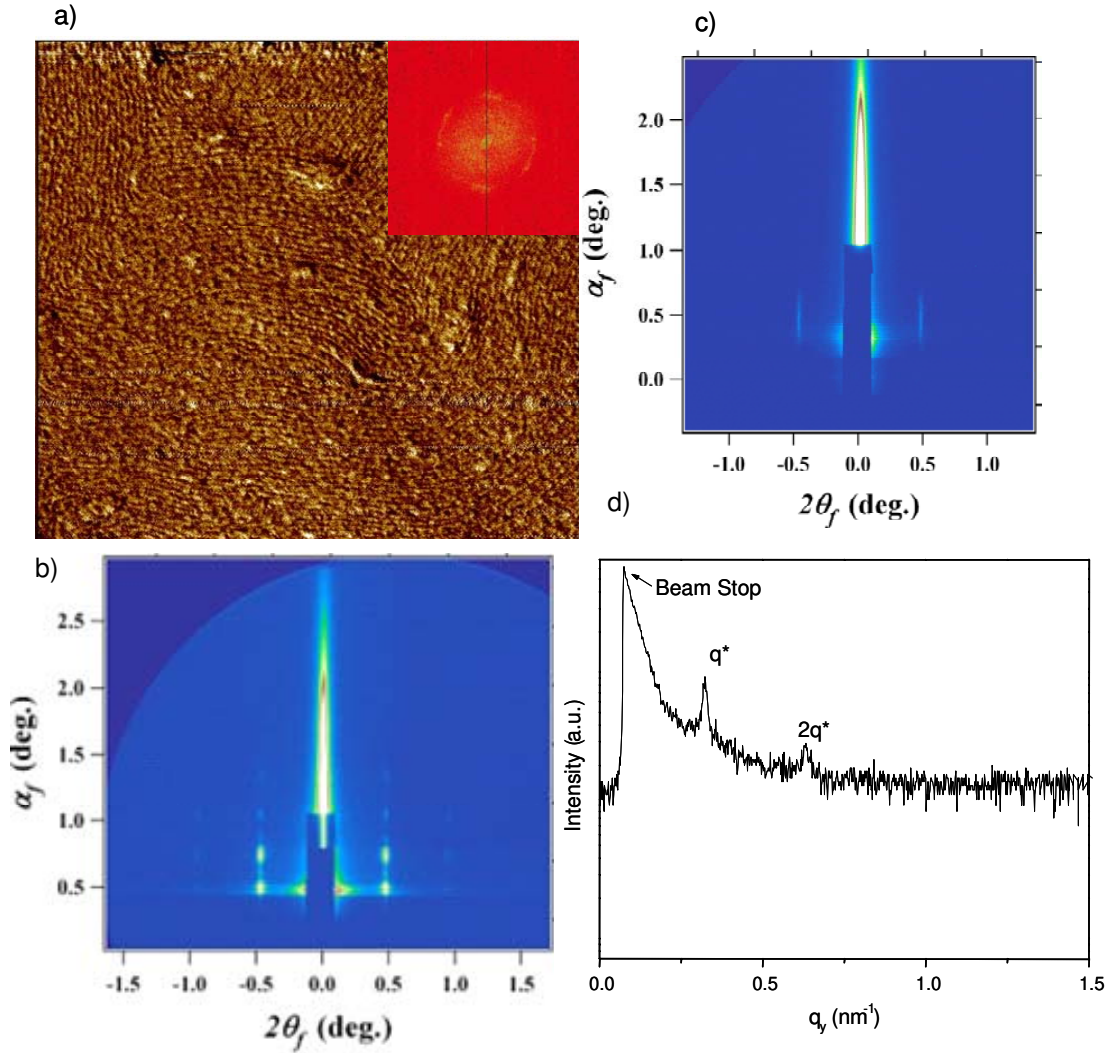


Figure 5.2. Surface analysis of POSS₁₀-S₁₃₀-POSS₁₀ triblock copolymer spin-coated on silicon with native silicon oxide layer. SFM (2 μm x 2 μm) phase image (a) revealed phase contrast with FFT (inset) of a ring that corresponds to 21.1 nm which is comparable to the bulk long period of the triblock. (b), GISAXS pattern of the thin film obtained at incident angle ($\alpha_i = 0.14^\circ$) probing only the surface of the film, scattering profile suggest that the microdomains are oriented perpendicular to the polymer/air interface. (c), GISAXS pattern of the thin film obtained at incident angle ($\alpha_i = 0.21^\circ$) probing the entire thickness of the film, scattering profile suggest that the lamellae microdomains are oriented perpendicular to the substrate and perforations layers are present parallel to the substrate. (d) 1-dimensional SAXS profile of the triblock sample obtained from the GISAXS pattern shown in 2c.

Fig. 5.2b shows the GISAXS pattern of the entire thickness of the thin film obtained at $\alpha_i = 0.21^\circ$. The scattering profile shows Bragg rods along the q_z axis and a number of sharp scattering reflections over a wide range of scattering angles. The absence of ring structures in the scattering profile shows the microdomains are orientated either along the q_z axis or the q_y axis. The 1-dimensional SAXS profile (Fig. 5.2d) of intensity versus scattering wave vector (q_y) showed that the relative scattering wave vector profile of the Bragg rods is $q^*: 2q^*$ indicating lamellae morphology. The relative positions of the scattering peaks indicate that the lamellae throughout the thickness of the film are orientated perpendicular to the substrate. Scattering peaks along the q_y or $2\theta_f$ axis are due to the cylinders observed in the lamellae microdomains and are oriented parallel to the substrate of the film. Based on the bulk morphology and the volume fraction of the triblock copolymer, POSS cylinders perforate through the PS microdomains. Similar GISAXS pattern was observed by Lee *et al.* for hexagonally perforated lamellae of polystyrene-*b*-polyisoprene diblock copolymer.³⁰ The strong reflections at $2\theta_f = 0.48^\circ$ are due to the reflected beam and weak reflections can be assigned to the transmitted beam. These perforations provide a 3-dimensional structure of the POSS phase in the thin films.

Typically, external stimuli an electric field, shear force or treatment of the surface is required to obtain the perpendicular orientation of the block copolymer domains. PS and POSS microdomains with perpendicular orientation are obtained on native silicon oxide layer without any treatment of the surface. The triblock copolymers were also spin coated on high surface energy gold substrate to understand the effect of the substrate on the orientation of the microdomains. The scattering profile obtained from the GISAXS image of the thin film (Fig. 5.3) is similar to the scattering profile of the triblock on a

native silicon oxide surface. Thus the orientation of the microdomains on both the silicon oxide surface and the gold surface is the same i.e. PS and POSS lamellae are perpendicular to the substrate and POSS cylinders are parallel to the substrate through the PS microdomains.

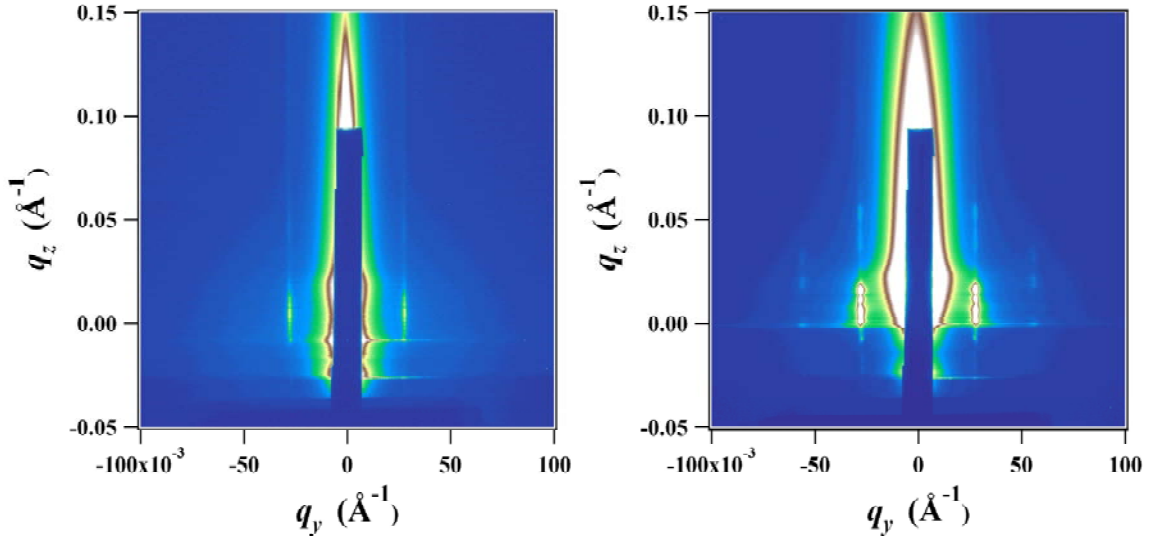


Figure 5.3. Surface analysis of POSS₁₀-S₁₃₀-POSS₁₀ triblock copolymer spin-coated on gold substrate. (left), GISAXS pattern of the thin film obtained at incident angle ($\alpha_i = 0.14^\circ$) probing only the surface of the film, scattering profile suggest that the microdomains are oriented perpendicular to the polymer/air interface. (right), GISAXS pattern of the thin film obtained at incident angle ($\alpha_i = 0.20^\circ$) probing the entire thickness of the film, scattering profile suggest that the lamellae microdomains are oriented perpendicular to the substrate and perforations layers are present parallel to the substrate.

The perpendicular orientation of the block copolymer microdomains are obtained if differences in the surface energy of the connecting blocks is zero or is very small.

However, factors such as the surface energy of the substrate and the architecture of the block copolymer chains strongly influence the orientation of the microdomains. Khanna *et al.* investigated the effect of the chain architecture of AB diblock and ABA triblock copolymers on the orientation of the microdomains in thin films.³¹ In the AB diblock

copolymer parallel orientations are favored because there is a gain in the surface energy due to the lower energy block occupying the polymer/air interface. However, in ABA triblock copolymers, there is a loss in entropy due to the looping of the chains at the interfaces, thus parallel orientations are obtained, if the gain in surface energy is greater than the loss in entropy. The opposing energy contributions stabilize the perpendicular orientation of the microdomains for the blocks having non-zero surface energy differences. Thus the ABA architecture can explain the perpendicular orientation of PMAPOSS and PS domains.

However, unlike in POSS₁₀-S₁₃₀-POSS₁₀ triblock copolymer, lamellae in POSS₈-S₁₃₀-POSS₈ triblock copolymer have microdomains parallel to the substrate. Other factors like thickness of the films, relative volume fractions and morphology of the block copolymer also influence the orientation of the microdomains in the block copolymers.³² The thickness of the POSS₈-S₁₃₀-POSS₈ thin films is twice the thickness of the POSS₁₀-S₁₃₀-POSS₁₀ thin films and ten times the long range period of the microdomains. When the thickness of the film is close to the period of the microdomains, due to the stretching imposed on the chains, the orientation of chains is parallel to the substrate and thus the resulting microdomains are perpendicular to the substrate.^{32,33} Morphology and relative volume fractions of the blocks also affect the stretching in the chains and hence influence the orientation of the domains.³² Thus the lamellae in triblock copolymers POSS₈-S₁₃₀-POSS₈ and POSS₁₀-S₁₃₀-POSS₁₀ are oriented in different directions.

5.3.2 Transformation of POSS to Silica

The perpendicularly oriented domains of POSS and PS can be used to generate ordered mesoporous silica structures. The triblock copolymers were thermally annealed at

375 °C in air to remove polystyrene (decomposition temperature of PS is 290 °C) and to oxidize the POSS cages to silica. The order-to-disorder temperature (T_{ODT}) of POSS₁₀-S₁₃₀-POSS₁₀ triblock copolymer is 185 °C (as estimated by SAXS), above which the polymer is in a phase-mix state. To avoid phase mixing, the PS phase was UV crosslinked at 254 nm for 1 h and then the thin films were thermally annealed at 375 °C for 24 h. For the POSS₁₀-S₁₃₀-POSS₁₀ films, XPS results before and after the thermal annealing are tabulated in table 5.2. The binding energy value of Si in POSS₁₀-S₁₃₀-POSS₁₀ before thermal annealing is 102.5 eV which corresponds to the literature value for the binding energy of Si in POSS and after the thermal annealing the binding energy of Si changes to 103.7 eV which is the binding energy of Si in silica.³⁴ During thermal annealing, the binding energy of the silicon increases due to the oxidation of silicon from the lower oxidation state in POSS to higher oxidation state in SiO₂. By XPS we also observe that the percentage of C at 15° and 75° take off angles before annealing are 62 % and 51 % respectively which reduce to 9 % and 5 % after the annealing process. The residual carbon after the annealing process could be due to silicon carbide, other inorganic carbon char formations, or organic impurities from the atmosphere.

Table 5.2. X-ray photoelectron spectroscopy (XPS) results of POSS₁₀-S₁₃₀-POSS₁₀ triblock copolymer before and after thermal annealing.

	Before Annealing			After Annealing		
Binding energy of Si (eV)	102.5			103.7		
	% C	% Si	% O	% C	% Si	% O
Incident Angle 15°	62	13	24	9	24	66
Incident Angle 75°	51	19	28	5	25	69

The surface of the thin film after the thermal annealing was investigated by SFM. The SFM phase image (Fig. 5.4a) showed strong phase contrast between the microdomains on the surface of the thin film. The phase contrast to be detected by SFM analysis indicates that both silica and air must be located at, or near, the surface. The phase contrast suggests that even after the thermal annealing process microdomains of silica are aligned normal to the surface. Fast Fourier Transform of the SFM phase image (Figure 5.4a Inset) yielded a ring corresponding to 20 nm, which is comparable to the period before the thermal annealing. Fig 5.4b shows the GISAXS scattering profile of the silica thin film after thermal annealing. In the scattering profile, Bragg rods were observed along the q_z axis with the scattering ratio $q^* : 2q^*$ indicating lamellar morphology. The position and the scattering pattern of the Bragg rods indicate that the silica microdomains are oriented normal to the substrate. During the annealing, the adhesion of the thin film to the substrate prevents the removal of the silica layer. Weak scattering peaks are observed along the q_y axis which suggest that the perforation are still present and are oriented parallel to the substrate. The diffused scattering peaks indicate that the microdomains are not sharp because of the accumulation of residual char. After the annealing process the thickness of the film reduces from 95 nm to 20 nm. This reduction in the thickness of the film is due to the loss of 90% organic content and the change of density of the microdomains ($\delta_{PS} - 1.05 \text{ g/cm}^3$, $\delta_{PMAPOSS} - 1.15 \text{ g/cm}^3$ and $\delta_{Silica} - 2.26 \text{ g/cm}^3$). Thus the poly(MAPOSS(isobutyl)-*b*-styrene-*b*-MAPOSS(isobutyl)) triblock copolymers offer an elegant route to make ordered silica structures on surfaces.

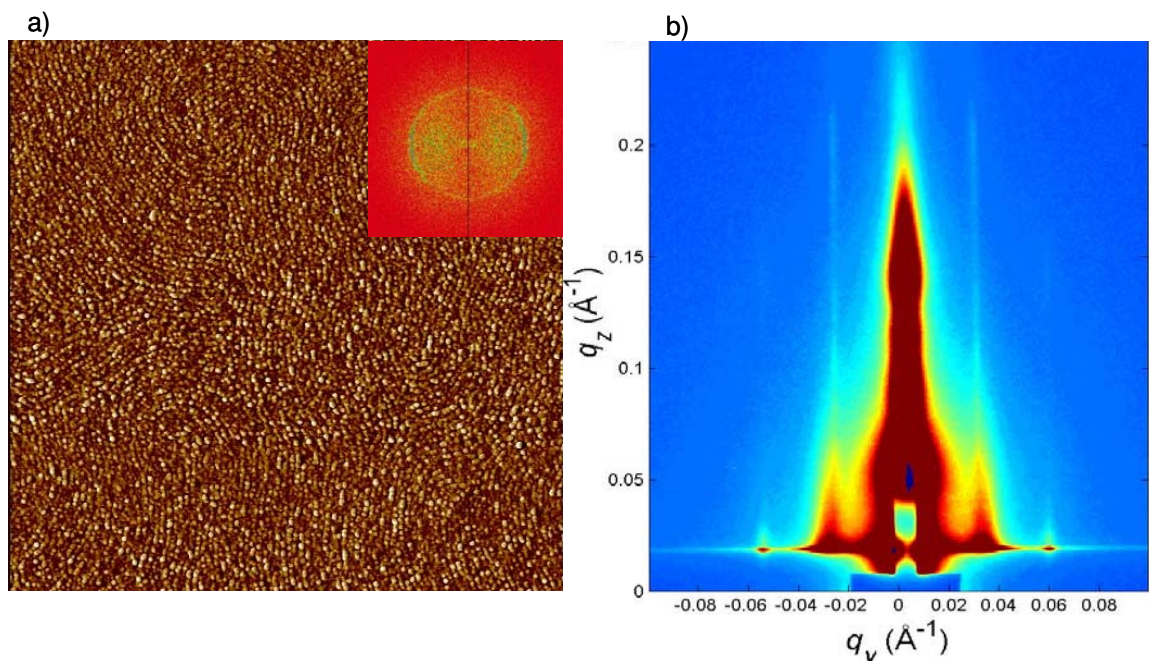


Figure 5.4. Surface analysis of POSS₁₀-S₁₃₀-POSS₁₀ triblock copolymer after thermal annealing at 375 °C. SFM (2 μm x 2 μm) phase image (a) revealed phase contrast with FFT (inset) of a ring that corresponds to 20 nm which is comparable to the long period of the triblock before thermal annealing. (b), GISAXS pattern of the thermally annealed thin film which suggests that the silica microdomains are perpendicular to the substrate.

5.3.3 Dielectric Constant of Silica Thin Film

In order to measure the dielectric constant (k) of the thin film by dielectric spectroscopy the minimum desired thickness of the film is 300 – 400 nm. Due to reduction in thickness of the film during the thermal annealing process it was difficult to obtain silica films of 300 – 400 nm. Thus the k values of the thin film was estimated using the Maxwell equation ($k \sim n^2$), where n is the refractive index of the material.³⁵ The refractive indexes (n) of the thin films before and after the thermal annealing were measured by Variable Angle Spectrometry Ellipsometry (VASE). The calculated n of the triblock copolymer before thermal annealing was 1.5 and after annealing n reduced to 1.24. The drop in n is attributed to the porosity created due to the removal of the organic phase during the thermal annealing process. The estimated dielectric constant of the silica

film using Maxwell equation is 1.53. The dielectric constant from Maxwell equation is generally lower than the dielectric constant calculated by dielectric spectroscopy.³⁵ This is due to the difference in frequency of the ellipsometry (10^{14} Hz) and frequency of dielectric spectroscopy (10^5 Hz). The dielectric constant depends linearly upon the permittivity of the material which is a frequency dependent property. At higher frequencies the permittivity is lower and thus the dielectric constant is also lower. Thus the dielectric constant calculated using Maxwell equation at higher frequency (10^{14} Hz) is generally lower than the dielectric constant calculated using dielectric spectroscopy (10^5 Hz).

The porosity of the annealed film was calculated using the Lorentz-Lorenz equation (equation (1)).³⁶

$$\frac{n_0^2 - 1}{n_0^2 + 2} (1 - P) = \frac{n^2 - 1}{n^2 + 2} \quad (1)$$

where n_0 is the refractive index of silica, n is the refractive index of the silica film and P is the porosity of the film. The porosity of the film is 44% due to removal of polystyrene organic phase and organic POSS peripheries. Thus ordered silica structures generated by poly(MAPOSS(isobutyl)-*b*-styrene-*b*-MAPOSS(isobutyl)) triblock copolymers have ultra-low dielectric constant and large porosity.

5.4 Summary

Thin film behavior of poly(MA-POSS(isobutyl)-*b*-Styrene-*b*-MA-POSS(isobutyl)) triblock copolymers of lamellae and hexagonal perforated lamellae bulk morphologies were studied on silicon oxide and gold substrates. Thin films of the triblock copolymers have similar morphologies on the substrates as in bulk. Lamellar triblock

copolymers with film thickness ten times the period of the microdomains align parallel to the substrate of the film while the lamellae in the perforated lamellae morphology orient perpendicular to the substrate. Chain architecture, film thickness, morphology and relative volume fractions affect the orientation of the microdomains. The cylinders of POSS lie parallel to the substrate and perforate through the PS lamellae. Due to perforated lamellae morphology, a 3-dimensional continuous structure of POSS is obtained on the surface. Ordered silica with 20 nm size features were obtained by thermal oxidation of POSS and removal of the organic phase. Silica generated by the oxidation of POSS has ultra low dielectric constant, high porosity and can be used as an insulator in microelectronic applications. Further work is on going to study the thin film morphology of the triblock copolymers on other substrates, and to use hybrid block copolymers for patterning applications.

5.5 References

- (1) Whitesides, G. M.; Grzybowski, B. *Science* **2002**, *295*, 2418-2421.
- (2) Stewart, M. D.; Willson, C. G. *MRS Bulletin* **2005**, *30*, 947-951.
- (3) Guarini, K. W.; Black, C. T.; Zhang, Y.; Kim, H.; Sikorski, E. M.; Babich, I. V. *Journal of Vacuum Science & Technology B* **2002**, *20*, 2788-2792.
- (4) Black, C. T.; Guarini, K. W.; Milkove, K. R.; Baker, S. M.; Russell, T. P.; Tuominen, M. T. *Applied Physics Letters* **2001**, *79*, 409-411.
- (5) Weiss, D.; Roukes, M. L.; Menschig, A.; Grambow, P.; Vonklitzing, K.; Weimann, G. *Physical Review Letters* **1991**, *66*, 2790-2793.
- (6) Volkmuth, W. D.; Austin, R. H. *Nature* **1992**, *358*, 600-602.

- (7) Volkmuth, W. D.; Duke, T.; Wu, M. C.; Austin, R. H.; Szabo, A. *Physical Review Letters* **1994**, *72*, 2117-2120.
- (8) Cheng, J. Y.; Ross, C. A.; Chan, V. Z. H.; Thomas, E. L.; Lammertink, R. G. H.; Vancso, G. J. *Advanced Materials* **2001**, *13*, 1174-1178.
- (9) Chou, S. Y.; Wei, M. S.; Krauss, P. R.; Fischer, P. B. *Journal of Applied Physics* **1994**, *76*, 6673-6675.
- (10) Park, S.; Lee, D. H.; Xu, J.; Kim, B.; Hong, S. W.; Jeong, U.; Xu, T.; Russell, T. *P. Science* **2009**, *323*, 1030-1033.
- (11) Hawker, C. J.; Russell, T. P. *MRS Bulletin* **2005**, *30*, 952-966.
- (12) Segalman, R. A. *Materials Science & Engineering R-Reports* **2005**, *48*, 191-226.
- (13) Bates, F. S.; Fredrickson, G. H. *Annual Review of Physical Chemistry* **1990**, *41*, 525-557.
- (14) Bucknall, D. G.; Anderson, H. L. *Science* **2003**, *302*, 1904-1905.
- (15) Park, M.; Harrison, C.; Chaikin, P. M.; Register, R. A.; Adamson, D. H. *Science* **1997**, *276*, 1401-1404.
- (16) Kim, H. C.; Jia, X. Q.; Stafford, C. M.; Kim, D. H.; McCarthy, T. J.; Tuominen, M.; Hawker, C. J.; Russell, T. P. *Advanced Materials* **2001**, *13*, 795-797.
- (17) Lin, Y.; Boker, A.; He, J. B.; Sill, K.; Xiang, H. Q.; Abetz, C.; Li, X. F.; Wang, J.; Emrick, T.; Long, S.; Wang, Q.; Balazs, A.; Russell, T. P. *Nature* **2005**, *434*, 55-59.
- (18) Templin, M.; Franck, A.; DuChesne, A.; Leist, H.; Zhang, Y. M.; Ulrich, R.; Schadler, V.; Wiesner, U. *Science* **1997**, *278*, 1795-1798.
- (19) Klaus, J. W.; Sneh, O.; George, S. M. *Science* **1997**, *278*, 1934-1936.

- (20) Maex, K.; Baklanov, M. R.; Shamiryany, D.; Iacopi, F.; Brongersma, S. H.; Yanovitskaya, Z. S. *Journal of Applied Physics* **2003**, *93*, 8793-8841.
- (21) Guliants, V. V.; Carreon, M. A.; Lin, Y. S. *Journal of Membrane Science* **2004**, *235*, 53-72.
- (22) Matejka, L.; Strachota, A.; Plestil, J.; Whelan, P.; Steinhart, M.; Slouf, M. *Macromolecules* **2004**, *37*, 9449-9456.
- (23) Leu, C. M.; Chang, Y. T.; Wei, K. H. *Macromolecules* **2003**, *36*, 9122-9127.
- (24) Zheng, L.; Farris, R. J.; Coughlin, E. B. *Macromolecules* **2001**, *34*, 8034-8039.
- (25) Zheng, L.; Kasi, R. M.; Farris, R. J.; Coughlin, E. B. *Journal of Polymer Science Part A-Polymer Chemistry* **2002**, *40*, 885-891.
- (26) Mather, P. T.; Jeon, H. G.; Romo-Uribe, A.; Haddad, T. S.; Lichtenhan, J. D. *Macromolecules* **1999**, *32*, 1194-1203.
- (27) Zheng, L.; Hong, S.; Cardoen, G.; Burgaz, E.; Gido, S. P.; Coughlin, E. B. *Macromolecules* **2004**, *37*, 8606-8611.
- (28) Pyun, J.; Matyjaszewski, K.; Wu, J.; Kim, G. M.; Chun, S. B.; Mather, P. T. *Polymer* **2003**, *44*, 2739-2750.
- (29) Hirai, T.; Leolukman, M.; Hayakawa, T.; Kakimoto, M.; Gopalan, P. *Macromolecules* **2008**, *41*, 4558-4560.
- (30) Lee, B.; Park, I.; Yoon, J.; Park, S.; Kim, J.; Kim, K. W.; Chang, T.; Ree, M. *Macromolecules* **2005**, *38*, 4311-4323.
- (31) Khanna, V.; Cochran, E. W.; Hexemer, A.; Stein, G. E.; Fredrickson, G. H.; Kramer, E. J.; Li, X.; Wang, J.; Hahn, S. F. *Macromolecules* **2006**, *39*, 9346-9356.

- (32) Ham, S.; Shin, C.; Kim, E.; Ryu, D. Y.; Jeong, U.; Russell, T. P.; Hawker, C. J. *Macromolecules* **2008**, *41*, 6431-6437.
- (33) Walton, D. G.; Kellogg, G. J.; Mayes, A. M.; Lambooy, P.; Russell, T. P. *Macromolecules* **1994**, *27*, 6225-6228.
- (34) Augustine, B. H.; Hughes, W. C.; Zimmermann, K. J.; Figueiredo, A. J.; Guo, X. W.; Chusuei, C. C.; Maidment, J. S. *Langmuir* **2007**, *23*, 4346-4350.
- (35) Huang, Q. R.; Volksen, W.; Huang, E.; Toney, M.; Frank, C. W.; Miller, R. D. *Chemistry of Materials* **2002**, *14*, 3676-3685.
- (36) Chen, H. J.; Fu, M. *Macromolecules* **2007**, *40*, 2079-2085.

CHAPTER 6

SUMMARY AND FUTURE OUTLOOK

This final chapter is comprised of two parts. The first part provides an overview of the studies described in chapters 2 through 5. In the second part, each chapter is revisited individually, providing an outline of future directions for the projects and suggesting some possible project extensions.

6.1 Summary

The goals of this thesis were to;

- Study the structure property relationship in POSS based polymer
- Incorporate POSS building blocks into polymers by a bottom-up approach
- Study the resulting microscopic structures of the novel hybrid block copolymers
- Understand the surface interactions of the hybrid block copolymers and to utilize them for patterning and low k application

In chapter 2 we studied the structure property relationship of PMA and styryl POSS homopolymers synthesized by ATRP and conventional free radical polymerization. The mass spectrometry data was obtained by electrospray ionization (ESI) and matrix assisted laser desorption-ionization (MALDI). We have succeeded in obtaining ESI and MALDI mass spectra on a variety of PMA and styryl POSS oligomers, in some cases as great as to masses $\sim 16,000$ g/mol. MALDI spectra were greatly enhanced with the use of a new matrix, 4,4'-dihydroxyoctafluoroazobenzene. ATRP syntheses were much more effective than conventional free radical procedures in creating

oligomers with a specified number of repeat units. ESI and MALDI mass spectra of the PMA POSS ATRP products showed the most intense peaks in the mass spectra corresponding to simple sodiated or potassiated species related to the substituted parent ion and less intense peaks arise from fragmentations (generally loss of one or more of the POSS side chains). The all-carbon backbone of the styryl materials was resistant to fragmentation, but the mass spectra obtained did show recombinations arising from the loss of the terminal Br atom not observed with the POSS PMAs. Differences in these ion chemistry products allowed us to draw conclusions about the structures of the styryl species.

In chapter 3, POSS building blocks were incorporated by a bottom-up approach in to low glass transition temperature, semi-crystalline poly(ethylene-butylene) based p(EB-*b*-MA-POSS(isobutyl)) diblock copolymers. Low PDI poly(ethylene-butylene) homopolymers and p(EB-*b*-MA-POSS(isobutyl)) diblock copolymers were synthesized by a combination of anionic polymerization and ATRP. Both phases of MA-POSS and EB crystallize depending upon the number of repeat units of MAPOSS and ethylene content in the EB chains. As both the phases are semi-crystalline interesting morphological behaviors were observed in these block copolymers. Three different morphologies i.e. cylinders, lamellae and spheres of the semicrystalline diblock copolymer were obtained by changing the relative volume fractions of EB and POSS phases. The cylindrical morphology which was obtained had a majority (60 volume %) EB block forming the cylindrical phase while the minor MAPOSS phase occupies the periphery around these cylinder. This inverse cylindrical morphology was observed presumably due to conformational asymmetry of the diblock copolymers and relative

flexibility of the connecting blocks. Order-order transitions from cylinders to lamellae morphology was observed in these diblock copolymers. Crystalline lamellae morphologies were formed due to crystallization of POSS cubes.

In chapter 4, POSS was incorporated as a building blocks by bottom-up approach in high glass transition temperature, amorphous polystyrene to obtain p(MA-POSS(isobutyl)-*b*-Styrene-*b*-MA-POSS(isobutyl)) triblock copolymers. Precise molecular weight and low PDI polystyrene homopolymers and p(MA-POSS(isobutyl)-*b*-Styrene-*b*-MA-POSS(isobutyl)) triblock copolymers were synthesized by a combination of anionic polymerization and ATRP. The use of CuBr₂ as co-catalyst increased the number of POSS units that can be attached by ATRP. Crystallization of POSS was confined in the hard domains of phase separated block copolymer. Three different morphologies, i.e. lamellae, cylinders and perforated lamellae have been observed by changing the relative volume fractions of POSS and PS. Perforated lamellae are a 3-dimensional monocontinuous morphology, were found with the lamellae of the minor component the PS phase were interrupted by POSS perforations connecting the majority phase. The phase diagram was slightly shifted due to the conformational asymmetry of the PS and POSS blocks. The size of the crystals and the d-spacing of the block copolymer could be controlled by varying the molecular weight of the copolymers.

In chapter 5, the thin film behavior of poly(MA-POSS(isobutyl)-*b*-Styrene-*b*-MA-POSS(isobutyl)) triblock copolymers of lamellae and hexagonal perforated lamellae bulk morphologies were studied on silicon oxide and gold substrates. Thin films of the triblock copolymers have similar morphologies on these substrates as in bulk. The microdomains can be oriented either parallel or perpendicular to the substrate. Chain architecture, film

thickness, morphology and relative volume fractions affect the orientation of the microdomains. Due to the perforated lamellae morphology, a 3-dimensional continuous structure of POSS was obtained on the surface. Ordered silica with 20 nm size features were obtained by thermal oxidation of POSS and removal of the organic phase. Silica generated by the oxidation of POSS has ultra low dielectric constant, high porosity and could be used as an insulator in microelectronic applications.

6.2 Future Outlook

Our study in chapters 2 – 5 have lead to many interesting results but have also raised some intriguing questions. In chapter 2, we have investigated POSS homopolymers by mass spectrometric studies using MALDI and ESI. The intensity of peaks in the MALDI spectra in most cases is sufficient to obtain ion mobility data. The structure property relationship of the homopolymers can be investigated ion mobility experiments.¹⁻⁴ A mass spectrometry and ion mobility setup at University of California, Santa Barbara can separate polymer chains based on conformations of the chains (Fig. 6.1). These studies will provide information about the structure and the conformation of the POSS molecules. The results from this study will minimize the experimental effort required to synthesize POSS molecules for specific applications. Ion mobility studies can be extended to complex structures for example block copolymers.

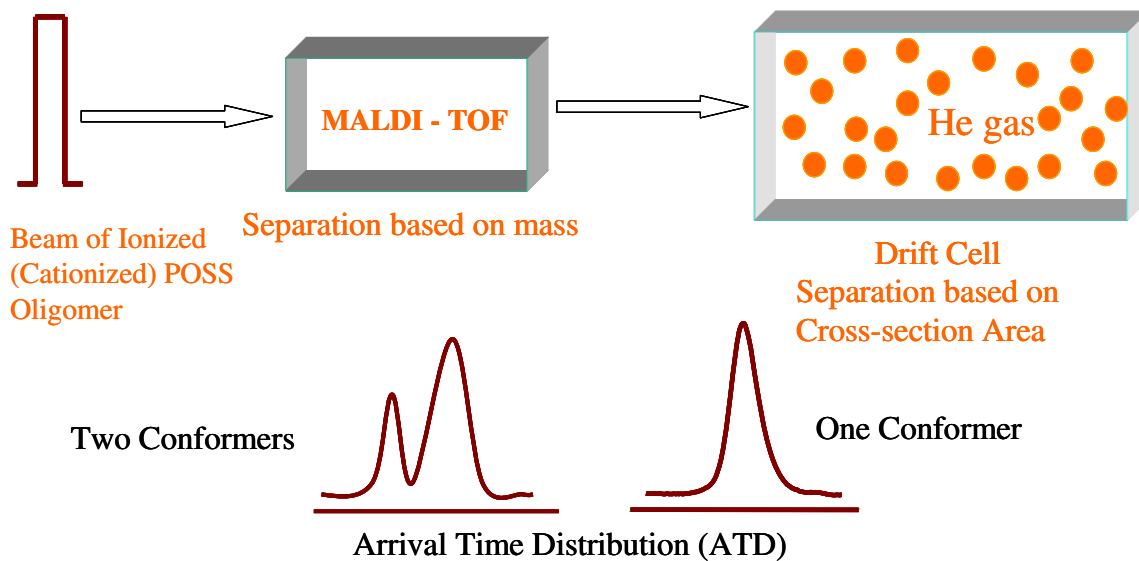


Figure 6.1 Study of conformation of polymers using MALDI-TOF and helium filled drift cell.

The results in chapter 3 have been the most intriguing. The combination of two semi-crystalline blocks has led to interesting morphological results. We have investigated a certain region of the phase diagram; further synthesis needs to be done to complete the study of the entire phase diagram. There is limited physical characterization data available for POSS molecules; to understand the phase behavior of these polymers it is necessary to obtain statistical segmental length, segmental volume of POSS molecules. On the morphological side it is essential to determine χ of these diblock copolymers. Factors such as annealing conditions, crystalline content can also affect the phase behavior and need to be investigated. Conformational asymmetry of the diblock copolymer needs to be determined experimentally and possibly theoretically or in conjunction with simulations. Based on the order-order transition from cylinders to lamellar morphology and lower d-spacing at high temperature, the possibility of an inverted phase diagram (i.e. lower χ at lower temperature) needs to be investigated.

In chapter 4 we have investigated POSS triblock copolymers with a high T_g polystyrene block. Perforated lamellar morphology obtained in this triblock studies, provides immense opportunity for further work. Further studies can be carried out to obtain bicontinuous gyroid morphology. Accurate determination of χ and conformational asymmetry would provide a better understanding of the phase diagram. Triblock copolymers with central POSS block and polystyrene end blocks can be synthesized for thin film studies.

In chapter 5 thin film behaviors of POSS triblock copolymer was studied on silica and gold surface and ordered low k silica was fabricated by thermal annealing of triblock copolymer. These investigations have shown that POSS has immense potential for application in nanopatterning as templates and in microelectronics as low k materials. Instead of thermal annealing, a technique like plasma oxidation needs to be investigated for nanopatterning applications. The orientations of the microdomains on other substrates also need to be studied. One of the limitations for large scale application is lack of long-range order of the microdomains. To induce long range order techniques such as shearing, zone annealing, chemical modification and trenches should be investigated.⁵⁻¹⁰ There is immense scope for basic scientific and application driven research on POSS molecules.

6.3 References

- (1) Anderson, S. E.; Baker, E. S.; Mitchell, C.; Haddad, T. S.; Bowers, M. T. *Chemistry of Materials* **2005**, *17*, 2537-2545.
- (2) Anderson, S. E.; Mitchell, C.; Haddad, T. S.; Vij, A.; Schwab, J. J.; Bowers, M. T. *Chemistry of Materials* **2006**, *18*, 1490-1497.

- (3) Baker, E. S.; Gidden, J.; Anderson, S. E.; Haddad, T. S.; Bowers, M. T. *Nano Letters* **2004**, *4*, 779-785.
- (4) Baker, E. S.; Gidden, J.; Fee, D. P.; Kemper, P. R.; Anderson, S. E.; Bowers, M. T. *International Journal of Mass Spectrometry* **2003**, *227*, 205-216.
- (5) Angelescu, D. E.; Waller, J. H.; Adamson, D. H.; Deshpande, P.; Chou, S. Y.; Register, R. A.; Chaikin, P. M. *Advanced Materials* **2004**, *16*, 1736-1740.
- (6) Bodycomb, J.; Funaki, Y.; Kimishima, K.; Hashimoto, T. *Macromolecules* **1999**, *32*, 2075-2077.
- (7) Berry, B. C.; Jones, R. L.; Karim, A. *PMSE Preprints* **2007**, *96*, 198-199.
- (8) Hashimoto, T.; Bodycomb, J.; Funaki, Y.; Kimishima, K. *Macromolecules* **1999**, *32*, 952-954.
- (9) Cheng, J. Y.; Ruiz, R.; Black, C. T.; Kim, H.-C. *Abstracts of Papers, 233rd ACS National Meeting, Chicago, IL, United States, March 25-29, 2007* **2007**, PMSE-122.
- (10) Park, S. M.; Stoykovich, M. P.; Ruiz, R.; Zhang, Y.; Black, C. T.; Nealey, P. E. *Advanced Materials* **2007**, *19*, 607-611.

APPENDIX

A. MALDI AND ESI DATA OF POSS OLIGOMERS

Table. MALDI SPECTRA

A1. $M = CH_3CH_2COOC-C(CH_3)_2-R_7T_7propylmethacrylate]_n -Br$

R = i-Butyl

linear^b	refl	M-Br+H+Na	M -Br+H+K	M +2H+Na-Br-F^a
		A	B	C
	1079.3			
	1081.3			
	1093.3		1086	
	1097.3			
	1165.4			1166
	1167.4			
	1173.2			
	1175.2			
1996.2	1995.6			
2023.5	2023.7	2026.4		
2040.6	2040.6		2042.5	
2109.4	2108.7			2110
	2965.8			
	2968.9	2970.1		

2967.1			
2983.1	2981.8		
	2984.8	2986.7	
3052.3	3050.8		3054
3910.2	3907.9		
	3912	3913.7	
3926.8	3924.9		
	3929.1		3929.8
3995.2			3998.8
4852.9	4854.3	4857.3	
4869.5	4868.2		
	4873.3		4873.4
4937.4			4942.4
			5886.1
5796.0		5800.9	
5811.9	5815.8		5817.1
5829.0			
5882.5			
6739.5		6744.6	

6755.5	6760.4		6760.7
6772.0			
6823.2			6829.7
7682.8		7688.3	
7698.7	7704		7704.4
7715.2			
7768.8			7773.3
7788.0			
8625.0		8620	
8642.1			8636
8661.0			
8709.8			8718
9573.1		9575.5	
9585.3			9591.6
9604.4			
9644.2			9639.6 (C-Br+3H-F)
9753.3			
10488.9			
10512.2		10519.2	
10530.8			10535.3
10595.9		10598.1 (M+Na)	10605.3
10643.6			10643.3 (C-H+K)

11473.9

11478.9

12437.8

12422.5

13341.5

13350.1

13507.6

$E = \text{CH}_3\text{CH}_2\text{OCOC}(\text{CH}_3)_2^-$; $F = \text{ibu}_7\text{Si}_8\text{O}_{12}(\text{CH}_2)_3^-$; $G = \text{ibu}_7\text{Si}_8\text{O}_{12}(\text{CH}_2)_3^-$

a. Alternatively, $G' = \text{ibu}_7\text{cage}(\text{CH}_2)_3\text{O}^-$ for $\mathbf{M}+2\mathbf{H}+\mathbf{K}-\mathbf{Br}-\mathbf{G}'$

b. blue = TOF linear mode

A2. M = CH₃CH₂COOC-C(CH₃)₂-R₇T₇propylmethacrylate]_n -Br

R = Phenyl

M -Br+H+Na M -Br+H+K M +2H+Na-Br-F M +Na+K-Br-F+EM +3Na+H-Br-2F

m/z

2064

2079

2190

2305 2306.3

~2322

2390 2392.4

3390 3389.8

3406 3405.9

3474 3475.9

3650 3644.3 3654.3

4473 4474.4

4489 4489.5

4558 4559.5

4687 4689.6

5557 5557

5572 5573.1

5641 5643.1

5768 5773.1

5800 5795.3

6641	6640.5			
6656		6656.6		
6725			6726.6	
6847?				6856.7
6880			6878.9	
7725	7724.1			
7739		7740.2		
7808			7810.2	
7930?				
7962			7962.4	7956.4
	8807.7?			
8823		8823.8		
8892			8893.8	
9043			9046	
9906				
9975				
10122			10129.6	

F = Phenyl₇Si₈O₁₂(CH₂)₃⁻

A3. M = C₆H₄(CO)₂NCH₂CH₂OCH₂CH₂OOC-C(CH₃)₂-R₇T₇propylmethacrylate]_n-Br

R = *i*-Butyl

	M - Br+H+Na	M - Br+H+K	M +2H+Na- Br-G ^a	M - Br+2H+K-G	M +H+K-G	M +2Na-G	M +Na+K- G
m/z							
2215	2215.6						
2231		2231.7					
2300			2302.7				
2316				2318.8			
2400					2396.7	2402.6	
2415							2418.7
3159	3159.2						
3175		3175.3					
3244			3246.3				
3259				3262.4			
3344					3340.3	3346.1	
3359							3362.3
4103	4102.9						
4119		4119					
4135							
4187			4190				
4203				4206.1			

4288			4284	4289.8	
4303					4305.9
5047	5046.5				
5063		5062.6			
5132			5133.6		
5148				5149.7	
5232			5227.6	5233.5	
5248					5249.6
5991	5990.1				
6007		6006.2			
~60					
76			6077.2		
6092				6093.4	
~61					
75			6171.2	6177.1	
6192					6193.2
6935	6933.8				
6951		6949.9			
7021			7020.9		
7034				7037	
7071					
7120			7114.9	7120.8	

7136		7136.9
7165		
7878	7877.4	
7894	7893.5	
	7964.5?	
7978		7980.6
8078		8080.5
8108		
8821		
?	8821.5	
8837	8837.2	



a. Alternatively, $G' = \text{ibu}_7\text{cage}(\text{CH}_2)_3\text{O}^-$ for $\mathbf{M}+2\mathbf{H}+\mathbf{K}-\mathbf{Br}-\mathbf{G}'$

A4. M =NH₂CH₂CH₂OCH₂CH₂OOC-C(CH₃)₂-[R₇T₇propylmethacrylate]_n -Br
R = i-Butyl

M -Br+H+K

m/z

2240

2340

2440

2458

2558

2659

2676

2777

2794

2801

2878

2895

2913

2977

2996

3013

3020

3096

3113

3131	
3214	
3232	
3314	
3332	
3432	
3532	
3550	
3650	
3669	
3750	
3769	
3869	
3886	
3969	
3989	3988.7
4087	
4207	
4307	
4932	4932.5
5876	5876.2
6819	6819.8

6898	
7032	
7763	7763.4
7982	
8708	
8920	
9652	9650.7
9861	

A5. M = [R₇T₇Propylmethacrylate]_n[(CH₃)₂CCN]_{m=1,2}
R = Cyclopentyl

	M + Na + H +		M + Na + 2ibuCN	M + K + 2ibuCN
	ibuCN			
m/z				
1794				
1927				
2148	2147.5			
2184				
2234				2230.7
2294				
2374				
3176	3175.2			
3194				
3243			3242.3	
3261				3258.4
4204	4203			
4220				
4272			4270	
4292				4286.1
5232	5230.7			
5320			5297.8?	5313.9
6262	6258.4			

~6349

6341.6

A6. M = R₇T₇Propylmethacrylate]_n[(CH₃)₂CCN]_{m=1,2}

R = i-Butyl

M+Na + 2ibuCN M+Na + ibuCN

m/z

1160

1173

1225

1232

1297

1340

1441

1532

1539

1576

1604

1906

1911

1913

1977

1979.4

2045

2046.6

2116

2288

2353		
2422		
2661		
2921		2923
2992	2990.1	
3057		
3865		3866.6
3937	3933.7	
4003		
4811		4810.3
4878	4877.4	
5753		5753.9
5824	5821	
6694		6697.6
6766	6764.6	
7640		7641.2
n/a	7708.3	

A7. $M = R_7T_7(C_6H_4CHCH_2)_n[(CH_3)_2CCN]_{m=1,2,3}$

R = i-Butyl

	$M + Na + H$	$M + Na + H +$ ibuCN	$M + Na +$ 2ibuCN	$M + Na +$ 3ibuCN
m/z				
1224				
1316				
1390				
1414				
1417				
1575				
1930		1931.3		
1943				
1998			1998.4	
2783	2783			
2824				
2851		2850.9		
2865				
2904				
2919			2918	
3771		3770.5		
3783				

3786		
3839		3837.7
4623	4623	
4692		4690.1
4759		4757.3
5611		5609.8
5678		5676.9
6531		6529.4
6599		6596.5
~7455		7449
7518		7516.1
7584		7584.2
8384		
8442		8435.7
9293		
9361		9355.4
10282		10275
11201		11194.6



R = i-Butyl

	Refl mode		M-Br+H+Na ^a	M-Br+H+K	M-Br+H+Na-phth
m/z					
1159					
1555.5					
2174			2167.6	2183.7	
2467.8	2469.1	2465.4			
~2777	2781.2	2778.2			2782.9
	2978.3	2974.8			
3096.1	3097.4	3094.4	3087.2		
	3362.5	3357.7			
3388.2	3388.5				
4016.5	4005.9	4011.8	4006.8		
	4017.9			4022.8	
		4403.3			
	4618.3	4611.1			4622.1
		4810.4			
	4924.7	4931	4926.4		
4935	4939.6			4942.5	
		5188.3			
5853		5850.4	5846		

	6443.8		
6771	6770	6765.6	6781.7
7692	7674.1	7685.3	
8599	8598.1	8604.9	
9528	9524.3	9524.5	
	10445.5	10444.1	
	11369.3	11363.7	
	12293.5	12283.3	
	13225.5	13203	
	14156.2	14122.6	
	15072.2		
	15997.5		
	16939.7		

- $m/z = 919$ repeat monomer unit.
- red = interpolated from spectrum
- blue = TOF linear mode

A9. M = C₆H₄(CO)₂N CH₂CH₂OCH₂CH₂OOC-C(CH₃)₂-R₇T₇(C₆H₄CHCH₂)_n-Br

R = Cyclopentyl

	Refl mode	M-Br+H+Na ^a	M-Br+H+K	M+K	M ₂ +Na	M-Br+H+K- X
m/z						
1048.3 ^b						1043.7
		2043.2				2047.4
~2340	2333	2335.7	2351.7			
	2347.1	2341.3				
	2354					
	2363.9					
2636.8	2637.1	2631.7			2639	
3029	2640					
	2657.1					
		3025.8				3051.1
	3337.4	3332.9	3339.9			
~3350	3350.3	3345.4	3354.9			
	3369.3	3362.5				
	3436.4	3430.2		3434.4		
	3541.5					
					3658.8	
3640.2	3660.5	3625			K	

4053						4054.8
~4325	4341.8	4351	4343.1			
	4354.8					
	4358			4359.2		
	4374.9					
	4387.1					
	4440				4438	
	4645	4636				4646.4
	4664.1					4662.4
5339		5352.8	5346.8	5362.8	5441.7	5058.5
~5650		5642				5650.1
6343		6336.2	6350.5	6366.5	6445.4	6062.2
		6647.3				6653.8
7364		7346.2	7354.2	7370.2		7065.9
		8351.7				

a. $m/z = 1003$ monomer repeat unit

b. blue = TOF linear mode

c. $X = C_6H_4(CO)_2NCH_2CH_2OCH_2CH_2OOC-C(CH_3)_2-$

A10. M = C₆H₄(CO)₂NCH₂CH₂OCH₂CH₂OOC-C(CH₃)₂-R₇T₇(C₆H₄CHCH₂)_n-Br
R = Cyclohexyl

m/z	refl		M-Br+H+K		
	mode		M+K ^a	M-Br+H+Na	M-Br+H+K-X
1442.6 ^b		1440.9			1444..5
	2079.8	2077			
2096.9	2096.9	2093			
	2113.8	2111			
2245.8	2244.9	2230			2244
	2542.9	2539			2544.9
~2850		2828	2627		
		3194			
		3322			
~3350		3338			3345
	3644.6	3638			
3733	3743.6	3735	3729		
4300	4298.1	4295			
	4446.3				4447.6
	4731.5	4739		4736	
	4745.4				4752
4828	4832.6		4830.8		
	4844.5				
		4923			

5936

5928 5932.7

7051

a. $m/z = 1101$ monomer repeat unit.

b. TOF linear mode

c. $\mathbf{X} = C_6H_4(CO)_2NCH_2CH_2OCH_2CH_2OOC-C(CH_3)_2-$

A11. M = NH₂CH₂CH₂OCH₂CH₂OOC-C(CH₃)₂-(Cyclohexyl)₇T₇(C₆H₄CHCH₂)_n-Br
R = Cyclohexyl

m/z	M-				
	M-Br+ ^a H+Na	M-Br+ H+K	Br+H+ Na-et	M- Br+2H	M-Br+H+ K-X
1059.4	1057 ^b				
			1125.8		
	1124		7		
1143.5	1142				1141.98
1145.5					
	1215				
1291.5	1290	1300.1		1278.11	
1321			1316.2		
1337	1345				
1439	1437				
1625					
2079	2077				
2081					
2084	2096				
2100					
2116					
			2227.7		
2228	2225			5	

2246	2244				2243.86
			2418.0		
	2391	2402	8		2379.99
3328	3323				3329.6

- $m/z = 1101$ monomer repeat unit.
- TOF linear mode
- $\mathbf{X} = \text{NH}_2\text{CH}_2\text{CH}_2\text{OCH}_2\text{CH}_2\text{OOC}-\text{C}(\text{CH}_3)_2-$

BIBLIOGRAPHY

- Abad, M. J.; Barral, L.; Fasce, D. P.; Williams, R. J. J. *Macromolecules* **2003**, *36*, 3128-3135.
- Agaskar, P. A. *Inorg. Chem.* **1991**, *30*, 2707-2708.
- Agaskar, P. A.; Klemperer, W. G. *Inorg. Chim. Acta* **1995**, *229*, 355-364.
- Aizenberg, J.; Weaver, J. C.; Thanawala, M. S.; Sundar, V. C.; Morse, D. E.; Fratzl, P. *Science* **2005**, *309*, 275-278.
- Alexandre, M.; Dubois, P. *Materials Science & Engineering R-Reports* **2000**, *28*, 1-63.
- Almar Posta, T. D., Richard Evans, Guoxin Li, Graeme Mod, Micheal O`Shea, *Macromolecules* **2006**, *39*, (16), 5293-5306.
- Anderson, S. E.; Bodzin, D.; Haddad, T. S.; Boatz, J. A.; Dupuis, N. F.; Mitchell, C.; and Bowers, M. T.: *Chem Mater.* **2008**, *20*, 4299-4309.
- Anderson, S. E.; Mitchell, C.; Bowers, M. T.; and T. S. Haddad, *Chem. Mater.*, **2005**, *17*, 2537-2545.
- Anderson, S. E.; Mitchell, C.; Haddad, T. S.; Vij, A.; Schwab, J. J.; Bowers, M. T., *Chemistry of Materials* **2006**, *18*, 1490-1497.
- Andrij Baumketner, Summer L. Bernstein, Thomas Wytttenbach, Gal Bitan, David B. Teplow, Michael T. Bowers, and Joan-Emma Shea, *Protein Sci.* **2006**, *15*, 420-428
- Angelescu, D. E.; Waller, J. H.; Adamson, D. H.; Deshpande, P.; Chou, S. Y.; Register, R. A.; Chaikin, P. M. *Advanced Materials* **2004**, *16*, 1736-1740.
- Antkowiak, D.; Tate, D. P.; Oberster, A. E.; Halasa, A. F. *Journal of Polymer Science Part a-1-Polymer Chemistry* **1972**, *10*, 1319-&.
- Augustine, B. H.; Hughes, W. C.; Zimmermann, K. J.; Figueiredo, A. J.; Guo, X. W.; Chusuei, C. C.; Maidment, J. S. *Langmuir* **2007**, *23*, 4346-4350.
- Auner, N.; Ziemer, B.; Herrschaft, B.; Ziche, W.; John, P.; Weis, J., *European Journal of Inorganic Chemistry*, **1999**, 1087-1094.
- Baker, E. S.; Gidden, J.; Anderson, S. E.; Haddad, T. S.; and Bowers, M.T., *Nano Lett.*, **2004**, *4*, 779-785.

- Baker, E. S.; Gidden, J.; Fee, D. P.; Kemper, P. R.; Anderson, S. E.; Bowers, M. T. *International Journal of Mass Spectrometry* **2003**, *227*, 205-216.
- Bakhtiar, R., *Rapid Communications in Mass Spectrometry*, **1999**, *13*, 87-89.
- Bakhtiar, R.; Feher, F. J., *Rapid Communications in Mass Spectrometry*, **1999**, *13*, 687-694.
- Baney, R. H.; Cao, X. In *Silicon Containing Polymers*; Jones, R. G., Ando, W., Chojnowski, J., Eds.; Klumer Academic Publishers: Netherlands, 2000, p 157-184.
- Baney, R. H.; Itoh, M.; Sakakibara, A.; Suzuki, T. *Chem. Rev.*, **1995**, *92*, 1409-1430.
- Baney, R. H.; Itoh, M.; Sakakibara, A.; Suzuki, T. *Chemical Reviews* **1995**, *95*, 1409-1430.
- Bassindale, A.R.; Parker, D.J.; Pourny, M.; Taylor, P. G.; Horton, P. N.; and Hursthouse, M.B., *J. Organomet. Chem.*, **2004**, *23*, 4400-4405.
- Bassindale, A.R.; Pourny, M.; Taylor, P.G.; Hursthouse, M.B.; Light, M.E. *Angew. Chem., Int. Ed.*, **2003**, *42*, 3488-3490.
- Bates, F. S.; Fredrickson, G. H. *Annual Review of Physical Chemistry* **1990**, *41*, 525-557.
- Bates, F. S.; Fredrickson, G. H. *Macromolecules* **1994**, *27*, 1065-1067.
- Bates, F. S.; Fredrickson, G. H. *Physics Today* **1999**, *52*, 32-38.
- Berry, B. C.; Jones, R. L.; Karim, A. *PMSE Preprints* **2007**, *96*, 198-199.
- Bharadwaj, R. K.; Berry, R. J.; Farmer, B. L. *Polymer* **2000**, *41*, 7209-7221.
- Bizet, S.; Galy, J.; Gerard, J. F. *Polymer* **2006**, *47*, 8219-8227.
- Black, C. T.; Guarini, K. W.; Milkove, K. R.; Baker, S. M.; Russell, T. P.; Tuominen, M. T. *Applied Physics Letters* **2001**, *79*, 409-411.
- Bodycomb, J.; Funaki, Y.; Kimishima, K.; Hashimoto, T. *Macromolecules* **1999**, *32*, 2075-2077.
- Bucknall, D. G.; Anderson, H. L. *Science* **2003**, *302*, 1904-1905.
- Bywater, S.; Worsfold, D. J. *Canadian Journal of Chemistry-Revue Canadienne De Chimie* **1962**, *40*, 1564-&.

- Capadona, J. R.; Shanmuganathan, K.; Tyler, D. J.; Rowan, S. J.; Weder, C. *Science* **2008**, *319*, 1370-1374.
- Capaldi, F. M.; Rutledge, G. C.; Boyce, M. C. *Macromolecules* **2005**, *38*, 6700-6709.
- Cardoen, G. B., K.; Emrick T.; Coughlin E.B. *Macromolecules* **2006**, *39*, 7170-7173.
- Cardoen, G. University of Massachusetts Amherst, 2006.
- Cardoen, G.; Coughlin, E. B. *Macromolecules* **2004**, *37*, 5123-5126.
- Castillo, R. V.; Muller, A. J.; Lin, M. C.; Chen, H. L.; Jeng, U. S.; Hillmyer, M. A. *Macromolecules* **2008**, *41*, 6154-6164.
- Chan, E. R.; Zhang, X.; Lee, C. Y.; Neurock, M.; Glotzer, S. C. *Macromolecules* **2005**, *38*, 6168-6180.
- Chen, H. J.; Fu, M. *Macromolecules* **2007**, *40*, 2079-2085.
- Cheng, J. Y.; Ross, C. A.; Chan, V. Z. H.; Thomas, E. L.; Lammertink, R. G. H.; Vancso, G. J. *Advanced Materials* **2001**, *13*, 1174-1178.
- Cheng, J. Y.; Ross, C. A.; Thomas, E. L.; Smith, H. I.; Vancso, G. J. *Advanced Materials* **2003**, *15*, 1599-+.
- Cheng, J. Y.; Ruiz, R.; Black, C. T.; Kim, H.-C. *Abstracts of Papers, 233rd ACS National Meeting, Chicago, IL, United States, March 25-29, 2007* **2007**, PMSE-122.
- Chiang, W. S.; Lin, C. H.; Yeh, C. L.; Nandan, B.; Hsu, P. N.; Lin, C. W.; Chen, H. L.; Chen, W. C. *Macromolecules* **2009**, *42*, 2304-2308.
- Chou, S. Y.; Wei, M. S.; Krauss, P. R.; Fischer, P. B. *Journal of Applied Physics* **1994**, *76*, 6673-6675.
- Constable, G. S.; Lesser, A. J.; Coughlin, E. B. *Macromolecules* **2004**, *37*, 1276-1282.
- Donald, A. M. *Materials Today* **2005**, *8*, 56.
- Drazkowski, D. B.; Lee, A.; Haddad, T. S.; Cookson, D. J. *Macromolecules* **2006**, *39*, 1854-1863.
- Eisenberg, P.; Erra-Balsells, R.; Ishikawa, Y.; Lucas, J.C.; Mauri, A. N.; Nonami, H.; Riccardi, C. C.; Williams, R. J. J.; *Macromolecules*, **2000**, *33*, 1940-1947.

- Erin Shammel Baker, John E. Bushnell, Stephen R. Wecksler, Mark D. Lim, Manuel J. Manard, Nicholas F. Dupuis, Peter C. Ford, and Michael T. Bowers, *J. Am. Chem. Soc.* **2005**, *127*, 18222-18228.
- Erin Shammel Baker, Summer L. Bernstein, and Michael T. Bowers, *J. Am. Soc. Mass Spectrom.* **2005**, *16*, 989-997.
- Farahani, M.; Antonucci, J. M.; Guttman, C. M., *Polymer Preprints (American Chemical Society, Division of Polymer Chemistry)*, **2004**, *45*, 350-351.
- Farahani, M.; Wallace, W. E.; Antonucci, J. M.; Guttman, C. M., *Journal of Applied Polymer Science*, **2006**, *99*, 1842-1847.
- Fasce, D. P.; Williams, R. J. J.; Erra-Balsells, R.; Ishikawa, Y.; Nonami, H., *Macromolecules*, **2001**, *34*, 3534-3539.
- Floudas, G.; Vazaiou, B.; Schipper, F.; Ulrich, R.; Wiesner, U.; Iatrou, H.; Hadjichristidis, N. *Macromolecules* **2001**, *34*, 2947-2957.
- Frankland, J. A.; Edwards, H. G. M.; Johnson, A. F.; Lewis, I. R.; Poshyachinda, S. *Spectrochimica Acta Part a-Molecular and Biomolecular Spectroscopy* **1991**, *47*, 1511-1524.
- Gehlsen, M. D.; Bates, F. S. *Macromolecules* **1994**, *27*, 3611-3618.
- Gettinger, C. L.; Heeger, A. J.; Drake, J. M.; Pine, D. J. *Journal of Chemical Physics* **1994**, *101*, 1673-1678.
- Gidden, J. ; Kemper, P.R.; Shammel, E. ; Fee, D.P.; Anderson, S.E.; and Bowers, M.T., *Int. J. Mass Spectrom.*, **2003** *222*, 63-73.
- Gido, S. P.; Schwark, D. W.; Thomas, E. L.; Goncalves, M. D. *Macromolecules* **1993**, *26*, 2636-2640.
- Gilman, J. W.; Schlitzer, D. S.; Lichtenhan, J. D. *Journal of Applied Polymer Science* **1996**, *60*, 591-596.
- Gomez-Romero, P. *Advanced Materials* **2001**, *13*, 163-174.
- Grason, G. M.; Kamien, R. D. *Macromolecules* **2004**, *37*, 7371-7380.
- Guarini, K. W.; Black, C. T.; Zhang, Y.; Kim, H.; Sikorski, E. M.; Babich, I. V. *Journal of Vacuum Science & Technology B* **2002**, *20*, 2788-2792.
- Gulians, V. V.; Carreon, M. A.; Lin, Y. S. *Journal of Membrane Science* **2004**, *235*, 53-72.

- Hadjichristidis, N.; Iatrou, H.; Pispas, S.; Pitsikalis, M. *Journal of Polymer Science Part a-Polymer Chemistry* **2000**, *38*, 3211-3234.
- Hahn, S. F. *Journal of Polymer Science Part a-Polymer Chemistry* **1992**, *30*, 397-408.
- Hajduk, D. A.; Takenouchi, H.; Hillmyer, M. A.; Bates, F. S.; Vigild, M. E.; Almdal, K. *Macromolecules* **1997**, *30*, 3788-3795.
- Halasa, A. F.; Lohr, D. F.; Hall, J. E. *Journal of Polymer Science Part a-Polymer Chemistry* **1981**, *19*, 1357-1360.
- Ham, S.; Shin, C.; Kim, E.; Ryu, D. Y.; Jeong, U.; Russell, T. P.; Hawker, C. J. *Macromolecules* **2008**, *41*, 6431-6437.
- Hamley, I. W. In *Interfaces Crystallization Viscoelasticity* 1999; Vol. 148, p 113-137.
- Hamley, I. W. In *Interfaces Crystallization Viscoelasticity*; Springer-Verlag Berlin: Berlin, 1999; Vol. 148, p 113-137.
- Harrison S., W. K., *Polymer Preprints (American Chemical Society, Division of Polymer Chemistry)* **2004**, *45*, (2), 545-546.
- Hashimoto, T.; Bodycomb, J.; Funaki, Y.; Kimishima, K. *Macromolecules* **1999**, *32*, 952-954.
- Hawker, C. J.; Russell, T. P. *MRS Bulletin* **2005**, *30*, 952-966.
- Hirai, T.; Leolukman, M.; Hayakawa, T.; Kakimoto, M.; Gopalan, P. *Macromolecules* **2008**, *41*, 4558-4560.
- Hsieh, H. L.; Quirk, R. P.; Editors *Anionic Polymerization : Principles And Practical Applications 1st Edition*, 1996.
- <http://research.chem.psu.edu/hragroup/biomaterials.htm>.
- <http://www.egr.msu.edu/cmscl/>.
- <http://www.hybridplastics.com>.
- http://www.tainstruments.com/main.aspx?n=2&id=181&main_id=348&siteid=11.
- Huang, Q. R.; Volksen, W.; Huang, E.; Toney, M.; Frank, C. W.; Miller, R. D. *Chemistry of Materials* **2002**, *14*, 3676-3685.
- Intasanta, N.; Russell, T. P.; Coughlin, E. B. *Abstracts of Papers of the American Chemical Society* **2004**, *227*, U513-U513.

- Jeon, H. G.; Mather, P. T.; Haddad, T. S. *Polymer International* **2000**, *49*, 453-457.
- Joshi, M.; Butola, B. S. *Journal of Macromolecular Science-Polymer Reviews* **2004**, *C44*, 389-410.
- Karak, N. *Journal of Polymer Materials* **2006**, *23*, 1-20.
- Karas, M.; Krueger, R., Ion formation in MALDI: *Chemical Reviews*, **2003**, *103*, 427-439.
- Khandpur, A. K.; Forster, S.; Bates, F. S.; Hamley, I. W.; Ryan, A. J.; Bras, W.; Almdal, K.; Mortensen, K. *Macromolecules* **1995**, *28*, 8796-8806.
- Khanna, V.; Cochran, E. W.; Hexemer, A.; Stein, G. E.; Fredrickson, G. H.; Kramer, E. J.; Li, X.; Wang, J.; Hahn, S. F. *Macromolecules* **2006**, *39*, 9346-9356.
- Kickelbick, G. *Progress in Polymer Science* **2003**, *28*, 83-114.
- Kim, H. C.; Jia, X. Q.; Stafford, C. M.; Kim, D. H.; McCarthy, T. J.; Tuominen, M.; Hawker, C. J.; Russell, T. P. *Advanced Materials* **2001**, *13*, 795-797.
- Kim, K. M.; Keum, D. K.; Chujo, Y. *Macromolecules* **2003**, *36*, 867-875.
- Kim, K. M.; Ouchi, Y.; Chujo, Y. *Polymer Bulletin* **2003**, *49*, 341-348.
- Klaus, J. W.; Sneh, O.; George, S. M. *Science* **1997**, *278*, 1934-1936.
- Knochenmuss, R., *The Analyst*, **2006**, *131*, 966-86.
- Kopesky, E. T.; Haddad, T. S.; Cohen, R. E.; McKinley, G. H. *Macromolecules* **2004**, *37*, 8992-9004.
- Kopesky, E. T.; McKinley, G. H.; Cohen, R. E. *Polymer* **2006**, *47*, 299-309.
- Kresge, C. T.; Leonowicz, M. E.; Roth, W. J.; Vartuli, J. C.; Beck, J. S. *Nature* **1992**, *359*, 710-712.
- Larsson, K. *Arkiv for Kemi* **1961**, *16*, 209-214.
- Lecolley, F.; Waterson, C.; Carmichael, A. J.; Mantovani, G.; Harrisson, S.; Chappell, H.; Limer, A.; Williams, P.; Ohno, K.; Haddleton, D. M. *Journal of Materials Chemistry* **2003**, *13*, 2689-2695.
- Lee, A.; Lichtenhan, J. D. *Journal of Applied Polymer Science* **1999**, *73*, 1993-2001.
- Lee, A.; Lichtenhan, J. D. *Macromolecules* **1998**, *31*, 4970-4974.

- Lee, B.; Park, I.; Yoon, J.; Park, S.; Kim, J.; Kim, K. W.; Chang, T.; Ree, M. *Macromolecules* **2005**, *38*, 4311-4323.
- Leibler, L. *Macromolecules* **1980**, *13*, 1602-1617.
- Leu, C. M.; Chang, Y. T.; Wei, K. H. *Macromolecules* **2003**, *36*, 9122-9127.
- Leu, C. M.; Reddy, G. M.; Wei, K. H.; Shu, C. F. *Chemistry of Materials* **2003**, *15*, 2261-2265.
- Li, G. Z.; Pittman, C. U., Chapter 5 in *Macromolecules Containing Metals and Metal-like Elements*. Vol. 5 Group IVA Polymers, Abd El Aziz, A.S.; Carraher, C.E.; Pittman, C.U.; Zeldin, M., Editors, John Wiley & Sons, Hoboken, NJ, 2005, pp 79-131.
- Li, G. Z.; Wang, L. C.; Ni, H. L.; Pittman, C. U. *J. Inorg. Organomet. Polym.*, **2001**, *11* 123-154.
- Lichtenhan, J. D. *Comments Inorg. Chem.*, **1995**, *17*, 115-130.
- Lichtenhan, J. D. in *Polymeric Materials Encyclopedia*, J. C. Salamore (ed.) CRC Press, NY, **1996** 7769-7778.
- Lin, Y.; Boker, A.; He, J. B.; Sill, K.; Xiang, H. Q.; Abetz, C.; Li, X. F.; Wang, J.; Emrick, T.; Long, S.; Wang, Q.; Balazs, A.; Russell, T. P. *Nature* **2005**, *434*, 55-59.
- Mackay, M. E.; Tuteja, A.; Duxbury, P. M.; Hawker, C. J.; Van Horn, B.; Guan, Z. B.; Chen, G. H.; Krishnan, R. S. *Science* **2006**, *311*, 1740-1743.
- Maex, K.; Baklanov, M. R.; Shamiryan, D.; Iacopi, F.; Brongersma, S. H.; Yanovitskaya, Z. S. *Journal of Applied Physics* **2003**, *93*, 8793-8841.
- Mark, J. E. *Accounts of Chemical Research* **2004**, *37*, 946-953.
- Matejka, L.; Strachota, A.; Plestil, J.; Whelan, P.; Steinhart, M.; Slouf, M. *Macromolecules* **2004**, *37*, 9449-9456.
- Mather, P. T.; Jeon, H. G.; Romo-Uribe, A.; Haddad, T. S.; Lichtenhan, J. D. *Macromolecules* **1999**, *32*, 1194-1203.
- Matsen, M. W.; Bates, F. S. *Journal of Chemical Physics* **1997**, *106*, 2436-2448.
- Matsen, M. W.; Bates, F. S. *Journal of Polymer Science Part B-Polymer Physics* **1997**, *35*, 945-952.

- Matsen, M. W.; Bates, F. S. *Macromolecules* **1996**, *29*, 7641-7644.
- Matsen, M. W.; Schick, M. *Macromolecules* **1994**, *27*, 4014-4015.
- Matsen, M. W.; Schick, M. *Macromolecules* **1994**, *27*, 6761-6767.
- Matsen, M. W.; Schick, M. *Macromolecules* **1994**, *27*, 7157-7163.
- Matsen, M. W.; Schick, M. *Physical Review Letters* **1994**, *72*, 2660-2663.
- Miao, J. J.; Cui, L.; Lau, H. P.; Mather, P. T.; Zhu, L. *Macromolecules* **2007**, *40*, 5460-5470.
- Milner, S. T. *Macromolecules* **1994**, *27*, 2333-2335.
- Moresesequela, B.; Stjacques, M.; Renaud, J. M.; Prudhomme, J. *Macromolecules* **1980**, *13*, 100-106.
- Nair, M. B.; Blum, F. D. *Abstracts of Papers of the American Chemical Society* **2005**, *229*, U961-U961.
- Osuji, C. O.; Chen, J. T.; Mao, G.; Ober, C. K.; Thomas, E. L. *Polymer* **2000**, *41*, 8897-8907.
- Papadakis, C. M.; Almdal, K.; Mortensen, K.; Posselt, D. *Europhysics Letters* **1996**, *36*, 289-294.
- Park, M.; Harrison, C.; Chaikin, P. M.; Register, R. A.; Adamson, D. H. *Science* **1997**, *276*, 1401-1404.
- Park, S. M.; Stoykovich, M. P.; Ruiz, R.; Zhang, Y.; Black, C. T.; Nealey, P. E. *Advanced Materials* **2007**, *19*, 607-611.
- Park, S.; Lee, D. H.; Xu, J.; Kim, B.; Hong, S. W.; Jeong, U.; Xu, T.; Russell, T. P. *Science* **2009**, *323*, 1030-1033.
- Phillips, S. H.; Haddad, T. S.; Tomczak, S. J. *Curr. Opin. Sol. State Mat. Sci.*, **2004**, *8*, 21-29.
- Pielichowski, K.; Njuguna, J.; Janowski, B.; Pielichowski, J. In *Supramolecular Polymers Polymeric Betains Oligomers* 2006; Vol. 201, p 225-296.
- Pracella, M.; Chionna, D.; Fina, A.; Tabuani, D.; Frache, A.; Camino, G. *Macromolecular Symposia* **2006**, *234*, 59-67.
- Pyun, J.; Matyjaszewski, K. *Chemistry of Materials* **2001**, *13*, 3436-3448.

- Pyun, J.; Matyjaszewski, K. *Macromolecules* **2000**, *33*, 217-220.
- Pyun, J.; Matyjaszewski, K.; Wu, J.; Kim, G. M.; Chun, S. B.; Mather, P. T. *Polymer* **2003**, *44*, 2739-2750.
- Quirk, R. P.; Yoo, T.; Lee, B. J. *Journal of Macromolecular Science-Pure and Applied Chemistry* **1994**, *A31*, 911-926.
- Rashid, E. S. A.; Ariffin, K.; Kooi, C. C.; Akil, H. M. *Materials & Design* **2009**, *30*, 1-8.
- Rubner, M. *Nature* **2003**, *423*, 925-926.
- Sanchez, C.; Arribart, H.; Guille, M. M. G. *Nature Materials* **2005**, *4*, 277-288.
- Sanchez, C.; Julian, B.; Belleville, P.; Popall, M. *Journal of Materials Chemistry* **2005**, *15*, 3559-3592.
- Scott, D. W. *Journal of the American Chemical Society* **1946**, *68*, 356-358.
- Segalman, R. A. *Materials Science & Engineering R-Reports* **2005**, *48*, 191-226.
- Semenov, A. N. *Macromolecules* **1993**, *26*, 6617-6621.
- Singha, N. K.; Mohandas, T. P. *Journal of Macromolecular Science-Pure and Applied Chemistry* **1997**, *A34*, 2269-2278.
- Soh, M. S.; Sellinger, A.; Yap, A. U. J. *Current Nanoscience* **2006**, *2*, 373-381.
- Somogyi, A.; Elandaloussi, E. H.; Hall, D. E.; Buyle Padias, A.; Bates, R. B.; Hall, H. K., Jr., *Macromolecules*, **2007**, *40*, 5311-5321.
- Somogyi, A.; Shu, P.; Padias, A. B. ; Hall, D. E.; Hall, H. K., Jr. "MALDI-TOF Analysis of Polymers by Using Tailor-Made Fluorinated Azobenzene and Stilbene Matrices", presented at 55th ASMS Conference on Mass Spectrometry and Allied Topics, **2007**, Indianapolis, IN
- Stewart, M. D.; Willson, C. G. *MRS Bulletin* **2005**, *30*, 947-951.
- Sur, G. S.; Sun, H. L.; Lyu, S. G.; Mark, J. E. *Polymer* **2001**, *42*, 9783-9789.
- Templin, M.; Franck, A.; DuChesne, A.; Leist, H.; Zhang, Y. M.; Ulrich, R.; Schadler, V.; Wiesner, U. *Science* **1997**, *278*, 1795-1798.
- Tuteja, A.; Choi, W.; Ma, M. L.; Mabry, J. M.; Mazzella, S. A.; Rutledge, G. C.; McKinley, G. H.; Cohen, R. E. *Science* **2007**, *318*, 1618-1622.

- Uddin, M. H.; Rodriguez, C.; Lopez-Quintela, A.; Leisner, D.; Solans, C.; Esquena, J.; Kunieda, H. *Macromolecules* **2003**, *36*, 1261-1271.
- Uraneck, C. A. *Journal of Polymer Science Part a-1-Polymer Chemistry* **1971**, *9*, 2273-&.
- Valencia, M.; Dempwolf, W.; Guenzler, F.; Knoepfelmacher, O.; Schmidt-Naake, G., *Macromolecules*, **2007**, *40*, 40-46.
- Valerie Gabelica, Erin Shammel Baker, Marie-Paule Teulade-Fichou, Edwin De Pauw, and Michael T. Bowers, *J. Am. Chem. Soc.* **2007**, *129*, 895-904.
- Vavasour, J. D.; Whitmore, M. D. *Macromolecules* **1993**, *26*, 7070-7075.
- Vavasour, J. D.; Whitmore, M. D. *Macromolecules* **1996**, *29*, 5244-5244.
- Volkmuth, W. D.; Austin, R. H. *Nature* **1992**, *358*, 600-602.
- Volkmuth, W. D.; Duke, T.; Wu, M. C.; Austin, R. H.; Szabo, A. *Physical Review Letters* **1994**, *72*, 2117-2120.
- Voronkov, M. G.; Lavrentyev, V. I. *Top. Curr. Chem.* **1982**, *102*, 199-236.
- Waddon, A. J.; Coughlin, E. B. *Chemistry of Materials* **2003**, *15*, 4555-4561.
- Waddon, A. J.; Zheng, L.; Farris, R. J.; Coughlin, E. B. *Nano Letters* **2002**, *2*, 1149-1155.
- Wallace, W. E.; Guttman, C. M.; Antonucci, J. M., *Polymer*, **1999**, *41*, 2219-2226.
- Wallace, W.E.; Guttman, C. M.; and Antonucci, J.M., *J. Am. Soc. Mass Spectrom.*, **1999**, *10*, 224-230.
- Walton, D. G.; Kellogg, G. J.; Mayes, A. M.; Lambooy, P.; Russell, T. P. *Macromolecules* **1994**, *27*, 6225-6228.
- Weiss, D.; Roukes, M. L.; Menshig, A.; Grambow, P.; Vonklitzing, K.; Weimann, G. *Physical Review Letters* **1991**, *66*, 2790-2793.
- Whitesides, G. M.; Grzybowski, B. *Science* **2002**, *295*, 2418-2421.
- Whitesides, G. M.; Mathias, J. P.; Seto, C. T. *Science* **1991**, *254*, 1312-1319.
- Williams, R. J. J.; Erra-Balsells, R.; Ishikawa, Y.; Nonami, H.; Mauri, A. N.; Riccardi, C. C., *Macromolecular Chemistry and Physics*, **2001**, *202*, 2425-2433.

- Yang, P. D.; Deng, T.; Zhao, D. Y.; Feng, P. Y.; Pine, D.; Chmelka, B. F.; Whitesides, G. M.; Stucky, G. D. *Science* **1998**, 282, 2244-2246.
- Yang, P. D.; Zhao, D. Y.; Margolese, D. I.; Chmelka, B. F.; Stucky, G. D. *Nature* **1998**, 396, 152-155.
- Yu, J. M.; Dubois, P.; Teyssie, P.; Jerome, R. *Macromolecules* **1996**, 29, 6090-6099.
- Zeng, J.; Kumar, S.; Iyer, S.; Schiraldi, D. A.; Gonzalez, R. I. *High Performance Polymers* **2005**, 17, 403-424.
- Zhang, X.; Chan, E. R.; Glotzer, S. C. *Journal of Chemical Physics* **2005**, 123.
- Zhang, X.; Zhang, Z. L.; Glotzer, S. C. *Nanotechnology* **2007**, 18.
- Zhang, Z. L.; Horsch, M. A.; Lamm, M. H.; Glotzer, S. C. *Nano Letters* **2003**, 3, 1341-1346.
- Zhao, D. Y.; Feng, J. L.; Huo, Q. S.; Melosh, N.; Fredrickson, G. H.; Chmelka, B. F.; Stucky, G. D. *Science* **1998**, 279, 548-552.
- Zhao, J. Q.; Fu, Y.; Liu, S. M. *Polymers & Polymer Composites* **2008**, 16, 483-500.
- Zhao, Y. Q.; Schiraldi, D. A. *Polymer* **2005**, 46, 11640-11647.
- Zheng, L.; Farris, R. J.; Coughlin, E. B. *Journal of Polymer Science Part a-Polymer Chemistry* **2001**, 39, 2920-2928.
- Zheng, L.; Farris, R. J.; Coughlin, E. B. *Macromolecules* **2001**, 34, 8034-8039.
- Zheng, L.; Hong, S.; Cardoen, G.; Burgaz, E.; Gido, S. P.; Coughlin, E. B. *Macromolecules* **2004**, 37, 8606-8611.
- Zheng, L.; Kasi, R. M.; Farris, R. J.; Coughlin, E. B. *Journal of Polymer Science Part a-Polymer Chemistry* **2002**, 40, 885-891.
- Zheng, L.; Waddon, A. J.; Farris, R. J.; Coughlin, E. B. *Macromolecules* **2002**, 35, 2375-2379.
- Zou, H.; Wu, S. S.; Shen, J. *Chemical Reviews* **2008**, 108, 3893-3957.